

SUPRAMOLECULAR REAGENTS FOR THE CONSTRUCTION OF PREDICTABLE  
ARCHITECTURES

by

MICHELLE M. SMITH

B.S., The Nottingham Trent University, 2003

AN ABSTRACT OF A DISSERTATION

submitted in partial fulfillment of the requirements for the degree

DOCTOR OF PHILOSOPHY

Department Of Chemistry  
College of Arts and Sciences

KANSAS STATE UNIVERSITY  
Manhattan, Kansas

2008

## Abstract

Tailoring the properties of a bulk material such as a pharmaceutical compound, through non-covalent interactions, could lead to the enhancement of its physical properties without chemically modifying the individual molecules themselves. In order to obtain a degree of control and reliability of these non-covalent interactions, we must develop a series of synthons – patterns of non-covalent interactions between molecules.

A family of N-heterocyclic amides were synthesised and an assessment of their binding selectivities was made, by evaluation of the *supramolecular yield*, (the frequency of occurrence of the desired connectivities). It was found that the supramolecular yield increased with increasing basicity of the heterocyclic nitrogen atom. However, there is a point where the heterocycle becomes basic enough to produce salts, which often leads to unpredictable connectivity and stoichiometry.

Once the effectiveness of the N-heterocyclic amides as supramolecular reagents was established, a series of more closely-related ditopic hydrogen-bond acceptor molecules were synthesised. The supramolecular reagents contained imidazole and pyridine binding sites, so that the two sites differ in terms of their basicity and geometry. An assessment of the ability of these molecules to induce selectivity when a hydrogen bond donor such as a cyanoxime or a carboxylic acid is introduced was made. A total of nineteen crystal structures were obtained, of which one yielded a salt with unpredictable connectivity, and eighteen were co-crystals. Ten of these were 2:1 co-crystals, which shows that the two sites are accessible for binding. Eight were 1:1 stoichiometry, with five out of eight (63%) forming a hydrogen bond to the best acceptor. In addition, a series of molecular electrostatic potential calculations were employed to investigate the binding preferences and probe the best donor/best acceptor hypothesis. A ternary supermolecule was also constructed from a central, asymmetric hydrogen-bond acceptor and two different hydrogen-bond donor molecules. It was found that the best donor, the cyanoxime, bound to the best acceptor, the imidazole nitrogen atom, while the second best donor, a carboxylic acid, bound to the second

best acceptor. The calculated molecular electrostatic potential values were used to rationalize this event.

A series of substituted cyanophenylloxime, hydrogen bond donor molecules were synthesized and their effectiveness at forming co-crystals was examined. It was found that simple R group substitution could have a significant effect upon the co-crystal forming ability of the hydrogen bond donors, having improved the yield from 4% and 7% in a series of co-crystallizations with closely-related oximes, to 96% with the cyanoximes.

A series of di- and tritopic cyanoximes were synthesized and an assessment of their co-crystal-forming ability was made. They were found to be equally effective at producing co-crystals as the monotopic cyanoximes, having done so in 23 out of 24 cases. In contrast to their carboxylic acid counterparts, the polycyanoximes also exhibited excellent solubility.

Finally, a series of ditopic ligands (N-heterocyclic amide and pyridyl cyanoximes) were employed in the synthesis of metal complexes. The amide-based ligands were found to be very effective at organizing the metal architectures with coordination through the heterocyclic nitrogen atom and propagation of one-dimensional chains through carboxamide-carboxamide interactions. These interactions prevailed even in the presence of potentially disruptive species such as solvent molecules, (in Ag(I) complexes) counterions, or other hydrogen bond acceptors. The self-complementarity of the oxime moiety was found not to prevail in any of the cases, but the pyridyl cyanoximes were consistent in their behaviour, forming an O-H $\cdots$ O (oxime-oxygen) hydrogen bond to a carboxylate or *acac* moiety.

SUPRAMOLECULAR REAGENTS FOR THE CONSTRUCTION OF PREDICTABLE  
ARCHITECTURES

by

MICHELLE M. SMITH

B.S., The Nottingham Trent University, 2003

A DISSERTATION

submitted in partial fulfillment of the requirements for the degree

DOCTOR OF PHILOSOPHY

Department of Chemistry  
College of Arts And Sciences

KANSAS STATE UNIVERSITY  
Manhattan, Kansas

2008

Approved by:

Major Professor  
Christer B. Aakeröy

## Abstract

Tailoring the properties of a bulk material such as a pharmaceutical compound, through non-covalent interactions, could lead to the enhancement of its physical properties without chemically modifying the individual molecules themselves. In order to obtain a degree of control and reliability of these non-covalent interactions, we must develop a series of synthons – patterns of non-covalent interactions between molecules.

A family of N-heterocyclic amides were synthesised and an assessment of their binding selectivities was made, by evaluation of the *supramolecular yield*, (the frequency of occurrence of the desired connectivities). It was found that the supramolecular yield increased with increasing basicity of the heterocyclic nitrogen atom. However, there is a point where the heterocycle becomes basic enough to produce salts, which often leads to unpredictable connectivity and stoichiometry.

Once the effectiveness of the N-heterocyclic amides as supramolecular reagents was established, a series of more closely-related ditopic hydrogen-bond acceptor molecules were synthesised. The supramolecular reagents contained imidazole and pyridine binding sites, so that the two sites differ in terms of their basicity and geometry. An assessment of the ability of these molecules to induce selectivity when a hydrogen bond donor such as a cyanoxime or a carboxylic acid is introduced was made. A total of nineteen crystal structures were obtained, of which one yielded a salt with unpredictable connectivity, and eighteen were co-crystals. Ten of these were 2:1 co-crystals, which shows that the two sites are accessible for binding. Eight were 1:1 stoichiometry, with five out of eight (63%) forming a hydrogen bond to the best acceptor. In addition, a series of molecular electrostatic potential calculations were employed to investigate the binding preferences and probe the best donor/best acceptor hypothesis. A ternary supermolecule was also constructed from a central, asymmetric hydrogen-bond acceptor and two different hydrogen-bond donor molecules. It was found that the best donor, the cyanoxime, bound to the best acceptor, the imidazole nitrogen atom, while the second best donor, a carboxylic acid, bound to the second

best acceptor. The calculated molecular electrostatic potential values were used to rationalize this event.

A series of substituted cyanophenylloxime, hydrogen bond donor molecules were synthesized and their effectiveness at forming co-crystals was examined. It was found that simple R group substitution could have a significant effect upon the co-crystal forming ability of the hydrogen bond donors, having improved the yield from 4% and 7% in a series of co-crystallizations with closely-related oximes, to 96% with the cyanoximes.

A series of di- and tritopic cyanoximes were synthesized and an assessment of their co-crystal-forming ability was made. They were found to be equally effective at producing co-crystals as the monotopic cyanoximes, having done so in 23 out of 24 cases. In contrast to their carboxylic acid counterparts, the polycyanoximes also exhibited excellent solubility.

Finally, a series of ditopic ligands (N-heterocyclic amide and pyridyl cyanoximes) were employed in the synthesis of metal complexes. The amide-based ligands were found to be very effective at organizing the metal architectures with coordination through the heterocyclic nitrogen atom and propagation of one-dimensional chains through carboxamide-carboxamide interactions. These interactions prevailed even in the presence of potentially disruptive species such as solvent molecules, (in Ag(I) complexes) counterions, or other hydrogen bond acceptors. The self-complementarity of the oxime moiety was found not to prevail in any of the cases, but the pyridyl cyanoximes were consistent in their behaviour, forming an O-H $\cdots$ O (oxime-oxygen) hydrogen bond to a carboxylate or *acac* moiety.

# Table of Contents

<b>List of Figures</b> .....	<b>xviii</b>
<b>List of Tables</b> .....	<b>xxvi</b>
<b>Acknowledgements</b> .....	<b>xxx</b>
<b>Dedication</b> .....	<b>xxxi</b>
<b>Preface</b> .....	<b>xxxii</b>
<b>CHAPTER 1 - Introduction</b> .....	<b>1</b>
1.1 What is supramolecular chemistry? .....	1
1.1.1 Molecular recognition.....	2
1.1.2 Self-assembly – the production of a crystal .....	3
1.2 Intermolecular interactions and the important hydrogen bond .....	4
1.2.1 Graph set notation .....	6
1.2.2 Etter’s hydrogen-bond rules.....	6
1.3 Co-crystallization as a tool for examining the balance between intermolecular interactions .....	7
1.3.1 Definition of “co-crystal”.....	8
1.3.2 Higher-order molecular co-crystals.....	9
1.4 Molecular electrostatic potentials (MEPs) as a tool for ranking hydrogen bond donor and acceptor strength .....	10
1.5 Goals .....	12
<b>CHAPTER 2 - Bifunctional amides – Synthesis of Molecular Co-crystals</b> .....	<b>18</b>
2.1 Introduction.....	18
2.2 How reliable are the new heterocyclic amides as supramolecular reagents?.....	19
2.2.1 Goals .....	19
2.3 Experimental .....	21
2.3.1 Synthesis of amides.....	22
2.3.1.1 Synthesis 4-[(7-aza-indol-1-yl)methyl]benzotrile, 1.....	22
2.3.1.2 Synthesis of 4-[(7-aza-indol-1-yl)methyl]benzamide, 2 .....	22

2.3.1.3	Synthesis of 4-[(5,6-dimethylbenzimidazol-1-yl)methyl]benzotrile, 3 ...	23
2.3.1.4	Synthesis of 4-[(5,6-dimethylbenzimidazol-1-yl)methyl]benzamide, 4	23
2.3.1.5	Synthesis of 3-[(5,6-dimethylbenzimidazol-1-yl)methyl]benzotrile, 5 ...	24
2.3.1.6	Synthesis of 3-[(5,6-dimethylbenzimidazol-1-yl)methyl]benzamide, 6	24
2.3.1.7	Synthesis 4-[(2-phenylimidazol-1-yl)methyl]benzotrile, 7	25
2.3.1.8	Synthesis of 4-[(2-phenylimidazol-1-yl)methyl]benzamide, 8	25
2.3.1.9	Synthesis 3-[(2-phenylimidazol-1-yl)methyl]benzotrile, 9	25
2.3.1.10	Synthesis of 3-[(2-phenylimidazol-1-yl)methyl]benzamide, 10	26
2.3.2	Synthesis of co-crystals and salts	26
2.3.2.1	Synthesis of 4-[(7-aza-indol-1-yl)methyl]benzamide 4-nitrobenzoic acid (1:2), 2a	27
2.3.2.2	Synthesis of 4-[(7-aza-indol-1-yl)methyl]benzamide 3,5-dinitrobenzoic acid (1:1), 2b	27
2.3.2.3	Synthesis of 4-[(5,6-dimethylbenzimidazol-1-yl)methyl]benzamide 2,5-dichlorobenzoic acid (1:1), 4a	27
2.3.2.4	Synthesis of 3-[(5,6-dimethylbenzimidazol-1-yl)methyl]benzamide 2,3,4,5,6-pentamethylbenzoic acid (1:1), 6a	27
2.3.2.5	Synthesis of 3-[(5,6-dimethylbenzimidazolium-1-yl)methyl]benzamide 3,5-dinitrobenzoate (1:1), 6b	27
2.3.3	Infra-red spectroscopy and melting point	28
2.4	Results	28
2.4.1	IR spectroscopy	28
2.4.2	Crystal structure of 4-[(7-aza-indol-1-yl)methyl]benzamide, 2	30
2.4.3	Crystal structure of 4-[(7-aza-indol-1-yl)methyl]benzamide 4-nitrobenzoic acid (1:2), 2a	31
2.4.4	Crystal structure of 4-[(7-aza-indol-1-yl)methyl]benzamide 3,5-dinitrobenzoic acid (1:1), 2b	32



2.4.5	Crystal structure of 4-[(5,6-dimethylbenzimidazolium-1-yl)methyl]benzamide 2,5-dichlorobenzoate (1:1), 4a .....	32
2.4.6	Crystal structure of 3-[(5,6-dimethylbenzimidazol-1-yl)methyl]benzamide, 6 .....	33
2.4.7	Crystal structure of 3-[(5,6-dimethylbenzimidazol-1-yl)methyl]benzamide 2,3,4,5,6-pentamethylbenzoic acid (1:1), 6a .....	34
2.4.8	Crystal structure of 3-[(5,6-dimethylbenzimidazolium-1-yl)methyl]benzamide 3,5-dinitrobenzoate, 6b .....	34
2.4.9	Calculations.....	35
2.5	Discussion .....	36
2.5.1	Synthesis and Characterization .....	36
2.5.2	IR spectroscopy.....	36
2.5.3	X-ray Crystallography.....	37
2.5.3.1	Structural consistency of amides.....	37
2.5.3.2	Salt formation.....	37
2.5.4	Binding selectivities .....	42
2.6	Conclusions.....	44
<b>CHAPTER 3 - Asymmetric Ditopic Ligands in the Design and Synthesis of Binary Supermolecules..... 46</b>		
3.1	Introduction.....	46
3.2	How selective are the supramolecular reagents? .....	47
3.2.1	Goals .....	47
3.3	Experimental .....	48
3.3.1	Synthesis of asymmetric acceptors .....	48
3.3.1.1	Synthesis of 1-[(3-pyridyl)methyl]-5,6-dimethylbenzimidazole, 11 .....	48
3.3.1.2	Synthesis of 1-[(4-pyridyl)methyl]-5,6-dimethylbenzimidazole, 12 .....	48
3.3.1.3	Synthesis of 1-[(3-pyridyl)methyl]-2-phenylimidazole, 13 .....	49
3.3.1.4	Synthesis of 1-[(4-pyridyl)methyl]-2-phenylimidazole, 14 .....	49
3.3.1.5	Synthesis of 1-[(3-pyridyl)methyl]-7-azaindole and 7-[(3-pyridyl)methyl]-7-azaindole, 15 and 16.....	50

3.3.1.6	Synthesis of 1-[(4-pyridyl)methyl]-7-azaindole and 7-[(4-pyridyl)methyl]-7-azaindole, 17 and 18.....	51
3.3.2	Synthesis of co-crystals and salts.....	51
3.3.2.1	General synthesis of co-crystals.....	51
3.3.2.2	Syntheses of 1-[(4-pyridyl)methyl]-5,6-dimethylbenzimidazole and 1-[(3-pyridyl)methyl]-5,6-dimethylbenzimidazole co-crystals, 11(a-i) and 12(a-g).....	52
3.3.2.3	Syntheses of 1-[(4-pyridyl)methyl]-2-phenylimidazole and 1-[(3-pyridyl)methyl]-2-phenylimidazole co-crystals, 13a and 14a .....	52
3.3.2.4	Synthesis of 1-[(3-pyridyl)methyl]-7-azaindole pentamethylbenzoic acid, 15a.....	52
3.4	Results.....	53
3.4.1	Crystal structure of 1-[(3-pyridyl)methyl]-5,6-dimethylbenzimidazole, 11	55
3.4.2	Crystal structure of 1-[(3-pyridyl)methyl]-2-phenylimidazole, 13.....	55
3.4.3	Crystal structure of 1-[(3-pyridyl)methyl]-5,6-dimethylbenzimidazole 4-chlorobenzoic acid (1:1), 11a.....	56
3.4.4	Crystal structure of 1-[(3-pyridyl)methyl]-5,6-dimethylbenzimidazolium pentafluoro benzoate (1:1), 11b .....	57
3.4.5	Crystal structure of 1-[(3-pyridyl)methyl]-5,6-dimethylbenzimidazole fumaric acid hydrate (1:1), 11c .....	57
3.4.6	Crystal structure of 1-[(4-pyridyl)methyl]-5,6-dimethylbenzimidazole 4-N,N'-dimethylamino) benzoic acid (1:1), 12a.....	58
3.4.7	Crystal structure of 1-[(4-pyridyl)methyl]-5,6-dimethylbenzimidazole 3-iodobenzoic acid (1:1), 12b.....	58
3.4.8	Crystal structure of 1-[(3-pyridyl)methyl]-5,6-dimethylbenzimidazolium pentamethyl benzoate pentamethylbenzoic acid (1:1:1), 11d.....	59
3.4.9	Crystal structure of 1-[(3-pyridyl)methyl]-5,6-dimethylbenzimidazolium 2,3,5,6-tetrafluoro-4-iodobenzoate ethanol (1:1:1), 11e .....	59
3.4.10	Crystal structure of 1-[(3-pyridinium)methyl]-5,6-dimethylbenzimidazole 3,5-dinitrobenzoate 3,5-dinitrobenzoic acid (1:1:1), 11f.....	60

3.4.11	Crystal structure of 1-[(3-pyridyl)methyl]-5,6-dimethylbenzimidazole 4-nitrobenzoic acid (1:2), 11g .....	60
3.4.12	Crystal structure of 1-[(3-pyridyl)methyl]-5,6-dimethylbenzimidazole 4-iodobenzoic acid (2:3), 11h.....	61
3.4.13	Crystal structure of 1-[(3-pyridyl)methyl]-5,6-dimethylbenzimidazole 4-bromophenylcyanoxime, 11i.....	62
3.4.14	Crystal structure of 1-[(4-pyridyl)methyl]-5,6-dimethylbenzimidazole 3-cyanobenzoic acid (1:2), 12c.....	62
3.4.15	Crystal structure of 1-[(4-pyridyl)methyl]-5,6-dimethylbenzimidazole oxalic acid hydrate (1:1:1), 12d .....	63
3.4.16	Crystal structure of 1-[(4-pyridyl)methyl]-5,6-dimethylbenzimidazole 3-fluorobenzoic acid (1:2), 12e .....	63
3.4.17	Crystal structure of 1-[(4-pyridyl)methyl]-5,6-dimethylbenzimidazole tetrafluoroiodo aldoxime (1:1), 12f.....	64
3.4.18	Crystal structure of 1-[(4-pyridyl)methyl]-5,6-dimethylbenzimidazole 4-fluorophenylcyanoxime, 12g.....	64
3.4.19	Crystal structure of 1-[(3-pyridyl)methyl]-2-phenylimidazole 4-nitrobenzoic acid (1:2), 13a.....	65
3.4.20	Crystal structure of 1-[(4-pyridyl)methyl]-2-phenylimidazole 4-nitrobenzoic acid (1:2), 14a.....	65
3.4.21	Crystal structure of 1-[(3-pyridyl)methyl]-7-azaindole 2,3,4,5,6-pentamethyl benzoic acid (1:2), 15a .....	66
3.4.22	Calculations.....	67
3.5	Discussion .....	67
3.5.1	Synthesis and characterization .....	67
3.5.2	IR spectroscopy.....	68
3.5.3	X-ray Crystallography.....	68
3.5.4	Binding selectivities .....	69
3.5.5	Hydrogen bond lengths .....	70
3.5.6	Salts .....	71
3.5.7	Halogen bonding.....	71

3.6	Conclusions .....	74
<b>CHAPTER 4 - Probing the Reliability of Oximes as Hydrogen-bond Donors in the</b>		
	<b>Synthesis of Molecular Co-crystals .....</b>	<b>76</b>
4.1	Introduction .....	76
4.2	Oximes – Reliable Tools for Supramolecular Synthesis? .....	78
4.3	Experimental .....	80
4.3.1	Synthesis of cyanophenylloximes .....	80
4.3.2	Synthesis of Co-crystals .....	82
4.3.2.1	Synthesis of 3-chlorophenylcyanoxime 1,4-bis[(benzimidazol-1-yl)methyl]benzene (2:1), 21a .....	83
4.3.2.2	Synthesis of 2-fluorophenylcyanoxime 1,2-bis(4-pyridyl)ethylene (2:1), 23e .....	84
4.3.3	Calculations .....	84
4.3.4	X-ray crystallography .....	84
4.3.5	Infra-red spectroscopy and melting point .....	84
4.4	Results .....	85
4.4.1	IR Spectroscopy .....	85
4.4.2	Crystal structure of 3-chloro-phenylcyanoxime 1,4-di[(1-benzimidazolyl)methyl]benzene (2:1), 21a .....	86
4.4.3	Crystal structure of 2-fluoro-phenylcyanoxime 1,2-di(4-pyridyl)ethane (2:1), 23e .....	86
4.5	Discussion .....	88
4.5.1	Synthesis and NMR Characterization .....	88
4.5.2	IR Spectroscopy and melting point .....	88
4.5.3	X-ray Crystallography .....	89
4.6	Conclusions .....	91
<b>CHAPTER 5 - Probing the Reliability of Di- and Tricyanophenylloximes as</b>		
	<b>Hydrogen-bond Donors in the Synthesis of Molecular Co-crystals .....</b>	<b>96</b>
5.1	Introduction – Polyfunctional carboxylic acids in crystal engineering .....	96
5.1.1	From discrete to extended architectures .....	97

5.1.2	Problems with polyfunctional carboxylic acids as supramolecular reagents...	98
5.1.3	Why cyanoximes are a good alternative .....	100
5.1.4	Goals .....	100
5.2	Experimental .....	101
5.2.1	Synthesis of dicyanophenyloximes .....	101
5.2.1.1	Synthesis of 1,4-dicyanophenyloxime, 26 .....	101
5.2.1.2	Synthesis of 1,3-dicyanophenyloxime, 27 .....	102
5.2.2	Synthesis of tricyanophenyloxime .....	102
5.2.2.1	Synthesis of 1,3,5-tris(cyanomethyl)benzene, 28 .....	102
5.2.2.2	Synthesis of 1,3,5-tricyanophenyloxime, 29 .....	103
5.2.3	Molecular electrostatic potentials .....	103
5.2.4	Synthesis of co-crystals .....	103
5.2.4.1	Synthesis of 1,4-dicyanophenyloxime 1,2-di(4-pyridyl)ethane, 26a ...	104
5.2.4.2	Synthesis of 1,4-dicyanophenyloxime 1-[(3-pyridyl)methyl]-5,6-dimethylbenzimidazole, 26b .....	104
5.2.4.3	Synthesis of 1,4-dicyanophenyloxime 1-[(3-pyridyl)methyl]benzimidazole, 26c .....	105
5.2.4.4	Synthesis of 1,4-dicyanophenyloxime 1-[(4-pyridyl)methyl]-2-phenylimidazole, 26d .....	105
5.2.4.5	Synthesis of 1,4-dicyanophenyloxime 2,3,5,6-tetramethylpyrazine, 26e. ....	105
5.2.4.6	Synthesis of 1,3,5-tricyanophenyloxime 2-bromo-5-methylpyridine, 29a .....	105
5.2.4.7	Synthesis of 1,3,5-tricyanophenyloxime 1,2-di(4-pyridyl)ethane, 29b ....	105
5.2.5	X-ray crystallography .....	105
5.2.6	Infra-red spectroscopy and melting point .....	106
5.3	Results .....	106
5.3.1	Molecular Electrostatic potential calculations .....	106
5.3.2	Crystal structure of 1,4-dicyanophenyloxime, 26 .....	108

5.3.3	Crystal structure of 1,4-dicyanophenyloxime 1,2-di(4-pyridyl)ethane, 26a.....	108
5.3.4	Crystal structure of 1,4-dicyanophenyloxime 1-[(3-pyridyl)methyl]-5,6-dimethylbenzimidazole, 26b .....	109
5.3.5	Crystal structure of 1,4-dicyanophenyloxime 1-[(3-pyridyl)methyl]benzimidazole, 26c .....	109
5.3.6	Crystal structure of 1,4-dicyanophenyloxime 1-[(4-pyridyl)methyl]-2-phenylimidazole, 26d .....	110
5.3.7	Crystal structure of 1,4-dicyanophenyloxime 2,3,5,6-tetramethyl pyrazine, 26e .....	111
5.3.8	Crystal structure of (1,3,5-tricyanophenyloxime) 2-bromo-5-methylpyridine, 29a .....	111
5.3.9	Crystal structure of (1,3,5-tricyanophenyloxime) <sub>2</sub> [1,4-di(4-pyridyl)ethane] <sub>3</sub> , 29b.....	112
5.3.10	IR Spectroscopy .....	113
5.4	Discussion .....	113
5.4.1	Synthesis and characterization .....	113
5.4.2	IR Spectroscopy .....	114
5.4.3	X-ray Crystallography.....	115
<b>CHAPTER 6 - Construction, Deconstruction, and Reconstruction of Ternary</b>		
	<b>Supermolecules.....</b>	<b>117</b>
6.1	Introduction .....	117
6.1.1	Goals .....	118
6.2	Experimental .....	120
6.2.1	Synthesis of ditopic hydrogen-bond donor and acceptor molecules.....	120
6.2.1.1	Synthesis of 4-(2-methylbenzimidazol-1-yl)methyl pyridine, 30 .....	120
6.2.1.2	Synthesis of 1,4-carboxyphenylcyanoxime, 32.....	121
6.2.2	Synthesis of co-crystals.....	122
6.2.2.1	Synthesis of 4-(5,6-dimethylbenzimidazol-1-yl)methylpyridine 4-carboxyphenylcyanoxime (1:1), 12:32 .....	122

6.2.2.2	Synthesis of 4-(2-phenylimidazol-1-yl)methylpyridine 4-hydroxybenzoic acid (1:1), 14:4-OH BA.....	122
6.2.2.3	Synthesis of pentamethylbenzoic acid 4-(2-methylbenzimidazol-1-yl)methylpyridinephenylcyanoxime (1:1:1) 30:PMBA:25 .....	123
6.3	Results.....	123
6.3.1	Crystal structure of 4-(5,6-dimethylbenzimidazol-1-yl)methylpyridine 4-carboxyphenylcyanoxime (1:1), 12:32 .....	123
6.3.2	Crystal structure of 4-(2-phenylimidazol-1-yl)methylpyridine 4-hydroxybenzoic acid, 14:4-OH BA .....	124
6.3.3	Crystal structure of pentamethylbenzoic acid 4-(2-methylbenzimidazol-1-yl)methylpyridinephenylcyanoxime(1:1:1), 30:PMBA:25 .....	124
6.3.4	Molecular electrostatic potentials .....	125
6.4	Discussion .....	126
6.4.1	Calculating the strength of intermolecular interactions .....	127
6.5	Conclusions.....	129
<b>CHAPTER 7 - Application of Cyanoxime and Amide building blocks in the</b>		
	<b>Supramolecular Assembly of Metal-Containing 1D-Architectures .....</b>	<b>132</b>
7.1	Introduction.....	132
7.1.1	Supramolecular approach.....	132
7.1.2	Goals .....	134
7.1.3	Choice of metals.....	135
7.2	Experimental .....	136
7.2.1	Synthesis of pyridylcyanoximes .....	137
7.2.1.1	Synthesis of (3-pyridyl)-cyanoxime, 33.....	137
7.2.1.2	Synthesis of 4-(3-pyridylphenylacetonitrile), 34 .....	138
7.2.1.3	Synthesis of [1-(pyridin-3-yl)-4-(cyanoxime)phenyl], 35 .....	138
7.2.2	Synthesis of metal complexes 4b-d, 8a, 10a, 33a and 33b, 35a and 35b ....	139
7.2.2.1	Synthesis of bis[4-(5,6-dimethylbenzimidazol-1-yl)methylbenzamide] silver(I) tetrafluoroborate, 4b.....	139
7.2.2.2	Synthesis of bis[4-(5,6-dimethylbenzimidazol-1-yl)methylbenzamide] silver(I) hexafluoroarsenate, 4c.....	139

7.2.2.3	Synthesis of [4-(5,6-dimethylbenzimidazol-1-yl)methylbenzamide]bis-(hexafluoroacetylacetonato)copper(II), 4d.....	139
7.2.2.4	Synthesis of tetrakis( $\mu$ -2-fluorobenzoato-O,O')-bis(4-(2-phenylimidazol-1-yl)methylbenzamide)-dicopper(II), 8a.....	139
7.2.2.5	Synthesis of tetrakis( $\mu$ -2-fluorobenzoato-O,O')-bis(3-(2-phenylimidazol-1-yl)methylbenzamide)-dicopper(II), 10a.....	140
7.2.2.6	Synthesis of tetrakis( $\mu$ -2-fluorobenzoato-O,O')-bis-(3-pyridyl-cyanoxime)-dicopper(II), 33a .....	140
7.2.2.7	Synthesis of tetrakis( $\mu$ -acetato-O,O')-bis-(3-pyridyl-cyanoxime)-dicopper(II), 33b .....	140
7.2.2.8	Synthesis of [1-(pyridin-3-yl)-4-(cyanoxime)phenyl]bis-(dibenzoylmethanato)nickel(II), 35a.....	140
7.2.2.9	Synthesis of tetrakis( $\mu$ -acetato-O,O')-bis([1-(pyridin-3-yl)-4-(cyanoxime)phenyl]-dicopper(II), 35b.....	140
7.3	Results.....	141
7.3.1	Crystal structure of bis[4-(5,6-dimethylbenzimidazol-1-yl)methylbenzamide]silver(I) tetrafluoroborate, 4b.....	142
7.3.2	Crystal structure of bis[4-(5,6-dimethylbenzimidazol-1-yl)methylbenzamide]silver(I) hexafluoroarsenate, 4c .....	143
7.3.3	Crystal structure of [4-(5,6-dimethylbenzimidazol-1-yl)methylbenzamide]bis(hexafluoroacetylacetonato)copper(II) acetonitrile, 4d. 144	
7.3.4	Crystal structure of tetrakis( $\mu$ -2-fluorobenzoato-O,O')-bis(4-(2-phenylimidazol-1-yl)methylbenzamide)-dicopper(II) acetonitrile, 8a.....	144
7.3.5	Synthesis of tetrakis( $\mu$ -2-fluorobenzoato-O,O')-bis(3-(2-phenylimidazol-1-yl)methylbenzamide)-dicopper(II), 10a .....	145
7.3.6	Synthesis of tetrakis( $\mu$ -2-fluorobenzoato-O,O')-bis-(3-pyridyl-cyanoxime)-dicopper(II), 33a.....	146
7.3.7	Crystal structure of tetrakis( $\mu$ -acetato-O,O')-bis-(3-pyridyl-cyanoxime)-dicopper(II), 33b .....	146



7.3.8	Crystal structure of [1-(pyridin-3-yl)-4-(cyanoxime)phenyl]bis-(dibenzoylmethanato)nickel(II), 35a.....	146
7.3.9	Crystal structure of tetrakis( $\mu$ -acetato-O,O')-bis([1-(pyridin-3-yl)-4-(cyanoxime)phenyl]-dicopper(II), 35b.....	147
7.4	Discussion.....	148
7.5	Conclusions.....	152
<b>Appendix A - <math>^1\text{H}</math> and <math>^{13}\text{C}</math> NMR Data.....</b>		<b>157</b>
<b>Appendix B - Crystal Data and Structure Refinements.....</b>		<b>189</b>
<b>Appendix C - Infra red spectra.....</b>		<b>239</b>

## List of Figures

Figure 1.1 Representation of the construction of a building from smaller building blocks, bricks, and the construction of supermolecules from smaller building blocks, molecules.....	1
Figure 1.2 Illustration of the concept of molecular recognition.....	3
Figure 1.3 (a) Host containing two 2-aminopyridine groups, creating a receptor for isophthalic acid, (b). <sup>8</sup> .....	3
Figure 1.4 Hydrogen bonding in the base pairs of DNA. ....	5
Figure 1.5 Examples of supramolecular synthons involving strong hydrogen bonds. ....	5
Figure 1.6 Examples of graph-set notation. ....	6
Figure 1.7 Examples of structures in which the Etter rules are obeyed (a) co-crystal of succinic acid 2-aminopyrimidine, (b) co-crystal of 3-hydroxy-2-naphthoic acid 4,4'-bipyridine. ....	7
Figure 1.8 Schematic representation of recrystallization vs co-crystallization.....	8
Figure 1.9 Two examples of molecular co-crystals: (a) 4-nitrobenzoic acid hemikis-2,2'-bipyridine (2:1) and (b) 1,4- <i>bis</i> -[(imidazol-1-yl)methyl]benzene fumaric acid (1:1). 9	
Figure 1.10 Illustration of a ternary co-crystal. The central molecule must be equipped with two different binding sites so that the incoming molecules can selectively recognize and bind to a specific site.....	9
Figure 1.11 (a) proton transfer (b) hydrogen bond.....	10
Figure 1.12 Schematic representation of a hydrogen bond.....	10
Figure 1.13 $pK_a$ values of benzoic acid and phenol, compared to the calculated hydrogen bond donor constant values. ....	11
Figure 1.14 Plot showing the correlation between the calculated charge of a hydrogen bond donor ( $E_{max}$ ) and those values obtained from solution, $\alpha_2$ . <sup>32</sup> .....	11
Figure 1.15 Schematic of a ternary system showing the best donor (highest positive charge) interacting with the best acceptor (highest negative charge). ....	12

Figure 1.16 (a) Schematic representation of a linearly-ordered supermolecule. Each group contains complementary binding sites to a neighbouring molecule, enabling a highly ordered supermolecule (b) alignment of molecules in the crystal structure of barbituric acid and 2,4,6-triaminopyrimidine. <sup>34</sup>	14
Figure 2.1 Schematic of isonicotinamide, outlining the two possible binding sites.	18
Figure 2.2 Hydrogen bonding between isonicotinamide and (a) 4-fluorobenzoic acid and (b) <i>trans</i> -cinnamic acid.	18
Figure 2.3 Previously synthesized (benzimidazol-1-yl)methyl benzamides.	19
Figure 2.4 3-(Benzimidazol-1-yl)-benzamide 4-nitrobenzoic acid. <sup>5</sup>	19
Figure 2.5 N-heterocyclic amides synthesized and studied here.	20
Figure 2.6 General synthesis of N-heterocyclic amides.	21
Figure 2.7 Hydrogen-bond network in the crystal structure of 2.	31
Figure 2.8 Hydrogen bonding in the crystal structure of 2a.	31
Figure 2.9 Hydrogen bonding in the crystal structure of 2b.	32
Figure 2.10 Extended network in the crystal structure of 4a.	33
Figure 2.11 Extended one-dimensional chain in the crystal structure of 6.	33
Figure 2.12 One-dimensional chain in the crystal structure of 6a.	34
Figure 2.13 (a) Interaction of carboxylate with protonated benzimidazole moiety and amide <i>anti</i> proton (b) $R_4^4$ (12) pattern formed with two carboxylate and two amide $NH_2$ moieties in the crystal structure of 6b.	35
Figure 2.14 (a) $R_4^4$ (12) motif obtained with two carboxylate molecules and two amide molecules upon proton transfer (b) $R_4^2$ (8) motif.	38
Figure 2.15 Plot of calculated MEP vs $pK_a$ .	41
Figure 2.16 Plot of MEP of hydrogen bond acceptor vs the difference in MEPs between the hydrogen-bond acceptor and the hydrogen-bond donor.	42
Figure 2.17 Binding preferences of the supramolecular reagents.	43
Figure 3.1 Supramolecular reagent equipped with two binding sites.	46
Figure 3.2 Supramolecular reagents synthesized here.	47

Figure 3.3 (a) 1-[(3-pyridyl)methyl]-5,6-dimethylbenzimidazole in the crystal structure of 11.....	55
Figure 3.4 1-[(3-Pyridyl)methyl]-2-phenylimidazole in the crystal structure of 13. ....	56
Figure 3.5 Dimer in the crystal structure of 11a. ....	56
Figure 3.6 Ion pair in the crystal structure of 11b. ....	57
Figure 3.7 Infinite one-dimensional chain in the crystal structure of 11c. ....	57
Figure 3.8 Hydrogen bonding interaction in the crystal structure of 12a. ....	58
Figure 3.9 Hydrogen-bonding interactions in the crystal structure of 12b. ....	58
Figure 3.10 Hydrogen bonding in the crystal structure of 11d. ....	59
Figure 3.11 Hydrogen and halogen bonding in the crystal structure of 11e. ....	60
Figure 3.12 Hydrogen bonds in the crystal structure of 11f. ....	60
Figure 3.13 Hydrogen bonds in the crystal structure of 11g. ....	61
Figure 3.14 Hydrogen- and halogen-bonding in the crystal structure of 11h. ....	61
Figure 3.15 Dimer in the crystal structure of 11i. ....	62
Figure 3.16 Trimer in the crystal structure of 12c. ....	62
Figure 3.17 (a) Side view with water molecules included (b) hydrogen bonding interactions in the crystal structure of 12d, (water molecules have been omitted). ..	63
Figure 3.18 Trimer in the crystal structure of 12e. ....	64
Figure 3.19 Hydrogen- and halogen-bonding in the crystal structure of 12f. ....	64
Figure 3.20 Dimer in the crystal structure of 12g. ....	65
Figure 3.21 Trimer in the crystal structure of 13a. ....	65
Figure 3.22 Trimer in the crystal structure of 14a. ....	66
Figure 3.23 Trimer in the crystal structure of 15a. ....	66
Figure 3.24 Electrostatic potential surfaces of heterocycles 11-18. ....	67
Figure 3.25 Classification of crystal structures obtained from supramolecular reactions between supramolecular reagents and a variety of acids and oximes. The numbers obtained in each case are portrayed in brackets. Im = imidazole, Py = pyridine. ....	69
Figure 3.26 MEPs and $\Delta$ MEPs of supramolecular reagents. All values are in $\text{kJ mol}^{-1}$ . ....	69
Figure 3.27 MEP surfaces of (a) 3-iodo and (b) 4-iodobenzoic acid. ....	72

Figure 3.28 MEP surfaces of (a) tetrafluoroiodobenzoic acid and (b) tetrafluoroiodo-aldoxime.....	73
Figure 3.29 Comparison of bond lengths in (a) 4,4'-bipyridine and 1,4-diiodobenzene <sup>4</sup> and 4,4'-bipyridine 1,4-diiodotetrafluorobenzene <sup>5</sup> .....	73
Figure 4.1 Examples of supramolecular synthons composed with carboxylic acids and N-heterocycles.....	76
Figure 4.2 Homomeric interactions between (a) carboxylic acid and (b) oxime functionalities. The lower energy of the oxime-oxime interaction indicates a weaker interaction.....	76
Figure 4.3 (a) Salt formed between 3,5-dinitrobenzoic acid and 1-[(pyrazol-1-yl)methyl], 3-[(benzimidazol-1-yl)methyl]benzene, resulting in a 1:1:1 complex incorporating a free 3,5-dinitrobenzoic acid and (b) salt formed as a result of proton transfer between pentamethylbenzoic acid and 3-(4-pyridyl)-pyrazole, also resulting in a 1:1:1 complex.....	77
Figure 4.4 Molecular electrostatic potential values (maxima and minima) of three types of oxime.....	78
Figure 4.5 Two different conformations of oximes: (a) dimer and (d) catemeric.....	79
Figure 4.6 General synthesis of cyanophenyloximes.....	80
Figure 4.7 Set up for the synthesis of cyanophenyloximes.....	81
Figure 4.8 The trimeric supermolecule in 21a.....	86
Figure 4.9 The trimeric supermolecule in 23e.....	86
Figure 4.10 Electrostatic potentials of three oximes (a) cyanophenyloxime, (b) acetyloxime and (c) aldoxime.....	87
Figure 4.11 Trimeric supermolecules in the crystal structures of (a) 1,4-di[(1-benzimidazolyl)methyl]benzene 4-bromophenylcyanoxime and (b) 1,4-di[(1-imidazolyl)methyl]benzene 3-chlorophenylcyanoxime.....	90
Figure 5.1 Discrete trimer in the co-crystal of terephthalic acid pyridine (1:2). <sup>1</sup> .....	96
Figure 5.2 Tetrameric supermolecule in the crystal structure of trimesic acid and pyridine (1:3). <sup>1</sup> .....	97
Figure 5.3 Extended one-dimensional, zig-zag chain in the co-crystal of 1,3-bis(4-pyridyl)propane and terephthalic acid. <sup>3</sup> .....	97

Figure 5.4 ‘Chicken-wire’ framework in the co-crystal of trimesic acid with 4,4’-bipyridine. <sup>4</sup> .....	98
Figure 5.5 Crystal structure of 4,4’-bipyridine and trimesic acid. ....	98
Figure 5.6 Homomeric interactions between (a) carboxylic acid (b) oxime.....	100
Figure 5.7 General synthesis of dicyanophenyloximes.....	101
Figure 5.8 Molecular electrostatic potentials of the di- and tricyanoximes studied here. ....	106
Figure 5.9 (a) single molecule of 1,4-dicyanophenyloxime and (b) extended network of 1,4-dicyanophenyloxime, displaying the $R_4^4(34)$ motif. ....	108
Figure 5.10 Zig-zag one-dimensional chain in the crystal structure of 26a. ....	109
Figure 5.11 One-dimensional chain in the crystal structure of 26b. ....	109
Figure 5.12 Asymmetric unit in the crystal structure of 26c.....	110
Figure 5.13 (a) Beginning of the helical formation in 26c (b) helix in 26c, shown looking down the axis.....	110
Figure 5.14 Adjacent chains in the crystal structure of 26d.....	111
Figure 5.15 One-dimensional chain in the crystal structure of 26e. ....	111
Figure 5.16 Discrete hexamer in the crystal structure of 29a.....	112
Figure 5.17 (a) hydrogen bonding of three bipyridyl molecules to the tricyanoxime (b) extended two-dimensional grid in the crystal structure of 29b. ....	112
Figure 5.18 Corresponding carboxylic acids A26, A27, and A29. ....	113
Figure 6.1 Ternary supermolecule constructed from two different carboxylic acids of different acidities. <sup>3</sup> .....	117
Figure 6.2 Protocol for deconstructing and reconstructing ternary co-crystals. $D_1$ and $D_2$ = hydrogen-bond donors, $A_1$ and $A_2$ = hydrogen-bond acceptors. ....	119
Figure 6.3 Asymmetric ditopic donors and acceptors employed in this study. ....	119
Figure 6.4 Reaction scheme for the synthesis of 4-carboxyphenylacetonitrile, 31 .....	120
Figure 6.5 Recognition events in the crystal structure of 12:32.....	124
Figure 6.6 Recognition events in the crystal structure of 14:4-OH BA.....	124
Figure 6.7 Recognition events in the crystal structure of 30:PMBA:25. ....	125

Figure 6.8 Supramolecular reagents and their calculated molecular electrostatic potentials, Table 6.2. ....	125
Figure 6.9 Representation of the two possible binding outcomes between a ditopic hydrogen-bond acceptor molecule, and a monotopic donor. The interaction with the highest negative value of $\Delta\Delta G$ would be the most favored. ....	127
Figure 6.10 Representation of the possible binding outcomes between two hydrogen bond donors of different hydrogen-bonding strength and a ditopic acceptor. ....	128
Figure 7.1 Metal coordination and supramolecular chemistry in the crystal structures of (a) (isonicotinamide)silver(I)trifluoromethanesulfonate dihydrate and (b) Diaqua-bis-(isonicotinamide-N)bis(2-fluorobenzoato)-O-copper(II). ....	132
Figure 7.2 (Benz-) and [(phenylimidazol-1-yl)methyl]benzamides vs isonicotinamide. ....	133
Figure 7.3 3-Pyridyl cyanoxime and [1-(pyridin-3-yl)-4-(cyanoxime)phenyl].....	134
Figure 7.4 (a) Metal coordination and supramolecular chemistry in the crystal structure of bis(3-aldoximepyridine)silver(I)hexafluorophosphate and (b) coordination modes in the crystal structure of catena-(( $\mu_2$ -1-(3-pyridylethanoneoxime-N,N')-( $\mu_2$ -iodo)-copper(II)). ....	134
Figure 7.5 Equatorial ‘blocked’ (a) <i>acac</i> complex and (b) “paddle-wheel” complex with axial sites (arrows) available for coordination. ....	136
Figure 7.6 Synthesis of pyridylcyanoximes. ....	137
Figure 7.7 Thermal ellipsoid plot (50% probability) and labeling scheme for 4b. ....	142
Figure 7.8 View of 4b showing $\pi$ - $\pi$ interactions between adjacent 1-D chains; tetrafluoroborate anions are disordered. ....	142
Figure 7.9 Thermal ellipsoid plot (50% probability) and labeling scheme for 4c. ....	143
Figure 7.10 Infinite 1-D cationic chain in 4b; [AsF <sub>6</sub> ] <sup>-</sup> anions have been removed for clarity. ....	143
Figure 7.11 One-dimensional chain in the crystal structure of 4d. ....	144
Figure 7.12 One-dimensional chain in the crystal structure of 8a. ....	145
Figure 7.13 1-D ‘wavy’ chain in the crystal structure of 10a. ....	145
Figure 7.14 One-dimensional chain in the crystal structure of 33a. ....	146
Figure 7.15 One dimensional chain in the crystal structure of 33b. ....	146

Figure 7.16 (a) Ligand coordination around the metal center in the crystal structure of 6a and (b) two Ni(II) centers with axial and equatorial coordination of [1-(pyridin-3-yl)-4-(cyanoxime)phenyl] ligands in the crystal structure of 35a.	
Dibenzoylmethanate ligands have been removed for clarity. ....	147
Figure 7.17 One-dimensional chain in the crystal structure of 35b. ....	148
Figure 7.18 Examples of where the supramolecular events are disrupted in the crystal structures of (a) bis[3-(2-methylbenzimidazol-1-yl)methylbenzamide]silver(I) hexafluoroarsenate methanol and (b) bis[3-(2-methylbenzimidazol-1-yl)methylbenzamide]silver(I) hexafluoroantimonate. ....	149
Figure 7.19 Cis and trans configurations around Ag(I) in the crystal structures of (a) bis[3-(2-methylbenzimidazol-1-yl)methylbenzamide]silver(I) hexafluoroantimonate and (b) bis[4-(5,6-dimethylbenzimidazol-1-yl)methylbenzamide]silver(I)hexafluoroarsenate ....	150
Figure 7.20 Interaction energies of (a) amide-amide dimer and (b) cyanoxime catemer. ....	151
Figure 7.21 Schematic representation of (a) two-point dimer interaction and (b) one-point catemeric interaction. ....	152
Figure A.1 <sup>1</sup> H NMR of 1 .....	157
Figure A.2 (a) <sup>1</sup> H and (b) <sup>13</sup> C NMR of 2.....	158
Figure A.3 <sup>1</sup> H NMR of 3.....	159
Figure A.4 (a) <sup>1</sup> H and (b) <sup>13</sup> C NMR of 4.....	160
Figure A.5 <sup>1</sup> H NMR of 5.....	161
Figure A.6 (a) <sup>1</sup> H and (b) <sup>13</sup> C NMR of 6.....	162
Figure A.7 <sup>1</sup> H NMR of 7.....	163
Figure A.8 (a) <sup>1</sup> H and (b) <sup>13</sup> C NMR of 8.....	164
Figure A.9 <sup>1</sup> H NMR of 9.....	165
Figure A.10 (a) <sup>1</sup> H and (b) <sup>13</sup> C NMR of 10.....	166
Figure A.11 (a) <sup>1</sup> H and (b) <sup>13</sup> C NMR of 11.....	167
Figure A.12 (a) <sup>1</sup> H and (b) <sup>13</sup> C NMR of 12.....	168
Figure A.13 (a) <sup>1</sup> H and (b) <sup>13</sup> C NMR of 13.....	169
Figure A.14 (a) <sup>1</sup> H and (b) <sup>13</sup> C NMR of 14.....	170



Figure A.15 $^1\text{H}$ NMR of 15.....	171
Figure A.16 $^1\text{H}$ NMR of 16.....	172
Figure A.17 (a) $^1\text{H}$ and (b) $^{13}\text{C}$ NMR of 17.....	173
Figure A.18 (a) $^1\text{H}$ and (b) $^{13}\text{C}$ NMR of 18.....	174
Figure A.19 $^1\text{H}$ NMR of 19.....	175
Figure A.20 $^1\text{H}$ NMR of 20.....	175
Figure A.21 $^1\text{H}$ NMR of 21.....	176
Figure A.22 $^1\text{H}$ NMR of 22.....	176
Figure A.23 $^1\text{H}$ NMR of 23.....	177
Figure A.24 $^1\text{H}$ NMR of 24.....	177
Figure A.25 $^1\text{H}$ NMR of 25.....	178
Figure A.26 (a) $^1\text{H}$ and (b) $^{13}\text{C}$ NMR of 26.....	179
Figure A.27 (a) $^1\text{H}$ and (b) $^{13}\text{C}$ NMR of 27.....	180
Figure A.28 $^1\text{H}$ NMR of 28.....	181
Figure A.29 (a) $^1\text{H}$ and (b) $^{13}\text{C}$ NMR of 29.....	182
Figure A.30 (a) $^1\text{H}$ and (b) $^{13}\text{C}$ NMR of 30.....	183
Figure A.31 $^1\text{H}$ NMR of 31.....	184
Figure A.32 (a) $^1\text{H}$ and (b) $^{13}\text{C}$ NMR of 32.....	185
Figure A.33 $^1\text{H}$ NMR of 33.....	186
Figure A.34 (a) $^1\text{H}$ NMR of 34.....	187
Figure A.35 (a) $^1\text{H}$ and (b) $^{13}\text{C}$ NMR of 35.....	188
Figure C.1 IR spectrum of 6.....	239
Figure C.2 IR spectrum of co-crystal of 6 and 3,5-dinitrobenzoic acid.....	239

## List of Tables

Table 2.1	pK <sub>a</sub> values of conjugate acids of the nitrogen-heterocycle amides (order most basic → least basic).....	20
Table 2.2	IR data (position of O-H···N stretches) from co-crystallization experiments ..	29
Table 2.3	Hydrogen-bond geometries for 2, 2a, and b, 4a and 6, 6a and b.....	30
Table 2.4	Molecular electrostatic potentials (MEPs).....	35
Table 2.5	pK <sub>a</sub> s of some carboxylic acids (least → most acidic).....	38
Table 2.6	ΔpK <sub>a</sub> values for the results here, complemented by some from the literature.	39
Table 2.7	Molecular electrostatic potential charges and their impact on proton transfer	40
Table 3.1	Crystal data for structures 11a-i, 12a-d, 13a, 14a, and 15a.....	53
Table 3.2	Results of co-crystallizations (from IR O-H···N bands) with supramolecular reagents 15, 16, 17 and 18.....	53
Table 3.3	Hydrogen bond geometries for 11a-i, 12a-g, 13a, 14a, and 15a .....	53
Table 3.4	Electrostatic potentials of heterocycles 11-18.....	67
Table 3.5	Hydrogen bond length comparisons for O-H···N interactions between the imidazole and pyridyl nitrogen atoms .....	71
Table 3.6	MEPs of iodobenzoic acids.....	72
Table 3.7	MEPs of tetrafluoroiodoaldoxime and benzoic acid.....	73
Table 4.1	Solubility data for trimesic, terephthalic, and isophthalic acid, respectively.....	78
Table 4.2	Cyanophenyloxime synthetic data .....	82
Table 4.3	Names of heterocyclic ligands and abbreviations, employed in this study.....	83
Table 4.4	IR data (position of O-H···N stretches) from co-crystallization experiments ..	85
Table 4.5	Hydrogen-bond geometries for 21a and 23e.....	85
Table 4.6	Electrostatic potentials of all the oximes studied here .....	87
Table 4.7	Supramolecular yield for each type of oxime. ....	88
Table 4.8	IR nitrile stretches of acetonitrile precursors vs cyanoxime products. ....	89

Table 4.9 Melting points of cyanoximes and corresponding carboxylic acids.....	89
Table 4.10 Percent occurrence of oxime configurations, based on results obtained from CSD search.....	91
Table 5.1 Solubility data of polycarboxylic acids.....	99
Table 5.2 Ligands employed in this study and their abbreviations.....	104
Table 5.3 Hydrogen bond geometries for 26, 26a-e, and 29a and b .	107
Table 5.4 IR stretches of co-crystals formed.....	113
Table 5.5 Melting point and solubilities of acids vs oximes.....	114
Table 6.1 Hydrogen-bond geometries for 12:32, 14:4-OH BA and 30:PMBA:25 .....	123
Table 6.2 Calculated molecular electrostatic potentials for molecules 30-33 and 35-39 .....	126
Table 6.3 Calculated interaction energies for co-crystals 12:32, 14:4-OH BA, 11i, 12f, 12g and 30:PMBA:25.....	128
Table 7.1 Selected bond distances and angles for 4b-d, 8a, 10a, 33a and 33b, 35a and 35b .....	141
Table 7.2 Hydrogen-bond geometries for 4b-d, 8a, 10a, 33a and 33b, 35a and 35b .....	141
Table B.1 Crystal data and structure refinement for 2 .....	189
Table B.2 Crystal data and structure refinement for 2a .....	190
Table B.3 Crystal data and structure refinement for 2b .....	191
Table B.4 Crystal data and structure refinement for 4a .....	192
Table B.5 Crystal data and structure refinement for 6 .....	193
Table B.6 Crystal data and structure refinement for 6a .....	194
Table B.7 Crystal data and structure refinement for 6b .....	195
Table B.8 Crystal data and structure refinement for 11 .....	196
Table B.9 Crystal data and structure refinement for 11a .....	197
Table B.10 Crystal data and structure refinement for 11b .....	198
Table B.11 Crystal data and structure refinement for 11c .....	199
Table B.12 Crystal data and structure refinement for 11d .....	200
Table B.13 Crystal data and structure refinement for 11e .....	201
Table B.14 Crystal data and structure refinement for 11f.....	202
Table B.15 Crystal data and structure refinement for 11g.....	203

Table B.16	Crystal data and structure refinement for 11h	204
Table B.17	Crystal data and structure refinement for 11i	205
Table B.18	Crystal data and structure refinement for 12a	206
Table B.19	Crystal data and structure refinement for 12b	207
Table B.20	Crystal data and structure refinement for 12c	208
Table B.21	Crystal data and structure refinement for 12d	209
Table B.22	Crystal data and structure refinement for 12e	210
Table B.23	Crystal data and structure refinement for 12f	211
Table B.24	Crystal data and structure refinement for 12g	212
Table B.25	Crystal data and structure refinement for 13	213
Table B.26	Crystal data and structure refinement for 13a	214
Table B.27	Crystal data and structure refinement for 14a	215
Table B.28	Crystal data and structure refinement for 15a	216
Table B.29	Crystal data and structure refinement for 21a	217
Table B.30	Crystal data and structure refinement for 23e	218
Table B.31	Crystal data and structure refinement for 26	219
Table B.32	Crystal data and structure refinement for 26a	220
Table B.33	Crystal data and structure refinement for 26b	221
Table B.34	Crystal data and structure refinement for 26c	222
Table B.35	Crystal data and structure refinement for 26d	223
Table B.36	Crystal data and structure refinement for 26e	224
Table B.37	Crystal data and structure refinement for 29a	225
Table B.38	Crystal data and structure refinement for 29b	226
Table B.39	Crystal data and structure refinement for 12:32	227
Table B.40	Crystal data and structure refinement for 14:4-OH BA	228
Table B.41	Crystal data and structure refinement for 30:PMBA:25	229
Table B.42	Crystal data and structure refinement for 4b	230
Table B.43	Crystal data and structure refinement for 4c	231
Table B.44	Crystal data and structure refinement for 4d	232
Table B.45	Crystal data and structure refinement for 8a	233
Table B.46	Crystal data and structure refinement for 10a	234

Table B.47	Crystal data and structure refinement for 33a .....	235
Table B.48	Crystal data and structure refinement for 33b .....	236
Table B.49	Crystal data and structure refinement for 35a .....	237
Table B.50	Crystal data and structure refinement for 35b .....	238

## **Acknowledgements**

First and foremost, I would like to thank my major professor, Dr Christer Aakeröy, whose door was always open and without his endless help and support, this thesis, and my research as a whole, would not have been possible. It is thanks to him that I developed my confidence and became a better scientist.

To members of the Aakeröy group, past and present, who I attend conferences with and had good times, both inside and outside of the lab. It was a joy to work with you all.

Thanks to all of my Ph.D committee members Dr Maatta, Dr Klabunde, Dr Kanost and Dr Fan for their valuable time and input.

Thanks to Dr John Desper, who is responsible for collecting data sets and solving all of the crystal structures herein.

Thanks to Connie Cusimano, Kim Ross, Jim Hodgson, Richard Bachamp, Tobe Eggers, Arlon Meek, Earline Dikeman and Mary Dooley, for their various inputs behind the scenes. Thanks also to Martin Courtois for his invaluable help with the dissertation template!

Finally, I would like to thank everyone who has made a contribution to my life here at K-state to make the transition here go as smoothly as possible. This includes friends Ben, Jamie, Kris, Helene and Pernilla. As well as to my family for all their love, support and guidance not just over the past five years but throughout my life.

## **Dedication**

I dedicate this dissertation to my family: mom, dad, Mark and Neil, to my nan, Anne, and my boyfriend, Sam.

Mom and dad – Thank you both so much for your endless love and support. You both know that it has not been easy at times, but without you both I would not have got through. I will never be able to pay you back for everything you have done, but hopefully I have made you both proud.

Mark and Neil – the best brothers anyone could ever have. Thank you for supporting me (financially!!) every time I come home. Without you I definitely wouldn't have made it home as often.

Nan – thank you also for helping to get me through this time and also for your love and financial support. It won't be forgotten.

Sam – Thanks for the support you have shown me over the past year or so. I know it hasn't been easy for you either, but we got through.

Finally, this is for Grandad Ken and Uncle Andrew. Gone, but not forgotten.

## Preface

Research carried out at Kansas State University for this dissertation led to the following publications in scientific journals:

- 1) C. B. Aakeröy, J. Desper, M. M. Smith and J. F. Urbina, “[Benzimidazol-1-yl)methyl]benzamides as bifunctional reagents for reliable inorganic-organic supramolecular synthesis”, *Dalton Trans.*, **2005**, 14, 2462-2470.
- 2) C. B. Aakeröy, D. J. Salmon, M. M. Smith, and J. Desper, “Cyanophenyloximes: Reliable and Versatile Tools for Hydrogen-Bond Directed Supramolecular Synthesis of Cocrystals”, *Cryst. Growth & Design*, **2006**, 6, 1033-1042.
- 3) C. B. Aakeröy, M. M. Smith and J. Desper, “Constructing, deconstructing, and reconstructing ternary supermolecules”. *Chem. Commun.*, **2007**, 38, 3936-3938.
- 4) C. B. Aakeröy, B. M. T. Scott, M. M. Smith, J. F. Urbina and J. Desper, “Establishing amide...amide reliability and transferability in the supramolecular assembly of metal-containing 1-D architectures”, submitted to Dalton Transactions.



# CHAPTER 1 - Introduction

## 1.1 What is supramolecular chemistry?

The most impressive buildings in the world would not be what they are without the building blocks and glue that hold them together, that is the materials they are made from and the glue being the mortar. The same can be said for supermolecules, which would not be the entities that they are without the specific molecules that combine to make them, and the “glue” – the intermolecular interactions – that hold them together, Figure 1.1.

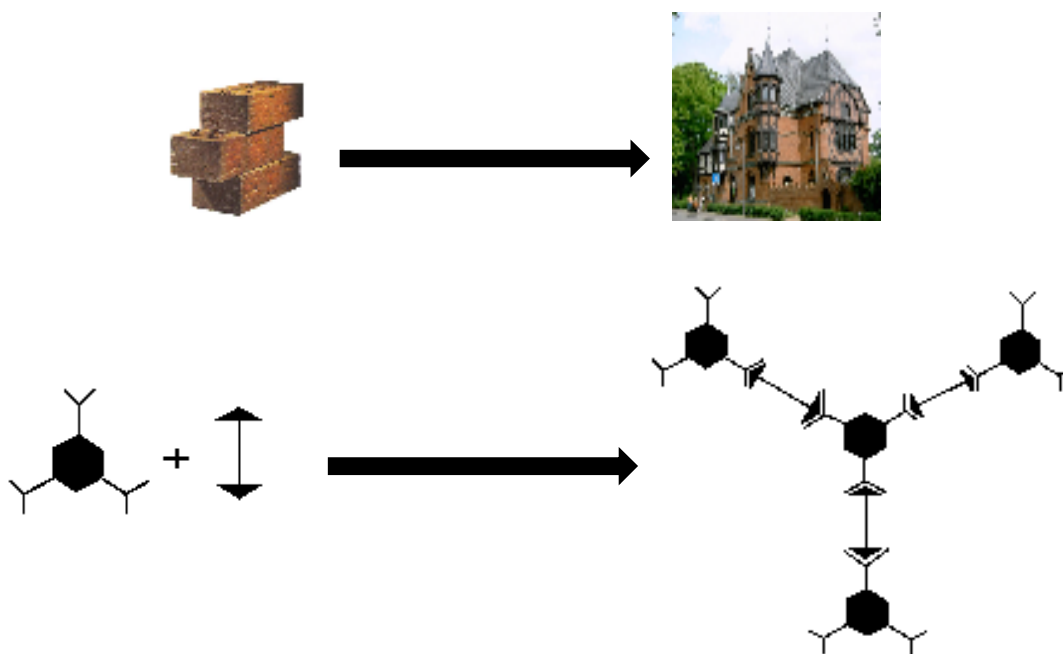


**Figure 1.1** Representation of the construction of a building from smaller building blocks, bricks, and the construction of supermolecules from smaller building blocks, molecules.

Supramolecular chemistry has been described as “chemistry beyond the molecule”.<sup>1</sup> Just as atoms combine into organic molecules through covalent bonds,

molecules make up supermolecules through non-covalent bonds, *intermolecular interactions*. For this reason, non-covalent synthesis has been described as “the supramolecular equivalent of organic synthesis”.<sup>2</sup> The result is an assembly of molecules whose structure and properties differ from those of the individual molecules themselves. “Just as there is a field of *molecular chemistry* based on the covalent bond, there is a field of *supramolecular chemistry*, the chemistry of molecular assemblies and of the intermolecular bond.”<sup>1</sup> The field of supramolecular chemistry, although still relatively new and rapidly developing, has concepts and principles that have manifested themselves in systems that form the basis of life. One such concept is molecular recognition.

### **1.1.1 Molecular recognition**

Molecular recognition refers to specific, selective connections between two or more molecules through non-covalent interactions, and plays an important part in biological systems. Examples include: enzyme-substrate recognition,<sup>3</sup> an antigen binding to its antibody,<sup>4</sup> the selective transport of molecules or ions into a cell,<sup>5</sup> and the intermolecular interactions in the base-pairs of DNA.<sup>6</sup> All these processes are highly sophisticated and require specific recognition events that are strong enough to be directional and selective, but are often required to be weak enough to be reversible. The concept of molecular recognition is both energetic and based upon a principle of *complementarity*. This means that it has to be energetically favourable, as well as involving molecules that are geometrically suited to each other (first illustrated by the steric fit “lock and key” concept of Emil Fischer.)<sup>7</sup> Jean-Marie Lehn described molecular recognition as “binding with a purpose”, since mere binding is not molecular recognition. The concept of molecular recognition is illustrated in Figure 1.2. The octagon would fit only one of the three hosts, due its specific shape and size, and molecules do the same thing by finding their match through size and geometry, a selective recognition and binding process.



**Figure 1.2** Illustration of the concept of molecular recognition.

A simple, real-life example of molecular recognition is the building block (a), containing a 1,3-connected phenyleneethynylene backbone, and a pair of 2-aminopyridine groups (Figure 1.3(a), providing excellent shape and complementarity to isophthalic acid, Figure 1.3(b).<sup>8</sup>

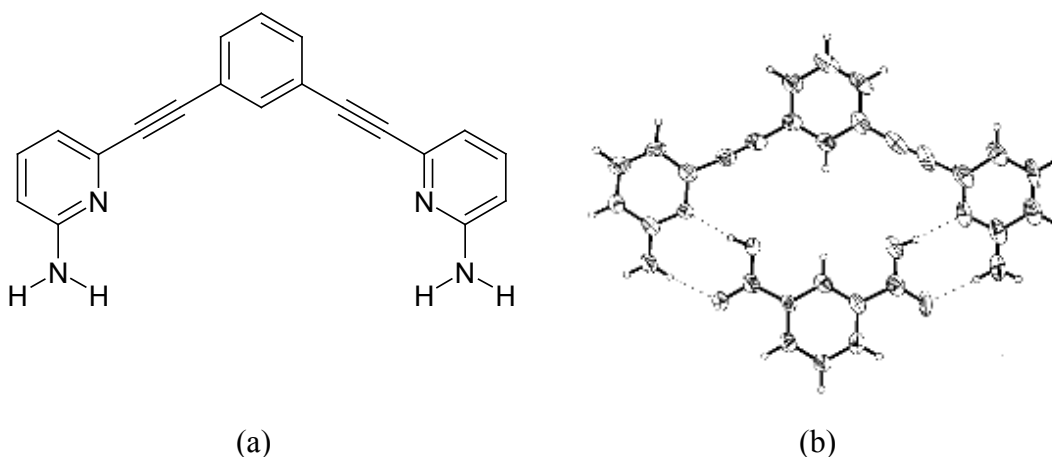


**Figure 1.3** (a) Host containing two 2-aminopyridine groups, creating a receptor for isophthalic acid, (b).<sup>8</sup>

### 1.1.2 Self-assembly – the production of a crystal

Large supermolecules are constructed through a process called *molecular self-assembly*, defined by Lehn as the ability of a system to spontaneously generate a “well-defined (functional) supramolecular architecture from its components under a given set of conditions”.<sup>1</sup> This refers to the construction of a supramolecular assembly through specific recognition events, leading to a supermolecule with well-defined shape and structure. The example in Figure 1.3 shows self-assembly as a result of molecules being

able to selectively recognize and bind to each other, forming a larger supermolecule. Macroscopic composition (supermolecules – such as a single crystal) and properties can hence be controlled by microscopic composition and arrangement in solids.

*“The crystal is, in a sense, the supramolecular par excellence – a lump of matter, of macroscopic dimensions, millions of molecules long, held together in a periodic arrangement by just the same kind of non-bonded interactions as those that are responsible for molecular recognition at all levels. Indeed, crystallization itself is an impressive display of supramolecular self-assembly, involving specific molecular recognition at an amazing level of precision” - Jack Dunitz.<sup>9</sup>*

Jean-Marie Lehn described supramolecular chemistry as “a sort of molecular sociology”.<sup>1</sup> The definition of sociology arising from the Latin for “companion” and the suffix –ology meaning “the study of”. One important goal of supramolecular chemistry is therefore, to investigate the social behavior of a molecule: what it likes and dislikes, its social interaction with other molecules – what it likes to do most and what it likes to do least, and the effect this has on the molecules surrounding it.

## **1.2 Intermolecular interactions and the important hydrogen bond**

In order to begin the process of deciphering what a molecule’s preferences are, we begin by probing the molecular interactions that it participates in. There are many kinds of intermolecular interactions utilized in supramolecular chemistry. This covers a wide range of attractive and repulsive forces, with ion-ion interactions,<sup>10</sup> dipole-dipole interactions,<sup>11</sup> ion-dipole interactions,<sup>12</sup> van der Waals forces,<sup>13</sup> and  $\pi$ - $\pi$  stacking,<sup>14</sup> being the most important. In the construction of supramolecular entities, hydrogen bonds have been extensively used since they are relatively strong and directional, which enables a degree of control during the self-assembly process. Hydrogen bonding has long demonstrated its importance in biological structures, in amino acids and peptides, and it is responsible for the shape of many proteins. It is of fundamental importance in the structure of water<sup>15,6</sup> without which many biological species would not exist, and is also present in the Watson-Crick hydrogen-bonded base pair,<sup>6</sup> Figure 1.4.

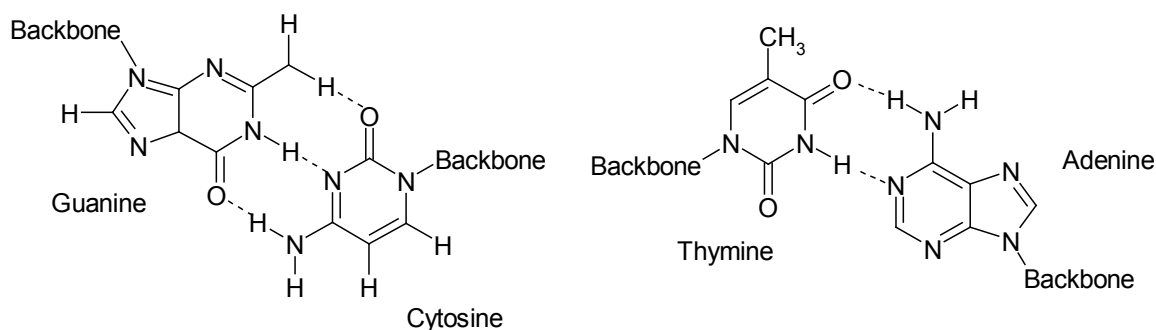


**Figure 1.4** Hydrogen bonding in the base pairs of DNA.

The bond lengths and energies of hydrogen bonds vary, since they depend greatly on their environment. The moderate-strength hydrogen bond has a bond energy ranging from 16-60 kJ mol<sup>-1</sup> and a bond length (donor-H...acceptor) of between 2.5 and 3.2 Å,<sup>16</sup> Margaret Etter first started examining hydrogen-bond patterns within organic compounds,<sup>17</sup> utilizing crystal engineering as a tool to study these interactions. Desiraju later labeled these patterns “*supramolecular synthons*”<sup>2</sup> which he defined as “structural units within molecules which can be formed and/or assembled by known or conceivable synthetic operations”. A few examples of supramolecular synthons are shown in Figure 1.5.

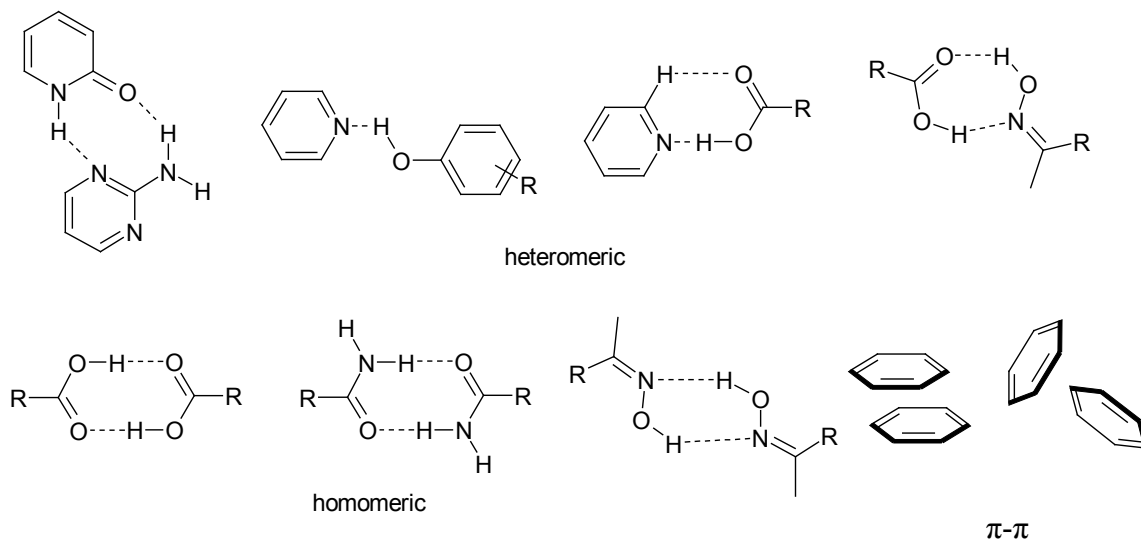


**Figure 1.5** Examples of supramolecular synthons involving strong hydrogen bonds.

### 1.2.1 Graph set notation

Hydrogen-bonded motifs can be described using a graph-set notation. Various groups contributed to this idea<sup>18</sup>, but the notation was refined by Etter et al,<sup>19</sup> who applied the concept to organic crystal structures, to differentiate between hydrogen-bond motifs, by the numbers of donors and acceptors present. General graph set notation is written as  $G_d^a(n)$ , where  $G$  denotes one of four possible patterns. Intramolecular hydrogen bonds are denoted by  $G=S$  (self), while intermolecular hydrogen bonds can be either: **C** (chain), **R** (ring), or **D** (discrete). The terms  $a$  and  $d$  refer to the number of acceptors ( $a$ ) and donors ( $d$ ) in the repeat motif, and are omitted when  $a=d=1$  (Figure 1.6(a)). Similarly,  $n$  is omitted in cases of **D** where there is only one hydrogen bond, Figure 1.6(b). Some examples of graph-set notations are given in Figure 1.6.

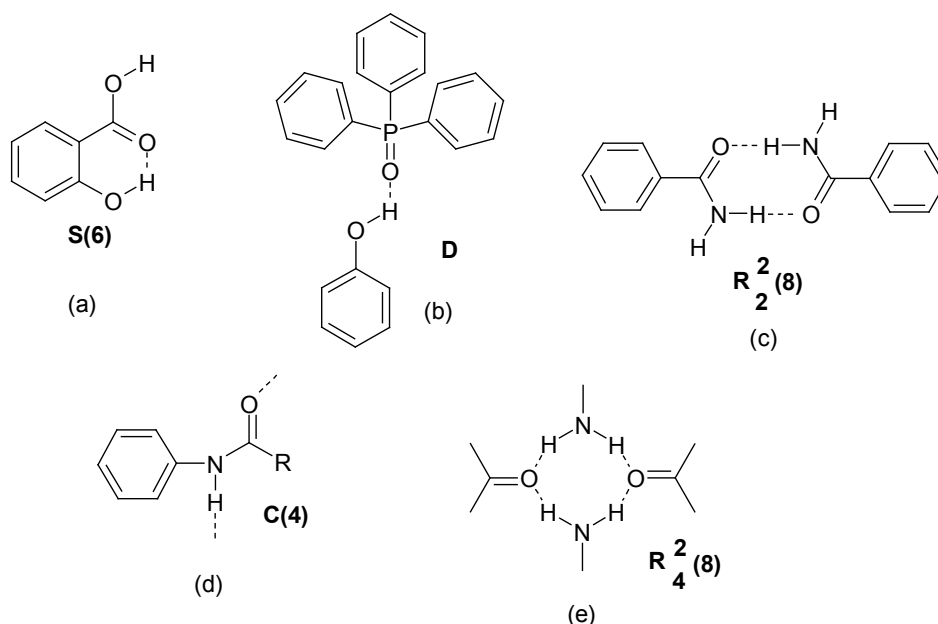


**Figure 1.6** Examples of graph-set notation.

### 1.2.2 Etter's hydrogen-bond rules

Based on systematic structural studies of crystal structures of organic compounds, Etter et al<sup>20,21</sup> established three guidelines applying to organic hydrogen-bonded structures:

- 1) all good proton donors and acceptors will be utilized in hydrogen bonding in the crystal structure of the compound<sup>22</sup>
- 2) if intramolecular hydrogen bonding can occur in the form of a six-membered ring, this will usually take place in preference to the formation of intermolecular hydrogen bonds
- 3) the best hydrogen bond donor and the best hydrogen bond acceptor remaining after intramolecular hydrogen bond formation will form hydrogen bonds to each other.

Some examples where the above rules are satisfied are shown in Figure 1.7.

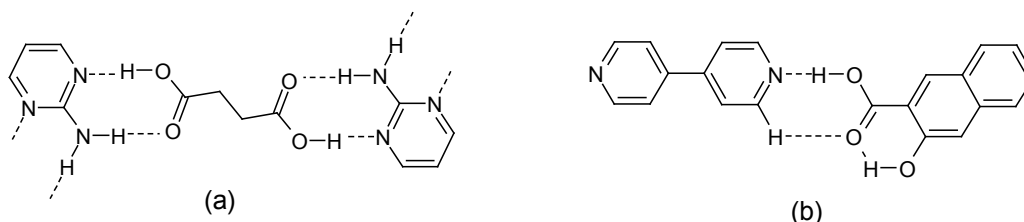


**Figure 1.7** Examples of structures in which the Etter rules are obeyed (a) co-crystal of succinic acid 2-aminopyrimidine,<sup>23</sup> (b) co-crystal of 3-hydroxy-2-naphthoic acid 4,4'-bipyridine.<sup>24</sup>

In (a) the best proton donor (the carboxylic acid) binds to the best hydrogen-bond acceptor (2-aminopyrimidine ring nitrogen atom), resulting in an  $R_2^2(8)$  motif, and (b) is an example of preferential formation of a six-membered intramolecular hydrogen bond.

### 1.3 Co-crystallization as a tool for examining the balance between intermolecular interactions

Co-crystallization is a tool by which we can probe the structural preferences and balances of, and between, molecules, and impart new properties not present in a “pure” (one-component material). This is the *deliberate* bringing together of two or more molecules (*binary*, *ternary* etc) into the same crystalline lattice without the making or breaking of covalent bonds.<sup>25</sup> The desired outcome is a heteromeric species, rather than homomeric, i.e two different components present instead of one component by itself.

The latter scenario has been relied upon as a means of purification for centuries, *recrystallization*, and occurs due to the inherent “selfishness” of molecules. Of all the publications detailing these procedures, just 2% of them describe co-crystallization, while 98% involve recrystallization, Figure 1.8.

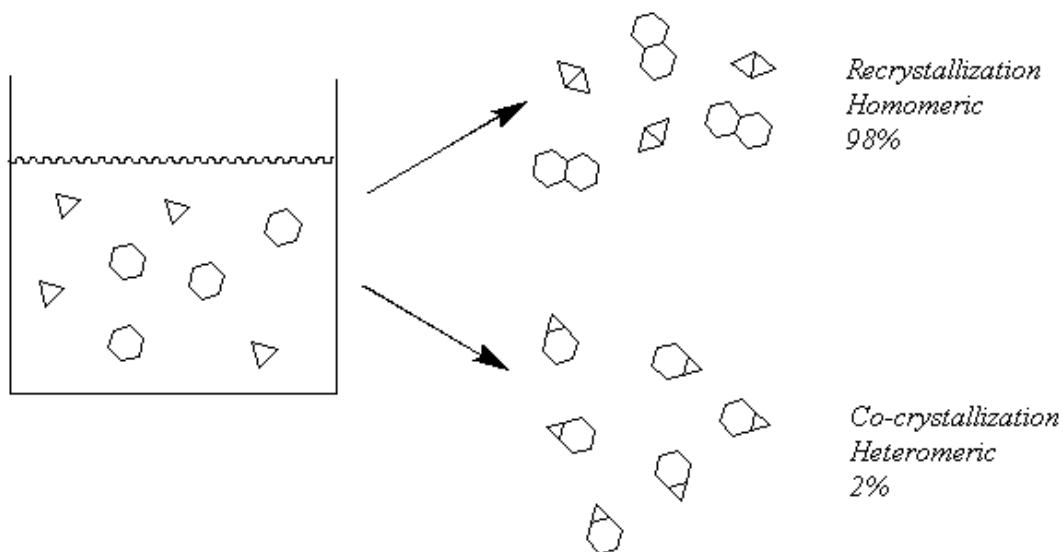


**Figure 1.8** Schematic representation of recrystallization vs co-crystallization.

Since the odds are clearly stacked against co-crystallization, new systematic strategies need to be developed in order to increase the chances of obtaining a heteromeric product. An important goal of this thesis is to create a library of synthons that can be relied upon in non-covalent synthesis.

### 1.3.1 Definition of “co-crystal”

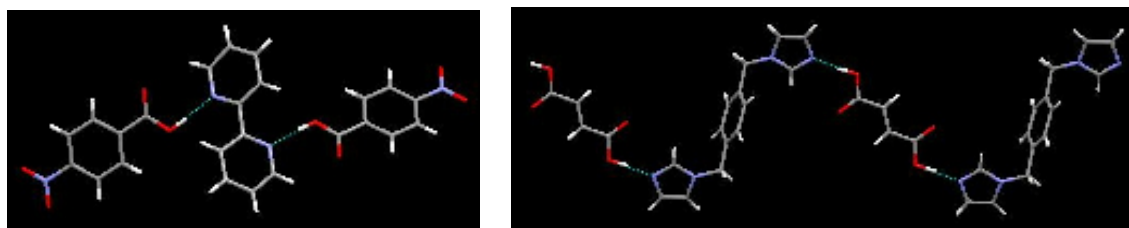
The definition of the term “co-crystal” has generated some controversy in recent years,<sup>26</sup> but such debates are to be expected within a relatively young and highly interdisciplinary field. Three main points will be followed in this thesis, however:

- 1) a “co-crystal” is a structurally homogeneous crystalline material<sup>25</sup> and is composed of two or more *neutral* species. The idea being that anything that is not neutral is considered a salt not a co-crystal.



- 2) The term co-crystal excludes solvates, hydrates, otherwise termed “clathrates”, where a molecule of solvent or other molecule becomes “accidentally” involved in the recognition process and was not the initial intent.
- 3) The “intent” must be clearly defined and the stoichiometric amounts should be specific.

Two examples of co-crystals are shown in Figure 1.9.



(a)

(b)

**Figure 1.9** Two examples of molecular co-crystals: (a) 4-nitrobenzoic acid hemikis-2,2'-bipyridine<sup>27</sup> (2:1) and (b) 1,4-*bis*-[(imidazol-1-yl)methyl]benzene fumaric acid (1:1).<sup>28</sup>

### 1.3.2 Higher-order molecular co-crystals

The molecular building blocks – *supramolecular reagents* - to be utilized for the understanding and controlling solid-state recognition events, can be selectively tuned as a means of controlling the hydrogen-bond interactions between them. Supramolecular reagents need to provide reliability, selectivity, and directionality. In the synthesis of a ternary supermolecule, the central supramolecular reagent needs to be equipped with two different binding sites so that molecules can selectively bind to them. In relation to the molecular recognition term earlier defined, this selectivity should also be matched geometrically. This concept is illustrated in Figure 1.10.



**Figure 1.10** Illustration of a ternary co-crystal. The central molecule must be equipped with two different binding sites so that the incoming molecules can selectively recognize and bind to a specific site.

Etter's rules stated that the best donor will form a hydrogen bond to the best acceptor, the second-best donor will form a hydrogen bond to the second-best acceptor and so on, but just as she stated, "good proton donors and good proton acceptors have to be defined",<sup>17</sup> we need to do the same for good hydrogen bond donors and good hydrogen bond acceptors. How do we do this?

## 1.4 Molecular electrostatic potentials (MEPs) as a tool for ranking hydrogen bond donor and acceptor strength

Previously, hydrogen bond donor and acceptor strengths have been classified in terms of  $pK_a$  values.<sup>20,29</sup> This has worked well within a family of compounds containing the same chemical functionalities<sup>30</sup> but, since they are a measure of proton transfer,  $pK_a$  values are not a direct measure of hydrogen-bond strength, and so are of less use when comparing and ranking hydrogen bond donor/acceptor strength of different functional groups.<sup>31</sup>

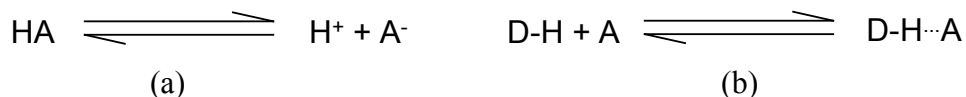


**Figure 1.11** (a) proton transfer (b) hydrogen bond.

Since hydrogen bonds are primarily electrostatic in nature, it makes sense to quantify them in terms of charge, Figure 1.12.

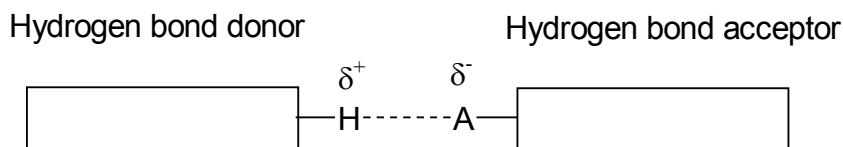


**Figure 1.12** Schematic representation of a hydrogen bond.

Hunter has shown in a recent publication<sup>32</sup> that it is possible to use calculated charges to quantify relative hydrogen-bond donor and acceptor strengths across a series of functionalities. These charges, molecular electrostatic potentials (MEPs) can be obtained at a relatively low level of theory (calculated at the AM1 level), making this a readily accessible tool. Hunter also showed that, despite the fact that a carboxylic acid is

more acidic than, say a phenol, the calculated MEPs suggest that phenols are better hydrogen-bond donors, Figure 1.13.

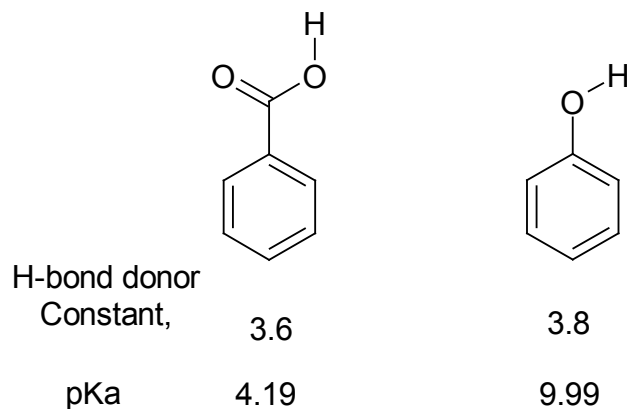


**Figure 1.13** pK<sub>a</sub> values of benzoic acid and phenol, compared to the calculated hydrogen bond donor constant values.

The values of  $\alpha$  and  $\beta$ , hydrogen bond donor and acceptor constants, respectively, are calculated from the MEP by dividing by a correction factor of 52 kJ mol<sup>-1</sup>, and have shown a good correlation with those values obtained from solution,  $\alpha_2$ , Figure 1.14

$$\alpha = E_{\max}/52 \text{ kJ mol}^{-1} = \text{hydrogen bond donor constant}$$

$$\beta = -E_{\min}/52 \text{ kJ mol}^{-1} = \text{hydrogen bond acceptor constant}$$

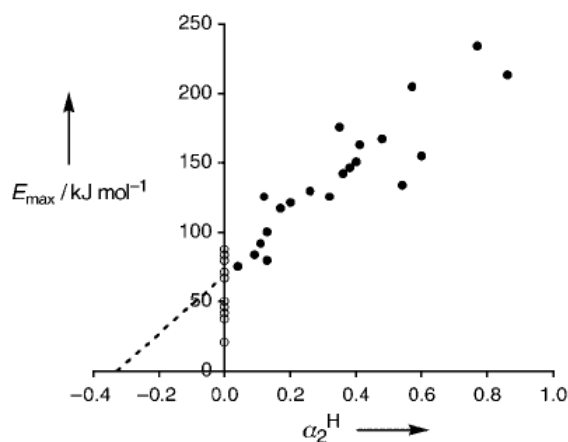


**Figure 1.14** Plot showing the correlation between the calculated charge of a hydrogen bond donor ( $E_{\max}$ ) and those values obtained from solution,  $\alpha_2$ .<sup>32</sup>

Molecular structures are constructed using Spartan '04 (Wavefunction, Inc. Irvine, CA). All molecules are optimized using AM1, with the maxima and minima in the electrostatic potential surface ( $0.002 \text{ e au}^{-1}$  isosurface) determined using a positive point charge in the vacuum as a probe.

MEPs can enable us to identify and rank hydrogen-bond donor and acceptor strengths of a variety of hydrogen bond donor and acceptor functionalities, and hence to probe the best-donor/best-acceptor hypothesis. Since a hydrogen bond is an attraction of two opposite charges, it would make sense that, the best hydrogen-bond donor would be the atom with the highest positive charge, and the best acceptor would be that with the highest negative charge, Figure 1.15.

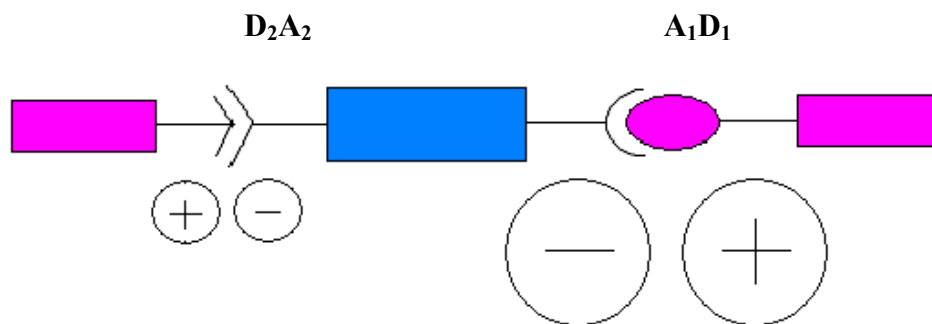


**Figure 1.15** Schematic of a ternary system showing the best donor (highest positive charge) interacting with the best acceptor (highest negative charge).

This approach hence enables a hierarchy of hydrogen bonding interactions to be developed, and could lead to the development of more complex supramolecular architectures.

## 1.5 Goals

The supramolecular library of available hydrogen bond donor and acceptor molecules needs to be expanded in order to increase our knowledge of their “molecular sociology”. There are currently only a handful of examples of ternary co-crystals in the literature,<sup>33</sup> all of which are composed of carboxylic acids. There is currently not an abundance of hydrogen-bond donors so there is a need to create new ones to expand our

knowledge into the behavior of different chemical functionalities, and then we can begin to think about employing different types of hydrogen bond donors in the synthesis of ternary co-crystals. Since  $pK_a$  values have been shown to be of little use across different chemical functionalities, we need to establish if it is possible to simplify the classification of hydrogen bond donors and acceptors in terms of charges, and use them to rank them in a hierarchical manner (best donor/best acceptor, second best donor/second best acceptor) etc). If we can do this, then it may be possible to develop a strategy for the synthesis of ternary supermolecules.

In summary, the goals of this thesis are to:

- 1) Synthesise several multifunctional supramolecular reagents.
- 2) Use these reagents to investigate a series of intermolecular interactions through co-crystallization experiments.
- 3) Determine the scope and limitations of using calculated MEPs to rationalize the binding preferences of the supramolecular reagents, by applying them to a range of chemical functionalities.
- 4) Synthesise a new family of hydrogen bond donors and determine their effectiveness in co-crystal synthons.
- 5) Determine to what extent simple covalent modifications can change the hydrogen bond donating or accepting ability of a supramolecular reagent.
- 6) Utilize intermolecular interactions in the construction of metal-organic networks of specific dimensionalities.

Gaining control of intermolecular interactions will provide opportunities to fine-tune specific properties, (electronic, optical, mechanical etc). If we can introduce long-range order of two different entities, Figure 1.16, this can lead to properties not exhibited by the individual molecules themselves. Lehn showed this was possible in the synthesis of a 3-D network that introduced polarity in the crystal structure of derivatives of barbituric acid and 2,4,6-triaminopyrimidine.<sup>34</sup> Such properties could find use in non-linear optical materials.<sup>35</sup>

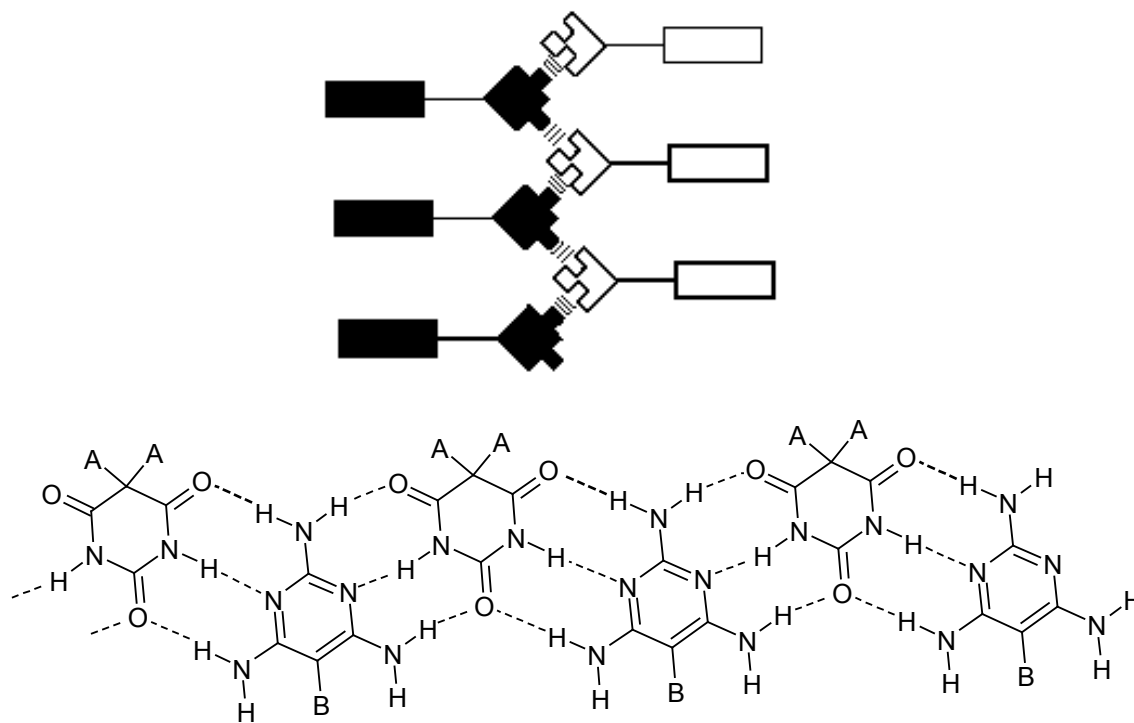


**Figure 1.16** (a) Schematic representation of a linearly-ordered supermolecule. Each group contains complementary binding sites to a neighbouring molecule, enabling a highly ordered supermolecule (b) alignment of molecules in the crystal structure of barbituric acid and 2,4,6-triaminopyrimidine.<sup>34</sup>

The orientation of groups along a strand is an illustration of changes being introduced at the microscopic level having an effect upon the properties at the macroscopic level. The patterns produced can vary depending on the individual molecules themselves, leading to the possibility of many types of properties. Such processes have a potential in the development of materials with electron transfer, energy transfer, or optical properties.

Furthermore, co-crystallization is currently being employed as a means of controlling the properties of active pharmaceutical ingredients.<sup>36</sup> Co-crystallization offers a way of controlling solubility, hygroscopicity, thermal stability etc through non-covalent reactions without *chemically* modifying the pharmaceutical compound itself.

---

## References

- <sup>1</sup> J-M. Lehn, *Supramolecular Chemistry*, vch publication, 1995.
- <sup>2</sup> G. R. Desiraju, *Angew. Chem. Int. Ed.*, 1995, **34**, 2311.
- <sup>3</sup> (a) H. Ura, K. Harata, I. Matsui, S. Kuramitsu, *J. Biochem.*, 2001, **129**, 173; (b) M. Mascal, P. S. Fallon, A. S. Batsanov, B. R. Heywood, S. Champ, M. Colclough, *J. Chem. Soc., Chem. Commun.*, 1995, 805.
- <sup>4</sup> J. van den Elsen, L. Vandeputte-Rutten, J. Kroon, P. Gros, *J. Biol. Chem.*, 1999, **274**, 1495.
- <sup>5</sup> (a) Y. Jiang, A. Lee, J. Chen, V. Ruta, M. Cadene, B. T. Chait, R. MacKinnon, *Nature*, 2003, **423**, 33; (b) [http://nobelprize.org/nobel\\_prizes/chemistry/laureates/2003/public.html](http://nobelprize.org/nobel_prizes/chemistry/laureates/2003/public.html)
- <sup>6</sup> G. A. Jeffrey, W. Saenger, *Hydrogen Bonding in Biological Structures*, Springer-Verlag, 1991.
- <sup>7</sup> E. Fischer, *Ber. Deutsch. Chem. Ges.*, 1894, **27**, 2985.
- <sup>8</sup> C. Bielawski, Y.-S. Chen, P. Zhang, P.-J. Prest, J. S. Moore, *Chem. Commun.*, 1998, 1313.
- <sup>9</sup> J. D. Dunitz, *Pure Appl. Chem.*, 1991, **63**, 177.
- <sup>10</sup> (a) D. J. Hoffart, J. Tiburcio, A. de la Torre, L. K. Knight, S. J. Loeb, *Angew. Chem. Int. Ed.*, 2008, **47**, 97; (b) D. Immke, S. J. Korn, *J. Gen. Physiol.*, 2000, **115**, 509.
- <sup>11</sup> S. Adhikari, A. Ueren, R. Roy, *J. Biol. Chem.*, 2008, **283**, 1334; (b) Y. Mu, Y. Q. Gao, *J. Chem. Phys.*, 2007, **127**, 105102; (c) B. N. J. Persson, R. Ryberg, *Phys. Rev. B*, 1981, **24**, 6954.
- <sup>12</sup> (a) C. Dosi, E. Giglio, V. Pavel, C. Ouagliata, *Acta Cryst.*, 1973, **A29**, 644; (b) J. O'M. Bockris, K. N. Reddy, M. Gamboa-Aldeco, *Modern Electrochemistry I*, Springer, 2000.
- <sup>13</sup> A I. Kitaigorodski, *Molecular Crystals and Molecules*, Academic press, New York, 1973.

- 
- <sup>14</sup> (a) A. Petitjean, R. G. Khoury, N. Kyritsakas, J. -M. Lehn, *J. Am. Chem. Soc.*, 2004, **126**, 6637; (b) A. Sygula, F. R. Fronczek, R. Sygula, P. W. Rabideau, M. M. Olmstead, *J. Am. Chem. Soc.*, 2007, **129**, 3842.
- <sup>15</sup> M. L. Huggins, *J. Phys. Chem.*, 1936, **40**, 723-731.
- <sup>16</sup> J. W. Steed, J. L. Atwood, *Supramolecular Chemistry*, Wiley publication, 2000.
- <sup>17</sup> M. C. Etter, *Acc. Chem. Res.*, 1990, **23**, 120.
- <sup>18</sup> (a) J. Donahue, *J. Phys. Chem.*, 1952, **56**, 502; (b) L. N. Kuleshova, P. M. Zorky, *Acta Cryst.*, 1980, **B36**, 2113; (c) P. M. Zorky, L. N. Kuleshova, *Zh. Strukt. Khim.*, 1980, **22**, 153; (d) F. Harary, *Graph Theory and Theoretical Physics*, Academic Press, New York, 1967; (e) R. E. Merrifield, H. E. Simmons, *Topological Methods in Chemistry*, Wiley and Sons, Inc, New York, 1989; (f) A. F. Wells, *Structural Inorganic Chemistry*, Clarendon Press, Oxford, 1962, 294; (g) W. C Hamilton, J. A. Ibers, *Hydrogen bonding in Solids*, W. A. Benjamin, Inc., New York, 1968, 19.
- <sup>19</sup> M. C. Etter, J. C. MacDonald, J. Bernstein, *Acta Cryst.*, 1990, **B46**, 256.
- <sup>20</sup> M. C. Etter, *J. Phys. Chem.*, 1991, **95**, 4601.
- <sup>21</sup> M. C. Etter, *Acc. Chem. Res.*, 1990, **23**, 120.
- <sup>22</sup> J. Donahue, *J. Phys. Chem.*, 1952, **56**, 502.
- <sup>23</sup> M. C. Etter, D. A. Adsmond, *J. Chem. Soc., Chem Commun.*, 1990, **8**, 589.
- <sup>24</sup> B.-Y. Lou, X.-D. Huang, X.-C. Lin, *Acta Cryst., Sect. C, Cryst. Struct. Commun.*, 2006, **62**, o310.
- <sup>25</sup> C. B. Aakeröy, D. J. Salmon, *CrystEngComm*, 2005, **7**, 439.
- <sup>26</sup> (a) G. R. Desiraju, *CrystEngComm*, 2003, **5**, 466; (b) J. D. Dunitz, *CrystEngComm*, 2003, **5**, 506.
- <sup>27</sup> CSD code: DAQZEB: J. R. Bowers, G. W. Hopkins, G. P. A. Yap, K. A. Wheeler, *Cryst. Growth Des.*, 2005, **5**, 727.
- <sup>28</sup> CSD code LATLAU: C. B. Aakeröy, J. Desper, B. Leonard, J. F. Urbina, *Cryst. Growth Des.*, 2005, **5**, 865.
- <sup>29</sup> C. B. Aakeröy, J. Desper, J. F. Urbina, *Chem. Commun.*, 2005, 2820.
- <sup>30</sup> B. G. Tehan, E. J. Lloyd, M. G. Wong, W. R. Pitt, J. G. Montana, D. T. Manallack, E. Gancia, *Quant. Struct. Act. Relat.*, 2002, **21**, 457.



- 
- <sup>31</sup> C. Laurence, H. Berthelot, *Perspect. Drug Discovery Des.*, 2000, **18**, 39.
- <sup>32</sup> C. A. Hunter, *Angew. Chem. Int. Ed.*, 2004, **43**, 5310.
- <sup>33</sup> (a) C. B. Aakeröy, J. Desper, J. F. Urbina, *Chem. Commun.*, 2005, 2820; (b) C. B. Aakeröy, A. M. Beatty, B. A. Helfrich, *Angew. Chem., Int. Ed.*, 2001, **40**, 3240.
- <sup>34</sup> J.-M. Lehn, M. Mascal, A. DeCian, J. Fischer, *J. Chem. Soc., Chem. Commun.*, 1990, 479.
- <sup>35</sup> (a) M. C. Etter, G. M. Frankenbach, *Chem. Mater.*, 1989, **1**, 10; (b) S. R. Marder, J. W. Perry, W. P. Schaefer, *Science*, 1989, **245**, 626; (c) R. E. Vizhi, S. Kalainathan, *Mat. Lett.* 2008, **62**, 791; (d) M. Moreno Oliva, J. Casado, J. T. Lopez Navarrete, G. Hennrich, M. C. Ruiz Delgado, J. Orduna, Jesus, *J. Phys. Chem. C*, 2007, **111**, 18778; (e) K. Jagannathan, S. Kalainathan, T. Gnanasekaran, N. Vijayan, G. Bhagavannarayana, *Cryst. Growth Des.*, 2007, **7**, 859; (f) V. V. Nesterov, M. Y Antipin, V. N. Nesterov, B. G. Penn, D. O. Frazier, T. V. Timofeeva, *Cryst. Growth Des.*, 2004, **4**, 521; (g) R. N. Rai, C. W. Lan, *J. Mat. Res.*, 2002, **17**, 1587.
- <sup>36</sup> (a) A. Jayasankar, D. J. Good, N. Rodriguez-Hornedo, *Molecular Pharmaceutics*, 2007, **4**, 360; (b) A. M. Chen, M. E. Ellison, A. Peresykin, R. M. Wenslow, N. Variankaval, C. G. Savarin, T. K. Natishan, D. J. Mathre, P. G. Dormer, D. H. Euler, R. G. Ball, Z. Ye, Y. Wang, I. Santos, *Chem. Commun.*, 2007, **4**, 419; (c) P. Vishweshwar, J. A. McMahon, M. L. Peterson, M. B. Hickey, T. R. Shattock, M. J. Zaworotko, *Chem. Commun.*, 2005, **36**, 4601; (d) N. Rodriguez-Hornedo, *Molecular Pharmaceutics*, 2007, **4**, 299; (e) P. M. Bhatt, N. V. Ravindra, R. Banerjee, G. R. Desiraju, *Chem. Commun.*, 2005, **8**, 1073; (f) P. Vishweshwar J. A. McMahon, J. A. Bis, M. J. Zaworotko, *J. Pharm.*, 2006, **95**, 499; (g) N. Blagden, M. Matas, P. T. Gavan, P. York, *Adv. Drug Deliv. Rev.* 2007, **59**, 617; (h) W. Jones, W. D. S. Motherwell, W. D. Samuel, A. V. Trask, *MRS Bull.*, 2006, **31**, 875; (i) N. J. Babu, L. S. Reddy, A. Nangia, *Molecular Pharmaceutics*, 2007, **4**, 417.

# CHAPTER 2 - Bifunctional amides – Synthesis of Molecular Co-crystals

## 2.1 Introduction

In the quest for supramolecular reagents capable of establishing intermolecular binding preferences, this study continues on the success that has been achieved with isonicotinamide.<sup>1</sup> Isonicotinamide has been used in the assembly of binary<sup>2</sup> and ternary<sup>3</sup> co-crystals, via two different binding sites, Figure 2.1.

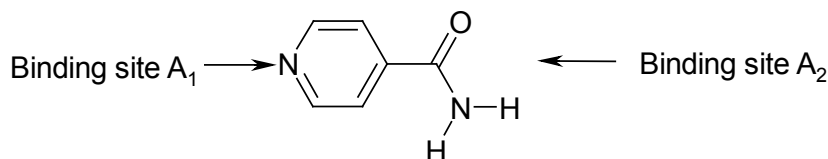


**Figure 2.1** Schematic of isonicotinamide, outlining the two possible binding sites.

Twenty-eight of the twenty-nine co-crystals consisting of isonicotinamide and a monocarboxylic acid (1:1 stoichiometry) in the Cambridge Structural Database, (97%) are connected through an O-H $\cdots$ N hydrogen-bond to the pyridyl nitrogen atom, leaving the amide to form a dimer with itself, Figure 2.2. These results represent a high *supramolecular yield*, i.e. a high frequency of occurrence of a given motif. They can be explained in terms of electrostatics: the best donor finds the best acceptor<sup>4</sup> when a carboxylic acid is introduced, i.e., the donor with the highest positive charge preferentially forms a hydrogen-bond with the acceptor with the highest negative charge.

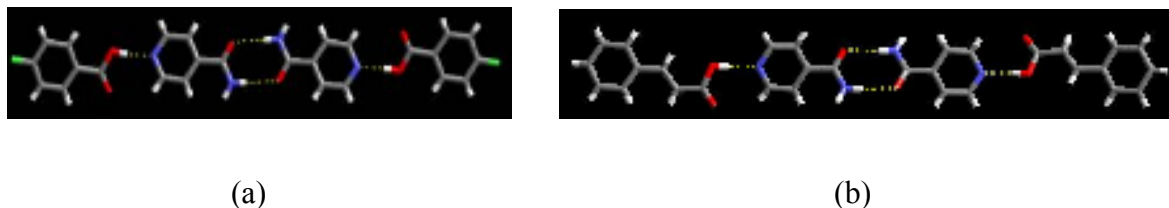


**Figure 2.2** Hydrogen bonding between isonicotinamide and (a) 4-fluorobenzoic acid and (b) *trans*-cinnamic acid.

In the continuation of this study, other N-heterocyclic amides, based on benzimidazole, were synthesized and their binding preferences were established, Figure 2.3.

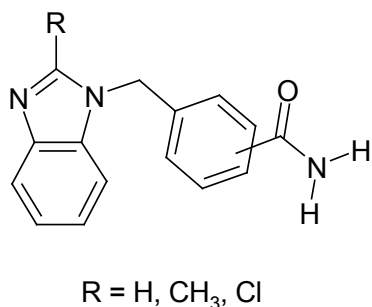


**Figure 2.3** Previously synthesized (benzimidazol-1-yl)methyl benzamides.<sup>5</sup>

There are only two crystal structures of benzimidazole benzamide:carboxylic acids of 1:1 stoichiometry in the CSD<sup>6</sup> and in each case, the acid opts for the imidazole nitrogen atom, and leaves the amide to form a dimer with itself, Figure 2.4.

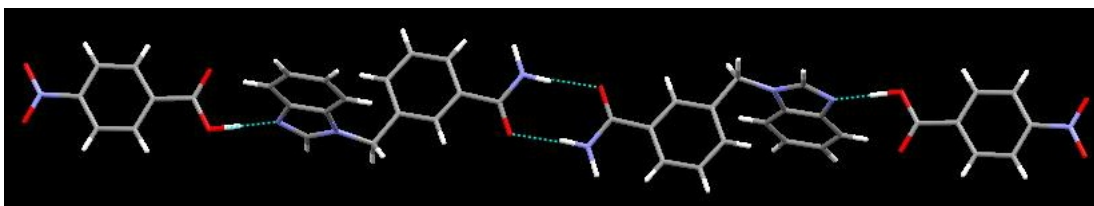


**Figure 2.4** 3-(Benzimidazol-1-yl)-benzamide 4-nitrobenzoic acid.<sup>5</sup>

## 2.2 How reliable are the new heterocyclic amides as supramolecular reagents?

### 2.2.1 Goals

In order to probe the validity of the best donor/best acceptor approach, five new N-heterocyclic amides of varying hydrogen-bond acceptor strength were synthesized, Figure 2.5

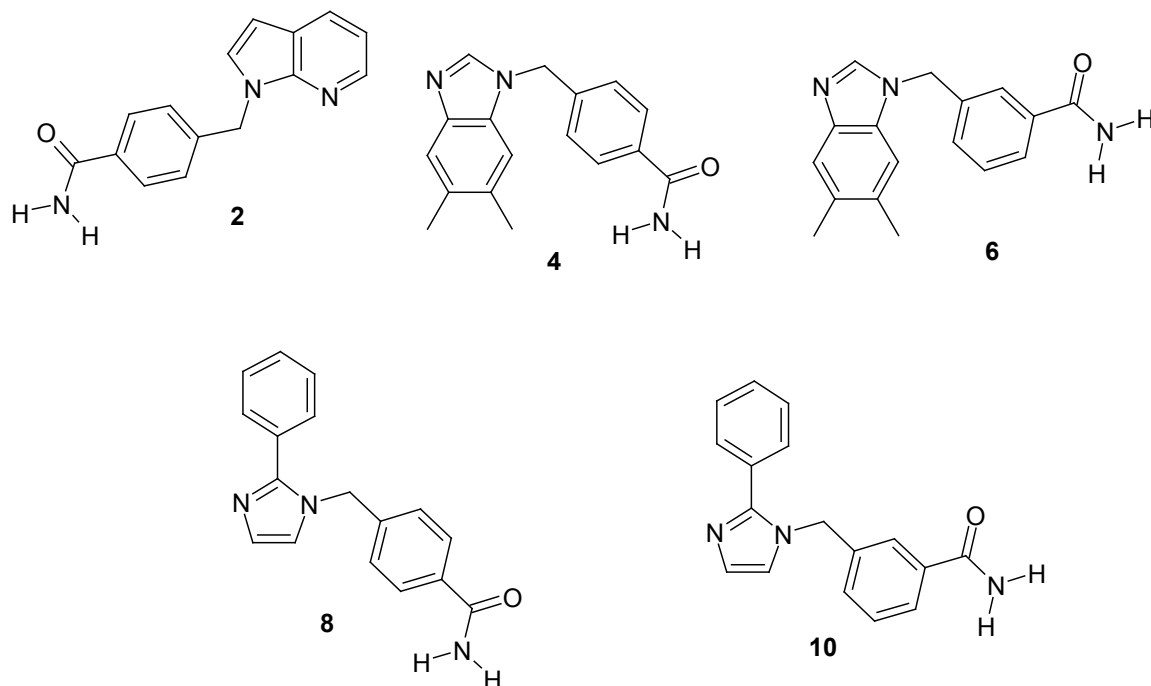


**Figure 2.5** N-heterocyclic amides synthesized and studied here.

The target molecules contain nitrogen atoms that cover a range of basicities, and include imidazole and pyridine-based fragments. The addition of methyl groups to the 5- and 6- positions on benzimidazole (amides **4** and **6**) increases the basicity of the nitrogen atom, Table 2.1. Incorporation of a phenyl group to the 2-position of imidazole (amides **8** and **10**) increases its basicity, making it more basic than 5,6-dimethylbenzimidazole, and the acceptor sites in **2** are less basic than **4**, **6**, **8** or **10**.

**Table 2.1**  $pK_a$  values of conjugate acids of the nitrogen-heterocycle amides<sup>7</sup> (order most basic  $\rightarrow$  least basic)

Molecule	$pK_a$
3-[(2-Phenylimidazol-1-yl)methyl]benzamide, <b>10</b>	6.37
4-[(2-Phenylimidazol-1-yl)methyl]benzamide, <b>8</b>	6.31
3-[(2-Methylbenzimidazol-1-yl)methyl]benzamide	5.93
4-[(5,6-Dimethylbenzimidazol-1-yl)methyl]benzamide, <b>4</b>	5.93
4-[(2-Methylbenzimidazol-1-yl)methyl]benzamide	5.92
3-[(5,6-Dimethylbenzimidazol-1-yl)methyl]benzamide, <b>6</b>	5.93
3-[Benzimidazol-1-yl)methyl]benzamide	5.46
4-[(7-Aza-indol-1-yl)methyl]benzamide, <b>2</b>	4.95
3-[(2-Chlorobenzimidazol-1-yl)methyl]benzamide	3.79
Isonicotinamide	3.39

Amides **4**, **6**, **8** and **10** all differ in basicity. The question is, do these differences correspond to differences in behavior in terms of binding preferences? There are no experimental  $pK_a$  values available for these molecules and so it would be beneficial if the calculated molecular electrostatic potentials could be relied upon as a means of predicting binding behavior. All of the N-heterocyclic amides should, in theory, behave as isonicotinamide, but do they? This study is conducted to achieve the following goals:

- 1) To synthesize and characterize a series of N-heterocyclic amides.
- 2) To establish their binding preferences with respect to a hydrogen bond donor, such as a carboxylic acid or an oxime, is introduced.
- 3) To make structural comparisons with relevant systems studied previously.
- 4) To establish whether molecular electrostatic potential calculations can be used as a reliable guideline for establishing binding preferences of these molecules.

### 2.3 Experimental

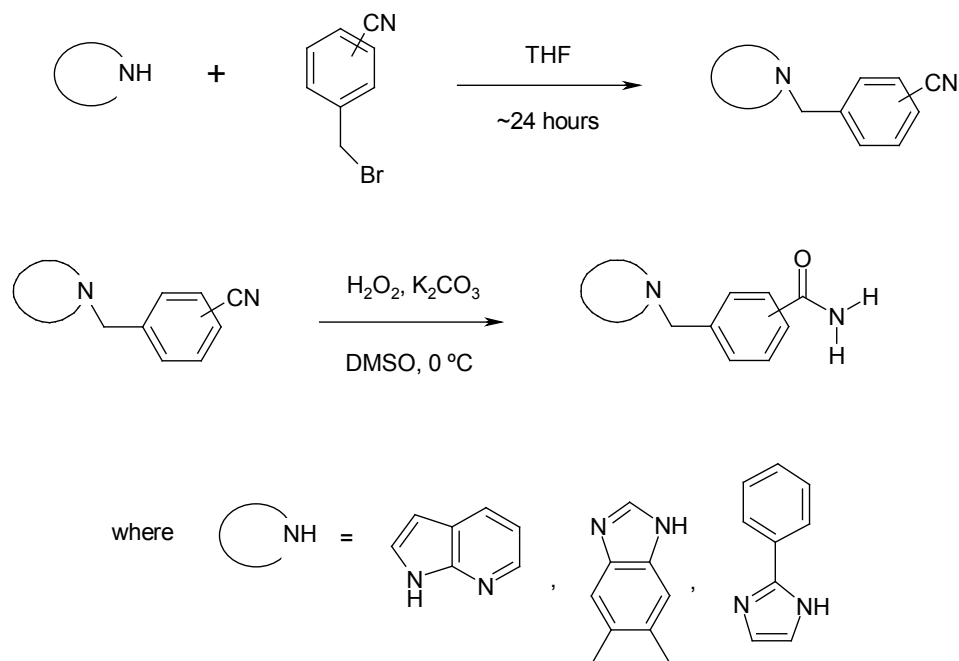


**Figure 2.6** General synthesis of N-heterocyclic amides.

### 2.3.1 Synthesis of amides

#### 2.3.1.1 Synthesis 4-[(7-aza-indol-1-yl)methyl]benzonitrile, 1

7-Azaindole (2.00 g, 16.8 mmol) was dissolved in dry THF (50mL) with stirring in a 250 mL round-bottomed flask. NaOH (7.00 g, 175 mmol) was added and the mixture was stirred for 2 hours under a dinitrogen atmosphere.  $\alpha$ -Bromo-*p*-tolunitrile (3.00 g, 1.69 mmol) was added to the reaction mixture in dry THF (40 mL). The reaction was stirred for 22 hours under a nitrogen atmosphere. Water (30 mL) was added to dissolve the NaOH. The two phases were separated using a separatory funnel, and the THF layer was dried over anhydrous MgSO<sub>4</sub>. MgSO<sub>4</sub> was filtered via vacuum filtration and THF was removed *via* rotary evaporation to produce a yellow solid. Recrystallisation from THF produced a yellow powder. Yield: 2.84g (71%); mp: 90-95°C; <sup>1</sup>H NMR: (400 MHz; CDCl<sub>3</sub>-*d*)  $\delta$  5.58 (s, 2H), 6.55 (d, 1H, *J* = 3.2 Hz), 7.12 (dd, 1H, *J*<sub>1</sub> = 4.8 Hz, *J*<sub>2</sub> = 4 Hz), 7.19 (d, 2H, *J* = 3.2 Hz), 7.48 (d, 1H, *J* = 8 Hz), 7.58 (d, 2H, *J* = 8.4 Hz) 7.96 (dd, 1H, *J*<sub>1</sub> = 1.6 Hz, *J*<sub>2</sub> = 8 Hz), 8.34 (dd, 1H, *J*<sub>1</sub> = 1.6 Hz, *J*<sub>2</sub> = 4.8 Hz). IR: 2224 cm<sup>-1</sup> (C≡N).

#### 2.3.1.2 Synthesis of 4-[(7-aza-indol-1-yl)methyl]benzamide, 2

**1** (1.40 g, 6.00 mmol) was dissolved in DMSO (25ml) with stirring in a 250ml round-bottomed flask under N<sub>2</sub> atmosphere. The reaction flask was then placed in an ice-water bath and anhydrous K<sub>2</sub>CO<sub>3</sub> (0.239g, 1.73 mmol) was added to the mixture. 30% wt H<sub>2</sub>O<sub>2</sub> (27.5ml) was syringed into the reaction mixture and the mixture turned yellow almost immediately. The reaction was allowed to warm to room temperature with continuous stirring under N<sub>2</sub> atmosphere, whilst covered in aluminum foil. Distilled water (14ml) was added and the reaction mixture was cooled in an ice-water bath. The yellow solid was filtered *via* vacuum filtration, dried, and recrystallized from ethanol/water to produce yellow needles. Yield: 0.373g (40%); mp: 175-179°C; <sup>1</sup>H NMR: (400 MHz; DMSO-*d*<sub>6</sub>)  $\delta$  5.53 (s, 2H), 6.53 (d, 1H, *J* = 3.6 Hz), 7.11 (dd, 1H), 7.25 (d, 2H, *J* = 8.4 Hz), 7.32 (bs, 1H), 7.65 (d, 1H, *J* = 3.2 Hz), 7.77 (d, 2H, *J* = Hz), 7.90 (bs, 1H), 7.99 (dd, 1H, *J*<sub>1</sub> = 1.6 Hz, *J*<sub>2</sub> = 8 Hz), 8.25 (dd, 1H, *J*<sub>1</sub> = 1.2 Hz, *J*<sub>2</sub> = 4.4 Hz); <sup>13</sup>C NMR: (200 MHz; DMSO-*d*<sub>6</sub>)  $\delta$  46.84, 79.16, 99.69, 115.81, 120.01, 126.89, 127.67, 128.64, 129.18, 133.34, 141.59, 142.58, 167.52; IR:  $\nu$  1684 cm<sup>-1</sup> (C=O), 3144-3310 cm<sup>-1</sup> (NH<sub>2</sub>).

### 2.3.1.3 Synthesis of 4-[(5,6-dimethylbenzimidazol-1-yl)methyl]benzonitrile, 3

5,6-Dimethylbenzimidazole (1.04 g, 6.84 mmol) was dissolved in dry THF (60 mL) with heat and stirring in a 250 mL round-bottomed flask. To the clear, light brown-colored solution was added NaOH (2.74 g, 68.4 mmol), which turned milky-brown in color. The mixture was stirred for 2 h at room temperature under an N<sub>2</sub> atmosphere. To this mixture was added dry THF containing  $\alpha$ -bromo-*p*-tolunitrile (30 mL solution, 1.34 g, 6.84 mmol). Stirring was continued for 16 h under an N<sub>2</sub> atmosphere, after which 7 mL of distilled water was added to dissolve the NaOH pellets and NaBr. The two layers formed were separated using a separatory funnel, and the THF layer was dried over anhydrous MgSO<sub>4</sub>. The MgSO<sub>4</sub> was filtered off by vacuum filtration, and the filtrate was concentrated *via* rotary evaporation to produce a pale yellow solid. Yield: 1.568 g (88%); mp: 153–155 °C, <sup>1</sup>H NMR (400 MHz, CDCl<sub>3</sub>-*d*):  $\delta$  2.32 (s, 3H), 2.36 (s, 3H), 5.39 (s, 2H), 6.94 (s, 1H), 7.21 (d, 2H, *J* = 8.8 Hz), 7.59 (s, 1H), 7.62 (d, 2H, *J* = 8.4 Hz), 7.86 (s, 1H); IR:  $\nu$  2223 cm<sup>-1</sup> (C $\equiv$ N).

### 2.3.1.4 Synthesis of 4-[(5,6-dimethylbenzimidazol-1-yl)methyl]benzamide, 4

**3** (1.568 g, 3.830 mmol) was dissolved in DMSO (9 mL) with heat and stirring in a 250 mL three-necked flask under an N<sub>2</sub> atmosphere. The reaction flask was then cooled in an ice-water bath and anhydrous K<sub>2</sub>CO<sub>3</sub> (0.0760 g, 0.547 mmol) was added to the reaction mixture. 30 wt% H<sub>2</sub>O<sub>2</sub> (9 mL) was syringed dropwise into the reaction mixture, and a white solid precipitated almost immediately. The reaction was then allowed to warm to room temperature with continued stirring for 1 h while covered in aluminum foil. After this distilled water (5 mL) was added to the reaction mixture. A white solid was obtained upon vacuum filtration, which was washed with two small portions of distilled water and dried. Recrystallization of the solid from hot acetonitrile afforded the product as colorless plates. Yield: 1.489 g (89%); mp: 245–250 °C; <sup>1</sup>H NMR (400 MHz, DMSO-*d*<sub>6</sub>):  $\delta$  2.26 (s, 3H), 2.28 (s, 3H), 5.49 (s, 2H), 7.25 (s, 1H), 7.29 (d, 2H, *J* = 8.0 Hz), 7.35 (bs, 1H), 7.42 (s, 1H), 7.81 (d, 2H, *J* = 8.0 Hz), 7.92 (bs, 1H), 8.25 (s, 1H); <sup>13</sup>C NMR (400 MHz, DMSO-*d*<sub>6</sub>)  $\delta$  19.89, 20.16, 47.18, 110.59, 119.61, 126.96, 127.89, 130.08, 131.16, 132.20, 133.66, 140.37, 142.21, 142.46, 167.54; IR:  $\nu$  1672 cm<sup>-1</sup> (C=O), 3167-3332 cm<sup>-1</sup> (NH<sub>2</sub>).

### 2.3.1.5 Synthesis of 3-[(5,6-dimethylbenzimidazol-1-yl)methyl]benzonitrile, 5

5,6-Dimethylbenzimidazole (4.085 g, 27.90 mmol) was dissolved in dry THF (50 mL) with heat and stirring in a 250 mL round-bottomed flask. To the clear, light brown-colored solution was added NaOH (11.60 g, 279.0 mmol), which turned milky-brown in color. The mixture was stirred for 2 h at room temperature under an N<sub>2</sub> atmosphere. To this mixture was added dry THF containing  $\alpha$ -bromo-*m*-tolunitrile (70 mL solution, 5.47 g, 27.90 mmol). Stirring was continued for 2 days h under an N<sub>2</sub> atmosphere, after which distilled water (100 mL) was added to dissolve the NaOH pellets and NaBr. The two layers formed were separated using a separatory funnel, and the THF layer was dried over anhydrous MgSO<sub>4</sub>. The MgSO<sub>4</sub> was filtered off by vacuum filtration, and the filtrate was concentrated *via* rotary evaporation to produce a pale yellow solid. Yield: 6.10 g (84%); mp: 172-175 °C, <sup>1</sup>H NMR (400 MHz, CDCl<sub>3</sub>-*d*):  $\delta$  2.35 (s, 3H), 2.38 (s, 3H), 5.38 (s, 2H), 6.98 (s, 1H), 7.33-7.35 (m, 1H), 7.44-7.48 (m, 2H), 7.61-7.62 (m, 2H), 7.89 (s, 1H); IR:  $\nu$  2228 cm<sup>-1</sup> (C $\equiv$ N).

### 2.3.1.6 Synthesis of 3-[(5,6-dimethylbenzimidazol-1-yl)methyl]benzamide, 6

**5** (6.10 g, 23.3 mmol) was dissolved in DMSO (90 mL) with heat and stirring in a 250 mL three-necked flask under an N<sub>2</sub> atmosphere. The reaction flask was then cooled in an ice-water bath and anhydrous K<sub>2</sub>CO<sub>3</sub> (0.46 g, 3.33 mmol) was added to the reaction mixture. 30 wt% H<sub>2</sub>O<sub>2</sub> (126 mL) was syringed dropwise into the reaction mixture. The reaction was then allowed to warm to room temperature with continued stirring for 1 h whilst covered in aluminum foil. After this distilled water (80 mL) was added to the reaction mixture, upon which a white solid precipitated. The solid was filtered via vacuum, which was washed with two small portions of distilled water and dried. NMR showed unreacted nitrile present, and the product was consequently purified via column chromatography. Recrystallization from hot acetonitrile gave colorless plates. Yield: 0.372g (6 %); mp: 217–222 °C; <sup>1</sup>H NMR (400 MHz, DMSO-*d*<sub>6</sub>):  $\delta$  2.26 (s, 3H), 2.27 (s, 3H), 5.47 (s, 2H), 7.26 (s, 1H), 7.39 (m, 2H), 7.41 (m, 1H), 7.42 (s, 1H), 7.75-7.76 (m, 1H), 7.77-7.78 (m, 1H), 7.99 (bs, 1H), 8.25 (s, 1H); <sup>13</sup>C NMR (DMSO-*d*<sub>6</sub>, 200 MHz)  $\delta$  19.87, 20.14, 47.30, 110.53, 119.56, 126.50, 126.55, 128.60, 130.00, 131.07, 132.18, 134.64, 137.42, 142.21, 143.43, 143.45, 167.51; IR:  $\nu$  1685 cm<sup>-1</sup> (C=O), 3169-3375 cm<sup>-1</sup> (NH<sub>2</sub>).



### 2.3.1.7 Synthesis 4-[(2-phenylimidazol-1-yl)methyl]benzonitrile, 7

2-Phenylimidazole (3.061g, 21.00 mmol) was dissolved in dry THF (40ml) with stirring in a 250 mL round-bottomed flask. To the colorless solution was added NaOH (8.40 g, 210 mmol) resulting in an orange solution, which was stirred for 2h at room temperature under a N<sub>2</sub> atmosphere. To this mixture was added a solution of dry THF (60ml) containing  $\alpha$ -bromo-*p*-tolunitrile (4.120 g, 21.03 mmol). Stirring was continued for 24h under a N<sub>2</sub> atmosphere, after which distilled water (20ml) was added to dissolve remaining NaOH pellets and the NaBr. The two layers formed were separated using a separatory funnel, and the THF layer was dried over anhydrous MgSO<sub>4</sub>. The MgSO<sub>4</sub> was filtered off, and the filtrate was concentrated *via* rotary evaporation to give a yellow solid. Yield: 5.26 g (96%); mp: 128-130 °C; <sup>1</sup>H NMR (400 MHz, CDCl<sub>3</sub>-*d*):  $\delta$  5.30 (s, 2H), 6.98 (d, 1H, *J* = 4Hz), 7.16 (d, 2H, *J* = 8Hz), 7.24 (d, 1H, *J* = 4Hz), 7.40-7.41 (m, 3H), 7.47-7.49 (m, 2H), 7.65 (d, 2H, *J* = 8Hz); IR:  $\nu$  2231 cm<sup>-1</sup> (C $\equiv$ N).

### 2.3.1.8 Synthesis of 4-[(2-phenylimidazol-1-yl)methyl]benzamide, 8

7 (5.20 g, 20.1 mmol) was dissolved in DMSO (30ml) with heat and stirring in a 250 mL three-necked flask under a N<sub>2</sub> atmosphere. The reaction flask was then cooled in an ice-water bath and anhydrous K<sub>2</sub>CO<sub>3</sub> (0.80 g, 5.77 mmol) was added to the reaction mixture. A 30 wt % H<sub>2</sub>O<sub>2</sub> solution (60mL) was added dropwise into the reaction mixture, and a white solid formed almost immediately. The reaction was then allowed to warm to room temperature with continued stirring for 1h while covered in aluminium foil. Distilled water (50ml) was added to the reaction mixture. A white solid was obtained upon vacuum filtration, which was washed with two small portions of distilled water and dried. Yield: 5.062 g (90%); mp: 75-80 °C; <sup>1</sup>H NMR (400 MHz, CDCl<sub>3</sub>-*d*):  $\delta$  5.28 (s, 2H), 5.82 (bs, 1H), 6.32 (bs, 1H), 6.99 (d, 1H, *J* = 4Hz), 7.14 (d, 2H, *J* = 8Hz), 7.22 (d, 1H, *J* = 4Hz), 7.38-7.40 (m, 3H), 7.49-7.52 (m, 2H), 7.80 (d, 2H, *J* = 4Hz); <sup>13</sup>C NMR: (400 MHz, CDCl<sub>3</sub>)  $\delta$  49.99, 121.23, 126.54, 128.15, 128.65, 128.68, 129.06, 129.09, 130.09, 133.04, 140.94, 148.29, 168.74; IR:  $\nu$  3293-3179 cm<sup>-1</sup> (NH<sub>2</sub>), 1649 cm<sup>-1</sup> (C=O).

### 2.3.1.9 Synthesis 3-[(2-phenylimidazol-1-yl)methyl]benzonitrile, 9

2-Phenylimidazole (3.016g, 20.9mmol) was dissolved in dry THF (50ml) with stirring in a 250mL round-bottomed flask. To the colourless solution was added NaOH

(8.36g, 209mmol) and the mixture was stirred for 2h at room temperature under a N<sub>2</sub> atmosphere. To this mixture was added a solution of dry THF (60ml) containing  $\alpha$ -bromo-m-tolunitrile (4.10g, 20.91mmol). Stirring was continued for 24h under a N<sub>2</sub> atmosphere, after which distilled water (10ml) was added to dissolve the NaOH pellets and NaBr. The two layers formed were separated using a separatory funnel, and the THF layer was dried over anhydrous MgSO<sub>4</sub>. The MgSO<sub>4</sub> was filtered off, and the filtrate was concentrated via vacuum filtration to produce a yellow oil. Purification by column chromatography (hexanes/ethyl acetate 10:1→4:1) yielded an orange oil (3.515g, 65%); <sup>1</sup>H NMR (400 MHz, CDCl<sub>3</sub>-d):  $\delta$  5.18 (s, 2H), 6.92 (1H, d,  $J$  = 4 Hz), 7.13 (1H, d,  $J$  = 4 Hz), 7.19 (1H, d,  $J$  = 8 Hz), 7.24 (1H, s), 7.30 (3H, m), 7.38 (1H, t,  $J$  = 8Hz), 7.39-7.42 (2H, m), 7.48 (1H, d,  $J$  = 8 Hz); IR:  $\nu$  2224 cm<sup>-1</sup> (C $\equiv$ N).

#### **2.3.1.10 Synthesis of 3-[(2-phenylimidazol-1-yl)methyl]benzamide, 10**

**9** (3.52 g, 13.6 mmol) was dissolved in DMSO (20ml) with heat and stirring in a 250 mL three-necked flask under a N<sub>2</sub> atmosphere. The reaction flask was then cooled in an ice-water bath and anhydrous K<sub>2</sub>CO<sub>3</sub> (0.570 g, 4.10 mmol) was added to the reaction mixture. 30 wt % H<sub>2</sub>O<sub>2</sub> solution (40mL) were added dropwise into the reaction mixture, and a white solid formed almost immediately. The reaction was then allowed to warm to room temperature with continued stirring for 1h while covered in aluminium foil. Distilled water (50ml) was added to the reaction mixture. A solid was obtained upon vacuum filtration, which was washed with two small portions of distilled water and dried. Recrystallisation from ethanol gave a white solid (3.343g, 88%); mp: 170-174 °C; <sup>1</sup>H NMR (400 MHz, CDCl<sub>3</sub>-d):  $\delta$  5.27 (s, 2H), 5.81 (bs, 1H), 6.25 (bs, 1H), 6.98 (d, 1H,  $J$  = 4 Hz), 7.19 (s, 1H), 7.21 (s, 1H), 7.39-7.41 (m, 3H), 7.43 (t, 1H,  $J$  = 4 Hz), 7.51-7.58 (m, 2H), 7.59 (s, 1H), 7.74 (d, 1H,  $J$  = 8 Hz); <sup>13</sup>C NMR: (200 MHz, CDCl<sub>3</sub>-d)  $\delta$  50.03, 121.13, 125.75, 126.79, 128.64, 128.73, 128.97, 129.24, 129.35, 129.99, 130.31, 134.10, 137.65, 168.62; IR:  $\nu$  3324-3180 cm<sup>-1</sup> (NH<sub>2</sub>), 1675 cm<sup>-1</sup> (C=O).

#### **2.3.2 Synthesis of co-crystals and salts**

The synthesis of a small number of co-crystals is presented here. Co-crystallizations were set up in a 1:1 ratio with carboxylic acids and cyanoximes. Only crystals suitable for

X-ray crystallography are reported here. Solids obtained were analyzed by IR spectroscopy. The results are presented in Table 2.2.

#### ***2.3.2.1 Synthesis of 4-[(7-aza-indol-1-yl)methyl]benzamide 4-nitrobenzoic acid (1:2), 2a***

**2** (15 mg, 0.060 mmol) was dissolved in methanol in a 100 mL beaker. To it was added a solution of 4-nitrobenzoic acid (10 mg, 0.060 mmol) in methanol. Yellow prisms were obtained via slow evaporation after 10 days; mp: 163-165 °C.

#### ***2.3.2.2 Synthesis of 4-[(7-aza-indol-1-yl)methyl]benzamide 3,5-dinitrobenzoic acid (1:1), 2b***

**2** (15 mg, 0.060 mmol) was dissolved in methanol in a 100 mL beaker. To it was added a solution of 3,5-dinitrobenzoic acid (10 mg, 0.060 mmol) in methanol. Yellow plates were obtained via slow evaporation after 1 day; mp: 176-178 °C.

#### ***2.3.2.3 Synthesis of 4-[(5,6-dimethylbenzimidazol-1-yl)methyl]benzamide 2,5-dichlorobenzoic acid (1:1), 4a***

**4** (14 mg, 0.060 mmol) was dissolved in ethanol with a few drops of water in a 100 mL beaker. To it was added a solution of 3,5-dinitrobenzoic acid (10 mg, 0.060 mmol) also in ethanol with a few drops of water. Amber prisms were obtained via slow evaporation after ~2 weeks; mp: 190-192 °C

#### ***2.3.2.4 Synthesis of 3-[(5,6-dimethylbenzimidazol-1-yl)methyl]benzamide 2,3,4,5,6-pentamethylbenzoic acid (1:1), 6a***

**6** (15 mg, 0.054 mmol) was dissolved in ethanol/acetonitrile, and 2,3,4,5,6-pentamethylbenzoic acid (10 mg, 0.054 mmol) was added to the solution. Colorless prisms were obtained after ~2 weeks; mp: 190-192 °C.

#### ***2.3.2.5 Synthesis of 3-[(5,6-dimethylbenzimidazolium-1-yl)methyl]benzamide 3,5-dinitrobenzoate (1:1), 6b***

**6** (15 mg, 0.054 mmol) was dissolved in ethanol/acetonitrile, and 3,5-dinitrobenzoic acid (11 mg, 0.054 mmol) was added to the solution. Colorless prisms were obtained after 1 week; mp: 193-195 °C.

### **2.3.3 *Infra-red spectroscopy and melting point***

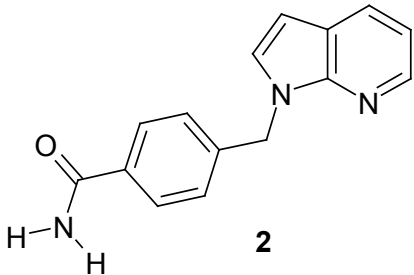
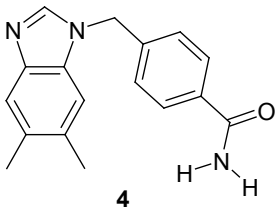
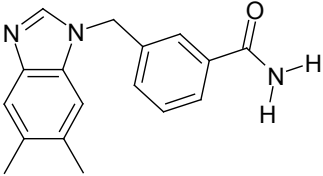
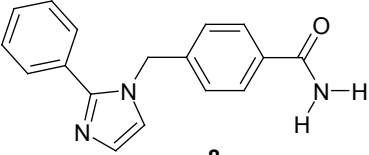
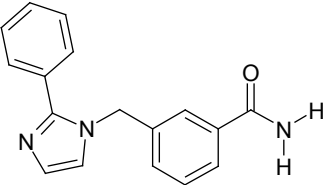
Infrared spectra of the products obtained in the co-crystallizations were acquired using a potassium bromide pellet. An approximate 8:1 ratio of KBr to solid product was combined in an oven-dried mortar and ground to a uniform powder with a pestle. A pellet press was employed to create a transparent KBr pellet that was used for analysis. A Nicolet FT-IR instrument equipped with OMNIC software was used to analyze the data. The main features used for identification of a co-crystal are the O-H...N hydrogen-bonding bands at 2500 and 1900  $\text{cm}^{-1}$ .<sup>8</sup> IR data is shown in Table 2.2. Melting points were performed on a Fisher-Johns apparatus and are uncorrected.

## **2.4 Results**

### **2.4.1 *IR spectroscopy***

The data obtained from IR spectroscopy performed on solids obtained from the supramolecular reactions is shown in Table 2.2.

**Table 2.2** IR data (position of O-H...N stretches) from co-crystallization experiments

Amide	Acid/oxime	O-H...N band (cm <sup>-1</sup> )
 <p><b>2</b></p>	4-Cyanobenzoic acid	2536, 1889
	3,5-Dinitrobenzoic acid	2550, 1942
	3-Bromo-5-Iodo benzoic acid	-
	Itaconic acid	-
	3,5-Difluorobenzoic acid	-
	4-Hydroxybenzoic acid	2524, 1869
	3-Iodobenzoic	-
	Naphthoic acid	-
	2,4-Dichlorobenzoic acid	-
	4-Nitrobenzoic acid	2422, 1904
	4-Ethylbenzoic acid	-
	4-Chlorophenylcyanoxime	-
	 <p><b>4</b></p>	4-Bromophenylcyanoxime
2-Chlorophenylcyanoxime		-
4-Chlorophenylcyanoxime		2545, 2048
2,5-Dichlorobenzoic acid		2484, 1905
Malic acid		2494, 1910
Benzoic acid		-
1,3,5-Tricyanophenylxime		2594, 1984
 <p><b>6</b></p>	4-Chlorophenylcyanoxime	2508, 1838
	4-Bromophenylcyanoxime	2495, 1818
	Pentamethylbenzoic acid	2481, 1964
	3,5-Dimethylbenzoic acid	-
	2-Chlorophenylcyanoxime	-
	3-Chlorophenylcyanoxime	2514, 1878
 <p><b>8</b></p>	4-Chlorophenylcyanoxime	2514, 1904
	2-Chlorophenylcyanoxime	2488, 1911
	4-Bromophenylcyanoxime	2521, 1911
	4-Nitrobenzoic acid	2481, 1931
	4-Hydroxybenzoic acid	2495, 1911
 <p><b>10</b></p>	1,3,5-Tricyanophenylxime	2508, 1885
	3-Fluorobenzoic acid	2514, 1984
	4-N, N'-Dimethylbenzoic acid	-
	3,5-Dinitrobenzoic acid	2448, 1964
	4-Toluic acid	2501, 1931
	2,5-Dichlorobenzoic acid	2495, 1951

**Table 2.3** Hydrogen-bond geometries for **2**, **2a**, and **b**, **4a** and **6**, **6a** and **b**.

Compound	D-H...A	d(D-H), Å	d(H...A), Å	d(D...A), Å	<(DHA), °
<b>2</b> <sup>i</sup>	N(27)-H(27A)...O27 <sup>a</sup>	0.879(19)	2.044(19)	2.9216(14)	175.9(16)
	N(27)-H(27B)...N(18A) <sup>b</sup>	0.845(19)	2.230(19)	3.055(3)	165.5(17)
	N(27)-H(27B)...N(11B) <sup>b</sup>	0.845(19)	2.04(3)	2.87(2)	168.9(19)
<b>2a</b> <sup>iii</sup>	O(37)-H(37)...O(27)	0.91(2)	1.60(2)	2.5055(14)	168.6(18)
	N(27)-H(27A)...O(38)	0.882(18)	2.035(18)	2.9047(14)	168.4(16)
	O(47)-H(47)...N(19)	1.078(17)	1.492(17)	2.5670(14)	174.3(15)
	N(27)-H(27B)...O(48) <sup>a</sup>	0.870(17)	2.101(18)	2.9430(14)	162.8(16)
<b>2b</b> <sup>v</sup>	O(31)-H(31)...O(17)	0.92(3)	1.64(3)	2.556(2)	172(2)
	N(17)-H(17A)...O(17) <sup>a</sup>	0.88(3)	2.02(3)	2.897(3)	173(2)
	N(17)-H(17B)...N(28) <sup>b</sup>	0.94(3)	2.13(3)	2.912(3)	139(2)
<b>4a</b> <sup>v</sup>	N(37)-H(37A)...O(41)	0.95(4)	2.00(5)	2.92(2)	164(3)
	N(37)-H(37A)...O(51)	0.95(4)	2.09(6)	3.01(4)	162(3)
	N(37)-H(37A)...O(61)	0.95(4)	2.01(5)	2.95(3)	169(3)
	N(37)-H(37B)...O(42) <sup>a</sup>	0.84(3)	2.12(4)	2.94(2)	164(4)
	N(37)-H(37B)...O(52) <sup>a</sup>	0.84(3)	2.30(5)	3.13(3)	168(3)
	N(37)-H(37B)...O(62) <sup>a</sup>	0.84(3)	2.17(5)	3.00(4)	171(4)
	N(13)-H(13)...O(41) <sup>b</sup>	0.93(4)	1.83(5)	2.75(2)	169(4)
	N(13)-H(13)...O(51) <sup>b</sup>	0.93(4)	1.57(5)	2.50(3)	172(5)
N(13)-H(13)...O(61) <sup>b</sup>	0.93(4)	1.80(5)	2.72(3)	172(4)	
<b>6</b> <sup>vi</sup>	N(37)-H(37B)...N(43)	0.95(3)	2.04(3)	2.971(4)	166(3)
	N(67)-H(67B)...N(13)	0.94(3)	2.03(3)	2.952(4)	167(3)
	N(37)-H(37A)...O(67) <sup>a</sup>	0.94(4)	1.96(4)	2.896(4)	172(3)
	N(67)-H(67A)...O(37) <sup>b</sup>	0.92(4)	1.98(4)	2.905(4)	175(3)
<b>6a</b> <sup>vii</sup>	N(37)-H(37A)...O(37) <sup>a</sup>	0.915(17)	1.928(17)	2.8396(14)	173.7(14)
	N(37)-H(37B)...O(42)	0.925(16)	1.958(17)	2.8432(15)	159.5(14)
	O(41)-H(41)...N(13) <sup>b</sup>	1.164(17)	1.382(17)	2.5191(14)	163.3(15)
<b>6b</b> <sup>viii</sup>	N(13)-H(13)...O(41)	1.02(4)	1.70(4)	2.711(3)	174(3)
	N(37)-H(37A)...O(42) <sup>a</sup>	0.91(4)	1.96(4)	2.841(3)	161(4)
	N(37)-H(37B)...O(41) <sup>b</sup>	0.82(4)	2.09(4)	2.886(3)	162(3)

Generator for A: i) <sup>a</sup> -x, -y+1, -z+2, <sup>b</sup> x-1, y, z; ii) <sup>a</sup> -x, -y+2, -z+2, <sup>b</sup> -x+1, -y+2, -z+1; iii) <sup>a</sup> -x, y+1/2, -z+3/2; iv) <sup>a</sup> -x+1, -y+2, -z, <sup>b</sup> -x, -y+1, -z; v) <sup>a</sup> -x+1, -y+1, -z+1, <sup>b</sup> x+1/2, -y+3/2, z-1/2; vi) <sup>a</sup> x, y, z-1, <sup>b</sup> x, y, z+1; vii) <sup>a</sup> -x+1, -y, -z+1, <sup>b</sup> x, y+1, z+1; viii) <sup>a</sup> x-1, y, z, <sup>b</sup> -x, -y+1, -z+1.

#### 2.4.2 Crystal structure of 4-[(7-aza-indol-1-yl)methyl]benzamide, **2**

The crystal structure of **2** contains a disordered molecule of 4-[(7-aza-indol-1-yl)methyl]benzamide. An amide-amide dimer is formed with an adjacent molecule, Figure 2.7, and the *anti* proton participates in an N-H...N hydrogen-bond with the pyridine nitrogen atom (Table 2.1).

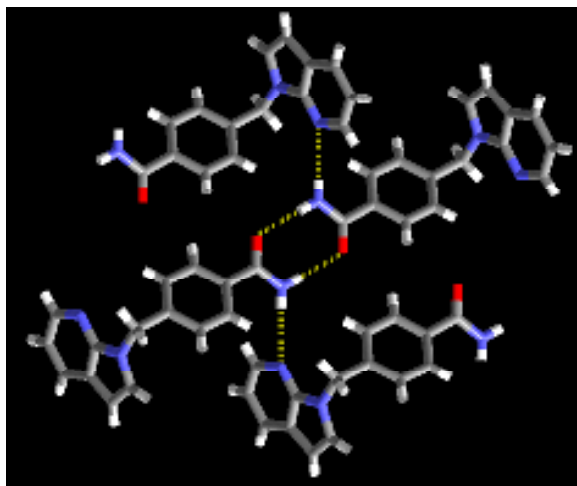


**Figure 2.7** Hydrogen-bond network in the crystal structure of **2**.

#### 2.4.3 Crystal structure of 4-[(7-aza-indol-1-yl)methyl]benzamide 4-nitrobenzoic acid (1:2), **2a**

The crystal structure of **2a** shows one molecule of 4-[(7-aza-indol-1-yl)methyl]benzamide and two molecules of 4-nitrobenzoic acid. The two 4-nitrobenzoic acid molecules form hydrogen bonds to the pyridyl nitrogen atom, and an acid-amide dimer, Figure 2.8. The amide *anti* proton participates in an N-H $\cdots$ O hydrogen bond with a carbonyl oxygen atom of an adjacent acid molecule.

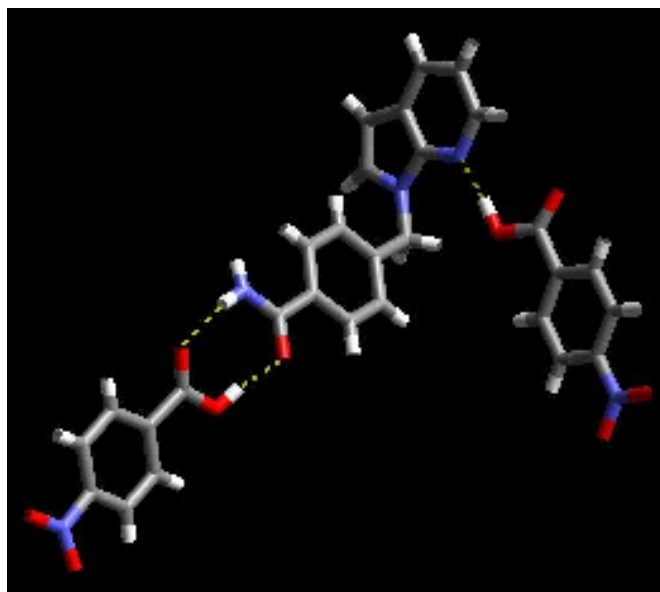


**Figure 2.8** Hydrogen bonding in the crystal structure of **2a**.

#### 2.4.4 Crystal structure of 4-[(7-aza-indol-1-yl)methyl]benzamide 3,5-dinitrobenzoic acid (1:1), 2b

The crystal structure of **2b** shows one molecule of 4-[(7-aza-indol-1-yl)methyl]benzamide and a molecule of 3,5-dinitrobenzoic acid. The acid forms an O-H $\cdots$ O hydrogen bond with the amide carbonyl oxygen atom. The amide-amide dimer has remained intact in the structure, with the amide *anti* proton opting to participate in an N-H $\cdots$ N hydrogen bond with the pyridyl nitrogen atom, Figure 2.9.

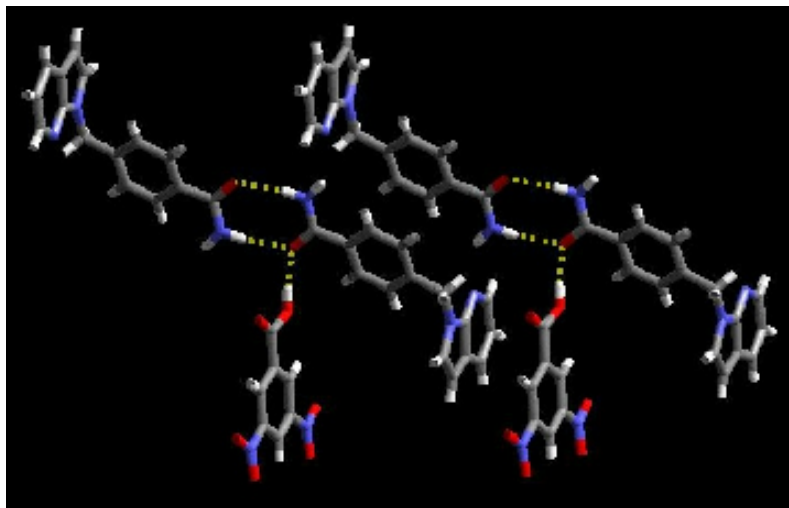


**Figure 2.9** Hydrogen bonding in the crystal structure of **2b**.

#### 2.4.5 Crystal structure of 4-[(5,6-dimethylbenzimidazolium-1-yl)methyl]benzamide 2,5-dichlorobenzoate (1:1), 4a

The crystal structure of **4a** shows that proton transfer has taken place to the benzimidazole nitrogen atom and the carboxylate participates in three N-H $\cdots$ O $^-$  hydrogen-bonds: two with an amide *anti* proton from two separate amide cations, and one with the protonated nitrogen atom of the benzimidazole moiety, Figure 2.10. There are no noteworthy interactions with either chlorine atom. The amide-amide dimer is disrupted to form a  $R_4^4(12)$  motif with four amide hydrogen atoms (from two different cations) and four carboxylate oxygen atoms (from two different anions), Figure 2.10.



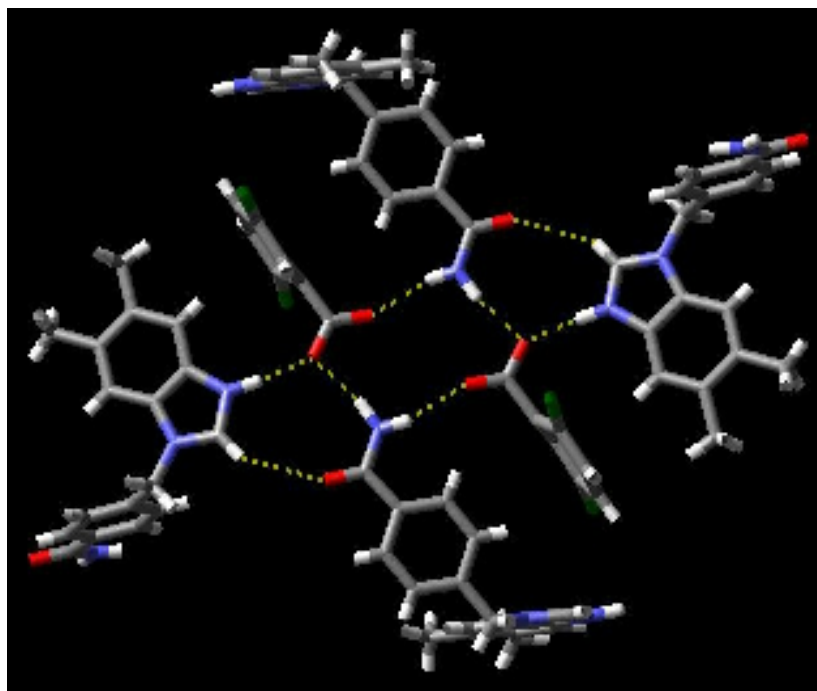


**Figure 2.10** Extended network in the crystal structure of **4a**.

#### 2.4.6 Crystal structure of 3-[(5,6-dimethylbenzimidazol-1-yl)methyl]benzamide, **6**

The crystal structure of **6** reveals two molecules of 3-[(5,6-dimethylbenzimidazol-1-yl)methyl]benzamide in the asymmetric unit. The molecules are connected through  $\pi$ - $\pi$  stacking interactions ( $\sim 3.460$  Å). There is a one-dimensional chain, propagated through amide-amide dimers, and an N-H $\cdots$ N hydrogen-bond between an amide *anti* proton and a benzimidazole nitrogen atom, in the structure, Figure 2.11.

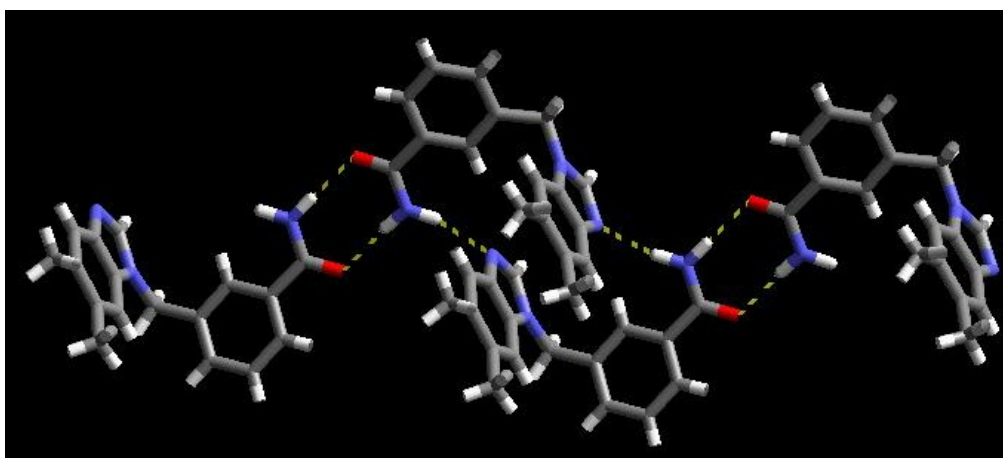


**Figure 2.11** Extended one-dimensional chain in the crystal structure of **6**.

#### 2.4.7 Crystal structure of 3-[(5,6-dimethylbenzimidazol-1-yl)methyl]benzamide 2,3,4,5,6-pentamethylbenzoic acid (1:1), **6a**

The crystal structure of **6a** shows one molecule of 3-[(5,6-dimethylbenzimidazol-1-yl)methyl]benzamide and one molecule of 2,3,4,5,6-pentamethylbenzoic acid. Pentamethylbenzoic acid forms an O-H $\cdots$ N interaction with the benzimidazole nitrogen atom, as well as an N-H $\cdots$ O (amide *anti* proton-acid carbonyl oxygen) hydrogen bond, Table 2.2. The result is an infinite one-dimensional chain, Figure 2.12.

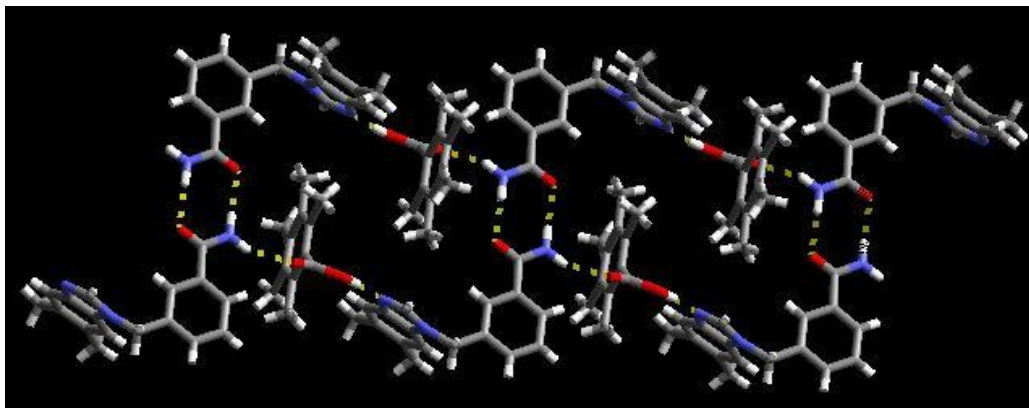
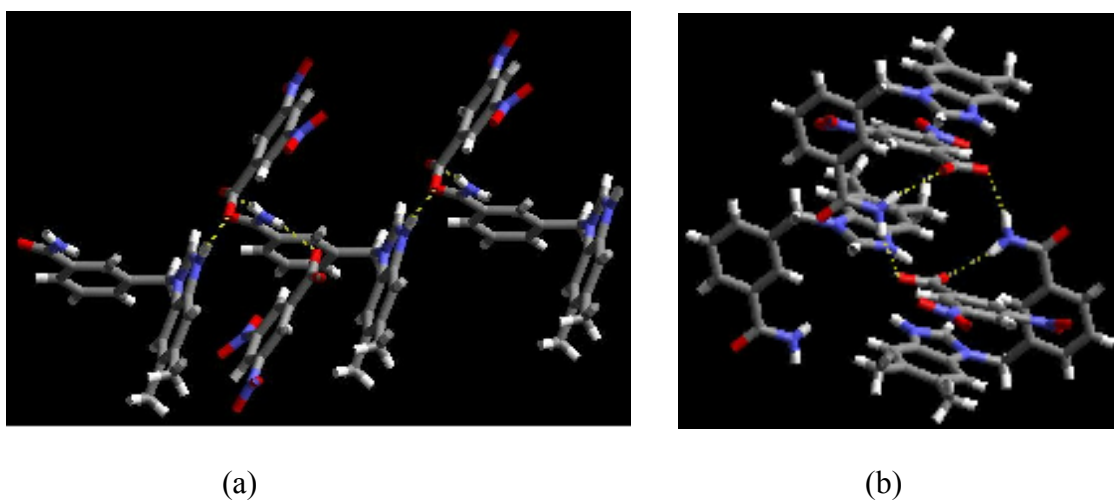


Figure 2.12 One-dimensional chain in the crystal structure of **6a**.

#### 2.4.8 Crystal structure of 3-[(5,6-dimethylbenzimidazolium-1-yl)methyl]benzamide 3,5-dinitrobenzoate, **6b**

The crystal structure of **6b** shows that proton transfer has taken place to the benzimidazole nitrogen atom and the carboxylate moiety forms two N-H $\cdots$ O hydrogen bonds with amide *anti* and *syn* protons from two separate amide cations, Figure 2.13(b). This means that the amide-amide dimer is disrupted, and the result is an  $R_4^4(12)$  motif similar to that observed in **4a**.



**Figure 2.13** (a) Interaction of carboxylate with protonated benzimidazole moiety and amide *anti* proton (b)  $R_4^4$  (12) pattern formed with two carboxylate and two amide  $NH_2$  moieties in the crystal structure of **6b**.

#### 2.4.9 Calculations

The molecular electrostatic potential calculations for each heterocyclic amide synthesized here, along with those studied previously, are presented in Table 2.4.

**Table 2.4** Molecular electrostatic potentials (MEPs)

Supramolecular reagent	Heterocycle N MEP (kJ mol <sup>-1</sup> )
Isonicotinamide	-262
3-[Benzimidazol-1-yl)methyl]benzamide	-296
3-[(2-Chlorobenzimidazol-1-yl)methyl]benzamide	-277
4-[(2-Methylbenzimidazol-1-yl)methyl]benzamide	-303
4-[(7-Aza-indol-1-yl)methyl]benzamide, <b>2</b>	-261
4-[(5,6-Dimethylbenzimidazol-1-yl)methyl]benzamide, <b>4</b>	-293
3-[(5,6-Dimethylbenzimidazol-1-yl)methyl]benzamide <b>6</b>	-305
4-[(2-Phenylimidazol-1-yl)methyl]benzamide, <b>8</b>	-321
3-[(2-Phenylimidazol-1-yl)methyl]benzamide, <b>10</b>	-317

## 2.5 Discussion

### 2.5.1 *Synthesis and Characterization*

All of the amides presented here are easily synthesized and purified, and the majority are obtained in good yields (40-90%). The yield for **6** was low, and this is due to the reaction not going to completion. A large amount of nitrile was recovered in this case. It is expected that if the reaction was repeated the yield would be greatly improved. The first step of the reaction, the coupling of the nitrile to the benzimidazole fragment, can be traced by following the shift of the methylene peak in the NMR spectrum from around 4.5 ppm to around 5.5 ppm. The appearance of the amide can be traced by the disappearance of the C≡N stretch around 2200 cm<sup>-1</sup> in the infrared spectrum. Two broad N-H peaks also appear in the <sup>1</sup>H NMR spectrum, and are also evident in the IR spectrum around 3300 cm<sup>-1</sup>.

### 2.5.2 *IR spectroscopy*

Analysis of the IR spectra of the solids obtained from co-crystallization reactions show considerable differences between each substituent. Representative spectra of a co-crystal and the ligand by itself are shown in Figures C.1 and C.2 (Appendix). Amide **2** formed co-crystals in just 4 out of 12 cases, a supramolecular yield of 33%. This could either mean that the acid opts to bind to the amide carbonyl group, that the lower charge on the nitrogen atom has played a part, or the addition of a fused ring to the pyridyl moiety causes the amide to be considerably less soluble than its isonicotinamide counterpart. IR data often showed spectra of either the carboxylic acid or the amide by itself, and so the latter explanation of the low solubility of the amide caused both components to crystallize homomericly seems fitting. Amides **4** and **6** were shown to have formed co-crystals in 4 out of 7 cases, a supramolecular yield of 57%, and in 6 out of 8 cases (a supramolecular yield of 75%), respectively. Although no crystal structures were obtained with amides **8** and **10**, they were shown to have formed co-crystals in 5 out of 5, and 4 out of 5 cases – supramolecular yields of 100% and 80%, respectively. The results show that the supramolecular yield increases with increasing basicity and calculated MEP of the nitrogen atom on each heterocycle (azaindole<benzimidazole<phenylimidazole), Tables 2.1 and 2.4. This is not necessarily true outside of this study, since isonicotinamide, a base comparable (in

terms of charge) to azaindole amide **4**, forms co-crystals driven by O-H $\cdots$ N interactions 97% of the time according to the CSD.

The positions of the O-H $\cdots$ N bands are varied, due to them being so broad. Consequently, they give no indication as to the strength of the hydrogen bond they represent. Bond lengths are a good indication of bond strengths, and these are obtained from X-ray crystallography.

### 2.5.3 X-ray Crystallography

Seven crystal structures are presented here, of which two are of amides by themselves, three are co-crystals and two are salts.

#### 2.5.3.1 Structural consistency of amides

Crystal structures **1** and **6** are of 4-[(7-aza-indol-1-yl)methyl]benzamide and 3-[(5,6-dimethylbenzimidazol-1-yl)methyl]benzamide, respectively. The two structures are similar, with an amide-amide dimer being present and the amide *anti* proton forming an N-H $\cdots$ N hydrogen bond with the heterocyclic nitrogen. In a recent study of the CSD,<sup>9</sup> it was found that 24 out of 35 structures of either substituted benzamides or N-heterocyclic amides (69%) contained an amide-amide dimer. Of the 18 N-heterocyclic (including 3 N-oxide) amides, 11 of them contained an amide-amide dimer (61%), with 7 of these containing an N-H $\cdots$ N amide *anti* proton-heterocycle hydrogen bond. This means that 64% of all the dimers formed contain an N-H (amide *anti* proton) $\cdots$ N (heterocycle) interaction.

The crystal structure of **6** is very similar to that of 3-[(2-chlorobenzimidazol-1-yl)methyl]benzamide, with an amide dimer present and the two benzimidazole fragments  $\pi$ - $\pi$  stacking with each other (3.847 Å compared to 3.804 Å in **6**).

#### 2.5.3.2 Salt formation

Proton transfer took place in two cases, both containing benzimidazole fragments. In both cases, an R $\begin{smallmatrix} 4 \\ 4 \end{smallmatrix}$  (12) motif is obtained, Figure 2.14.

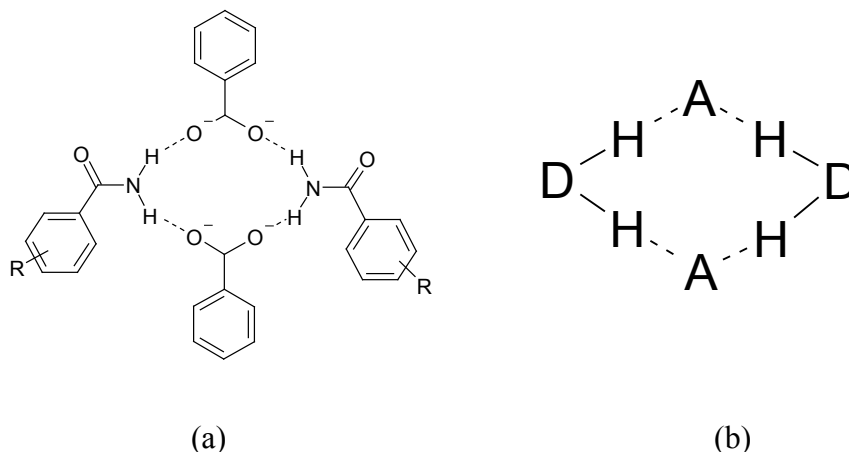


**Figure 2.14** (a)  $R_4^4$  (12) motif obtained with two carboxylate molecules and two amide molecules upon proton transfer (b)  $R_4^2$  (8) motif.

There are no previous occurrences of this motif reported in the literature. It does, however, resemble the  $R_4^2$  (8) (Figure 2.14 (b)), of which there are over 12,000 cases of in the CSD.<sup>10</sup>

### 2.5.3.3 Can salt formation be predicted?

Salt formation is often problematic, and frequently leads to undesired and unpredictable compositions and motifs.<sup>11</sup> The formation of a salt in the cases here could be due to the combination of a strong base with a strong acid, since a weaker acid, pentamethylbenzoic acid, produces a co-crystal (Table 2.5).

**Table 2.5** pK<sub>a</sub>s of some carboxylic acids (least → most acidic)

Acid	pK <sub>a</sub>
Pentamethylbenzoic acid	4.00
4-Nitrobenzoic acid	3.40
3,5-Nitrobenzoic acid	2.80

A search of the CSD shows that proton transfer occurs in 50% of all the structures containing a benzimidazole fragment and a carboxylic acid. Addition of methyl groups to

the 5- and 6- positions on benzimidazole increases the basicity of the benzimidazole nitrogen atom and thus would increase the probability of proton transfer occurring. A well-known rule, the  $pK_a$  rule,<sup>12</sup> has been used as a guideline for the occurrence of proton transfer. Johnson and Rumon stated that a  $pK_a$  difference of 3.7 is large enough to allow proton transfer from a carboxylic acid to a pyridine. Etter et al also carried out some studies of this type with phenols and pyridines. So far then, this rule has only concerned pyridine as a base. The  $\Delta pK_a$  values for the systems here are presented in Table 2.6.

**Table 2.6**  $\Delta pK_a$  values for the results here, complemented by some from the literature

Crystal	$pK_a$ base	$pK_a$ acid	$\Delta pK_a$ ( $pK_{a(\text{base})} - pK_{a(\text{acid})}$ )	Proton transfer?
<b>2b</b>	4.95	2.80	2.15	N
<b>4a</b>	5.93	2.47	3.46	Y
<b>6a</b>	5.93	4.00	1.93	N
<b>6b</b>	5.93	2.80	3.13	Y
<b>3-bzimamide 4-NO<sub>2</sub>-BA</b>	5.93	2.80	3.13	N
<b>3-(2-Me)bzimamide 4-NO<sub>2</sub>-BA</b>	5.46	2.80	2.66	N

Where **3-bzimamide 4-NO<sub>2</sub>-BA**: 3-[benzimidazol-1-yl)methyl]benzamide 4-nitrobenzoic acid, **3-(2-Me)bzimamide 4-NO<sub>2</sub>-BA**: 3-[(2-methylbenzimidazol-1-yl)methyl]benzamide 4-nitrobenzoic acid.

The  $\Delta pK_a$  values do show that proton transfer takes place at higher  $\Delta pK_a$  values. However, it seems that proton transfer occurs at those lower than stated in the literature, with proton transfer occurring at  $\Delta pK_a = 3.13$  and 3.46. It would make sense that a lower  $\Delta pK_a$  is required for salt formation, since imidazole is a stronger base than pyridine. It is interesting to see that, in another system with the same  $\Delta pK_a$  of 3.13, proton transfer did not take place. With a few extra data points, there may well be a distinct correlation between  $\Delta pK_a$  and the likelihood of proton transfer.

As an extension of the  $pK_a$  rule, it may be possible to predict the occurrence of proton transfer through the use of molecular electrostatic potentials. The MEPs were calculated for each molecule in each of the salts obtained here, complemented by some examples from the literature, to see if this is the case, Table 2.7.

**Table 2.7** Molecular electrostatic potential charges and their impact on proton transfer

Crystal	Acceptor MEP/ kJ mol <sup>-1</sup>	Donor MEP/ kJ mol <sup>-1</sup>	$\Delta$ MEP (MEP <sub>donor</sub> -MEP <sub>acceptor</sub> ) kJ mol <sup>-1</sup>	Proton transfer?
<b>4a</b>	-291.6	+144.6	436.2	Y
<b>6b</b>	-304.5	+193.5	498.0	Y
<b>6a</b>	-304.5	+129.1	433.6	N
<b>2b</b>	-260.9	+170.3	431.2	N
<b>Isonic BA</b>	-261.6	+133.7	395.3	N
<b>Isonic hex-2A</b>	-261.6	+131.6	393.2	N
<b>Isonic 4-NO<sub>2</sub>BA</b>	-261.6	+170.3	431.9	N
<b>Isonic 3,5-(NO<sub>2</sub>)<sub>2</sub> BA</b>	-261.6	+193.5	455.1	N
<b>3-bzimamide 4-NO<sub>2</sub>-BA</b>	-296.1	+170.3	466.4	N
<b>3-(2-Me)bzimamide 4-NO<sub>2</sub>-BA</b>	-300.0	+170.3	470.3	N
<b>Im CBDA</b>	-312.7	+152.8	465.5	Y
<b>Im BA</b>	-312.7	+133.7	446.4	Y
<b>BzIm CBDA</b>	-304.5	+152.8	457.3	Y

Where: **Isonic BA**: Isonicotinamide benzoic acid, **Isonic hex-2A**: isonicotinamide hex-2-enoic acid, **Isonic 4-NO<sub>2</sub>BA**: isonicotinamide 4-nitrobenzoic acid, **Isonic 3,5-(NO<sub>2</sub>)<sub>2</sub> BA**: isonicotinamide 3,5-dinitrobenzoic acid, **3-bzimamide 4-NO<sub>2</sub>-BA**: 3-[benzimidazol-1-yl)methyl]benzamide 4-nitrobenzoic acid, **3-(2-Me)bzimamide 4-NO<sub>2</sub>-BA**: 3-[(2-methylbenzimidazol-1-yl)methyl]benzamide 4-nitrobenzoic acid, **Im CBDA**: imidazole cyclobutanediacid, **Im BA**: imidazole benzoic acid, and **BzIm CBDA**: benzimidazole cyclobutanediacid.

A plot of MEP and pK<sub>a</sub> shows that there is a good correlation between the calculated charge on the hydrogen bond donor or acceptor and the calculated charge, i.e, a strong base would have a high negative charge and a strong acid would have a high positive charge, Figure 2.15.



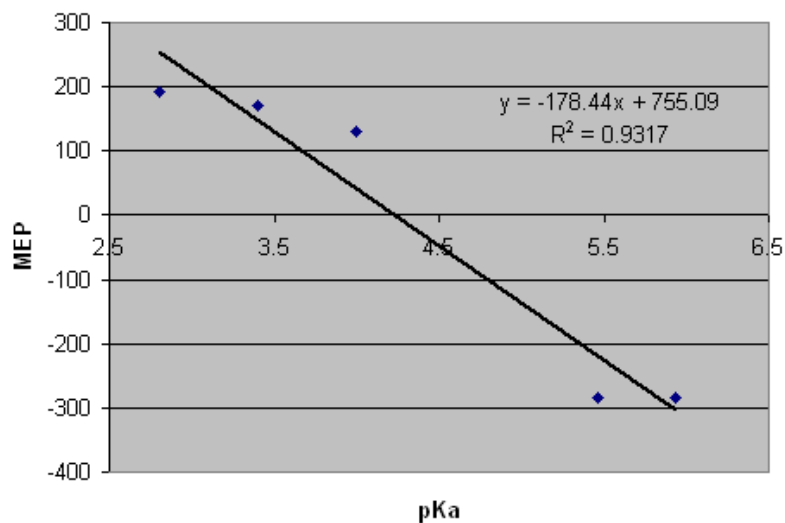


**Figure 2.15** Plot of calculated MEP vs pK<sub>a</sub>.

The calculations show that there is no real cut-off point as to when proton transfer occurs. All the cases of proton transfer occurred when the  $\Delta$ MEP of donor and acceptor was above 436 kJ mol<sup>-1</sup>. This does not mean, however, that every case with a calculated  $\Delta$ MEP above 436 kJ mol<sup>-1</sup> will exhibit proton transfer. This is shown by the three examples with  $\Delta$ MEPs ranging from 455.1 to 455.3 kJ mol<sup>-1</sup>. It can be said, however, that, with a  $\Delta$ MEP greater than 436 kJ mol<sup>-1</sup> there is a higher probability of proton transfer occurring.

The plot of the charge difference between the acceptor and donor shows that all of the cases where charge transfer took place occurred when the acceptor had a charge greater than -290 kJ mol<sup>-1</sup> and when the charge difference was greater than 430 kJ mol<sup>-1</sup>. There are three outliers in this region that remained a co-crystal, Figure 2.16, and so there is a degree of uncertainty as to whether proton transfer would take place.

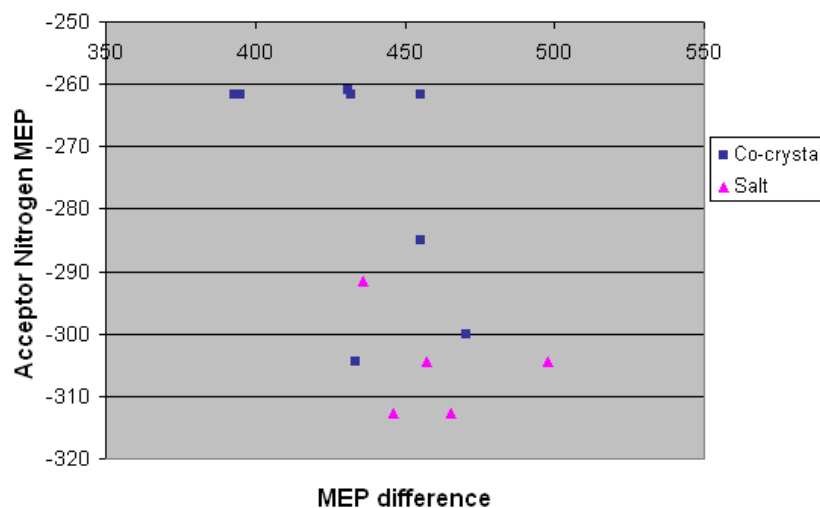


**Figure 2.16** Plot of MEP of hydrogen bond acceptor vs the difference in MEPs between the hydrogen-bond acceptor and the hydrogen-bond donor.

Every case where proton transfer occurs is where the acceptor nitrogen has a charge of  $-290 \text{ kJ mol}^{-1}$  or more. However, there are two cases here where the acceptor has a charge of  $-300 \text{ kJ mol}^{-1}$  and  $-304.5 \text{ kJ mol}^{-1}$ , and proton transfer does not occur. Although the probability of proton transfer is more likely when an acceptor nitrogen has a charge of  $-290 \text{ kJ mol}^{-1}$  or more, it does not happen 100% of the time. It can, however, be predicted with reasonable confidence that a nitrogen atom on a heterocycle with a charge of  $-260 \text{ kJ mol}^{-1}$  or below will not accept a proton. The results of crystal structure **2b** and those with isonicotinamide support this, since there are very few crystal structures (just two in the CSD) containing isonicotinamide and a carboxylic acid where proton transfer has taken place onto the pyridyl ring nitrogen atom.<sup>13</sup> There are also very few examples of crystal structures containing a weak base (i.e an MEP less than isonicotinamide) that has been protonated by a carboxylic acid.<sup>14</sup>

## 2.5.4 Binding selectivities

### 2.5.4.1 Azaindole amide

Although the molecular electrostatic potential of the pyridyl nitrogen atom of 7-azaindole amide is comparable to that of isonicotinamide, the two crystal structures

obtained with it cannot really prove or disprove the hypothesis that it should have similar behavior to isonicotinamide. The first is a 2:1 crystal structure where one molecule of 4-nitrobenzoic acid forms an O-H $\cdots$ N interaction with the pyridyl nitrogen atom, and another forms an O-H $\cdots$ O interaction with the amide carbonyl oxygen atom. Isonicotinamide behaves in the same way when co-crystallized with a carboxylic acid in a 2:1 ratio. The second co-crystal, although a 1:1 crystal structure, sees the carboxylic acid abandon the interaction with the pyridyl nitrogen atom and opt for an O-H $\cdots$ O interaction with the amide carbonyl oxygen atom. More crystal structures would be required to say for certain as to whether this behavior is typical of this supramolecular reagent and, indeed, whether it can be relied upon in supramolecular synthesis.

#### 2.5.4.2 Benzimidazole amides

Isonicotinamide has proven itself to be selective in its binding preferences, with only 1 case out of 29 seeing binding take place to the amide moiety. There are fewer examples of 1:1, neutral crystal structures with benzimidazoles, only two in fact. They do both, however, show binding to the most basic side. There is only one 1:1 example of azaindole amide, and this shows binding to the amide moiety. The supramolecular yields are displayed in Figure 2.17.

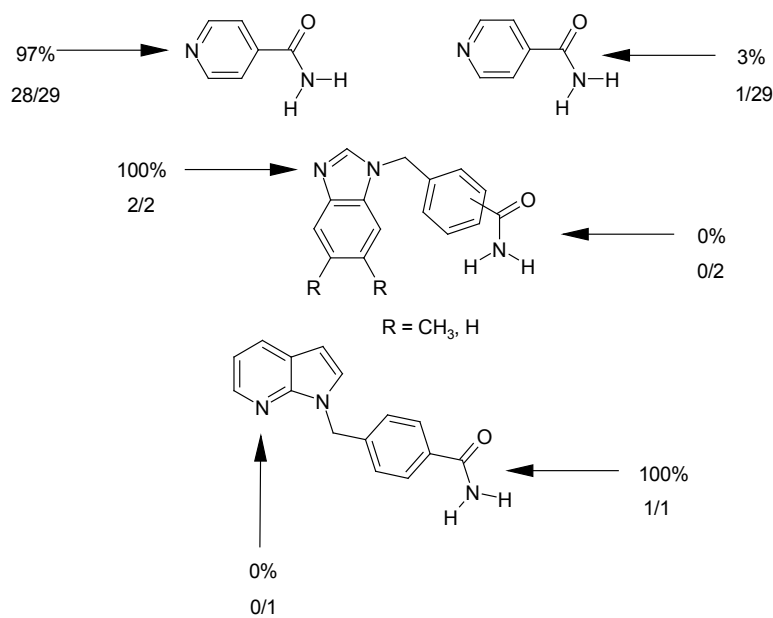


**Figure 2.17** Binding preferences of the supramolecular reagents.

## 2.6 Conclusions

Five new N-heterocyclic amides were synthesised and five co-crystals were obtained with them. Both of the crystal structures obtained with the benzimidazole amides, displayed best donor/best acceptor behaviour. IR spectroscopy showed O-H...N bands in 8 out of 13 cases. The phenylimidazole amides showed O-H...N bands in 10 out of 11 cases. Azaindole amide **2** only showed O-H...N bands in 4 out 12 cases. It seems that the increase in basicity (and increased negative MEP) corresponds to an increased selectivity for a carboxylic acid for the heterocyclic nitrogen over the amide moiety. Calculated electrostatic potentials can offer a reasonable guideline into the prediction of the selectivity of these supramolecular reagents.

This study has highlighted some of the problems that can occur during supramolecular synthesis. First, the solubility of the supramolecular reagent has to be comparable the reacting component to prevent it from crystallizing homomerically. Second, in order to induce selectivity, the two binding sites have to be different, but the basicity has to be such that the supermolecule remains neutral. This is important in order to maintain structural predictability.

---

## References:

- <sup>1</sup> (a) C. B. Aakeröy, A. M. Beatty, B. A. Helfrich, *J. Am. Chem. Soc.*, 2002, **124**, 14425; (b) I. D. H. Oswald, W. D. S. Motherwell, S. Parsons, *Acta Cryst., Sect. E: Struct. Rep. Online*, 2005, E**61**, o3161; (c) S. L. Reddy, N. J. Babu, A. Nangia, *Chem. Comm.*, 2006, **13**, 1369; (d) S. Basavoju, D. Boström, S. P. Velaga, *Crys. Growth Des.*, 2006, **6**, 2699.
- <sup>2</sup> B. R. Bhogala, S. Basavoju, A. Nangia, *CrystEngComm*, 2005, **7**, 551; (b) C. B. Aakeröy, A. M. Beatty, B. A. Helfrich, M. Nieuwenhuyzen, *Cryst. Growth Des.*, 2003, **3**, 159; (c) C. C. Seaton, A. Parkin, C. C. Wilson, N. Blagden, *Cryst. Growth Des.*, 2008, **8**, 363.
- <sup>3</sup> (a) C. B. Aakeröy, A. M. Beatty, B. A. Helfrich, *Angew. Chem. Int. Ed.*, 2001, **40**, 3240; (b) C. B. Aakeröy, A. M. Beatty, B. A. Helfrich, M. Nieuwenhuyzen, *Cryst. Growth Des.*, 2003, **3**, 159.
- <sup>4</sup> M. C. Etter, *Acc. Chem. Res.*, 1990, **23**, 120; M. C. Etter, *J. Phys. Chem.*, 1991, **95**, 4601.
- <sup>5</sup> C. B. Aakeröy, J. Desper, J. F. Urbina, *Cryst. Growth Des.*, 2005, **5**, 1283.
- <sup>6</sup> CSD codes: WANCOE, WANCUK.
- <sup>7</sup> The predicted value of pK<sub>a</sub> was obtained using the ACD/I-Lab Web service (ACD/pKa 8.03), Advanced Chemistry Development, Inc. ([www.acdlabs.com](http://www.acdlabs.com)).
- <sup>8</sup> (a) N. V Drichko, G. Y. Kerenskai, V. M. Schreiber, *J. Mol. Struct.*, 1999, **477**, 127; (b) J. P. Castaneda, G. S. Denisov, S. Y. Kucherov, V. M. Schreiber, A. V. Shurukhina, *J. Mol. Struct.*, 2003, **660**, 25.
- <sup>9</sup> C. B. Aakeröy, B. M. T. Scott, J. Desper, *New J. Chem.*, 2007, **31**, 2044.
- <sup>10</sup> M. Rafilovich, J. Bernstein, M. B. Hickey, M. Tauber, *Cryst. Growth Des.*, 2007,
- <sup>11</sup> C. B. Aakeröy, M. E. Fasulo, J. Desper, *Mol. Pharm.*, 2007, **4**, 317.
- <sup>12</sup> (a) S. L. Johnson, K. A. Rumon, *J. Phys. Chem.*, 1965, **69**, 74; (b) K.-S Huang, D. Britton, M. C. Etter, S. R. Byrn, *J. Mater. Chem.*, 1997, **7**, 713–720.
- <sup>13</sup> (a) H. Aghabozorg, M. Ghadermazi, S. Sheshmani, *Anal. Sci.: X-ray Struct. Anal. Online.*, 2000, **22**, x251; (b) B. R. Bhogala, S. Basavoju, A. Nangia, *CrystEngComm.*, 2005, **7**, 551.
- <sup>14</sup> Search included pyrazole, triazole, indazole and 7-azaindole.

# CHAPTER 3 - Asymmetric Ditopic Ligands in the Design and Synthesis of Binary Supramolecules

## 3.1 Introduction

The previous chapter described bifunctional supramolecular reagents that differed significantly in terms of their binding sites. This chapter will deal with ditopic supramolecular reagents that are more closely related. This will enable a comparison in terms of their binding selectivities in a more sophisticated manner. Preliminary work in this area includes a series of pyridyl/benzimidazol-1-yl molecules where the two hydrogen bond acceptor sites differ primarily in terms of their basicity<sup>1</sup>, Figure 3.1.

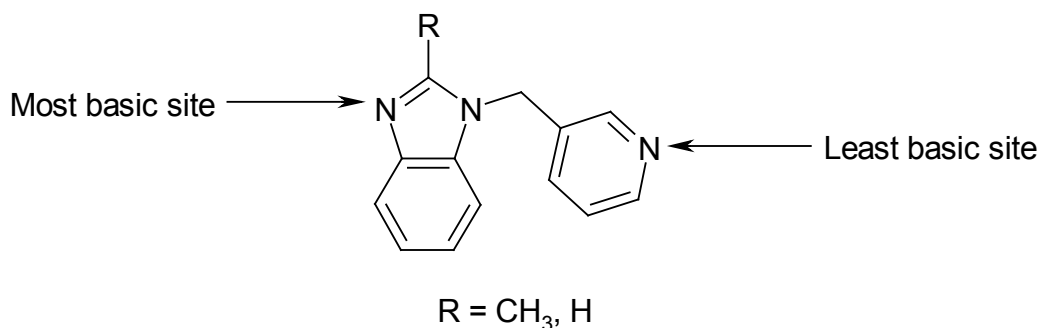


**Figure 3.1** Supramolecular reagent equipped with two binding sites.

These supramolecular reagents have worked well in the synthesis of ternary supermolecules,<sup>1</sup> with the strongest acid forming a hydrogen bond with the strongest base (imidazole) and the weaker acid binding to the weaker base (pyridine, based on pK<sub>a</sub> values). There are currently five ternary co-crystals with these types of molecules<sup>1</sup> (both in the literature and unpublished results) and two 1:1 co-crystals. To find out more about the binding preferences of these types of supramolecular reagents, this chapter will introduce other heterocycles of varying hydrogen-bond acceptor strength, Figure 3.2.

### 3.2 How selective are the supramolecular reagents?

In order to probe the binding preferences of the supramolecular reagents without bias, the two sites need to be geometrically similar, in order to remove any steric interference, Figure 3.2.

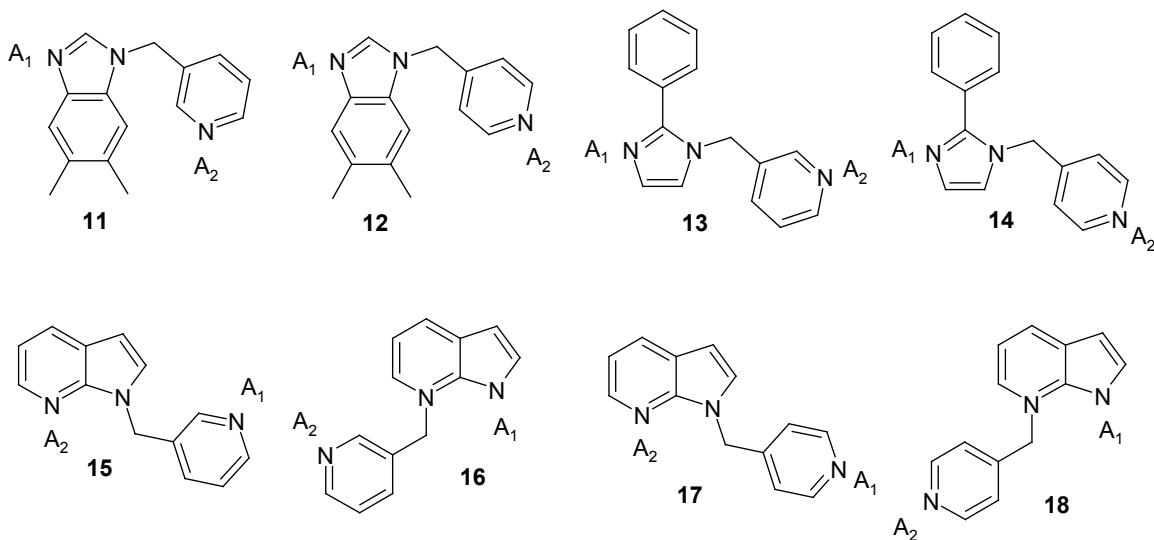


**Figure 3.2** Supramolecular reagents synthesized here.

Rather than using  $pK_a$  values as a guideline to finding the best donor/best acceptor, a series of AM1 calculations will be employed to calculate the charges on each molecule.

#### 3.2.1 Goals

- 1) To synthesise eight target molecules, Figure 3.2.
- 2) To carry out a series of AM1 calculations to rank the binding sites in terms of charge.
- 3) Employ **11-18** in a series of co-crystallization reactions in order to find if the best-donor/donor best-acceptor approach, in terms of charge calculations, is reliable.

## 3.3 Experimental

### 3.3.1 Synthesis of asymmetric acceptors

#### 3.3.1.1 Synthesis of 1-[(3-pyridyl)methyl]-5,6-dimethylbenzimidazole, 11

5,6-Dimethylbenzimidazole (1.04g, 7.10 mmol) was dissolved in 20 mL dry THF with heat and stirring in a 250 mL round-bottomed flask under a N<sub>2</sub> atmosphere. NaOH (2.84 g, 71.0 mmol) was added and the mixture was stirred for 2 h, upon which a suspension of 3-picolyl chloride hydrochloride (1.17 g, 7.10 mmol) in 20 mL dry THF, and subsequent washings with THF to ensure that all of the 3-picolyl chloride hydrochloride was transferred. The mixture was stirred at 75 °C for 3 days under a N<sub>2</sub> atmosphere, after which 7 mL distilled water was added to dissolve the NaOH and NaCl. The two layers were separated using a separatory funnel, and the THF was dried over anhydrous MgSO<sub>4</sub>. The MgSO<sub>4</sub> was filtered by vacuum filtration, and the filtrate was concentrated *via* rotary evaporation to produce a brownish-orange solid. The product was recrystallized from hot toluene to produce brown rods. Yield 0.703 g (42 %); mp: 150-153 °C; <sup>1</sup>H NMR (DMSO-*d*<sub>6</sub>, 400 MHz) δ 2.34 (s, 3H), 2.37 (s, 3H), 5.34 (s, 2H), 7.03 (s, 1H), 7.23-7.26 (m, 1H), 7.38 (d, 1H, *J* = 8.4 Hz), 7.59 (s, 1H), 7.86 (s, 1H), 8.57 (d, 1H *J* = 4.4 Hz), 8.60 (s, 1H); <sup>13</sup>C NMR (400 MHz, CDCl<sub>3</sub>-*d*) δ 20.11, 20.45, 46.08, 109.77, 120.28, 123.80, 131.43, 131.48, 132.94, 132.62, 134.47, 142.04, 142.26, 148.23, 150.20.

#### 3.3.1.2 Synthesis of 1-[(4-pyridyl)methyl]-5,6-dimethylbenzimidazole, 12

5,6-Dimethylbenzimidazole (2.175 g, 14.70 mmol) was dissolved in 30 mL dry THF with heat and stirring in a 250 mL round-bottomed flask under a N<sub>2</sub> atmosphere. NaOH (5.87 g, 147 mmol) was added and the mixture was stirred for 2 h, upon which, a suspension of 4-picolyl chloride hydrochloride (2.411 g, 14.70 mmol) in 30 mL dry THF, and subsequent washings with THF to ensure that all of the 4-picolyl chloride hydrochloride was transferred. The mixture was stirred at 75 °C for 16 h under a N<sub>2</sub> atmosphere, after which 15 mL distilled water was added to dissolve the NaOH and NaCl. The two layers were separated using a separatory funnel, and the THF was dried over anhydrous MgSO<sub>4</sub>. The MgSO<sub>4</sub> was filtered by vacuum filtration, and the filtrate



was concentrated *via* rotary evaporation to produce a pale brown solid. The product was recrystallized from THF and ethanol to produce colorless cubes. Yield 2.387 g (69%); m.p. 182-190 °C, <sup>1</sup>H NMR (DMSO-*d*<sub>6</sub>, 200 MHz) δ 2.26 (s, 3H), 2.28 (s, 3H) 5.51 (s, 2H), 7.13 (dd, 2H, *J*<sub>1</sub> = 1.2 Hz, *J*<sub>2</sub> = 4 Hz), 7.22 (s, 1H), 7.45 (s, 1H), 8.25 (s, 1H), 8.50 (dd, 2H *J*<sub>1</sub> = 1.6 Hz, *J*<sub>2</sub> = 4.4 Hz); <sup>13</sup>C NMR (400 MHz, CDCl<sub>3</sub>-*d*) δ 20.26, 20.57, 47.36, 109.79, 120.57, 121.28, 131.59, 132.14, 132.74, 142.43, 142.50, 144.95, 150.42.

### 3.3.1.3 *Synthesis of 1-[(3-pyridyl)methyl]-2-phenylimidazole, 13*

2-Phenylimidazole (3.020 g, 20.80 mmol) was dissolved in 30 mL dry THF with stirring in a 250 mL round-bottomed flask under a N<sub>2</sub> atmosphere. NaOH (8.32 g, 208 mmol) was added and the mixture was stirred for 2 h, upon which, a suspension of 3-picolyl chloride hydrochloride (3.41 g, 20.8 mmol) in 30 mL dry THF, and subsequent washings with THF to ensure that all of the 3-picolyl chloride hydrochloride was transferred. The mixture was stirred at 75 °C for 3 days under a N<sub>2</sub> atmosphere, after which 50 mL distilled water was added to dissolve the NaOH and NaCl. The two layers were separated using a separatory funnel, and the THF was dried over anhydrous MgSO<sub>4</sub>. The MgSO<sub>4</sub> was filtered by vacuum filtration, and the filtrate was concentrated *via* rotary evaporation to produce a brown oil. Yield: 0.586 g (12%); mp: 69-72 °C; <sup>1</sup>H NMR (400 MHz, DMSO-*d*<sub>6</sub>): δ 5.39 (s, 2H), 7.07 (d, 1H, *J* = 1.6 Hz), 7.35 (m, 3H), 7.43 (m, 3H), 7.55 (m, 2H), 8.25 (d, 1H, *J* = 1.2 Hz), 8.45 (dd, 1H *J* = (need values on NMR)); <sup>13</sup>C NMR (400 MHz, CDCl<sub>3</sub>-*d*) δ 48.05, 121.00, 123.89, 128.78, 128.84, 129.18, 129.32, 130.24, 132.56, 134.42, 148.24, 148.30, 149.47.

### 3.3.1.4 *Synthesis of 1-[(4-pyridyl)methyl]-2-phenylimidazole, 14*

2-Phenylimidazole (1.262 g, 8.75 mmol) was dissolved in 30 mL dry THF with stirring in a 250 mL round-bottomed flask under a N<sub>2</sub> atmosphere. NaOH (3.5 g, 87.5 mmol) was added and the mixture was stirred for 2 h, upon which, a suspension of 4-picolyl chloride hydrochloride (1.44 g, 8.75 mmol) in 30 mL dry THF, and subsequent washings with THF to ensure that all of the 4-picolyl chloride hydrochloride was transferred. The mixture was stirred at 75 °C for 2 days under a N<sub>2</sub> atmosphere, after which 10 mL distilled water was added to dissolve the NaOH and NaCl. The two layers

were separated using a separatory funnel, and the THF was dried over anhydrous MgSO<sub>4</sub>. The MgSO<sub>4</sub> was filtered by vacuum filtration, and the filtrate was concentrated *via* rotary evaporation to produce a brown oil. Subsequent purification via column chromatography (3:1 hexanes/ethyl acetate) yielded a pale brown solid. Yield: 0.994 g (48%); mp: 33-38 °C, <sup>1</sup>H NMR (400 MHz, CDCl<sub>3</sub>-*d*) δ 5.21 (s, 2H), 6.95-6.96 (m, 3H), 6.98 (d, 1H, *J* = 1.2 Hz), 7.22 (d, 1H, *J* = 1.2 Hz), 7.36-7.38 (m, 1H), 7.44-7.46 (m, 2H), 8.56 (dd, 1H, *J*<sub>1</sub> = 1.6 Hz, 4.4 Hz); <sup>13</sup>C NMR (CDCl<sub>3</sub>-*d*, 400 MHz) δ 49.20, 121.12, 121.29, 128.59, 128.71, 129.14, 129.33, 129.92, 146.11, 148.34, 150.33.

### 3.3.1.5 Synthesis of 1-[(3-pyridyl)methyl]-7-azaindole and 7-[(3-pyridyl)methyl]-7-azaindole, 15 and 16

7-Azaindole (2.02 g, 17.0 mmol) was dissolved in 30 mL dry THF with stirring in a 250 mL round-bottomed flask under a N<sub>2</sub> atmosphere. NaOH (6.84 g, 171 mmol) was added and the mixture was stirred for 2 h, upon which, a suspension of 3-picolyl chloride hydrochloride (2.79 g, 17.0 mmol) in 30 mL dry THF, and subsequent washings with THF to ensure that all of the 3-picolyl chloride hydrochloride was transferred. The mixture was stirred at 75 °C for 3 days under a N<sub>2</sub> atmosphere, after which 50 mL distilled water was added to dissolve the NaOH and NaCl. The two layers were separated using a separatory funnel, and the THF was dried over anhydrous MgSO<sub>4</sub>. The MgSO<sub>4</sub> was filtered by vacuum filtration, and the filtrate was concentrated *via* rotary evaporation to produce a brown oil. Purification by column chromatography (hexanes/ethyl acetate 15:1 → 100% Ethyl acetate) yielded the two isomers.

**15:** Colorless oil, yield: 0.343 g (10 %); <sup>1</sup>H NMR (400 MHz, CDCl<sub>3</sub>-*d*) δ 5.53 (s, 2H), 6.51 (d, 1H, *J* = 3.6 Hz), 7.10 (dd, 1H, *J*<sub>1</sub> = 8 Hz, *J*<sub>2</sub> = 4.8 Hz), 7.19 (d, 1H), 7.21 (dd, 1H, *J*<sub>1</sub> = Hz, *J*<sub>2</sub> = Hz), 7.49-7.42 (m, 1H), 7.94 (dd, 1H, *J*<sub>1</sub> = 8 Hz, *J*<sub>2</sub> = 1.2 Hz), 8.36 (dd, 1H, *J*<sub>1</sub> = 4.4 Hz, *J*<sub>2</sub> = 1.6 Hz), 8.52 (dd, 1H, *J*<sub>1</sub> = Hz, *J*<sub>2</sub> = Hz), 8.58 (d, 1H, *J* = 2 Hz).

**16:** Yellow oil, yield: 0.321 g (9%); <sup>1</sup>H NMR (400 MHz, CDCl<sub>3</sub>-*d*) δ 5.90 (s, 2H), 6.70 (d, 1H, *J* = 2.4 Hz), 6.85 (t, 1H, *J* = 6.8 Hz), 7.23 (dd, 1H, *J* = 7.6 Hz), 7.59 (d, 1H, *J* = 6.4 Hz), 7.73-7.76 (m, 1H), 7.94 (d, 1H, *J* = 2.4 Hz), 8.11 (d, 1H, *J*<sub>1</sub> = 7.2 Hz), 8.56 (dd, 1H, *J*<sub>1</sub> = 5.2 Hz, *J*<sub>2</sub> = 1.6 Hz), 8.69 (d, 1H, *J* = 2 Hz);

### 3.3.1.6 Synthesis of 1-[(4-pyridyl)methyl]-7-azaindole and 7-[(4-pyridyl)methyl]-7-azaindole, 17 and 18

7-Azaindole (4.66 g, 39.0 mmol) was dissolved in 30 mL dry THF with stirring in a 250 mL round-bottomed flask under a N<sub>2</sub> atmosphere. NaOH (15.6 g, 390 mmol) was added and the mixture was stirred for 2 h, upon which, a suspension of 4-picolyl chloride hydrochloride (8.96 g, 55.0 mmol) in 30 mL dry THF, and subsequent washings with THF to ensure that all of the 3-picolyl chloride hydrochloride was transferred, was added. The mixture was stirred at 75 °C for 3 days under a N<sub>2</sub> atmosphere, after which 30 mL distilled water was added to dissolve the NaOH and NaCl. The two layers were separated using a separatory funnel, and the THF was dried over anhydrous MgSO<sub>4</sub>. The MgSO<sub>4</sub> was filtered by vacuum filtration, and the filtrate was concentrated *via* rotary evaporation to produce a viscous, dark brown oil. Purification by column chromatography (hexanes/ethyl acetate 8:1 → 100% ethyl acetate) yielded the two isomers.

**17:** Colorless oil, yield: 1.322 g (16 %); <sup>1</sup>H NMR (400 MHz, CDCl<sub>3</sub>-*d*) δ 5.42 (s, 2H), 6.47 (d, 1H, *J* = 4.8 Hz), 6.92 (d, 2H, *J* = 5.6 Hz), 7.02 (dd, 1H, *J*<sub>1</sub> = 5.6 Hz, *J*<sub>2</sub> = 8.8 Hz), 7.11 (d, 1H, *J* = 3.6 Hz), 7.87 (d, 1H, *J* = 8 Hz), 8.27 (d, 1H, *J* = 4.8 Hz), 8.43 (d, 2H, *J* = 5.6 Hz); <sup>13</sup>C NMR (CDCl<sub>3</sub>-*d*, 200 MHz) δ 46.32, 100.43, 115.87, 120.03, 121.39, 127.50, 128.69, 142.92, 146.55, 129.67.

**18:** Yellow oil, yield: 0.637 g (8%); <sup>1</sup>H NMR (400 MHz, CDCl<sub>3</sub>-*d*) δ 5.77 (s, 2H), 6.64 (d, 1H, *J* = 2.4 Hz), 6.79 (dd, 1H, *J*<sub>1</sub> = 6.4 Hz, *J*<sub>2</sub> = 7.6 Hz), 7.03 (d, 2H, *J* = 6 Hz), 7.49 (d, 1H, *J* = 6 Hz), 7.83 (d, 1H, *J* = 2.8 Hz), 8.06 (dd, 1H, *J*<sub>1</sub> = 0.8 Hz, *J*<sub>2</sub> = 7.6 Hz), 8.43 (dd, 2H, *J*<sub>1</sub> = 1.6 Hz, *J*<sub>2</sub> = 4.4 Hz); <sup>13</sup>C NMR (CDCl<sub>3</sub>-*d*, 200 MHz) δ 54.29, 101.77, 109.23, 121.98, 128.63, 130.85, 143.95, 145.64, 148.56, 150.07, 150.20.

### 3.3.2 Synthesis of co-crystals and salts

#### 3.3.2.1 General synthesis of co-crystals

Although only the reactions that produced single crystals suitable for X-ray crystallography are listed here, each supramolecular reagent was set up in 10 or more co-crystallization reactions with different carboxylic acids and oximes. Since supramolecular reagents **15**, **16**, **17**, and **18** were oils, it was difficult to obtain single

crystals. Solids produced in these reactions were analyzed by IR spectroscopy and the results are presented in Table 3.2. All co-crystal reactions were set up in a 1:1 ratio of ligand to carboxylic acid or oxime, with the exception of **11d**, which was set up in a 2:1 ratio (ligand:carboxylic acid).

### ***3.3.2.2 Syntheses of 1-[(4-pyridyl)methyl]-5,6-dimethylbenzimidazole and 1-[(3-pyridyl)methyl]-5,6-dimethylbenzimidazole co-crystals, 11(a-i) and 12(a-g)***

1-[(4-Pyridyl)methyl]-5,6-dimethylbenzimidazole or 1-[(3-pyridyl)methyl]-5,6-dimethylbenzimidazole (0.02 g, 0.084 mmol) was dissolved in ethanol with slight heat. A solution of the acid or oxime (0.084 mmol) in ethanol was added and the solution was allowed to evaporate at room temperature. Crystals suitable for X-ray crystallography were usually obtained within approximately 2 weeks. The data for the co-crystals/salts obtained are displayed in Table 3.1.

### ***3.3.2.3 Syntheses of 1-[(4-pyridyl)methyl]-2-phenylimidazole and 1-[(3-pyridyl)methyl]-2-phenylimidazole co-crystals, 13a and 14a***

1-[(4-Pyridyl)methyl]-2-phenylimidazole or 1-[(3-pyridyl)methyl]-2-phenylimidazole (0.015 g, 0.064 mmol) was dissolved in ethanol. A solution of the acid or oxime (0.064 mmol) in ethanol was added and the solution was allowed to evaporate at room temperature. Crystals suitable for X-ray crystallography were usually obtained within approximately 2 weeks. The data for the co-crystals obtained are displayed in Table 3.1.

### ***3.3.2.4 Synthesis of 1-[(3-pyridyl)methyl]-7-azaindole pentamethylbenzoic acid, 15a***

1-[(3-pyridyl)methyl]-7-azaindole (0.017 g, 0.082 mmol) was dissolved in ethanol. Pentamethylbenzoic acid (0.016 g, 0.082 mmol) was added and the solution was allowed to evaporate at room temperature. Crystals suitable for X-ray crystallography were obtained after approximately 2 weeks (Table 3.1).

**Table 3.1** Crystal data for structures **11a-i**, **12a-d**, **13a**, **14a**, and **15a**

Co-crystal	Acid/oxime	Co-crystal mp (° C)	Stoichiometry	Morphology
<b>11a</b>	4-Chlorobenzoic acid	125-130	1:1	Colorless plate
<b>11b</b>	Pentafluorobenzoic acid	149-153	1:1	Colorless plate
<b>11c</b>	Fumaric acid	150-155	1:1	Colorless plate
<b>11d</b>	Pentamethylbenzoic acid	170-175	1:1	Colorless plate
<b>11e</b>	Tetrafluoroiodo- benzoic acid	155-158	1:1	Colorless prism
<b>11f</b>	3,5-Dinitrobenzoic acid	168-173	2:1	Colorless plate
<b>11g</b>	4-Nitrobenzoic acid	176-180	2:1	Amber plate
<b>11h</b>	4-Iodobenzoic acid	145-148	3:2	Colorless needle
<b>11i</b>	4-Bromo-phenylcyanoxime	110-115	1:1	Colorless plate
<b>12a</b>	4-N, N <sup>3</sup> -dimethyl aminobenzoic acid	136-140	1:1	Colorless plate
<b>12b</b>	3-Iodobenzoic acid	177-180	1:1	Colorless prism
<b>12c</b>	3-Cyanobenzoic acid	130-137	2:1	Colorless plate
<b>12d</b>	Oxalic acid	200-204	2:1	Colorless plate
<b>12e</b>	3-Fluorobenzoic acid	94-100	2:1	Colorless plate
<b>12f</b>	Tetrafluoroiodo aldoxime	190-195	1:1	Orange plate
<b>12g</b>	4-Fluoro-phenylcyanoxime	114-116	1:1	Colorless plate
<b>13a</b>	4-Nitrobenzoic acid	113-117	2:1	Orange plate
<b>14a</b>	4-Nitrobenzoic acid	165-170	2:1	Colorless plate
<b>15a</b>	Pentamethylbenzoic acid	100-110	2:1	Red plate

### 3.4 Results

**Table 3.2** Results of co-crystallizations (from IR O-H...N bands) with supramolecular reagents **15**, **16**, **17** and **18**

Supramolecular Reagent	No. Co-crystals Set up	No. Co-crystals formed	Supramolecular Yield
1-[(3-pyridyl)methyl]-7-azaindole, <b>15</b>	10	10	100%
1-[(3-pyridyl)methyl]-7-azaindole, <b>16</b>	8	6	75%
1-[(4-pyridyl)methyl]-7-azaindole, <b>17</b>	10	9	90%
1-[(4-pyridyl)methyl]-7-azaindole, <b>18</b>	10	3	30%

**Table 3.3** Hydrogen bond geometries for **11a-i**, **12a-g**, **13a**, **14a**, and **15a**

Co-crystal	D-H...A	D(D-H)	d(H...A)	d(D...A)	<(DHA)
<b>11a</b>	O(41)-H(41)...N(31)	1.01(2)	1.64(2)	2.643(2)	177(2)
<b>11b</b>	N(13)-H(13)...O(41)	1.000(16)	1.593(16)	2.5822(13)	169.0(14)

<b>11c<sup>i</sup></b>	O(41)-H(41)...N(13)	1.26(4)	1.29(4)	2.540(3)	174(3)
	O(51)-H(51)...N(31)	0.94(4)	1.71(4)	2.653(3)	175(3)
	O(1S)-H(1A)...O(42)	0.77(4)	2.12(5)	2.819(5)	151(6)
	O(1S)-H(1B)...O(42) <sup>a</sup>	0.74(4)	3.21(6)	3.308(6)	91(5)
<b>11d</b>	O(61)-H(61)...O(41)	1.03(3)	1.53(3)	2.547(2)	169(3)
	N(13)-H(13)...O(41)	1.03(2)	1.60(2)	2.629(2)	175(2)
<b>11e</b>	N(13)-H(13)...O(41)	0.91(2)	1.69(2)	2.5908(18)	172(2)
	O(1S)-H(1S)...O(41)	0.86(3)	1.87(3)	2.719(2)	170(3)
<b>11f</b>	N(31)-H(31)...O(51)	1.22(11)	1.39(11)	2.593(11)	169(10)
	O(41)-H(41)...N(13)	1.20(13)	1.51(13)	2.591(12)	146(10)
<b>11g</b>	O(41)-H(41)...N(31)	0.92(3)	1.72(3)	2.637(3)	179(3)
	O(51)-H(51)...N(13)	0.96(3)	1.64(3)	2.600(2)	175(3)
<b>11h</b>	O(41)-H(41)...N(31)	0.84	1.84	2.680(2)	179.3
	O(61)-H(61)...N(13)	0.84	1.89	2.723(3)	168.7
<b>11i</b>	O(47)-H(47)...N(13)	0.907(18)	1.704(18)	2.6100(15)	177.6(17)
<b>12a</b>	O(41)-H(41)...N(31)	1.08(4)	1.52(4)	2.604(4)	174(3)
<b>12b</b>	O(31)-H(31)...N(21)	0.84	1.76	2.600(4)	178.2
	O(61)-H(61)...N(51)	0.84	1.77	2.608(5)	171.6
<b>12c</b>	O(41)-H(41)...N(13)	0.941(16)	1.682(16)	2.6204(14)	174.9(14)
	O(51)-H(51)...N(31)	0.963(16)	1.681(17)	2.6328(14)	169.0(15)
<b>12d<sup>ii</sup></b>	O(41)-H(41)...N(13)	0.958(13)	1.663(13)	2.6137(10)	170.8(12)
	O(1S)-H(1A)...O(44)	0.883(15)	1.925(15)	2.8068(10)	176.2(13)
	O(1S)-H(1B)...O(1S) <sup>a</sup>	0.89(3)	1.94(3)	2.8287(16)	172(3)
	O(1S)-H(1C)...O(1S) <sup>b</sup>	0.87(3)	1.96(3)	2.8252(16)	178(3)
<b>12e</b>	O(41)-H(41)...N(13)	0.90(2)	1.71(2)	2.603(2)	174(2)
	O(51)-H(51)...N(31)	1.03(2)	1.58(2)	2.596(2)	171(2)
<b>12f</b>	O(47)-H(47)...N(13)	0.76(2)	1.93(2)	2.6836(17)	180(3)
<b>12g</b>	O(47)-H(47)...N(13)	(1.047(10))	1.596(10)	2.6047(10)	175.9(8)
<b>13a</b>	O(41)-H(41)...N(13)	0.84	1.76	2.567(4)	159.9
	O(51)-H(51)...N(21)	0.84	1.83	2.662(4)	167.8

<b>14a</b>	O(41)-H(41)...N(11)	1.020(17)	1.561(17)	2.5748(14)	171.4(15)
	O(51)-H(51)...N(31)	1.031(17)	1.575(17)	2.6029(14)	174.7(15)
<b>15a</b>	O(41)-H(41)...N(21)	0.92(5)	1.78(5)	2.699(4)	177(5)
	O(61)-H(61)...N(18)	1.06(5)	1.66(5)	2.712(5)	174(4)

(i)<sup>a</sup> -x+2,-y+1,-z+1; (ii)<sup>a</sup> -x,y,-z+1/2; <sup>b</sup> -x,-y+1,-z+1.

### 3.4.1 Crystal structure of 1-[(3-pyridyl)methyl]-5,6-dimethylbenzimidazole, **11**

The crystal structure of **11** shows a single molecule of 1-[(3-pyridyl)methyl]-5,6-dimethylbenzimidazole, Figure 3.3. Both the imidazole and pyridyl nitrogen atoms are interacting with methylene protons of adjacent molecules of **11**. (C-H...N: 3.445 Å and 3.541 Å, respectively). The proton in the 2-position on benzimidazole, the most acidic of the molecule, does not participate in any noteworthy interactions.

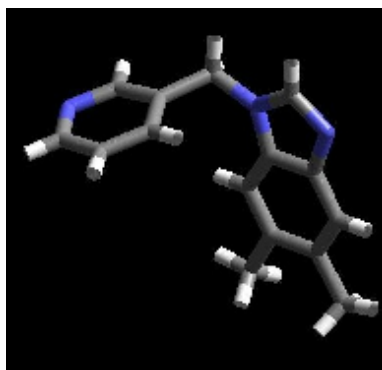


**Figure 3.3** (a) 1-[(3-pyridyl)methyl]-5,6-dimethylbenzimidazole in the crystal structure of **11**.

### 3.4.2 Crystal structure of 1-[(3-pyridyl)methyl]-2-phenylimidazole, **13**

The crystal structure of **13** shows a single molecule of 1-[(3-pyridyl)methyl]-2-phenylimidazole, Figure 3.4. The imidazole nitrogen atom interacts with an aromatic C-H proton of an adjacent pyridyl ring (C-H...N: 3.402 Å), and the pyridyl nitrogen atom interacts with a methylene C-H proton (C-H...N: 3.374 Å). There are no  $\pi$ - $\pi$  interactions within the crystal structure of this molecule.

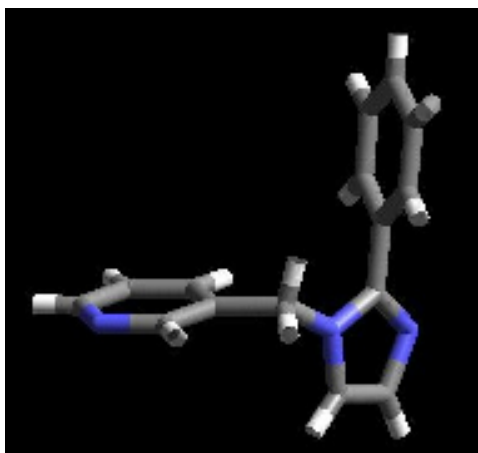


**Figure 3.4** 1-[(3-Pyridyl)methyl]-2-phenylimidazole in the crystal structure of **13**.

### *3.4.3 Crystal structure of 1-[(3-pyridyl)methyl]-5,6-dimethylbenzimidazole 4-chlorobenzoic acid (1:1), 11a*

The crystal structure of **11a** contains one molecule of 1-[(3-pyridyl)methyl]-5,6-dimethylbenzimidazole and one molecule of 4-chlorobenzoic acid, Figure 3.5. 4-chlorobenzoic acid forms a hydrogen bond to the pyridyl nitrogen atom through an O-H...N interaction (Table 3.3). There are no noteworthy interactions with the benzimidazole nitrogen atom.

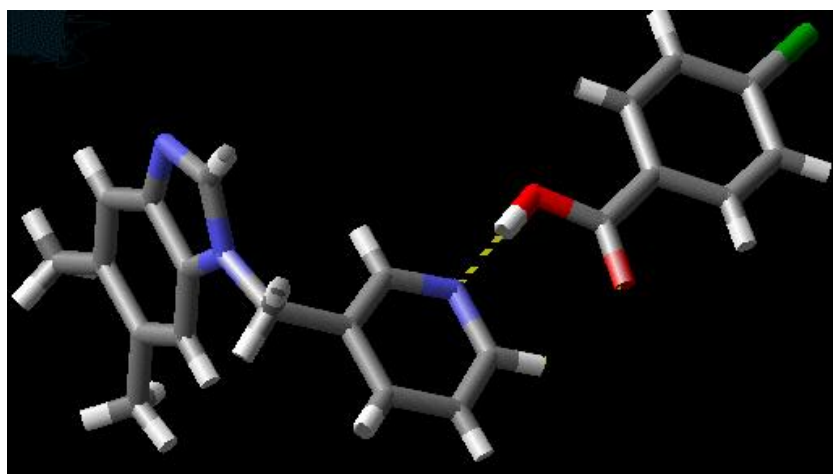


**Figure 3.5** Dimer in the crystal structure of **11a**.



#### 3.4.4 Crystal structure of 1-[(3-pyridyl)methyl]-5,6-dimethylbenzimidazolium pentafluoro benzoate (1:1), *11b*

The crystal structure of **11b** contains one cation of 1-[(3-pyridyl)methyl]-5,6-dimethylbenzimidazole and one pentafluorobenzoate ion, Figure 3.6. Proton transfer has taken place to the benzimidazole nitrogen atom, and there is an N-H $\cdots$ O $^-$  bond connecting the ion pairs (Table 3.3). There are no noteworthy interactions with the pyridyl nitrogen atom.

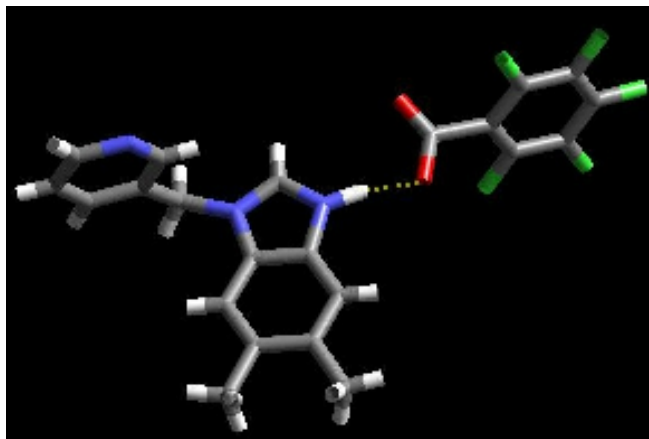


**Figure 3.6** Ion pair in the crystal structure of **11b**.

#### 3.4.5 Crystal structure of 1-[(3-pyridyl)methyl]-5,6-dimethylbenzimidazole fumaric acid hydrate (1:1), *11c*

The crystal structure of **11c** contains an infinite one-dimensional chain propagated via O-H $\cdots$ N hydrogen bonds between the fumaric acid molecules and the imidazole and pyridyl nitrogen atoms. The structure also contains a molecule of water in the lattice, which forms an O-H $\cdots$ O hydrogen bond with the carbonyl groups of fumaric acid, Figure 3.7. (Table 3.3).

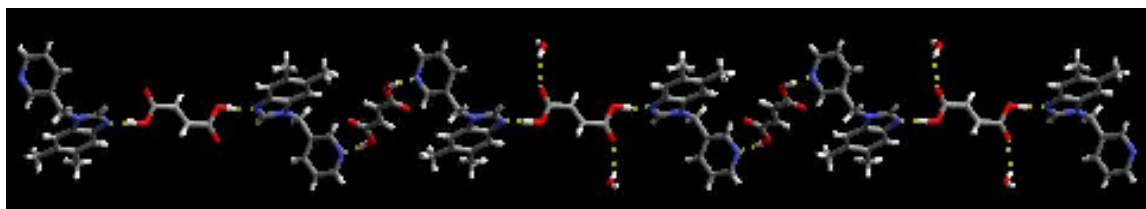


**Figure 3.7** Infinite one-dimensional chain in the crystal structure of **11c**.

### 3.4.6 Crystal structure of 1-[(4-pyridyl)methyl]-5,6-dimethylbenzimidazole 4-*N,N'*-(dimethylamino) benzoic acid (1:1), 12a

The crystal structure of **12a** contains one molecule of 1-[(4-pyridyl)methyl]-5,6-dimethylbenzimidazole and one molecule of 4-*N,N'*-(dimethylamino) benzoic acid, Figure 3.8, which are connected through an O-H $\cdots$ N hydrogen-bonding interaction between the carboxylic acid moiety and the pyridyl nitrogen atom (Table 3.3). There are no noteworthy interactions with the benzimidazole nitrogen atom.

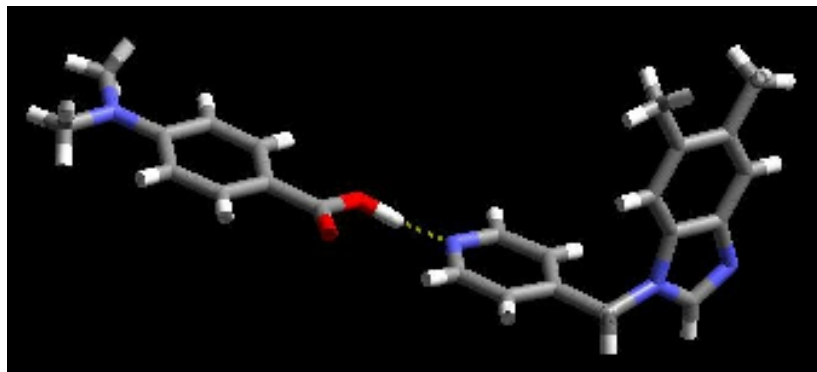


**Figure 3.8** Hydrogen bonding interaction in the crystal structure of **12a**.

### 3.4.7 Crystal structure of 1-[(3-pyridyl)methyl]-5,6-dimethylbenzimidazole 3-iodobenzoic acid (1:1), 12b

The crystal structure of **12b** contains two crystallographically inequivalent molecules of 1-[(3-pyridyl)methyl]-5,6-dimethylbenzimidazole and 3-iodobenzoic acid, Figure 3.9. 3-Iodobenzoic acid forms a hydrogen bond to the pyridyl nitrogen atom through an O-H $\cdots$ N interaction (Table 3.3). There are no noteworthy interactions with the imidazole nitrogen atom.

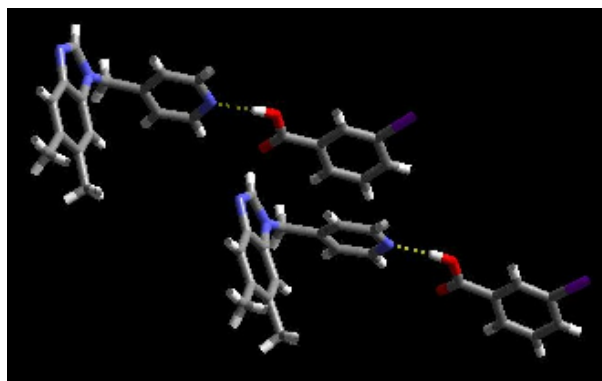


**Figure 3.9** Hydrogen-bonding interactions in the crystal structure of **12b**.

### 3.4.8 Crystal structure of 1-[(3-pyridyl)methyl]-5,6-dimethylbenzimidazolium pentamethyl benzoate pentamethylbenzoic acid (1:1:1), 11d

The crystal structure of **11d** contains one cation of 1-[(3-pyridyl)methyl]-5,6-dimethylbenzimidazole, a pentamethyl benzoate anion, and one molecule of pentamethyl benzoic acid, Figure 3.10. Proton transfer has taken place to the benzimidazole nitrogen atom, resulting in a free molecule of pentamethylbenzoic acid also being present in the lattice. The carboxylate forms an  $\text{N}^+\text{-H}\cdots\text{O}^-$  hydrogen bond with the protonated benzimidazole nitrogen atom. There are no noteworthy interactions with the pyridine nitrogen atom.

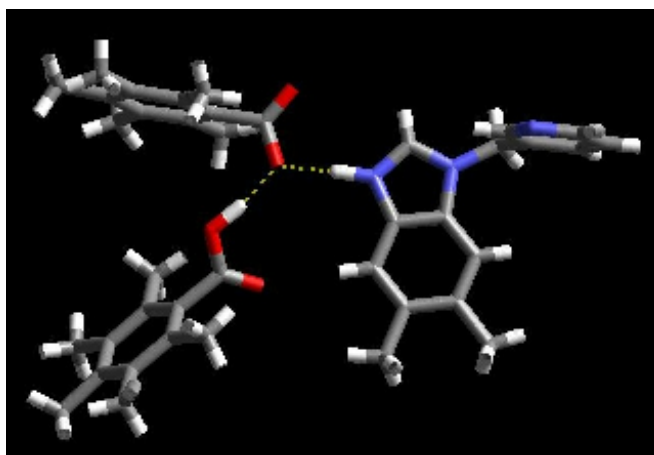


**Figure 3.10** Hydrogen bonding in the crystal structure of **11d**.

### 3.4.9 Crystal structure of 1-[(3-pyridyl)methyl]-5,6-dimethylbenzimidazolium 2,3,5,6-tetrafluoro-4-iodobenzoate ethanol (1:1:1), 11e

The crystal structure of **11e** contains a 1-[(3-pyridyl)methyl]-5,6-dimethylbenzimidazole cation, one 2,3,5,6-tetrafluoro-4-iodobenzoate anion, and one molecule of ethanol, Figure 3.11. Proton transfer has taken place to the benzimidazole nitrogen atom, and the carboxylate forms an  $\text{N}^+\text{-H}\cdots\text{O}^-$  hydrogen bond with the protonated benzimidazole nitrogen atom. The pyridine nitrogen atom participates in a weak halogen bond with the iodine atom (4.961 Å).

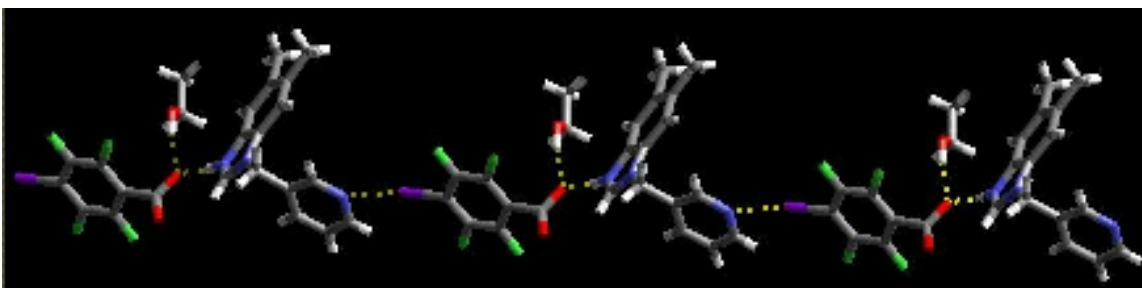


**Figure 3.11** Hydrogen and halogen bonding in the crystal structure of **11e**.

**3.4.10 Crystal structure of 1-[(3-pyridinium)methyl]-5,6-dimethylbenzimidazole 3,5-dinitrobenzoate 3,5-dinitrobenzoic acid (1:1:1), 11f**

The crystal structure of **11f** contains one cation of 1-[(3-pyridinium)methyl]-5,6-dimethylbenzimidazole, one 3,5-dinitrobenzoate ion, and one molecule of 3,5-dinitrobenzoic acid, Figure 3.12. Proton transfer has taken place to the pyridyl nitrogen atom. The carboxylate forms an  $\text{N}^+\text{-H}\cdots\text{O}^-$  hydrogen bond with the protonated pyridyl nitrogen atom. Another molecule of 3,5-dinitrobenzoic acid participates in an  $\text{O-H}\cdots\text{N}$  hydrogen bond with the benzimidazole nitrogen atom (Table 3.3).

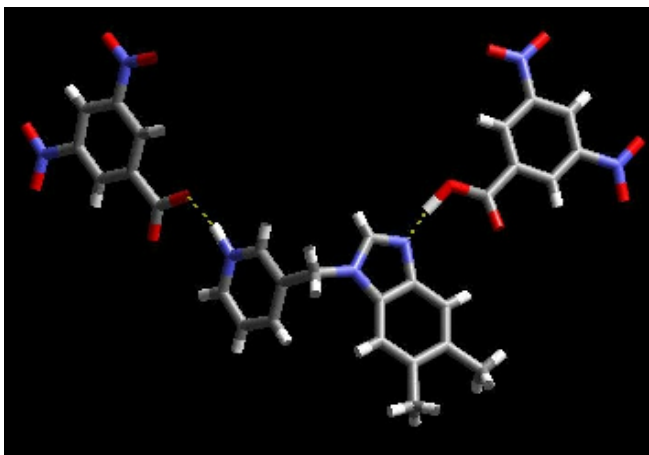


**Figure 3.12** Hydrogen bonds in the crystal structure of **11f**.

**3.4.11 Crystal structure of 1-[(3-pyridyl)methyl]-5,6-dimethylbenzimidazole 4-nitrobenzoic acid (1:2), 11g**

The crystal structure of **11g** contains one molecule of 1-[(3-pyridyl)methyl]-5,6-dimethylbenzimidazole, and two molecules of 4-nitrobenzoic acid, Figure 3.13. The two

acid molecules form O-H $\cdots$ N hydrogen bonds to the imidazole and pyridyl nitrogen atoms (Table 3.3).

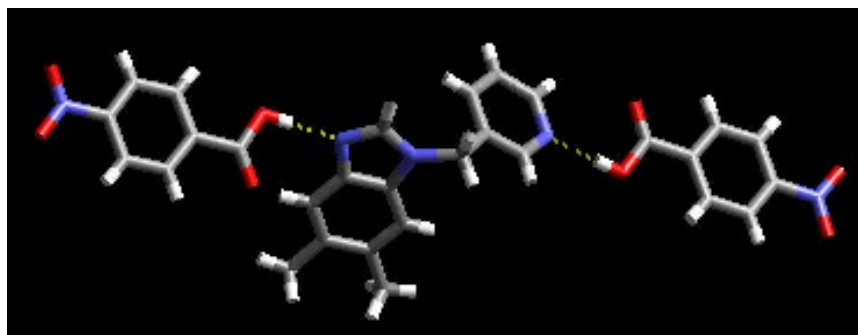


**Figure 3.13** Hydrogen bonds in the crystal structure of **11g**.

#### *3.4.12 Crystal structure of 1-[(3-pyridyl)methyl]-5,6-dimethylbenzimidazole 4-iodobenzoic acid (2:3), 11h*

The crystal structure of **11h** contains two molecules of 1-[(3-pyridyl)methyl]-5,6-dimethylbenzimidazole, and three molecules of 4-iodobenzoic acid, Figure 3.14. One molecule of 4-iodobenzoic acid forms two interactions with two molecules of 1-[(3-pyridyl)methyl]-5,6-dimethylbenzimidazole, one is an O-H $\cdots$ N hydrogen bond to an imidazole nitrogen atom, and the other is an N $\cdots$ I halogen bond with an imidazole nitrogen atom from another 1-[(3-pyridyl)methyl]-5,6-dimethylbenzimidazole molecule (N $\cdots$ I, 3.056 Å). There are no other noteworthy interactions present in this structure, and so there is no one-dimensional chain.

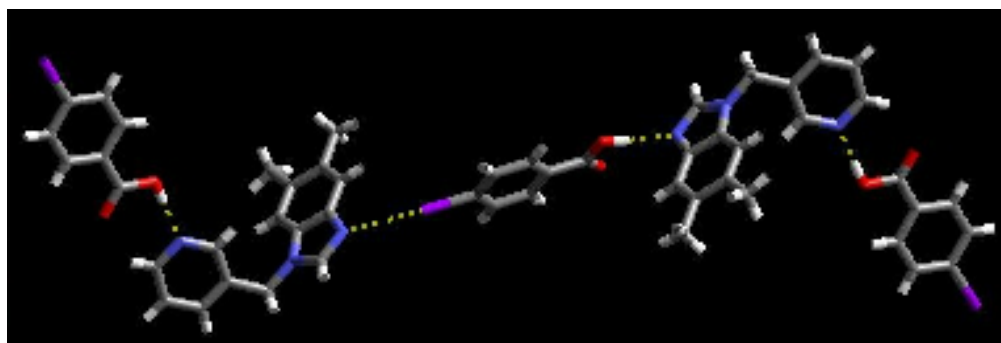


**Figure 3.14** Hydrogen- and halogen-bonding in the crystal structure of **11h**.

### 3.4.13 Crystal structure of 1-[(3-pyridyl)methyl]-5,6-dimethylbenzimidazole 4-bromophenylcyanoxime, *11i*

The crystal structure of **11i** contains one molecule of 1-[(3-pyridyl)methyl]-5,6-dimethylbenzimidazole, and one molecule of 4-bromophenylcyanoxime, Figure 3.15. The oxime forms an O-H $\cdots$ N interaction with the benzimidazole nitrogen atom (Table 3.3). The pyridyl nitrogen atom forms a weak interaction with an adjacent aromatic proton. (C-H $\cdots$ N: 3.528 Å).

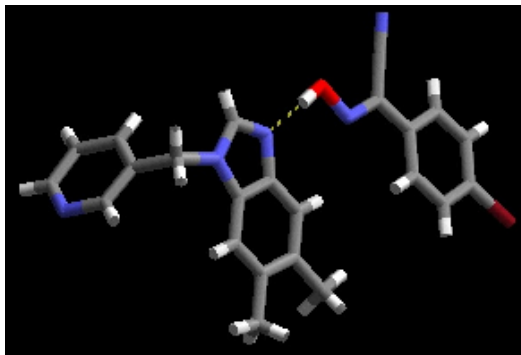


**Figure 3.15** Dimer in the crystal structure of **11i**.

### 3.4.14 Crystal structure of 1-[(4-pyridyl)methyl]-5,6-dimethylbenzimidazole 3-cyanobenzoic acid (1:2), *12c*

The crystal structure of **12c** contains one molecule of 1-[(4-pyridyl)methyl]-5,6-dimethylbenzimidazole, and two molecules of 3-cyanobenzoic acid, Figure 3.16. Both molecules of 3-cyanobenzoic acid form O-H $\cdots$ N hydrogen bonds with the pyridyl and the benzimidazole nitrogen atoms (Table 3.3).

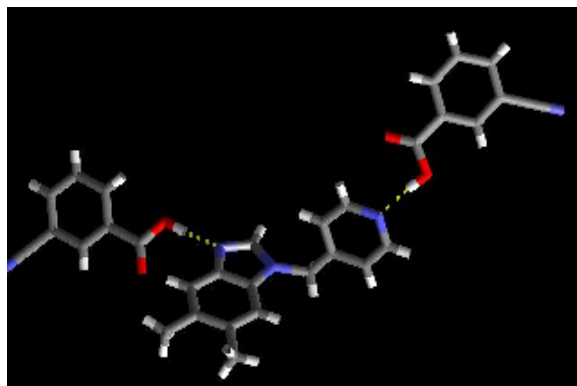


**Figure 3.16** Trimer in the crystal structure of **12c**.

#### 3.4.15 Crystal structure of 1-[(4-pyridyl)methyl]-5,6-dimethylbenzimidazole oxalic acid hydrate (1:1:1), **12d**

The crystal structure of **12d** contains one molecule of 1-[(4-pyridyl)methyl]-5,6-dimethylbenzimidazole, one molecule of oxalic acid, and one molecule of water, Figure 3.17. The oxalic acid molecule forms O-H $\cdots$ N hydrogen-bonding interactions with the benzimidazole nitrogen atom and the pyridyl nitrogen atom (Table 3.3). The water molecule forms an interaction with an oxalic acid carbonyl oxygen atom (Table 3.33). Interestingly, one of the carboxylic acid moieties adopts an unusual *anti* conformation, Figure (b).

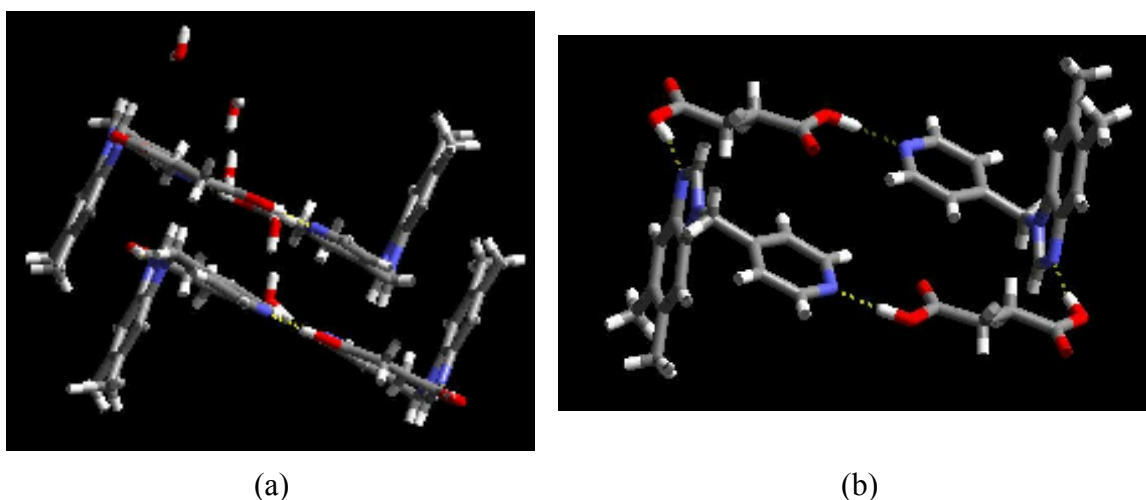


**Figure 3.17** (a) Side view with water molecules included (b) hydrogen bonding interactions in the crystal structure of **12d**, (water molecules have been omitted).

#### 3.4.16 Crystal structure of 1-[(4-pyridyl)methyl]-5,6-dimethylbenzimidazole 3-fluorobenzoic acid (1:2), **12e**

The crystal structure of **2e** contains one molecule of 1-[(4-pyridyl)methyl]-5,6-dimethylbenzimidazole and two disordered molecules of 3-fluorobenzoic acid, Figure 3.18. Both acids form O-H $\cdots$ N hydrogen bonds with the benzimidazole and pyridyl nitrogen atoms (Table 3.3).

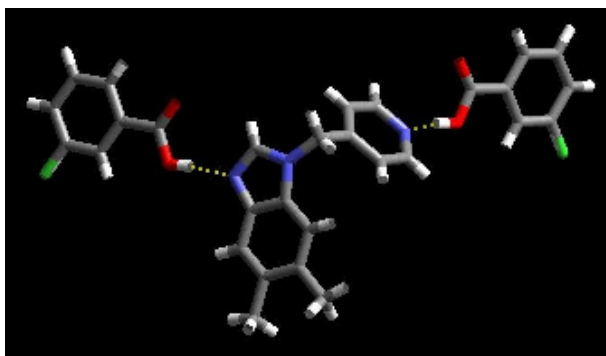


**Figure 3.18** Trimer in the crystal structure of **12e**.

**3.4.17 Crystal structure of 1-[(4-pyridyl)methyl]-5,6-dimethylbenzimidazole tetrafluoroiodo aldoxime (1:1), 12f**

The crystal structure of **12f** contains one molecule of 1-[(4-pyridyl)methyl]-5,6-dimethylbenzimidazole and one molecule of tetrafluoroiodoaldoxime, Figure 3.18. The oxime moiety participates in an O-H $\cdots$ N hydrogen-bonding interaction with the imidazole nitrogen atom (Table 3.3), and the iodine atom participates in a halogen bond with the pyridyl nitrogen atom (N $\cdots$ I: 2.786 Å). The result is an infinite one-dimensional chain, Figure 3.19.

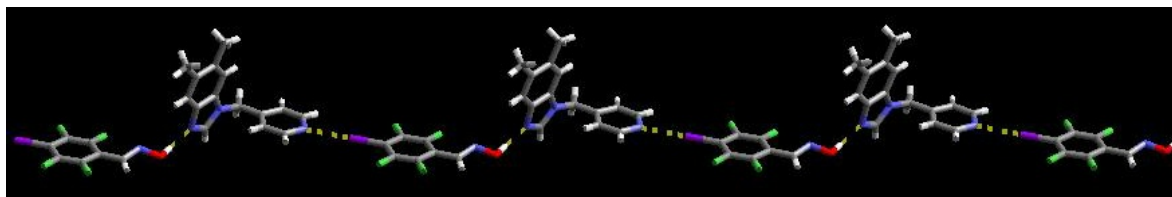


**Figure 3.19** Hydrogen- and halogen-bonding in the crystal structure of **12f**.

**3.4.18 Crystal structure of 1-[(4-pyridyl)methyl]-5,6-dimethylbenzimidazole 4-fluorophenylcyanoxime, 12g**

The crystal structure of **12g** contains one molecule of 1-[(4-pyridyl)methyl]-5,6-dimethylbenzimidazole and one molecule of 4-fluorophenylcyanooxime, Figure 3.20. The oxime moiety participates in an O-H $\cdots$ N hydrogen-bonding interaction with the benzimidazole nitrogen atom (Table 3.3), resulting in a discrete entity.



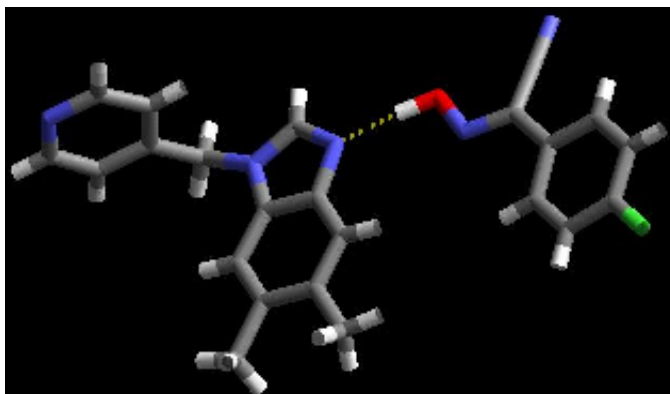


**Figure 3.20** Dimer in the crystal structure of **12g**.

**3.4.19 Crystal structure of 1-[(3-pyridyl)methyl]-2-phenylimidazole 4-nitrobenzoic acid (1:2), 13a**

The crystal structure of **13a** contains one molecule of 1-[(3-pyridyl)methyl]-2-phenylimidazole and two molecules of 4-nitrobenzoic acid, Figure 3.21. Both acids form O-H $\cdots$ N hydrogen-bonds with the imidazole and pyridyl nitrogen atoms (Table 3.3).

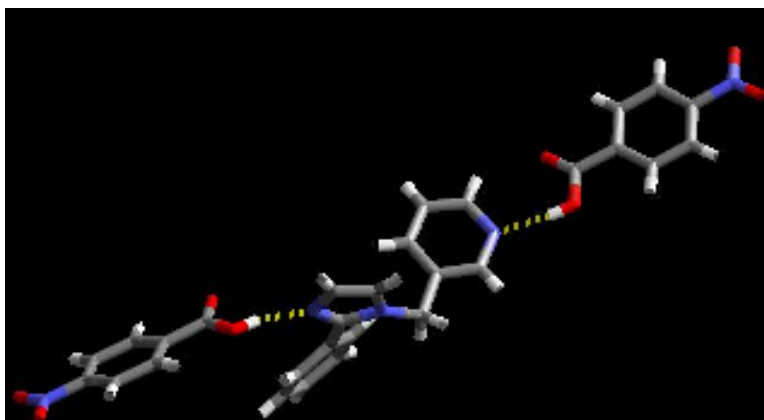


**Figure 3.21** Trimer in the crystal structure of **13a**.

**3.4.20 Crystal structure of 1-[(4-pyridyl)methyl]-2-phenylimidazole 4-nitrobenzoic acid (1:2), 14a**

The crystal structure of **14a** also contains one molecule of 1-[(4-pyridyl)methyl]-2-phenylimidazole and two molecules of 4-nitrobenzoic acid, Figure 3.22. Both acids form O-H $\cdots$ N hydrogen-bonds with the imidazole and pyridyl nitrogen atoms (Table 3.3).

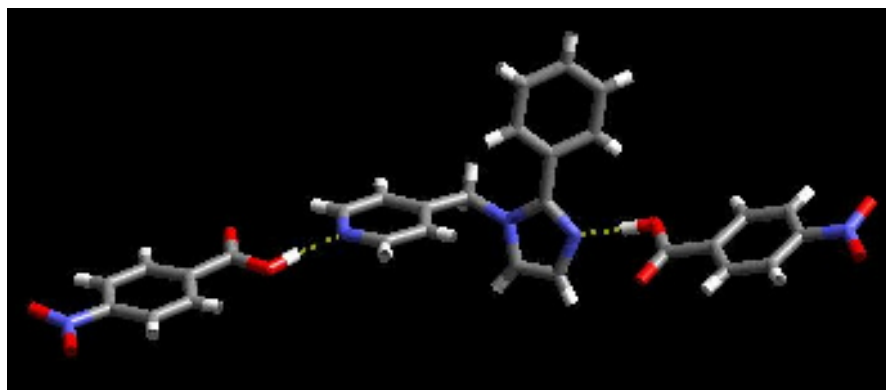


**Figure 3.22** Trimer in the crystal structure of **14a**.

**3.4.21 Crystal structure of 1-[(3-pyridyl)methyl]-7-azaindole 2,3,4,5,6-pentamethyl benzoic acid (1:2), 15a**

The crystal structure of **15a** also contains one molecule of 1-[(3-pyridyl)methyl]-7-azaindole and two molecules of pentamethylbenzoic acid, Figure 3.23. Both acids form O-H...N hydrogen-bonds with the pyridyl moieties (Table 3.3).

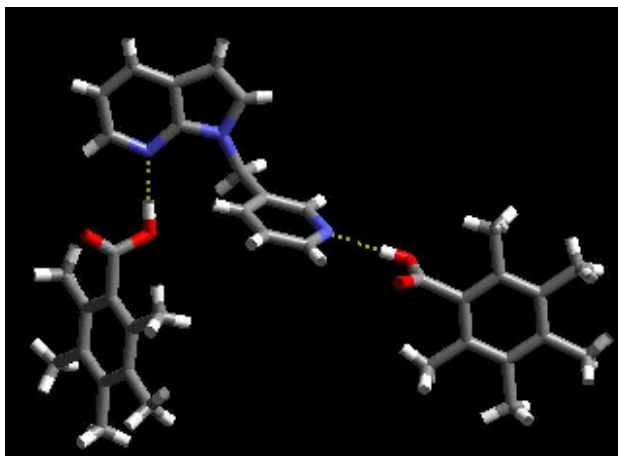


**Figure 3.23** Trimer in the crystal structure of **15a**.

### 3.4.22 Calculations

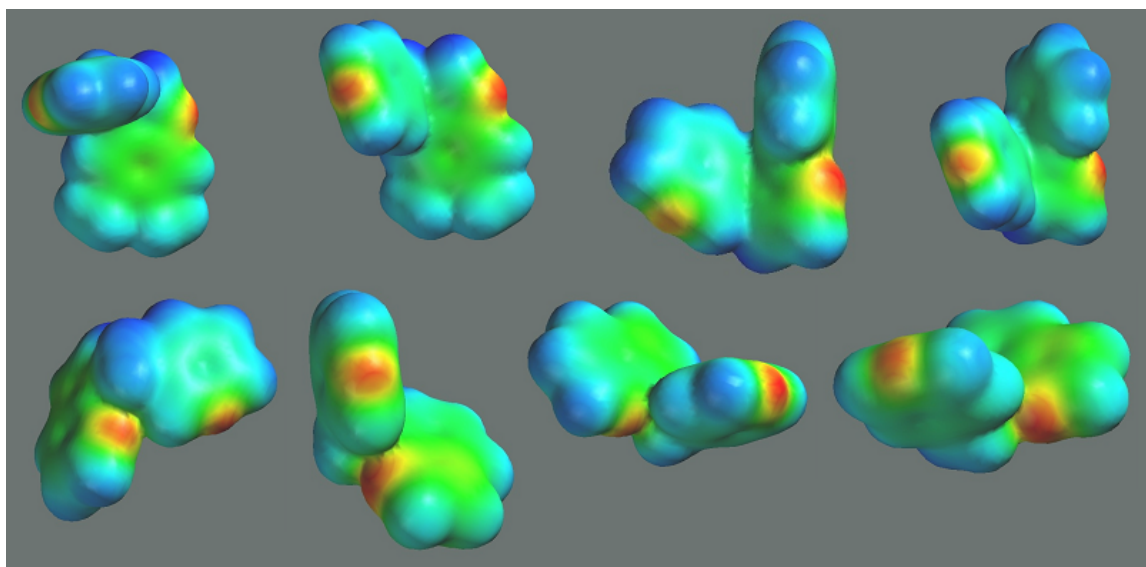


**Figure 3.24** Electrostatic potential surfaces of heterocycles **11-18**.

**Table 3.4** Electrostatic potentials of heterocycles **11-18**.

Heterocycle	MEP A <sub>1</sub> / kJ mol <sup>-1</sup>	MEP A <sub>2</sub> / kJ mol <sup>-1</sup>
1-[(3-Pyridyl)methyl]-5,6-dimethylbenzimidazole, <b>11</b>	-301	-255
1-[(4-Pyridyl)methyl]-5,6-dimethylbenzimidazole, <b>12</b>	-299	-274
1-[(3-Pyridyl)methyl]-2-phenylimidazole, <b>13</b>	-321	-260
1-[(4-Pyridyl)methyl]-2-phenylimidazole, <b>14</b>	-311	-271
1-[(3-Pyridyl)methyl]-7-azaindole, <b>15</b>	-282	-262
7-[(3-Pyridyl)methyl]-7-azaindole, <b>16</b>	-308	-282
1-[(4-Pyridyl)methyl]-7-azaindole, <b>17</b>	-280	-254
7-[(4-Pyridyl)methyl]-7-azaindole, <b>18</b>	-303	-266

## 3.5 Discussion

### 3.5.1 Synthesis and characterization

All asymmetric supramolecular reagents, **11-18**, have been prepared in variable

yields (10-69%). They also all show good solubility in a range of solvents (ethanol, methanol, ethyl acetate, acetonitrile, chloroform, methylene chloride). As a result the reagents readily formed several co-crystals and salts with a range of carboxylic acids and oximes. The coupling of the pyridyl moiety to the nitrogen atom can be traced by following the shift of the methylene in the NMR spectrum ( $\sim 4.5 \rightarrow \sim 5.5$  ppm).

### 3.5.2 IR spectroscopy

All of the supramolecular reagents show a great ability to form co-crystals. Supramolecular reagents **13** and **14** were shown to produce co-crystals that were oils (shown by dry grinding and dry mixing experiments). Consequently, there were not an abundance of crystal structures for these compounds. Table 3.2 shows that supramolecular reagents **15-18** were also capable of forming co-crystals, having done so in good supramolecular yields. Compound **18** produced solids that did not produce satisfactory IR spectra. Only three could be confirmed as co-crystals having formed, one not formed and four were inconclusive.

The O-H $\cdots$ N bands are very broad (Figure C.2, Appendix) and consequently, give no indication as to the strength of the hydrogen bond they represent. In 2:1 co-crystal formation, IR gave no indication that two different hydrogen bonds were present. Consequently, it would be necessary to look at the bond lengths of the two different hydrogen bonds present in the 2:1 structures. These are obtained from X-ray crystallography.

### 3.5.3 X-ray Crystallography

A total of 21 crystal structures are presented here, of which two are of the supramolecular reagents themselves, fifteen are co-crystals, and four are salts. Three of the salts displayed either 2:1 or 1:1 stoichiometry, and were included in the numbers for either a 2:1 or 1:1 co-crystal, Figure 3.25.

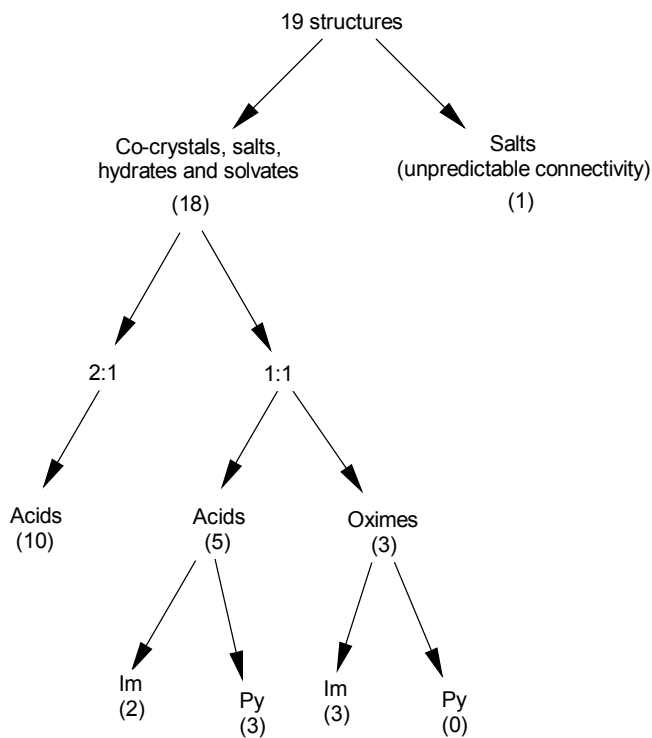


**Figure 3.25** Classification of crystal structures obtained from supramolecular reactions between supramolecular reagents and a variety of acids and oximes. The numbers obtained in each case are portrayed in brackets. Im = imidazole, Py = pyridine.

### 3.5.4 Binding selectivities

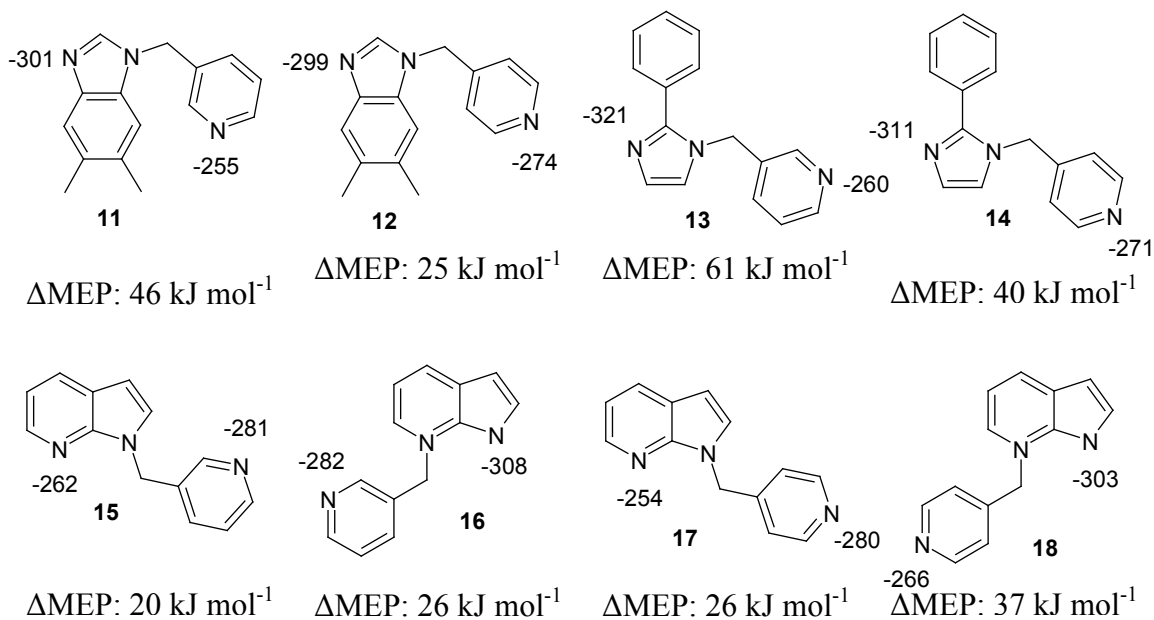


**Figure 3.26** MEPs and  $\Delta$ MEPs of supramolecular reagents. All values are in kJ mol<sup>-1</sup>.

Eight of the eighteen structures exhibited 1:1 stoichiometry. Of these, five were obtained with carboxylic acids and three were with oximes. In the three cases with oximes, all of them displayed best donor-best acceptor behavior, binding to the imidazole nitrogen atom (a supramolecular yield of 100%). In the five structures with carboxylic acids, two of them bound to the imidazole nitrogen atom. Both cases were salts (**11b** and **11e**), with proton transfer taking place to the imidazole nitrogen atom. The remaining three structures containing carboxylic acids showed a preference for the pyridyl nitrogen atom. Two of them were with supramolecular reagent **12**, which has a  $\Delta$ MEP of just 25 mol<sup>-1</sup>. This difference may be so small that the two binding sites cannot be distinguished (Figure 3.26). Another reason may be due to the geometric match between the pyridyl ring and the carboxylic acid. The aromatic C-H proton may aid this interaction, and hence make this the preferred site for carboxylic acids. In all three cases the acid carbonyl group and the adjacent C-H proton are almost co-planar, with the torsion angle ranging from 5 to 10 °.

The overall supramolecular yield is 63%, five out of eight cases displaying best donor/best acceptor behavior. This means that the reagents display a degree of reliability in terms of the best donor/best acceptor approach, and the molecular electrostatic potential calculations complement this, and can be used to rationalize the binding preferences when two different binding sites are present.

In the cases of 2:1 co-crystal formation, both the imidazole and pyridyl nitrogen atoms participate in hydrogen bonding interactions. This merely shows that both binding sites are not sterically hindered, and are accessible to an incoming hydrogen-bond donor without any geometric bias.

### 3.5.5 *Hydrogen bond lengths*

The hydrogen bond lengths for those interactions with the imidazole nitrogen atom (Im) compared to those with the pyridyl nitrogen atom (Py), as well as the hydrogen bond lengths for acceptor 1 (A<sub>1</sub>) and acceptor 2 (A<sub>2</sub>) in crystal structure **15a** are shown in Table 3.5.

**Table 3.5** Hydrogen bond length comparisons for O-H...N interactions between the imidazole and pyridyl nitrogen atoms

Crystal structure	Im(N)...H-O (Å)	<Im(N)...H-O (°)	Py(N)...H-O (Å)	<Py(N)...H-O (°)
<b>11c</b>	2.540	174.0	2.653	175.0
<b>11g</b>	2.600	175.0	2.637	179.0
<b>11h</b>	2.723	168.7	2.680	179.3
<b>12c</b>	2.620	174.9	2.633	169.0
<b>12d</b>	2.614	170.0	2.624	176.5
<b>12e</b>	2.603	174	2.596	171
<b>13a</b>	2.567	159.9	2.662	167.8
<b>14a</b>	2.575	171.4	2.603	174.7
	A <sub>1</sub> (N)...H-O (Å)	<A <sub>1</sub> (N)...H-O (°)	A <sub>2</sub> (N)...H-O (Å)	<A <sub>2</sub> (N)...H-O (°)
<b>15a</b>	2.698	177.0	2.712	174.0

In seven out of nine cases, the shortest hydrogen bond length is for that between the best donor and best acceptor. This shows that this interaction is stronger than that between the second best donor and second best acceptor.

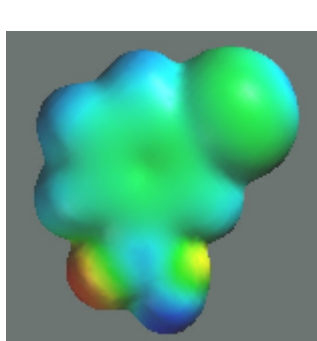
### 3.5.6 Salts

Of the four salts obtained, two displayed unpredictable composition. Structure **11d** contained another molecule of pentamethylbenzoic acid present as a result of proton transfer. The crystal structure of **11e** contained an ethanol molecule. Despite this, the main recognition events were undisrupted. The carboxylate forms a hydrogen bond with the best acceptor, the imidazole nitrogen atom (as determined by the charge calculations), whilst the iodine atom forms a halogen bond with the weaker acceptor, the pyridyl nitrogen atom. The other two cases did not display any unpredictable behavior, with no additional molecules appearing in the structure as a result of proton transfer.

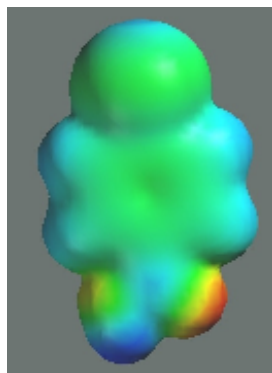
### 3.5.7 Halogen bonding

Halogen bonding has gained considerable attention recently,<sup>2</sup> and appeared in

three of the structures reported here: **11e**, **11h** and **12f**, each of them containing N $\cdots$ I interactions.<sup>3</sup> Crystal structure **11h** saw 4-iodobenzoic acid participating in a halogen bond with the pyridyl nitrogen atom. Interestingly, in the crystal structure containing 3-iodobenzoic acid (**12b**), no halogen bonding was seen to occur with the iodine atom. This is despite the fact that the MEPs of the iodine atoms in both acids are of comparable charge, Figure 3.27 and Table 3.6.



(a)



(b)

**Figure 3.27** MEP surfaces of (a) 3-iodo and (b) 4-iodobenzoic acid.

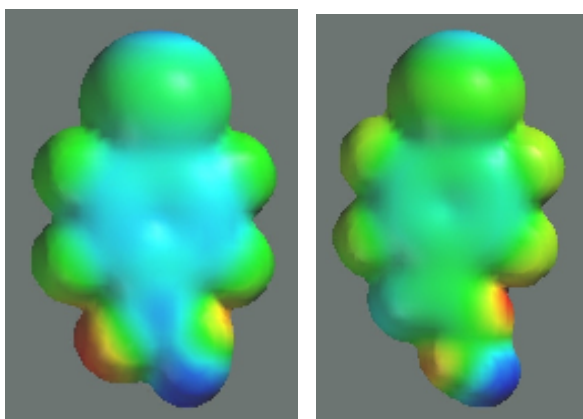
There were no iodobenzoic acid crystal structures with pyridines available for comparison in the CSD.

Crystal structures **11e** and **11h** were with tetrafluoroiodo benzoic acid and aldoxime analogues. **11e** was a salt, due to the strong acid produced on adding the fluoro groups to the ring. Nevertheless, both structures contained one-dimensional chains. The iodine atom forms a stronger halogen bond in the aldoxime structure compared to the carboxylic acid (2.786 Å compared to 2.890 Å). It is to be expected that the halogen bond with the tetrafluoro derivatives would be stronger than the iodobenzoic acid counterparts since the iodine atom in the former case has been “activated”, i.e. has a higher positive charge due to the addition of electron-withdrawing fluorine atoms, Figure 3.28.

**Table 3.6** MEPs of iodobenzoic acids

Acid	Iodine atom MEP kJ mol <sup>-1</sup>
4-Iodobenzoic acid	70
3-Iodobenzoic acid	71





(a) (b)

**Figure 3.28** MEP surfaces of (a) tetrafluoroiodobenzoic acid and (b) tetrafluoroiodoaloxime.

**Table 3.7** MEPs of tetrafluoroiodoaloxime and benzoic acid

Tetrafluoroiodo analogue	Iodine atom MEP kJ mol <sup>-1</sup>
Aldoxime	70
Benzoic acid	92

This is demonstrated in the cases of 4,4'-bipyridine and 1,4-diiodobenzene<sup>4</sup>, and 4,4'-bipyridine 1,4-diiidotetrafluorobenzene<sup>5</sup>, Figure 3.29.

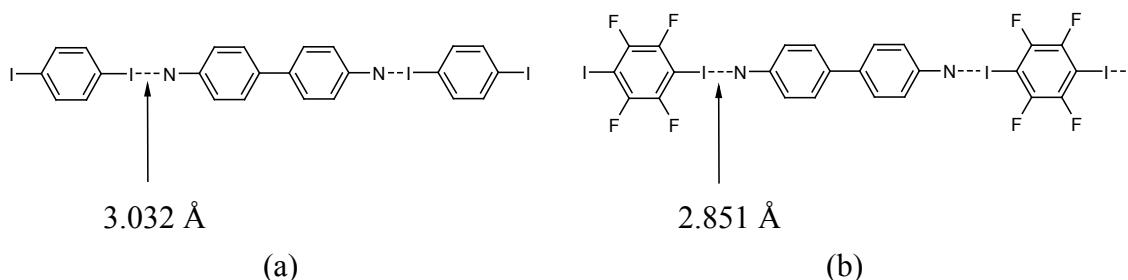


**Figure 3.29** Comparison of bond lengths in (a) 4,4'-bipyridine and 1,4-diiodobenzene<sup>4</sup> and 4,4'-bipyridine 1,4-diiidotetrafluorobenzene<sup>5</sup>.

Two out of three structures exhibited best donor/best acceptor behavior, with the best donor (the hydrogen bond moiety) forming a hydrogen bond with the best acceptor, and the second best donor (the iodine atom) forming a halogen bond with the second best acceptor (the pyridyl nitrogen atom). Only **11h** behaved unexpectedly (in terms of connectivity), with two acid molecules interacting with both binding sites, and an imidazole-iodine interaction.

It has been shown that halogen bonding is a secondary interaction, and the structural assembly is primarily driven by O-H $\cdots$ N hydrogen bonds. The combination of hydrogen and halogen bonding provides an additional handle on the synthesis and assembly of supramolecules. This makes it a versatile supramolecular strategy, capable of bringing molecular building blocks together in a hierarchical manner.

### 3.6 Conclusions

It has been shown that a series of ditopic hydrogen bond-acceptor molecules, with binding sites of similar geometry, can induce selectivity by means of their basicity. The calculated MEPs of the supramolecular reagents can be used as a reliable guideline to the prediction of their binding preferences. The accessibility of each binding site was deciphered by obtaining co-crystals of 2:1 composition, while those of 1:1 stoichiometry tells us something about the selectivity of the particular molecule.

---

---

## References

- <sup>1</sup> C. B. Aakeröy, J. Desper, J. F. Urbina, *Chem. Commun.*, 2005, 2820.
- <sup>2</sup> (a) M. Fourmigue, *Struct. Bond.*, 2008, **126**, 181; (b) P. Metrangolo, G. Resnati, T. Pilati, S. Biella, *Struct. Bond.*, **126**, 105; (c) W. T. Pennington, T. W. Hanks, H. D. Arman, *Struct. Bond.*, 2008, **126**, 65; (d) M. Vartanian, A. C. B. Lucassen, L. J. W. Shimon, M. E. van der Boom, *Cryst. Growth Des.*, 2008, **8**, 786; (e) P. Metrangolo, F. Meyer, T. Pilati, D. M. Proserpio, G. Resnati, *Cryst. Growth Des.*, 2008, **8**, 654; (f) P. Metrangolo, F. Meyer, T. Pilati, D. M. Proserpio, G. Resnati, *Chem. -- Eur. J.*, 2007, **13**, 5765; (g) C. B. Aakeröy, N. Schultheiss, J. Desper, C. Moore, *CrystEngComm*, 2007, **9**, 421; (h) F. Zordan, L. Brammer, P. Sherwood, *J. Am. Chem. Soc.*, 2005, **127**, 5979.
- <sup>3</sup> (a) N.S. Goroff, S. M. Curtis, J. A. Webb, F. W. Fowler, J. W. Lauher, *Org. Lett.*, 2005, **7**, 1891; (b) R. B. Walsh, C. W. Padgett, P. Metrangolo, G. Resnati, T. W. Hanks, W. T. Pennington, *Cryst. Growth Des.*, 2001, **1**, 165
- <sup>4</sup> P. Metrangolo, H. Neukirch, P. Tullio, G. Resnati, *Acc. Chem. Res.*, 2005, **38**, 386.
- <sup>5</sup> See ref 3(b)

# CHAPTER 4 - Probing the Reliability of Oximes as Hydrogen-bond Donors in the Synthesis of Molecular Co-crystals

## 4.1 Introduction

Well-studied synthons include those of the interaction between an N-heterocycle and a carboxylic acid, Figure 4.1.

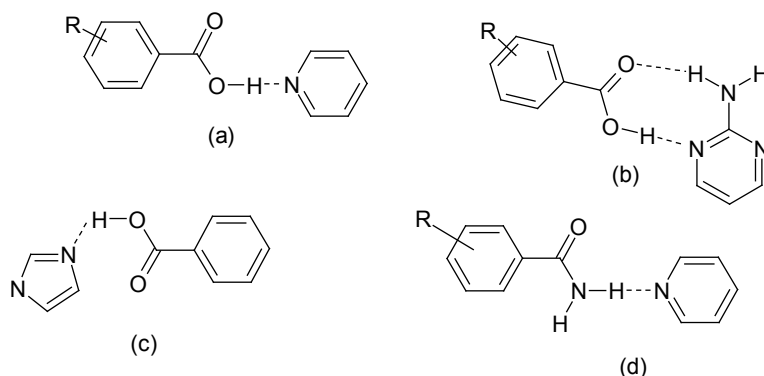


**Figure 4.1** Examples of supramolecular synthons composed with carboxylic acids and N-heterocycles.

The most prominent of the above is the acid-pyridine synthon, which has proven itself to be an effective and robust tool in supramolecular synthesis.<sup>1</sup> Alcohols<sup>2</sup> and amines<sup>3</sup> have also been used successfully as reagents in the supramolecular synthesis of co-crystals. Carboxylic acids have probably been the most effective of all at forming co-crystals, however there are also a few drawbacks associated with them.

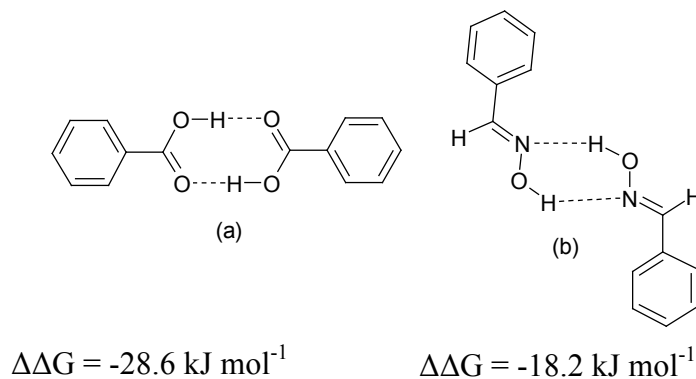


**Figure 4.2** Homomeric interactions between (a) carboxylic acid and (b) oxime functionalities. The lower energy of the oxime-oxime interaction indicates a weaker interaction.

First, the acid-acid dimer (Figure 4.2 (a)) often prevails in the presence of other components.<sup>4</sup> A reason for this is the hydrogen-bond accepting ability of the carbonyl oxygen atom. The nitrogen atom of the oxime moiety is much weaker in comparison. The values from these electrostatic potential calculations can also be used to calculate the energies ( $\Delta\Delta G$ )<sup>5</sup> of the acid-acid dimer vs that of the oxime-oxime, Figure 4.2. The relative weakness of the oxime dimer could be advantageous in co-crystallization reactions, since this motif is easier to disrupt when another component is introduced.

Second, proton transfer often occurs in crystal structures involving a carboxylic acid and a basic N-heterocycle. This leads to unpredictable connectivities (Figure 4.3), with the carboxylate often bringing in another free acid or solvent molecule, in order to satisfy the carboxylate anion. Instead, it has been shown<sup>6</sup> that the connectivity is much more predictable if the acid retains a neutral charge, i.e. unexpected stoichiometry or chemical composition are much less likely to occur. Such events can be avoided with oximes, since proton transfer is much less likely to occur.

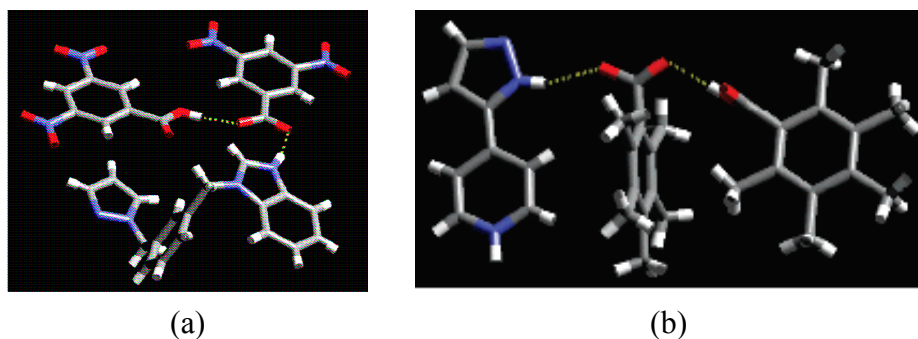


**Figure 4.3** (a) Salt formed between 3,5-dinitrobenzoic acid and 1-[(pyrazol-1-yl)methyl], 3-[(benzimidazol-1-yl)methyl]benzene, resulting in a 1:1:1 complex incorporating a free 3,5-dinitrobenzoic acid and (b) salt formed as a result of proton transfer between pentamethylbenzoic acid and 3-(4-pyridyl)pyrazole, also resulting in a 1:1:1 complex.

Third, in order to synthesize co-crystals, it is advantageous if the solubilities of the two components are similar. If one component is considerably less soluble than the other then there is a high probability it will precipitate from solution by itself and the result will be a homomeric

species. The solubility of many acids is poor, Table 4.1, which may prevent co-crystal synthesis. Oximes can offer an improvement in this area.

**Table 4.1** Solubility data for trimesic, terephthalic, and isophthalic acid, respectively.

Carboxylic Acid	Solubility in ethanol	Solubility in methanol	Solubility in water
	soluble	soluble <sup>a</sup>	slightly
	insoluble	insoluble	insoluble
	soluble	soluble <sup>a</sup>	slightly

<sup>a</sup> With heat

## 4.2 Oximes – Reliable Tools for Supramolecular Synthesis?

Oximes may offer an alternative to carboxylic acids since they are relatively easy to synthesize, can offer an improved solubility, and, most importantly, provide an opportunity to “fine-tune” the charge on the proton on the oxime moiety through simple substitution of the R group. Figure 4.4 shows three types of oximes, acetyloxime (a), aldoxime (b), and cyanoxime (c).

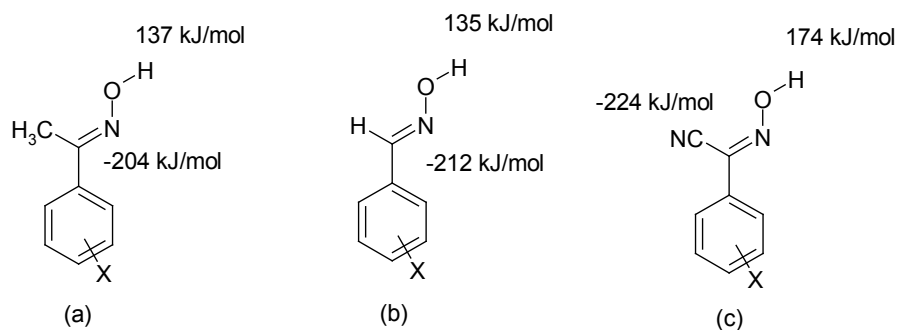


**Figure 4.4** Molecular electrostatic potential values (maxima and minima) of three types of oxime.

The co-crystal forming ability of acetyloximes and aldoximes have previously been studied, and have been found to be considerably poor.<sup>7</sup> A simple covalent modification of changing the R group to that of a nitrile has a significant effect upon the MEP of the oxime proton. The effect that changing this charge has upon the co-crystal-forming ability of cyanoximes will be probed here, and the following questions will be addressed:

- 1) Are cyanoximes effective/reliable co-crystallizing agents?
- 2) Does this increased positive charge translate into a better hydrogen bond donating ability of the oxime?
- 3) Does changing the charge affect oxime-oxime interactions? It will be interesting to investigate what the preferred configuration of the oxime moiety is in the crystalline state, and the structures that they adopt, the catemeric or the dimer configuration, and whether there is a difference between the three different types of oxime, Figure 4.5.

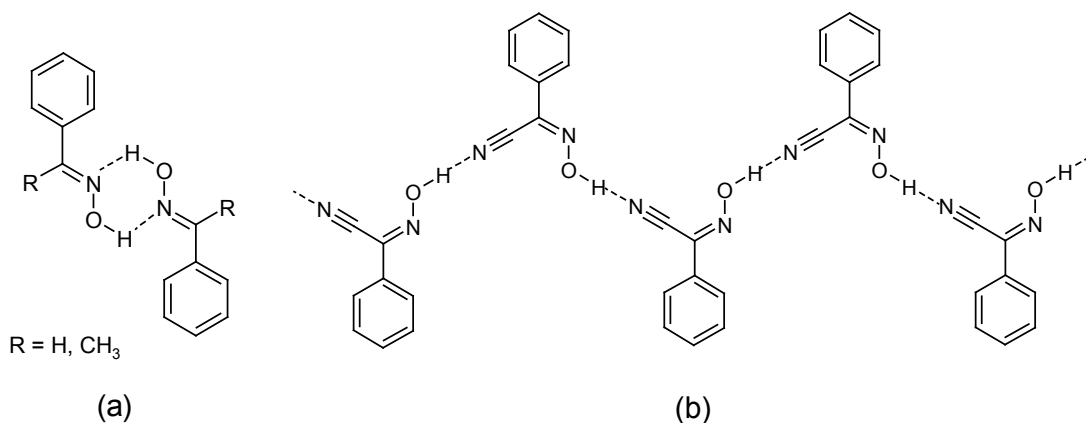


**Figure 4.5** Two different conformations of oximes: (a) dimer and (d) catemeric.

In order to answer these questions, a series of co-crystallization reactions were conducted with cyanoximes (Figure 4.4 (c)) and a set of symmetric hydrogen-bond acceptors.

## 4.3 Experimental

### 4.3.1 Synthesis of cyanophenyloximes

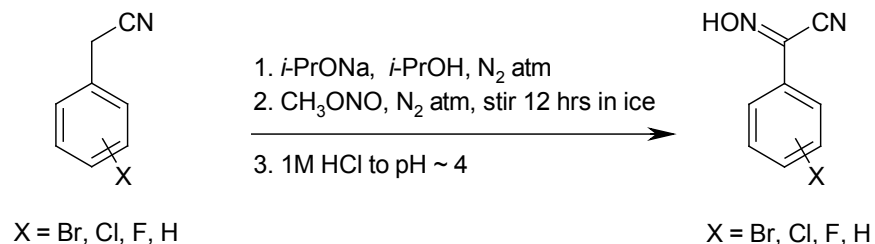


**Figure 4.6** General synthesis of cyanophenyloximes.

The preparation of the cyanophenyloximes, Figure 4.6, was carried out as previously reported.<sup>8,9</sup> 2-Propanol (250 mL) was placed in a 500-mL Erlenmeyer flask, and a magnetic stir bar was added. A dinitrogen atmosphere was introduced by bubbling nitrogen gas into the 2-propanol via a thin glass tube. N<sub>2</sub> was allowed to flow into the solution for around 10 min before sodium metal (0.183 g, 7.94 mmol), this varied from each cyanoxime – see below) was added in tiny pieces over a 15-min period. The Na metal was allowed to dissolve under the N<sub>2</sub> atmosphere (generally 2-3 h). The X-phenylacetonitrile (X = H, 4-Br, 2-Cl, 3-Cl, 4-Cl, 4-F, 2-F; 7.94 mmol, unless otherwise stated – see Table 4.2) was dissolved in 5 mL of additional 2-propanol and added to the stirring *i*-PrONa solution. The solution changed from colorless to a light peach color. A separate 500-mL three-necked flask was equipped with a stir bar, 10 g of NaNO<sub>2</sub>, 100 mL of distilled H<sub>2</sub>O, and 50 mL of methanol. The NaNO<sub>2</sub> was allowed to dissolve with stirring. A greased septum was introduced into one neck, and a greased one-hole rubber stopper was placed firmly into the central neck. A dropper funnel (125 mL) was greased and attached to the third neck with a Keck clip. A solution of 2:1 H<sub>2</sub>O/H<sub>2</sub>SO<sub>4</sub> (50 mL) was prepared and kept in an ice bath (~4 °C). After a glass U-tube apparatus was assembled between the *i*-PrONa/acetonitrile solution in the Erlenmeyer flask and the NaNO<sub>2</sub>/H<sub>2</sub>O/MeOH solution in the three-necked flask Figure 4.7, the acid/water solution was placed into the dropper funnel, and the acid/water solution was slowly added dropwise to the NaNO<sub>2</sub>/H<sub>2</sub>O/MeOH solution inside the flask.



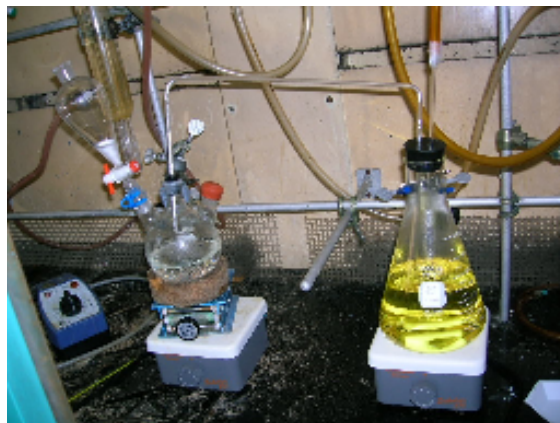


**Figure 4.7** Set up for the synthesis of cyanophenyloximes.

Small bubbles of the evolving  $\text{CH}_3\text{ONO}$  gas were immediately seen upon the reaction of the acid with the sodium nitrite. Evidence of the methyl nitrite gas flow into the Erlenmeyer flask was seen as evidence of gas bubbles under the surface of the *i*-PrONa/acetonitrile solution. This solution immediately changed from the light peach color to a bright yellow. The acid/water mixture was slowly added dropwise to the  $\text{NaNO}_2/\text{H}_2\text{O}/\text{MeOH}$  solution in small aliquots until all was added (about 1 h). The U-tube apparatus was dismantled, and the now bright yellow *i*-PrONa/acetonitrile/ $\text{CH}_3\text{ONO}$  solution was placed under an  $\text{N}_2$  atmosphere. The Erlenmeyer flask was placed into an ice bath and allowed to stir overnight at  $\sim 4^\circ\text{C}$ . The next morning a small amount of white solid had precipitated from the bright yellow solution. This solid was filtered off and determined to be the sodium cyanophenyloximate salt via  $^1\text{H}$  NMR. The remaining solvent was removed from the reaction mixture via rotary evaporation, resulting in a light yellow solid. If  $^1\text{H}$  NMR showed starting material present, the solid was dissolved in 50 mL of water at room temperature, and excess starting material was filtered off (the cyanophenyloximate salt is soluble in water). The water was removed, and the resulting solid was determined to be the pure sodium cyanophenyloximate salt via  $^1\text{H}$  NMR. All of the sodium cyanophenyloximate salt was collected in a 250 mL beaker and dissolved in 40 mL of distilled water. A magnetic stir bar was added, and the beaker was placed in an ice bath on a stir plate. The starting pH of the mixture was  $\sim 10$ .  $\text{HCl}$  (1 M) was added in 2-mL aliquots, and the pH was measured via pH paper after each addition. A white precipitate began forming when the solution was at pH 8. Acid was continuously added until the pH of the solution was determined to be  $\sim 5$ .

At pH 5, the solution was very cloudy and white. This white precipitate was filtered off and determined to be the free oxime, and characterized by melting point, <sup>1</sup>H NMR and IR.

**Table 4.2** Cyanophenyloxime synthetic data

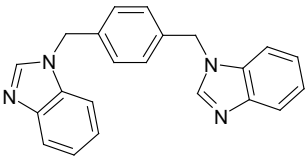
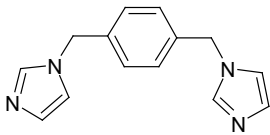
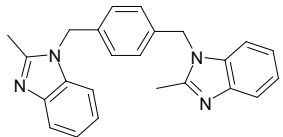
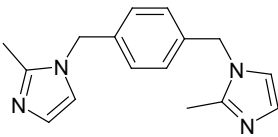
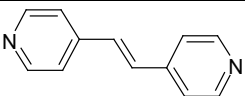
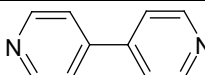
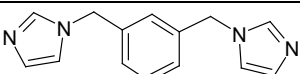
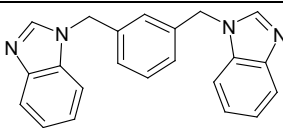
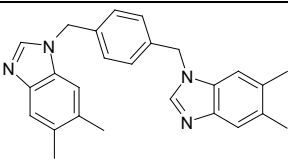
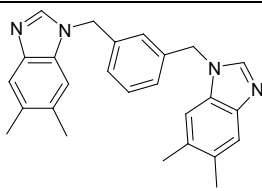
Cyanoxime	Yield (g)	Yield (%)	MP (° C)	Lit. MP (° C)	<sup>1</sup> H NMR (δ ppm) (200 MHz, DMSO- <i>d</i> <sub>6</sub> )	ν (C≡N) (cm <sup>-1</sup> )	ν (C=N) (cm <sup>-1</sup> )
4-Br, <b>19</b>	1.408	79	129-131	135	7.42-7.53 (dd, 4H), 14.1 (bs, 1H)	2216	1672
2-Cl, <b>20</b>	1.002	71	110-112	112	7.47-7.66 (m, 4H), 14.1 (bs, 1H)	2236	1653
3-Cl, <b>21</b>	4.239 <sup>a</sup>	70	107-108	105	7.46-7.49 (m, 2H), 7.60-7.66 (m, 2H)	2229	1653
4-Cl, <b>22</b>	1.020	71	95-98	95	7.58-7.62 (d, 2H, <i>J</i> = ), 7.72-7.76 (d, 2H, <i>J</i> = ), 14.1 (bs, 1H)	2216	1679
2-F, <b>23</b>	4.571 <sup>b</sup>	75	118-120	118	7.32-7.46 (m, 2H), 7.55-7.74 (m, 2H), (bs, 1H)	2228	1646
4-F, <b>24</b>	1.748 <sup>c</sup>	72	83-85	89	7.34-7.43 (m, 2H), 7.74-7.81 (m, 2H), 13.84 (bs, 1H)	2245	1600
H, <b>25</b>	5.339 <sup>d</sup>	85	125-126	128-129 <sup>10</sup>	7.72-7.77 (m, 3H), 7.53-7.56 (m, 2H), 13.8 (s, 1H)	2236	1646

\*Starting with <sup>a</sup> 33.3, <sup>b</sup> 37.0, <sup>c</sup> 15.9, and <sup>d</sup> 42.7 mmol of X-phenylacetonitrile

### 4.3.2 Synthesis of Co-crystals

Co-crystals/solids were obtained through slow evaporation at room temperature. Solids produced were analyzed by IR spectroscopy, and crystals were analyzed by IR spectroscopy and X-ray crystallography.

**Table 4.3** Names of heterocyclic ligands and abbreviations, employed in this study.

Ligand Abbreviation <sup>a</sup>	Ligand Structure	Ligand Abbreviation	Ligand Structure
1,4-bibix <b>a</b>		1,4-bix <b>b</b>	
1,4-(2-Me)-bibix <b>c</b>		1,4-(2-Me)-bix <b>d</b>	
4,4'-bpe <b>e</b>		4,4'-bipy <b>f</b>	
1,3-bix <b>g</b>		1,3-bibix <b>h</b>	
1,4-(5,6-dime)-bibix <b>i</b>		1,3-(5,6-dime)-bibix <b>j</b>	

<sup>a</sup> 4,4'-bipy = 4,4'-bipyridine; 4,4'-bpe = *trans*-1,2-bis(4-pyridine)ethylene

Commercially available heterocycles were purchased from Aldrich. Bis-imidazoles and bis-benzimidazoles employed in this study, Table 4.3, were synthesized using published procedures.<sup>11</sup> Co-crystals of cyanophenylloxime plus the nitrogen-containing heterocycles that produced both single crystals and solids were synthesized as follows:

#### 4.3.2.1 Synthesis of 3-chlorophenylcyanoxime 1,4-bis[(benzimidazol-1-yl)methyl]benzene (2:1), 21a

**21** (8.0 mg, 0.045 mmol) was dissolved in 1:1 ethanol/ethyl acetate in a 50 mL beaker. A 1:1 ethyl acetate/ethanol solution of 1,4-bibix (15 mg, 0.045 mmol) was added. Fluffy crystals not suitable for X-ray crystallography were obtained after 2 days. These needles were redissolved in methanol and colorless plates were obtained via slow evaporation after ~ 2 weeks; mp: 160-179 °C.

#### 4.3.2.2 *Synthesis of 2-fluorophenylcyanoxime 1,2-bis(4-pyridyl)ethylene (2:1), 23e*

**23** (13 mg, 0.082 mmol) and 4,4' bpe (13 mg, 0.082 mmol) were both dissolved separately in acetonitrile. Slow evaporation over 5 days yielded very skinny needles not suitable for X-ray diffraction. Consequently the needles were redissolved in methanol, which produced suitable crystals (colorless plates); mp: 167-170 °C .

#### 4.3.3 *Calculations*

The charges on the three oximes used in this study were calculated using Spartan '04 (Wavefunction, Inc. Irvine, CA). The three molecules were optimized using AM1, and the maxima and minima in the molecular electrostatic potential surface (0.002 e/au isosurface) were determined using a positive point charge as a vacuum as the probe. The electrostatic maxima and minima as determined by AM1 for cyanophenylloximes, along with those for acetyloxime and benzaldoximes, are shown in Table 4.6.

#### 4.3.4 *X-ray crystallography*

Data sets were collected on a Bruker SMART APEX diffractometer using molybdenum K $\alpha$  radiation at 100 K. Data were collected using SMART.<sup>12</sup> The asymmetric units for all structures contained one oxime and one-half bis(imidazole) molecule. Single-crystal structure determinations were carried out on two cyanophenylloxime-based co-crystals. The relevant crystallographic data are displayed in Tables B.27 and B.28 and hydrogen-bond geometries for both are listed in Table 4.5.

#### 4.3.5 *Infra-red spectroscopy and melting point*

Infrared spectra of the products obtained in the co-crystallizations were acquired using a potassium bromide pellet. An approximate 8:1 ratio of KBr to solid product was combined in an oven-dried mortar and ground to a uniform powder with a pestle. A pellet press was employed to create a transparent KBr pellet that was used for analysis. A Nicolet FT-IR instrument equipped with OMNIC software was used to analyze the data. The main features used for identification are the O-H...N hydrogen-bonding bands at 2500 and 1900 cm<sup>-1</sup>.<sup>13</sup> Melting points were performed on a Fisher-Johns apparatus and are uncorrected.

## 4.4 Results

The relevant IR data for the attempted co-crystallization reactions are summarized in Table 4.4.

### 4.4.1 IR Spectroscopy

**Table 4.4** IR data (position of O-H...N stretches) from co-crystallization experiments

Heterocycle	IR O-H...N bands (cm <sup>-1</sup> )					
	Oximes					
	Phenylcyanoximes					
	19	20	21	22	23	24
4,4'-bipy	2522, 1845	2545, 1834	2482, 1839	2540, 1823	2525, 1808	2494, 1823
4,4'-bpe	2488, 1859	2489, 1833	2449, 1839	2484, 1849	2489, 1849	2484, 1849
1,4-bix	2488, 1819	2501, 1858	2442, 1825	2508, 1832	2488, 1891	2488, 1898
1,4-bibix	2482, 1812	2484, 1885	2442, 1819	2504, 1772	2499, 1844	2528, 1785
1,4-(2-Me)-bix	2462, 1825	2508, 1885	2508, 1912	2501, 1904	2508, 1878	2514, 1898
1,4-(2-Me)-bibix	2482, 1799	*	2488, 1806	*	*	*
1,3-bix	2501, 1845	2489, 1885	2535, 1878	2521, 1911	2821, 1865	2504, 1890
1,3-bibix	2515, 1859	2499, 1885	2522, 1865	2508, 1845	2514, 1885	2521, 1851
1,3-(5,6-dime)-bibix	2548, 1931	*	*	2520, 1833	*	*
1,4-(5,6-dime)-bibix	2495, 1818	-	-	2514, 1865	2488, 1885	2541, 1898

- indicates no co-crystal was formed, \* indicates no co-crystallization was attempted

**Table 4.5** Hydrogen-bond geometries for **21a** and **23e**

Co-crystal	D-H...A	d(D-H), Å	d(H...A), Å	d(D...A), Å	<(DHA), °
<b>21a</b>	O(37)-H(37)...N(13)	0.93(2)	1.69(2)	2.6145(2)	176.3(2)
<b>23e</b>	O(17)-H(17)...N(21)	1.03(3)	1.60(3)	2.628(3)	178(3)

#### 4.4.2 Crystal structure of 3-chloro-phenylcyanoxime 1,4-di[(1-benzimidazolyl)methyl]benzene (2:1), 21a

The single-crystal structure of **21a** reveals the presence of a trimeric supermolecule, Figure 4.8, a 2:1 co-crystal assembled via two equivalent O-H...N hydrogen bonds. There are no other noticeable interactions in this crystal structure. The oxime moiety is planar with the aromatic backbone, and the phenyl-benzimidazole torsion angle is approximately 77°.

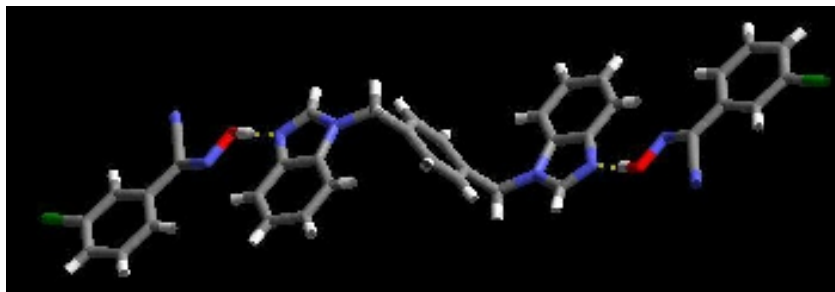


**Figure 4.8** The trimeric supermolecule in **21a**

#### 4.4.3 Crystal structure of 2-fluoro-phenylcyanoxime 1,2-di(4-pyridyl)ethane (2:1), 23e

A trimeric supermolecule is also present in the crystal structure of **23e**, which contains a fluoro-substituted phenylcyanoxime, Figure 4.9. The supermolecule is assembled through O-H...N hydrogen-bond interactions. Again, the structure contains a trimeric supermolecule, a 2:1 co-crystal assembled through two equivalent O-H...N hydrogen bonds. There are no other noticeable interactions in this crystal structure. The oxime moiety is not planar with the aromatic backbone, tilted at an angle of approximately 30°.

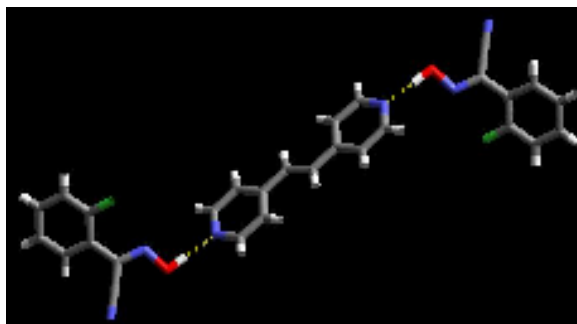


**Figure 4.9** The trimeric supermolecule in **23e**.

#### 4.4.4 Calculations

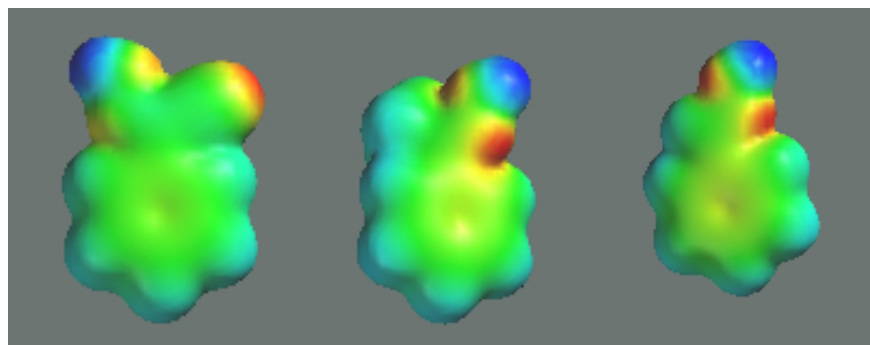


**Figure 4.10** Electrostatic potentials of three oximes (a) cyanophenylloxime, (b) acetyloxime and (c) aldoxime

Table 4.6 shows the results of the electrostatic potentials calculated for the oximes studied here, and Figure 4.10 shows the electrostatic potential figures for each type of oxime.

**Table 4.6** Electrostatic potentials of all the oximes studied here

Oxime	$E_{\max}$ (kJ/mol) (=NOH)	$E_{\min}$ (kJ/mol) (position)
4-bromophenylcyanoxime, <b>19</b>	183.99	-215.13 (C≡N)
2-chlorophenylcyanoxime, <b>20</b>	172.24	-224.55 (C≡N)
3-chlorophenylcyanoxime, <b>21</b>	180.78	-208.78 (C≡N)
4-chlorophenylcyanoxime, <b>22</b>	180.60	-211.46 (C≡N)
2-fluorophenylcyanoxime, <b>23</b>	176.54	-229.09 (C≡N)
4-fluorophenylcyanoxime, <b>24</b>	181.36	-210.30 (C≡N)
phenylcyanoxime, <b>25</b>	171.61	-219.56 (C≡N)
3-bromoacetyloxime	140.04	-204.83 (C=N)
4- bromoacetyloxime	145.38	-201.94 (C=N)
acetyloxime	135.56	-217.112 (C=N)
3-bromoaldoxime	145.90	-176.87 (C=N)
4- bromoaldoxime	150.85	-179.53(C=N)

## 4.5 Discussion

### 4.5.1 Synthesis and NMR Characterization

Cyanoximes can be prepared relatively easily in good yields, requiring only recrystallization as a means of purification. Their formation can be easily traced using IR and NMR spectroscopy. On conversion to the cyanoxime, the methylene peak in the acetonitrile precursor that usually appears around 3.8 ppm disappears. The cyanoxime proton is also identifiable as a broad singlet around 14 ppm, in contrast to the oxime proton in aldoximes and acetophenone, which appears at 11.20-11.44 ppm in the  $^1\text{H}$  NMR spectra ( $\text{DMSO-}d_6$ ). The oxime proton in 3-chlorophenylcyanoxime **21** was not observed in DMSO however, in  $\text{CDCl}_3$  the peaks observed were as follows: (200 MHz)  $\delta$  7.401 (t, 1H), 7.462 (d, 1H), 7.675 (d, 1H), 7.810 (s, 1H), 8.583 (bs, 1H). The oximes also exhibit excellent solubility in a variety of solvents (ethyl acetate, ethanol, methanol, chloroform).

**Table 4.7** Supramolecular yield for each type of oxime.

	Cyanophenyl-oximes	Benzaldoximes	acetyloximes
no. cocrystals formed	50	1	2
total co-crystallizations set up	52	24	24
% supramolecular yield	96	4	8

### 4.5.2 IR Spectroscopy and melting point

The results of the co-crystallization reactions obtained here, complemented by those obtained previously,<sup>7</sup> clearly show that substitution of the R group from a simple hydrogen or alkyl group, to a nitrile, (which increases the positive charge on the oxime proton) has a significant effect upon successful co-crystal formation. The acetyloximes/benzaldoximes were found to be less effective co-crystal formers, having formed co-crystals in just three out of a total of 48 attempts. Melt experiments performed between heterocyclic compounds and acetophenoximes and benzaldoximes also show that solubility is not a factor in prevention of co-crystal formation, since these also failed to produce co-crystals. Cyanophenylloximes on the other hand, formed co-crystals in 50 out of a total of 52 attempts, a supramolecular yield of 96%. (Table 4.7).



On conversion from the acetonitrile starting material to the cyanoxime, the nitrile stretch in the IR spectrum also shows a shift to lower wavenumbers ranging from 6 to 33 (Table 4.8). The melting points of the cyanophenyloximes are, in general, considerably lower than their carboxylic acid counterparts (Table 4.9), and this finding may be explained due to the stronger acid-acid dimer being harder to break up than the oxime dimer/catemer (Figure 4.2).

**Table 4.8** IR nitrile stretches of acetonitrile precursors vs cyanoxime products.

Substituent	Acetonitrile (C≡N) cm <sup>-1</sup>	Oxime (C≡N) cm <sup>-1</sup>
4-Br	2249	2216
2-Cl	2248	2236
3-Cl	2256	2229
4-Cl	2249	2216
2-F	2256	2236
4-F	2249	2243
H	2249	2236

**Table 4.9** Melting points of cyanoximes and corresponding carboxylic acids.

Substituent	Carboxylic acid <sup>a</sup> (°C)	Cyanoxime <sup>a</sup> (°C)
4-Br	252-254	135
2-Cl	138-140	112
3-Cl	153-157	105
4-Cl	238-241	95
2-F	122-125	118
4-F	182-184	89
H	121-125	128-129

<sup>a</sup> values taken from literature values

#### 4.5.3 X-ray Crystallography

Six other single crystal structures are present in the literature,<sup>7</sup> in addition to the two obtained here. One contained an acetyloxime and five contained various cyanophenyloximes. Each one showed the predicted/desired supramolecular motif in the formation of discrete,

trimeric supermolecules held together by O-H $\cdots$ N interactions (oxime $\cdots$ N-heterocycle), Figure 4.11.

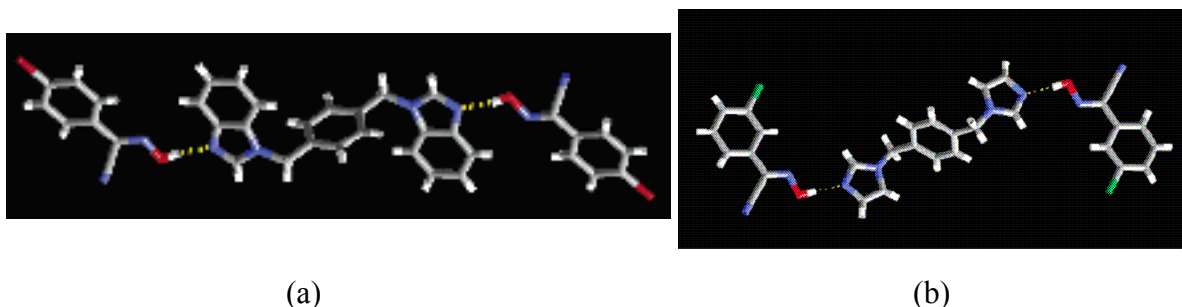


**Figure 4.11** Trimeric supermolecules in the crystal structures of (a) 1,4-di[(1-benzimidazolyl)methyl]benzene 4-bromophenylcyanoxime and (b) 1,4-di[(1-imidazolyl)methyl]benzene 3-chlorophenylcyanoxime.

The O-H $\cdots$ N hydrogen bonds that are principally responsible for the assembly of the binary co-crystals constructed from N-heterocycles and cyanoximes are all, as expected for strong hydrogen bonds, close to linear (Table 4.5). The N $\cdots$ O distances also fall within a relatively narrow range, apart from the interaction involving the less acidic acetyloxime. The O $\cdots$ N distance in the crystal structure of substantially longer, 2.774 Å, than any of the analogous contacts from a cyanophenylloxime to the N-based hydrogen bond acceptor (2.58-2.67 Å). Bond lengths suggest that the acetyloxime forms weaker hydrogen bonds with the N-based heterocycles than the corresponding cyanoximes.

A search of the CSD shows a total of four cyanoximes that have been structurally characterized to date<sup>14</sup>, along with twelve aldoximes<sup>15</sup> and three acetyloximes<sup>16</sup>. The search excluded ions, salts, any structures that include potential disruptive groups hydroxy, methoxy etc, and was limited to aromatic oximes.

**Table 4.10** Percent occurrence of oxime configurations, based on results obtained from CSD search.

	Dimer (%)	Catemer (%)	Other (%)
Aldoxime	67	25	8
acetyloxime	67	33	0
Cyanoxime	0	100	0

The results show that the preferred motif of aldoximes and acetyloximes is the dimer formation, whilst that of the cyanophenyloximes is the catemer, Table 4.10. The dimer is in ten out of a total of fifteen cases (aldoximes/acetyloxime), with four being the catemeric formation and the remaining one a ring structure. The occurrence of the *anti* conformation prevents formation of the dimer and so in all cases where the *anti* configuration is adopted the catemer is present. The *syn* conformation is observed in all of the crystal structures obtained in the above study, and comparing these findings with those from the CSD only four out of a total of twenty-eight structures (14%) contained the *anti* conformation. These findings do not appear to be dependent on the substituent (F, Cl, Ph, NO<sub>2</sub> etc).

A possible reason as to why the preferred structure of the cyanophenyloximes is the catemeric formation is due to the introduction of the nitrile group, a better hydrogen bond acceptor than the oxime nitrogen. In the regular oximes, the  $E_{\min}$  lies on the oxime nitrogen atom, whilst in the cyanophenyloximes it lies on the nitrile nitrogen atom (Figure 4.4). This encourages the oxime proton to abandon the interaction with the oxime nitrogen atom for the atom with the higher  $E_{\min}$ , the nitrile nitrogen atom, promoting the catemeric structure. This is supported by the calculated values for the respective intermolecular interactions, Figure 4.4, R = CN.  $\Delta\Delta G$  (a) = 15.8 kJ mol<sup>-1</sup>,  $\Delta\Delta G$  (b) = 27.7 kJ mol<sup>-1</sup>.<sup>17</sup>

## 4.6 Conclusions

The results presented here show that effective and versatile supramolecular synthesis is possible through simple covalent modifications. We have also introduced a new family of co-

crystallization agents and have expanded the toolbox for developing synthons that can be employed in the synthesis of more complex supermolecules.

---

## References

<sup>1</sup> (a) C. B. Aakeröy, A. M. Beatty, B. A. Helfrich, M. Nieuwenhuyzen, *Cryst. Growth Des.*, 2003, **3**, 159; (b) C.B.Aakeröy, J.Desper, B.A.Helfrich, *CrystEngComm*, 2004, **6**, 19; (c) B. R. Bhogala, P. Vishweshwar, A. Nangia, *Cryst.Growth Des.*, 2002, **2**, 325; (d) P. S. Wheatley, A. J. Lough, G. Ferguson, C. Glidewell, *Acta Crystallogr., Sect.C: Cryst.Struct.Commun.*, 1999, **55**, 1489; (e) X.-Z. Sun, M.-H. Zeng, B.-H Ye, *Acta Crystallogr., Sect.E: Struct.Rep.Online*, 2004, **60**, o2103; (f) T. L. Nguyen, F. W. Fowler, J. W. Lauher, *J.Am.Chem.Soc.*, 2001, **123**, 11057; (g) K. K. Arora, J. PrakashaReddy, V. R. Pedireddi, *Tetrahedron*, 2005, **61**, 10793; (h) H. Koshima, T. Nakagawa, T. Matsuura, H. Miyamoto, F. Toda, *J.Org.Chem.*, 1997, **62**, 6322; (i) J. R. Bowers, G. W. Hopkins, G. P. A. Yap, K. A. Wheeler, *Cryst.Growth Des.*, 2005, **5**, 727; (j) G. S. Papaefstathiou, A. J. Kipp, L. R. MacGillivray, *Chem.Commun.*, 2001, 2462; (k) V. R. Pedireddi, A. Ranganathan, S. Chatterjee, *Tetrahedron Lett.*, 1998, **39**, 9831.

<sup>2</sup> (a) J. A. Bis, O. L. McLaughlin, P. Visheshwar, M. J. Zaworotko, *Cryst. Gr. & Des.*, 2006, **6**, 2648; (b) O. Ermer, A. Eling, *J. Chem. Soc. Perk. Trans. 2: Physical Organic Chemistry*, 1994, **5**, 925; (c) M. Ratajczak-Sitarz, A. Katrusiak, K. Gawronska, J. Gawronski, *Tet.: Asymm.*, 2007, **18**, 765; (d) V. R. Vangala, R. Mondal, C. K. Broder, J. A. K. Howard, G. R. Desiraju, *Cryst. Growth. Des.*, 2005, **5**, 99; (e) J. H. Loehlin, M. C. Etter, C. Gendreau, E. Cervasio, *Chem. Mater.*, 1994, **6**, 1218; (f) B. R. Sreekanth, P. Vishweshwar, K. Vyas, *Chem. Comm.*, 2007, **23**, 2375; (g) C. J. Burchell, C. Glidewell, A. J. Lough, G. Ferguson, *Acta Cryst., Sect.: Struc. Sc.*, 2007, B57(2), 201.

<sup>3</sup> (a) V. Bertolasi, P. Gilli, V. Ferretti, G. Gilli, *N. J. Chem.*, 2001, **25**, 408; (b) M. L. Cheney, G. J. McManus, J. A. Perman, Z. Wang, M. J. Zaworotko, *Cryst. Gr. & Des.*, 2007, **7**, 616; (c) R. S. Armstrong, I. M. Atkinson, E. Carter, M. S. Mahinay, B. W. Skelton, P. Turner, G. Wei, A. H. White, L. F. Lindoy, *Proc. Nat. Acad. Sc. USA*, 2002, **99**, 4987; (d) T-F. Tan, J. Han, M-L. Pang, H-B. Song, Y-X. Ma, J-B. Meng, *Cryst. Gr. & Des.*, 2006, **6**, 1186. See also 2 (b), (d) and (e)

- 
- 4 (a) P. L. Wash, E. Maverick, J. Chiefari, D. A. Lightner, *J. Am. Chem. Soc.*, 1997, **119**, 3802; (b) C. B. Aakeröy, A. M. Beatty, K. R. Lorimer, *Dalton*, 2000, **21**, 3869.
- <sup>5</sup> C. A. Hunter, *Angew. Chem. Int. Ed.*, 2004, **43**, 5310. Free energies of hydrogen-bonding interactions are calculated using the following equation:  $\Delta\Delta G = 2(-(\alpha\beta))$ , where  $\alpha = E_{\max}/52 \text{ kJ/mol}^{-1}$  and  $\beta = -E_{\min}/52 \text{ kJ/mol}^{-1}$ . Benzoic acid:  $\alpha = 133.65/52 = 2.6$ ,  $\beta = 285.84/52 = 5.5$ .  $\Delta\Delta G = -2(2.6 \times 5.5) = -28.6 \text{ kJ mol}^{-1}$ . Benzaldoxime:  $\alpha = 134.75/52 = 2.6 \text{ kJ mol}^{-1}$ ,  $\beta = 182.96/52 = 3.5 \text{ kJ mol}^{-1}$ .  $\Delta\Delta G = -2(2.6 \times 3.5) = -18.2 \text{ kJ mol}^{-1}$ .
- <sup>6</sup> C. B. Aakeröy, M. E. Fasulo, J. Desper, *Mol. Pharm.*, 2007, **4**, 317.
- <sup>7</sup> C. B. Aakeröy, D. J. Salmon, M. M. Smith, J. Desper, *Cryst. Growth Des.*, 2006, **6**, 1033.
- <sup>8</sup> D. Robertson, C. Barnes, N. Gerasimchuk, *J. Coord. Chem.*, 2004, **57**, 1205.
- <sup>9</sup> D. Robertson, J. F. Cannon, N. Gerasimchuk, *Inorg. Chem.*, 2005, **44**, 8326.
- <sup>10</sup> D. Boschi, G. Sorba, M. Bertinaria, R. Fruttero, R. Calvino, A. Gasco, *J. Chem. Soc., Perkin Trans. I*, 2001, 1751–1757.
- <sup>11</sup> (a) B. F. Abrahams, B. F. Hoskins, R. Robson, D. A. Slizys, *Acta Crystallogr. C*, 1998, **54**, 1666; (b) C. B. Aakeröy, J. Desper, B. Leonard, J. F. Urbina, *Cryst. Growth Des.*, 2004, **5**, 865.
- <sup>12</sup> SMART v5. 060, Bruker Analytical X-ray Systems, Madison, WI, 1997-1999.
- <sup>13</sup> (a) N. V Drichko, G. Y. Kerenskai, V. M. Schreiber, *J. Mol. Struct.*, 1999, **477**, 127; (b) J. P. Castaneda, G. S. Denisov, S. Y. Kucherov, V. M. Schreiber, A. V. Shurukhina, *J. Mol. Struct.*, 2003, **660**, 25.
- <sup>14</sup> (a) A. A. Espenbetov, Y. T. Struchkov, L. V. Rybakovam, *Zh. Strukt. Khim. (Russ.) (J. Struct. Chem.)*, 1986, **27**, 180; (b) D. Robertson, J. F. Cannon, N. Gerasimchuk, *Inorg. Chem.*, 2005, **44**, 8326.
- <sup>15</sup> (a) J. Jia, X.-Z. Wang, Y. Zhang, J.-W. Wang, *Acta Crystallogr., Sect. E: Struct. Rep. Online*, 2006, **62**, o2683; (b) C.-X. Wu, X.-Q Lu, *Acta Crystallogr., Sect. E: Struct. Rep. Online*, 2006, **62**, o2826; (c) A. D. Ward, V. R. Ward, E. R. T. Tiekink, *Z. Kristallogr.-New Cryst. Struct.*, 2001, **216**, 561; (d) A. D. Ward, V. R. Ward, E. R. T. Tiekink, *Z. Kristallogr.-New Cryst. Struct.*, 2001, **216**, 563; (e) K. G. Jensen, *Acta Chem. Scand.*, 1970, **24**, 3293; (f) E. Arte, J. P. Declercq, G. Germain, M. van Meerssche, *Bull. Soc.*

---

*Chim. Belg.*, 1980, **89**, 155; (g) C. Glidewell, J. N. Low, J. M. S. Skakle, J. L. Wardell, *Acta Crystallogr., Sect. E: Struct. Rep. Online*, 2004, **60**, o422; (h) F. Bachechi, L. Zambonelli, *Acta Crystallogr., Sect. B: Struct. Crystallogr. Cryst. Chem.*, 1972, **28**, 2489; (i) F. Bachechi, L. Zambonelli, *Acta Crystallogr., Sect. B: Struct. Crystallogr. Cryst. Chem.*, 1973, **29**, 2598; (j) B. Jerslev, S. Larsen, *Acta Crystallogr., Sect. C: Cryst. Struct. Commun.*, 1992, **48**, 136; (k) D.-T. Zhang, F.-G. Sun, G.-Y. Duan, J.-W. Wang, *Acta Crystallogr., Sect. E: Struct. Rep. Online*, 2006, **62**, o715.

<sup>16</sup> (a) A. Gieren, T. Hubner, C. Ruiz-Perez, *Chem.Zeit.*, 1986, **110**, 73; (b) A. Gieren, T. Hubner, C. Ruiz-Perez, *Chem.Zeit.*, 1986, **110**, 76; (c) S. Fortier, G. I. Birnbaum, G. W. Buchanan, B. A. Dawson, *Can. J. Chem.*, 1980, **58**, 191.

<sup>17</sup> Values were calculated as follows: (a)  $\alpha = 171.61/52 = 3.3$ ,  $\beta = 123.6/52 = 2.4$ ,  $\Delta\Delta G = 15.8 \text{ kJ mol}^{-1}$ . (b)  $\alpha = 171.61/52 = 3.3$ ,  $\beta = 219.56/52 = 4.2$ ,  $\Delta\Delta G = 27.7 \text{ kJ mol}^{-1}$ .

# CHAPTER 5 - Probing the Reliability of Di- and Tricyanophenylloximes as Hydrogen-bond Donors in the Synthesis of Molecular Co-crystals

## 5.1 Introduction – Polyfunctional carboxylic acids in crystal engineering

Previous crystal engineering using “polyfunctional” carboxylic acids (carboxylic acids that incorporate two or more carboxylic acid functionalities onto one backbone), has led to the construction of both discrete and extended architectures.

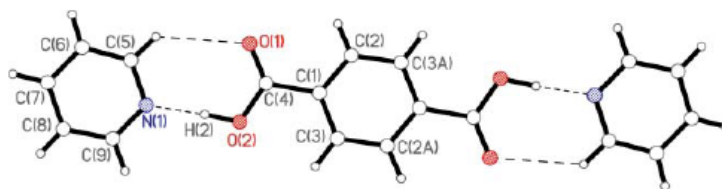


**Figure 5.1** Discrete trimer in the co-crystal of terephthalic acid pyridine (1:2).<sup>1</sup>

For example, the co-crystal of terephthalic acid and pyridine<sup>1</sup> contains a 1:2 discrete, trimeric supermolecule, driven by the formation of O-H $\cdots$ N hydrogen-bonding interactions Figure 5.1.

Trimesic acid<sup>2</sup> is a polyfunctional acid of particular interest to the supramolecular chemist, since it has desirable properties including structural planarity, chemical robustness, and an ability to propagate self-assembly in two dimensions. Co-crystallization of trimesic acid with pyridine sees the formation of a 1:3 co-crystal, Figure 5.2.<sup>1</sup>



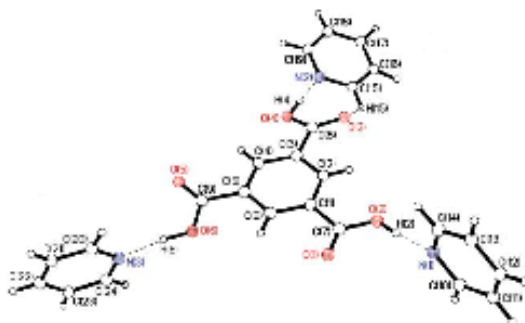


**Figure 5.2** Tetrameric supermolecule in the crystal structure of trimesic acid and pyridine (1:3).<sup>1</sup>

### 5.1.1 From discrete to extended architectures

By replacing a monotopic N-heterocycle with a ditopic analogue it is possible to move from discrete to extended assemblies. For example, replacing pyridine with 1,3-bis(4-pyridyl)propane leads to an extended network, zig-zag chains<sup>3</sup>, Figure 5.3.

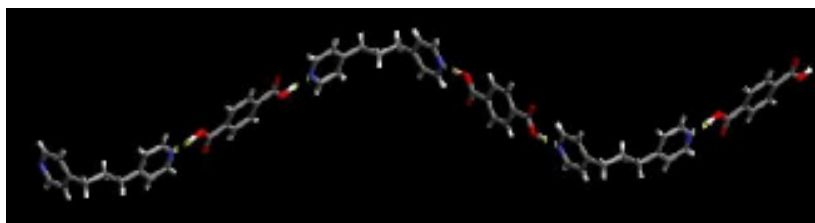


**Figure 5.3** Extended one-dimensional, zig-zag chain in the co-crystal of 1,3-bis(4-pyridyl)propane and terephthalic acid.<sup>3</sup>

The same is possible with the second example, trimesic acid. An elegant example of a 2-D network is the combination of trimesic acid and 4,4'-bipyridine,<sup>4</sup> (Figure 5.4) which produces a two-dimensional honeycomb grid with large cavities, even after interpenetration.

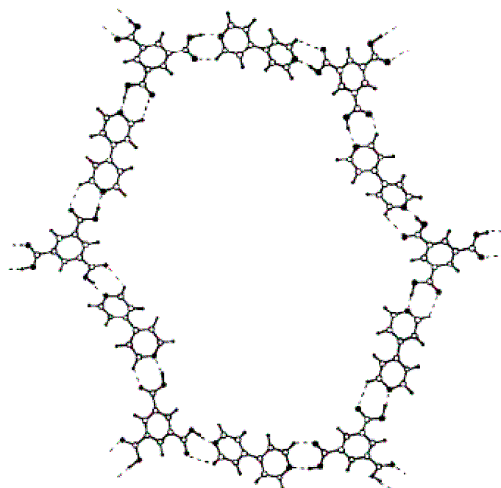


**Figure 5.4** ‘Chicken-wire’ framework in the co-crystal of trimesic acid with 4,4'-bipyridine.<sup>4</sup>

### 5.1.2 Problems with polyfunctional carboxylic acids as supramolecular reagents

A problem with carboxylic acids in supramolecular synthesis is that they frequently undergo proton transfer upon co-crystallization with a basic N-heterocycle,<sup>5</sup> which often leads to unpredictable outcomes. For example, the crystal structure of 4,4'-bipyridine and trimesic acid is a hexahydrate,<sup>6</sup> Figure 5.5, with proton transfer taking place from one of the carboxylic acid moieties onto the pyridine nitrogen atom.

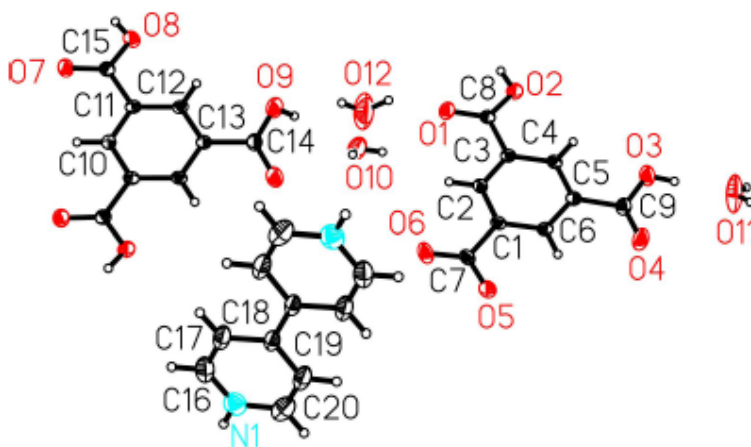


**Figure 5.5** Crystal structure of 4,4'-bipyridine and trimesic acid.<sup>6</sup>

A search of the Cambridge Structural Database shows just a handful of co-crystals of true co-crystals (by definition) involving trimesic acid.<sup>7</sup> Out of a total of 41 crystal structures, 18 are co-crystals (44%), five are salts, and 18 are solvates, hydrates, or

hydrated solvates. The search only involved structures containing trimesic acid and a hydrogen bond acceptor as the other compound. In order to maintain predictability and reliability, it is beneficial to avoid the formation of hydrates and solvates, and salts.

Trimesic acid has huge potential, however its use as a supramolecular reagent has been hampered due to its poor solubility in most solvents. Solubility data of some polycarboxylic acids is shown in Table 5.1.

**Table 5.1** Solubility data of polycarboxylic acids

Carboxylic Acid	Solubility in ethanol	Solubility in methanol	Solubility in water
	soluble	soluble <sup>a</sup>	slightly
	insoluble	insoluble	insoluble
	soluble	soluble <sup>a</sup>	slightly

<sup>a</sup> With heat

A third problem with carboxylic acids is their self-complementarity. The acid-acid dimer is very robust (Figure 5.6). Consequently has proven difficult to break apart when other components are introduced.

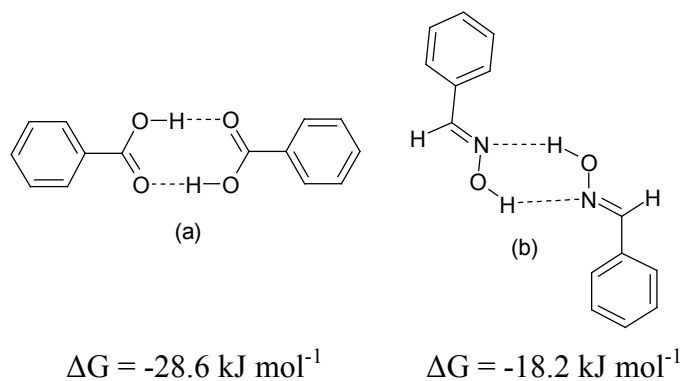


**Figure 5.6** Homomeric interactions between (a) carboxylic acid (b) oxime

Carboxylic acids have also remained key supramolecular reagents, because they are readily available and cheap. We would like to create a new set of polyfunctional supramolecular reagents that improve on the disadvantages of carboxylic acids, that are readily accessible.

### 5.1.3 *Why cyanoximes are a good alternative*

We have already seen that cyanophenyl oximes are extremely good co-crystal formers, and produce discrete, trimeric supermolecules with ditopic symmetric hydrogen-bond acceptors (see Chapter 4). The oxime-oxime interaction is easier to break apart than that of an acid, (Chapter 4 and Figure 5.6). The mono-cyanophenyl oximes exhibited excellent solubility in a variety of solvents and it is expected that the polyfunctional cyanophenyl oximes will behave in the same manner. This will offer an improvement compared to the carboxylic analogues, whose solubility is poor in most solvents. Proton transfer is also much less likely with cyanoximes, highlighted in Chapter 4, where no salts were formed in any of the crystal structures obtained. Carboxylic acids also have a lower  $pK^a$  than oximes, and so are more likely to lose their proton and form salts.

### 5.1.4 *Goals*

We will now investigate whether it is possible to extend these discrete trimers into one-dimensional frameworks, as with the carboxylic acids shown above. If two or more oxime functionalities were to be placed on the same backbone, would 1,4-dicyanophenyl oxime, 1,3-dicyanophenyl oxime, and 1,3,5-tricyanophenyl oxime offer

some advantages over their analogues: terephthalic, isophthalic, and trimesic acid, respectively? The goals of this study are therefore to:

- 1) synthesize and characterize 1,4- and 1,3-dicyanoxime.
- 2) prepare both one- and two-dimensional supramolecular architectures using them, and investigate how effective they are at achieving this goal.
- 3) synthesize and characterize 1,3,5-tricyanophenyloxime.
- 4) construct both discrete, and two-dimensional frameworks with these tricyanoximes.

## 5.2 Experimental

### 5.2.1 Synthesis of dicyanophenyloximes

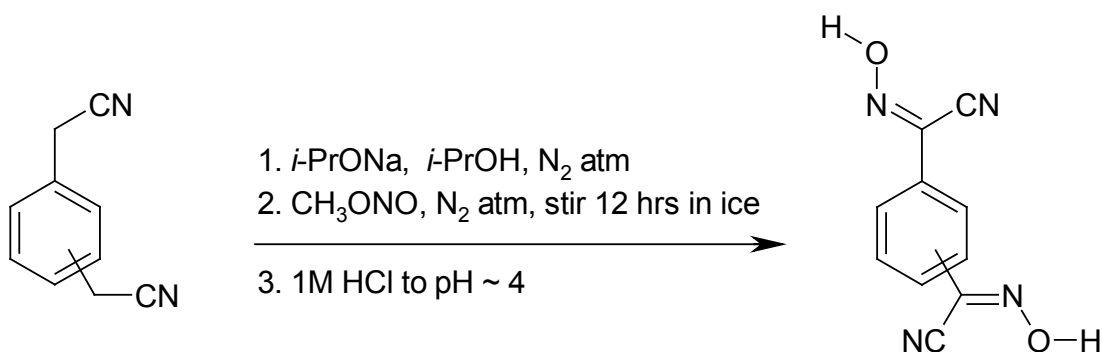


**Figure 5.7** General synthesis of dicyanophenyloximes.

#### 5.2.1.1 Synthesis of 1,4-dicyanophenyloxime, 26

A solution of 1,4-phenylenediacetonitrile dissolved in 2-propanol (0.4 g, 2.56 mmol) was added to a solution of Na metal (0.250 g, 10.87 mmol), dissolved in 2-propanol (540 mL). The solution immediately turned blue. Methyl nitrite gas was generated *in situ* (see full procedure, 4.3.1) and passed through the solution. The solution changed color from blue to green to yellow, and the solution turned cloudy thereafter. The solution was left to stir for 3 days, after which the solid was filtered off. It was then dissolved in water and upon acidification to ~pH 2 a white precipitate emerged. The remaining 2-propanol was removed from the filtrate to leave behind an orange solid. The solid was dissolved in water and acidified with 1M HCl to form a pale yellow solid,

which was then recrystallized from water to yield colorless plates. Yield: 0.451 g (87%).  $^1\text{H}$  NMR (DMSO- $d_6$ , 200 MHz):  $\delta$  7.87 (s, 4H), 14.05 (s, 2H);  $^{13}\text{C}$  NMR (DMSO- $d_6$ , 200 MHz)  $\delta$  115.73, 122.15, 128.03, 132.93; IR:  $\nu$  2238  $\text{cm}^{-1}$  (C $\equiv$ N), 1623  $\text{cm}^{-1}$  (C=N),  $\nu$  3441  $\text{cm}^{-1}$  (O-H); mp: 240-247  $^\circ\text{C}$  (decomp.).

### 5.2.1.2 Synthesis of 1,3-dicyanophenyloxime, 27

Na metal (0.370 g, 16.09 mmol) was dissolved in 540 mL 2-propanol. 1,3-phenylenediacetonitrile (1.24 g, 7.90 mmol) was dissolved in 100 mL 2-propanol and added to the sodium solution. Methyl nitrite gas was generated *in situ* (see full procedure, 4.3.1) and passed through the solution, and the solution turned color to yellow. The solution was left to stir for 3 days, after which a white precipitate emerged. The solid was filtered off and then dissolved in water. Upon acidification  $\sim\text{pH}$  2 a white precipitate appeared. Yield: 1.521 g (90%);  $^1\text{H}$  NMR (DMSO- $d_6$ , 200 MHz):  $\delta$  7.65-7.73 (m, 1H), 7.84-7.89 (m, 2H), 8.04 (s, 1H), 14.03 (bs, 2H);  $^{13}\text{C}$  NMR (DMSO- $d_6$ , 400 MHz)  $\delta$  109.88, 122.05, 124.87, 127.57, 139.46; IR: 2243  $\text{cm}^{-1}$  (C $\equiv$ N),  $\text{cm}^{-1}$  (C=N); mp: 210-212  $^\circ\text{C}$  (decomp.).

### 5.2.2 Synthesis of tricyanophenyloxime

1,3,5-tris(bromomethyl)benzene was purchased from Aldrich and used without further purification.

#### 5.2.2.1 Synthesis of 1,3,5-tris(cyanomethyl)benzene, 28

To a solution of 1,3,5-tris(bromomethyl)benzene (3.02 g, 8.5 mmol) in THF (25 ml) was added sodium bicarbonate (saturated solution, 30 mL) and sodium cyanide (4.17 g, 85 mmol), followed by 30 mL water. The solution was left to stir for 48 h after which it was acidified with 1 M HCl, the THF was removed *via* rotary evaporation to leave behind a beige solid. Yield: 1.529 g (92%);  $^1\text{H}$  NMR (200 MHz,  $\text{CDCl}_3$ - $d$ ):  $\delta$  3.81 (s, 6H), 7.31 (s, 3H); IR:  $\nu$  2253  $\text{cm}^{-1}$  (C $\equiv$ N); mp: 110-115  $^\circ\text{C}$ .

#### 5.2.2.2 *Synthesis of 1,3,5-tricyanophenyloxime, 29*

Na metal (0.54 g, 23.52 mmol) was dissolved in 540 mL 2-propanol. 1,3,5-tricyano(methylbenzene) (0.80 g, 4.10 mmol) was dissolved in ~100 mL 2-propanol and added to the sodium solution. Methyl nitrite gas was generated *in situ* (see full procedure, 4.3.1) and passed through the solution, and the solution turned yellow in color. The solution was left to stir for 5 days, after which a precipitate emerged. The solid was filtered off and dried. It was then dissolved in water and acidified to ~pH 2 where a brown precipitate appeared. The 2-propanol was removed from the filtrate and the resulting solid was dissolved in water and acidified to ~pH 2, resulting in a brown precipitate. The water was removed from both layers, all fractions were dissolved in methylene chloride and a small amount of methanol, and purified by column chromatography. (3:1 hexanes/ethyl acetate) to yield a white solid. Yield: 0.822 g (71 %);  $^1\text{H}$  NMR (400 MHz,  $\text{DMSO-}d_6$ ):  $\delta$  8.11 (s, 3H), 14.24 (s, 3H);  $^{13}\text{C}$  NMR (400 MHz,  $\text{DMSO-}d_6$ ):  $\delta$  110.34, 124.29, 130.49, 132.17; IR:  $\nu$  2248  $\text{cm}^{-1}$  ( $\text{C}\equiv\text{N}$ ),  $\nu$  11633  $\text{cm}^{-1}$  ( $\text{C}=\text{N}$ ),  $\nu$  3395  $\text{cm}^{-1}$  (O-H); mp: 255-259 °C (decomp.).

#### 5.2.3 *Molecular electrostatic potentials*

The charges on oximes used in this study were calculated using Spartan '06 (Wavefunction, Inc. Irvine, CA). The four molecules were optimized using AM1, and the maxima and minima in the molecular electrostatic potential surface (0.002 e/au isosurface) were determined using a positive point charge as a vacuum as the probe.

#### 5.2.4 *Synthesis of co-crystals*

Some of the ligands employed in this study are shown in Table 5.2. Co-crystals/solids were obtained through slow evaporation on the bench top at room temperature. Only syntheses of those that produced crystals suitable for X-ray crystallography are described here. Solids produced were analyzed by IR spectroscopy (Table 5.4), and crystals were analyzed by IR spectroscopy and X-ray crystallography.

**Table 5.2** Ligands employed in this study and their abbreviations.

Ligand Abbreviation <sup>a</sup>	Ligand Structure	Ligand Abbreviation	Ligand Structure
4,4'-bipy		4,4'-dpe	
3-py-(5,6-dime)bzim		4-py-(5,6-dime)bzim	
3-py-(2-phim)		4-py-(2-phim)	
1,3,5-(5,6-dime)-tribix		2,3,5,6-tmpz	
1,4-(5,6-dime)bibix		1,3-(5,6-dime)bibix	

#### 5.2.4.1 Synthesis of 1,4-dicyanophenylloxime 1,2-di(4-pyridyl)ethane, 26a

**26** (10 mg,  $5.05 \times 10^{-5}$  mol) was dissolved in methanol in a 50 mL beaker. A solution of 4,4'-dpe (11 mg,  $5.97 \times 10^{-5}$  mol) in methanol was added. Colourless prisms suitable for X-ray crystallography were obtained after ~1 week. Mp: 278-283 °C.

#### 5.2.4.2 Synthesis of 1,4-dicyanophenylloxime 1-[(3-pyridyl)methyl]-5,6-dimethylbenzimidazole, 26b

**26** (7 mg,  $3.54 \times 10^{-5}$  mol) was dissolved in methanol in a 50 mL beaker. A solution of 3-py-(5,6-dime)-bzim (10 mg,  $4.22 \times 10^{-5}$  mol) was added. Colourless prisms suitable for X-ray crystallography were obtained after 3 days. Mp: 225-235 °C.



#### **5.2.4.3 Synthesis of 1,4-dicyanophenyloxime 1-[(3-pyridyl)methyl]benzimidazole, 26c**

**26** (8 mg,  $4.04 \times 10^{-5}$  mol) was dissolved in methanol in a 50 mL beaker. A solution of 3-py-(bzim) (10 mg,  $5.53 \times 10^{-5}$  mol) was added. Orange plates suitable for X-ray crystallography were obtained after 1 week. MP: 205-209 °C.

#### **5.2.4.4 Synthesis of 1,4-dicyanophenyloxime 1-[(4-pyridyl)methyl]-2-phenylimidazole, 26d**

**26** (9.00 mg, 0.035 mmol) was dissolved in methanol in a 50 mL beaker. A solution of 4-py-(2-phim) (13.0 mg, 0.048 mmol) was added. Colourless plates suitable for X-ray crystallography were obtained after 1 week. MP: 215-225 °C.

#### **5.2.4.5 Synthesis of 1,4-dicyanophenyloxime 2,3,5,6-tetramethylpyrazine, 26e**

**26** (10.0 mg, 0.062 mmol) was dissolved in methanol in a 50 mL beaker. A solution of 2,3,5,6-tmpyz (8.00 mg, 0.059 mmol) was added. Colourless needles suitable for X-ray crystallography were obtained after 1 week. MP: 268-272 °C.

#### **5.2.4.6 Synthesis of 1,3,5-tricyanophenyloxime 2-bromo-5-methylpyridine, 29a**

**29** (5.00 mg, 0.018 mmol) was dissolved in ethyl acetate in a 50 mL beaker. A solution of 2-bromo-5-methylpyridine (9.00 mg, 0.053 mmol) was added. Colourless prisms were yielded after approximately one week. Mp: 200-203 °C.

#### **5.2.4.7 Synthesis of 1,3,5-tricyanophenyloxime 1,2-di(4-pyridyl)ethane, 29b**

**29** (5.00 mg, 0.018 mmol) was dissolved in ethyl acetate in a 50 mL beaker. A solution of 4,4'-dpe (5.00 mg, 0.027 mmol) was added. This yielded a powdery white solid that was recrystallized from acetonitrile to yield yellow plates. Mp: 246-248 °C.

### **5.2.5 X-ray crystallography**

Data sets were collected on a Bruker SMART APEX diffractometer using molybdenum K $\alpha$  radiation at 100 K. Data were collected using SMART.<sup>8</sup> Single-crystal structure determinations were carried out on five dicyanophenyloxime-based co-crystals, a tricyanoxime-based co-crystal, and a dicyanophenyloxime by itself. The

crystallographic data are displayed in Table 5.2 and hydrogen-bond geometries for all four structures are listed in Table 5.3.

### 5.2.6 *Infra-red spectroscopy and melting point*

Infrared data of the products obtained in the cocrystallizations were acquired using a potassium bromide pellet. An approximate 8:1 ratio of KBr to solid product was combined in an oven-dried mortar and ground to a uniform powder with a pestle. A pellet press was employed to create a transparent KBr pellet that was used for analysis. A Nicolet FT-IR instrument equipped with OMNIC software was used to analyze the data. The resulting IR spectra were printed and analyzed. The main features used for identification are the O-H...N hydrogen-bonding bands at 2500 and 1900  $\text{cm}^{-1}$ .<sup>9</sup> Melting points were performed on a Fisher-Johns apparatus and are uncorrected.

## 5.3 Results

### 5.3.1 *Molecular Electrostatic potential calculations*

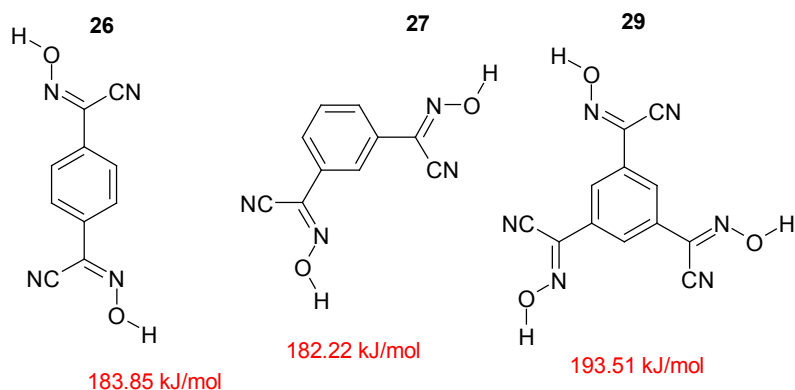


**Figure 5.8** Molecular electrostatic potentials of the di- and tricyanoximes studied here.

Figure 5.8 shows the molecular electrostatic potentials for each dicyanoxime and tricyanoxime. It can be seen that the values do not differ significantly from the substituted mono-cyanophenyl oximes seen previously. Based on this, there should be no notable difference in ability to form co-crystals in terms of donor ability. However, it still remains to be seen as to whether the solubility of these molecules is sufficient enough to bring about heteromeric species from solution. Additionally, an assessment of the

effectiveness of these molecules at forming extended networks will be made, and it will be established as to whether the incorporation of multiple functionalities placed on the same backbone will impede this in any way. To answer these questions the di- and tricyanoxime species will be synthesized and employed in a series of co-crystallization reactions.

Five new co-crystals and a crystal structure of 1,4-dicyanophenyloxime are presented here, along with O-H...N stretches of attempted co-crystallization reactions between the various heterocycles and oximes, Table 5.4.

**Table 5.3** Hydrogen bond geometries for **26**, **26a-e**, and **29a** and **b** .

Co-crystal	D-H...A	d(D-H), Å	d(H...A), Å	d(D...A), Å	<(DHA), °
<b>26<sup>i</sup></b>	O(17)-H(37)...N(18)	0.902(17)	1.900(17)	2.7947(14)	171.2(15)
<b>26a</b>	O(17A)-H(17A)...N(21)	1.008(11)	1.576(11)	2.5780(10)	171.9(11)
	O(17B)-H(17B)...N(21)	1.01(3)	1.71(9)	2.513(11)	133(8)
<b>26b</b>	O(47)-H(47)...N(13)	1.010(16)	1.640(16)	2.6444(13)	171.9(11)
	O(57)-H(57)...N(31)	1.065(17)	1.548(17)	2.6004(14)	168.6(15)
<b>26c<sup>ii</sup></b>	O(37)-H(37)...N(21)	0.95 (3)	1.74 (3)	2.674 (3)	168 (3)
	O(39)-H(39)...N(13)	1.33 (3)	1.35 (3)	2.673 (3)	171 (2)
<b>26d<sup>iii</sup></b>	O(47)-H(47)...N(21)	1.00(2)	1.66(2)	2.6548(16)	171(2)
	O(49A)-H(49A)...N(13) <sup>a</sup>	0.84	1.78	2.6177(16)	171.8
	O(49B)-H(49B)...N(13) <sup>a</sup>	0.84	1.81	2.639(10)	169.3
<b>26e</b>	O(17)-H(17)...N(21)	0.986(14)	1.697(14)	2.6832(10)	177.9(12)
<b>29a<sup>iv</sup></b>	O(21)-H(21)...N(71)	0.91(3)	1.83(3)	2.733(3)	168(3)
	O(41)-H(41)...N(81)	0.66(3)	2.02(3)	2.671(2)	174(4)
	O(61)-H(61)...N(42) <sup>a</sup>	0.70(3)	2.07(3)	2.768(2)	175(3)
<b>29b<sup>v</sup></b>	O211-H211...N311	0.84	1.81	2.609(2)	157.8
	O231-H231...N41A1	0.84	1.84	2.676(2)	170.6
	O231-H231...N41B1	0.84	1.59	2.405(15)	161.1
	O251-H251...N51A1	0.84	1.91	2.718(3)	161.6
	O251-H251...N51B1	0.84	1.56	2.372(13)	160.7
	O212-H212...N312 <sup>a</sup>	0.84	1.80	2.598(2)	157.7
	O232-H232...N41A2#2	0.858(11)	1.82	2.620(4)	157.5
	O232-H232...N41B2#2	0.858(11)	1.96	2.76(3)	157.9
	O252-H252...N51A2#3	0.84	1.77	2.591(4)	165.8
	O252-H252...N51B2#3	0.84	2.02	2.811(14)	156.9

Operators for generating equivalent atoms: (i) <sup>a</sup>-x+5/2, y-1/2; z (ii) -x+3/2, y+1/2, -z+1/2; (iii) <sup>a</sup> x+1, y-1, z-1; (iv) -x,-y+1,-z; (v) <sup>a</sup> x+1, y, z+1; <sup>b</sup> x-1, y+1, z; <sup>c</sup> x, y-1, z.

### 5.3.2 Crystal structure of 1,4-dicyanophenyloxime, 26

The single-crystal structure determination of **26** shows a single molecule of 1,4-dicyanophenyloxime in the asymmetric unit. The oxime moieties are nearly coplanar with the aromatic backbone. The notable interactions occurring within the structure are O-H $\cdots$ N interactions between the oxime and the nitrile (O-H $\cdots$ N: 2.795 Å). These connect four molecules to form a  $R_4^4(34)$  motif resulting in cavities measuring approximately 8.6 x 7.7 Å, Figure 5.9.

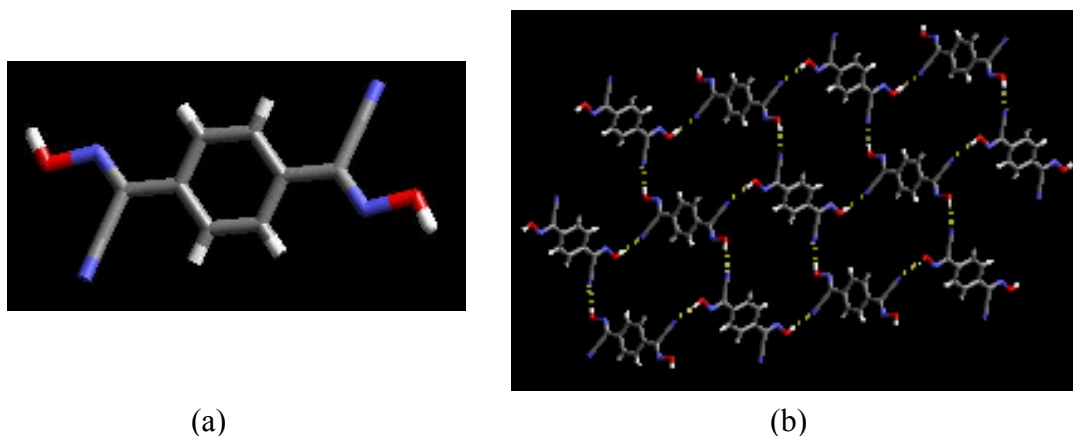


**Figure 5.9** (a) single molecule of 1,4-dicyanophenyloxime and (b) extended network of 1,4-dicyanophenyloxime, displaying the  $R_4^4(34)$  motif.

### 5.3.3 Crystal structure of 1,4-dicyanophenyloxime 1,2-di(4-pyridyl)ethane, 26a

The single-crystal structure determination of **1a** shows a 1:1 co-crystal containing infinite 1D zig-zag chains constructed from O-H $\cdots$ N interactions, Figure 5.10, Table 5.3. The chains are connected through an interaction between the nitrile nitrogen atom and an adjacent C-H proton of a neighbouring dicyanoxime (C-H $\cdots$ N (3.362 Å)). The oxime moiety is coplanar with the aromatic backbone.

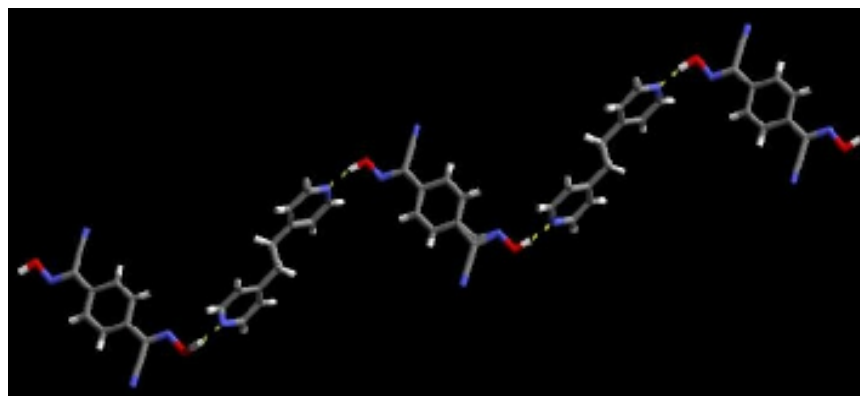


**Figure 5.10** Zig-zag one-dimensional chain in the crystal structure of **26a**.

#### 5.3.4 Crystal structure of 1,4-dicyanophenyloxime 1-[(3-pyridyl)methyl]-5,6-dimethylbenzimidazole, **26b**

The crystal structure of **26b** shows a 2:1 (dicyanoxime:pyridylbenzimidazole) co-crystal containing infinite one-dimensional chain. The chains are formed through primary O-H $\cdots$ N interactions (Table 5.3). Adjacent chains are connected through an interaction between the nitrile nitrogen atom and a methylene proton of the pyridyl(methyl)benzimidazole. (C-H $\cdots$ N: 3.604 Å). The oxime moieties are nearly coplanar with the aromatic backbone.

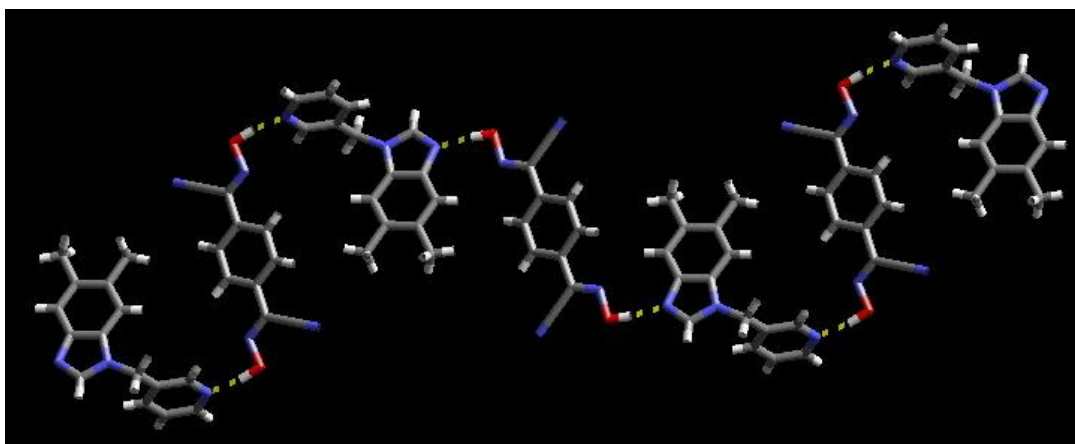


**Figure 5.11** One-dimensional chain in the crystal structure of **26b**.

#### 5.3.5 Crystal structure of 1,4-dicyanophenyloxime 1-[(3-pyridyl)methyl]benzimidazole, **26c**

The crystal structure of **26c** shows a 1:1 co-crystal, with the dicyanoxime forming an O-H $\cdots$ N hydrogen bond to the imidazole moiety, Figure 5.12. A one-dimensional

chain is present in a spiral formation. The nitrile nitrogen atom participates in interactions with adjacent methylene protons ( $C-H \cdots N$ : 3.482 Å). Figure 5.12 shows the helical formation.

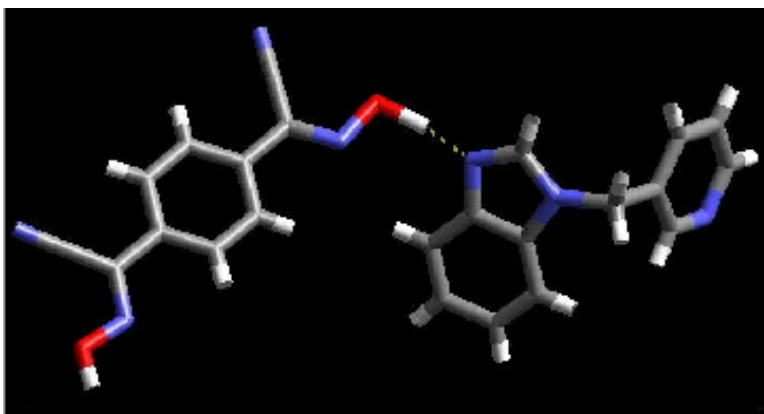
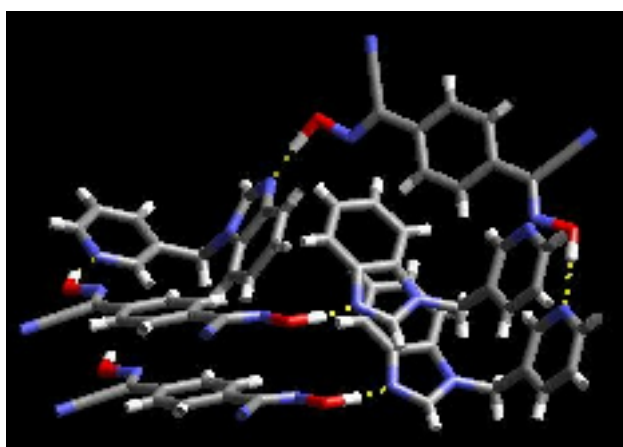
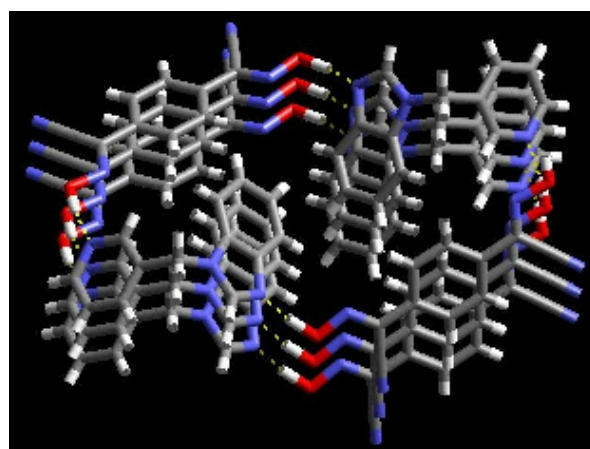


**Figure 5.12** Asymmetric unit in the crystal structure of **26c**.



(a)



(b)

**Figure 5.13** (a) Beginning of the helical formation in **26c** (b) helix in **26c**, shown looking down the axis.

### 5.3.6 Crystal structure of 1,4-dicyanophenyloxime 1-[(4-pyridyl)methyl]-2-phenylimidazole, **26d**

The crystal structure of **26d** shows a 1:1 co-crystal with the oxime moiety interacting with the pyridyl nitrogen atom, resulting in a one-dimensional chain, Figure 5.14. Chains are connected through an interaction between the nitrile nitrogen atom and

an adjacent C-H proton on a dicyanoxime molecule ( $C-H \cdots N$  3.382 Å). The oxime moieties are almost coplanar with the aromatic backbone.

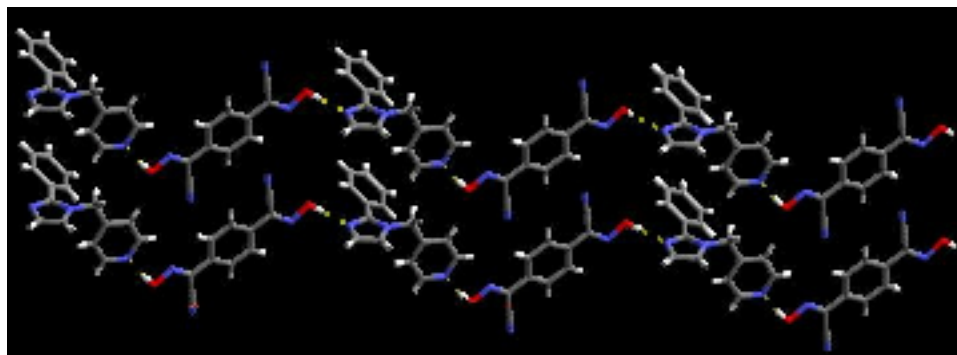


**Figure 5.14** Adjacent chains in the crystal structure of **26d**.

### 5.3.7 *Crystal structure of 1,4-dicyanophenyloxime 2,3,5,6-tetramethyl pyrazine, 26e*

The 1:1 (1,4-dicyanophenyloxime: 2,3,5,6-tetramethyl pyrazine) crystal structure of **26e** shows an infinite one-dimensional chain propagated through O-H $\cdots$ N interactions between the oxime moiety and the pyrazine nitrogen atom. In addition to the O-H $\cdots$ N hydrogen bond there is also an interaction between the nitrogen atom of the oxime moiety and a pyrazine methyl group proton. ( $C-H \cdots C$ : 3.474 Å).

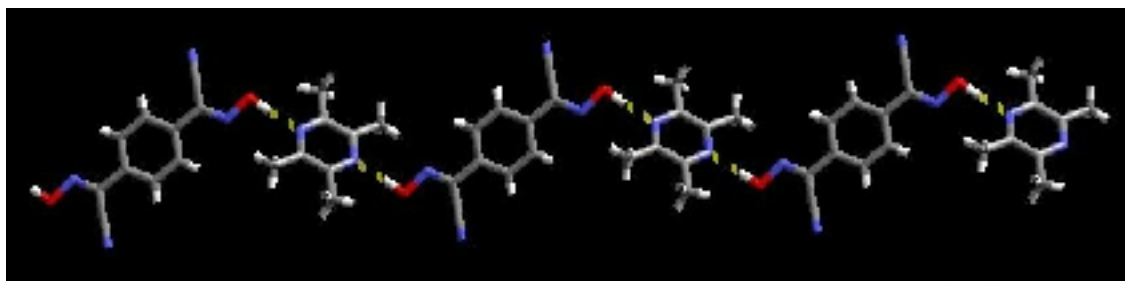


**Figure 5.15** One-dimensional chain in the crystal structure of **26e**.

### 5.3.8 *Crystal structure of (1,3,5-tricyanophenyloxime) 2-bromo-5-methylpyridine, 29a*

The crystal structure of **29a** shows two molecules of 2-bromo-5-methylpyridine and one molecule of tricyanophenyloxime. The two pyridine molecules are connected to the tricyanoxime through O-H $\cdots$ N interactions. The third oxime moiety forms an O-H $\cdots$ N interaction with a nitrile group of an adjacent tricyanoxime moiety, forming a discrete hexamer, Figure 5.16.

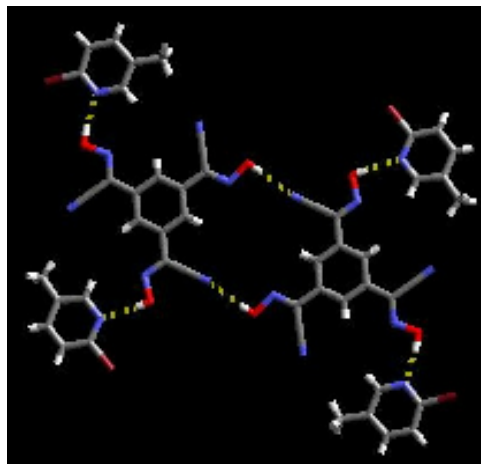
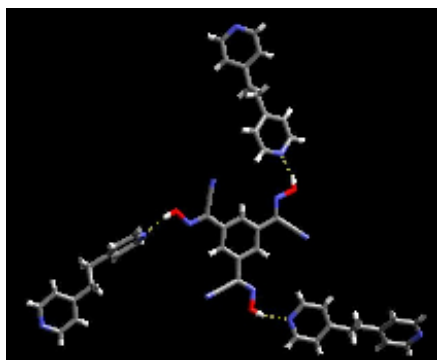


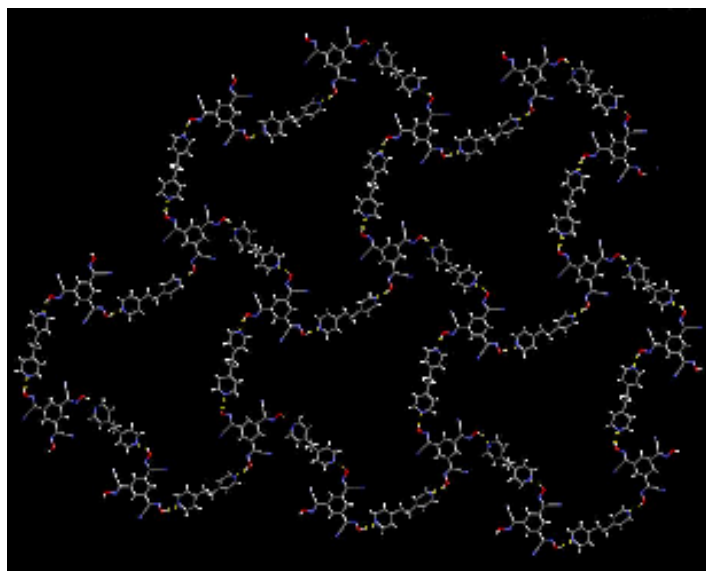
**Figure 5.16** Discrete hexamer in the crystal structure of **29a**.

### 5.3.9 Crystal structure of $(1,3,5\text{-tricyanophenylloxime})_2 [1,4\text{-di}(4\text{-pyridyl})\text{ethane}]_3$ , **29b**

The crystal structure of **29b** shows two molecules of tricyanophenylloxime, three molecules of dipyridylethane, and a molecule of solvent. The three dipyridylethane molecules are attached to all three cyanoxime groups via O-H $\cdots$ N hydrogen bonds, Figure 5.13(a). The structure is a two-dimensional honeycomb grid, Figure 5.17(b). The grids are connected through  $\pi$ - $\pi$  interactions of two tricyanophenylloxime molecules (3.996 Å).



(a)



(b)

**Figure 5.17** (a) hydrogen bonding of three bipyridyl molecules to the tricyanoxime (b) extended two-dimensional grid in the crystal structure of **29b**.



### 5.3.10 IR Spectroscopy

**Table 5.4** IR stretches of co-crystals formed

Heterocycle	IR O-H...N bands (cm <sup>-1</sup> )		
	oxime		
	1,4-dicyanox	1,3- dicyanox	1,3,5-tricyanox
4,4'-bipy	2468, 2095	2555, 1838	2501, 1851
4,4'-dpe	2473, 1941	2484, 1844	2495, 1845
3-py-(5,6-dime)bzim	2520, 1874	2508, 1825	2521, 1851
4-py-(5,6-dime)bzim	2508, 2044	2528, 1858	2514, 1865
3-py-(2-phim)	*	2508, 1838	-
4-py-(2-phim)	2501, 1832	2534, 1838	2504, 1874
1,3,5(5,6-dime)-tribix	*	*	2501, 1871
2,3,5,6-tmpz	2514, 1818	2581, 1765	*
1,4-(5,6-dimebibix)	*	2534, 1984	2567, 1845
1,3-(5,6-dimebibix)	*	2541, 1832	2495, 1865

- indicates no O-H...N stretches were present in the IR spectrum, \* indicates no co-crystallization was attempted.

## 5.4 Discussion

### 5.4.1 Synthesis and characterization

The di- and tricyanoximes have been prepared in good yields and are easy to purify, the dicyanoximes are isolable from the reaction mixture, whilst the tricyanoximes can be easily purified by the means of column chromatography. The polycyanoximes also show extreme promise with their superior solubility over the corresponding carboxylic acids, Table 5.5 and Figure 5.18.

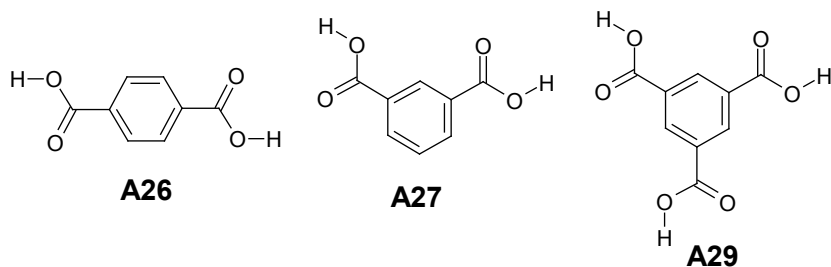


**Figure 5.18** Corresponding carboxylic acids A26, A27, and A29.

**Table 5.5** Melting point and solubilities of acids vs oximes.

Melting point (° C)		Solubility		
		Ethanol	Water	Diethyl ether
<b>26</b>	240-247 (decomp)	soluble	soluble <sup>a</sup>	partially
<b>A26</b>	>300	insoluble	insoluble	insoluble
<b>27</b>	210-212 (decomp.)	soluble	soluble	partially
<b>A27</b>	341-343	soluble	slightly	soluble
<b>29</b>	255-259 (decomp.)	soluble	soluble <sup>a</sup>	soluble
<b>A29</b>	>300	very	slightly	soluble

<sup>a</sup> with heat

The tricyanoxime is soluble in a range of solvents, including ethanol, methanol, diethyl ether, ethyl acetate and acetonitrile. This is in stark contrast to trimesic acid, which is insoluble in most solvents<sup>10</sup>. Both dicyanoximes are also soluble in most solvents, often without heat. The excellent solubility enables both components to *co-crystallize* and reduces the chance of formation of homomeric species. The cyanoximes also have a lower melting point and tend to decompose compared to their carboxylic acid counterparts. Both the solubilities and melting points can be attributed to the acid-acid dimer being more robust than the oxime catemer, as shown in Figure 5.6.

The formation of the oxime moiety can also be traced by the appearance of a broad singlet in the NMR spectrum ~14.0 ppm (dicyanoximes and 14.2 ppm (tricyanoxime), (DMSO-*d*<sub>6</sub>).

#### 5.4.2 IR Spectroscopy

As in the cases of monocyanoximes, co-crystal formation was monitored by the appearance of O-H...N stretches (~1900, ~2500 cm<sup>-1</sup>) in the IR. The dicyanoximes were shown to be just as effective at forming co-crystals as the monocyanoximes. The 1,4-dicyanophenyloxime was shown to be able to form crystals of superior quality compared to the 1,3-dicyanophenyloxime and hence is the reason why more crystal structures have

been obtained. However, according to IR spectroscopy, co-crystals were formed in a total of 9 attempts out of a total 10.

### 5.4.3 *X-ray Crystallography*

A total of six co-crystals were successfully formed and analyzed using X-ray crystallography. In all five dicyanoxime crystal structures, the desired/expected motif was observed, in the formation of infinite one-dimensional chains. In one of these cases, a helical formation of this chain was observed. In all cases an interaction between the nitrile nitrogen atom and a methylene proton is observed. In cases **26a**, **b**, and **d**, where a one-dimensional chain is formed, these interactions are utilized in the connection of adjacent chains. In the case of **26e**, no interactions with the nitrile nitrogen atom are observed, and in **26c** an interaction occurs between the nitrile nitrogen atom and both a methylene proton (3.482 Å) and an aromatic C-H proton (3.551 Å). These interactions are all weak, with bond distances ranging from 3.382-3.604 Å. There are no interactions with the 2-proton on benzimidazole, in either of the structures containing benzimidazole moieties. This is somewhat surprising since this is the most acidic proton on these molecules.

In the tricyanoxime crystal structures the crystal structure with pyridine didn't quite lead to a discrete tetramer in **29a**, however this is just one crystal structure and the tricyanoxime still has the potential to form these types of supermolecules. The predicted/desired supramolecular motif was, however, achieved in **29b**, in the formation of a 2-dimensional honeycomb network. The synthesis of a three-point hydrogen bond donor with excellent solubility has led to the construction of a predictable architecture. The potential of guest inclusion can also be investigated, since the structure forms a porous network. This molecule has great potential and could surpass trimesic acid as a supramolecular reagent, due to its improved properties.

---

---

## References

- <sup>1</sup> S. N. Dale, M. R. J. Elsegood, M. Hemmings, A. C. Wilkinson, *CrystEngComm.*, 2004, **6**, 207.
- <sup>2</sup> (a) D. G. Branzea, A. Guerri, O. Fabelo, C. Ruiz-Perez, L.-M. Chamoreau, C. Sangregorio, A. Caneschi, M. Andruh, *Cryst. Growth Des.*, 2008, **8**, 941; (b) R. Thomas, G. U. Kulkarni, *J. Mol. Struct.* 2008, **873**, 160; (c) K. G. Nath, O. Ivasenko, J. M. MacLeod, J. A. Miwa, J. D. Wuest, A. Nanci, D. F. Perepichka, F. Rosei, *J. Phys. Chem. C*, 2007, **111**, 16996; (d) H. Zhou, H. Dang, J.-H. Yi, A. Nanci, A. Rochefort, J. D. Wuest, *J. Am. Chem. Soc.*, 2007, **129**, 13774; (e) I. Goldberg, J. Bernstein, *Chem. Commun.*, 2007, **2**, 132. (f) M. Du, Z.-H. Zhang, X.-J. Zhao, *Cryst. Growth Des.*, 2005, **5**, 1247.
- <sup>3</sup> Y.-M. Dai, [H.-Y. Shen](#), [J.-F. Huang](#), *Acta Cryst.* 2005, **E61**, o3410-o3411.
- <sup>4</sup> C. V. K. Sharma, M. J. Zawarotko, *Chem. Comm.*, 1996, 2655.
- <sup>5</sup> C. B. Aakeröy, M. E. Fasulo, J. Desper, *Mol. Pharm.*, 2007, **4**, 317.
- <sup>6</sup> X.-H. Li, X.-X. Lei, S. Wang, *Acta. Cryst. Sect E. Struct Rep.*, 2005, **E61**, o1802–o1804.
- <sup>7</sup> C. B. Aakeröy, D. J. Salmon, *CrystEngComm*, 2005, **7**, 439.
- <sup>8</sup> SMART v5. 060, Bruker Analytical X-ray Systems, Madison, WI, 1997-1999.
- <sup>9</sup> (a) N. V. Drichko, G. Y. Kerenskai, V. M. Schreiber, *J. Mol. Struct.*, 1999, **477**, 127; (b) J. P. Castaneda, G. S. Denisov, S. Y. Kucherov, V. M. Schreiber, A. V. Shurukhina, *J. Mol. Struct.*, 2003, **660**, 25.
- <sup>10</sup> R. C. Weast, *Handbook of Chemistry and Physics*, 51<sup>st</sup> Edition, 1970-1971.

# CHAPTER 6 - Construction, Deconstruction, and Reconstruction of Ternary Supermolecules

## 6.1 Introduction

Molecular co-crystals have received considerable attention recently. Despite numerous publications featuring new co-crystals,<sup>1</sup> however, (just a handful of recent examples are referenced here), very few of them are constructed from three components or more using precise and well-defined supramolecular synthons<sup>2</sup>. There is no doubt that bringing three different molecular species into one crystalline lattice without making or breaking covalent bonds, is still exceedingly difficult. It has previously been shown that ditopic hydrogen-bond acceptors based on pyridyl/benzimidazole can act as a hub for the assembly of ternary co-crystals in combination with two carboxylic acids of different strengths.<sup>3</sup> The stronger acid (based upon  $pK_a$  values) binds to the best hydrogen-bond acceptor (the more basic N-heterocycle), whereas the weaker acid binds to the second-best acceptor site, Figure 6.1.

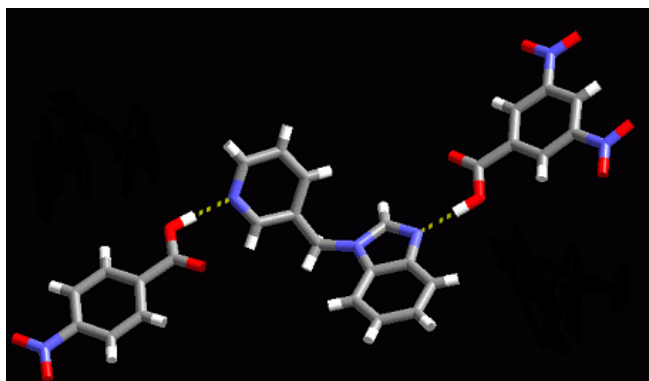


**Figure 6.1** Ternary supermolecule constructed from two different carboxylic acids of different acidities.<sup>3</sup>

The use of  $pK_a$  values for identifying the better hydrogen-bond donor can work within a family of compounds,<sup>4</sup> but such data offers no reliable information when comparing hydrogen-bond donor/acceptor strength for different functional groups.<sup>5</sup> Instead, Hunter has shown how calculated molecular electrostatic potential (MEP)

surfaces can be employed for assigning (and ranking) the relative hydrogen-bond donor/acceptor strengths across a wide range of chemical functionalities.<sup>6</sup> The calculations can be performed at a relatively low level of theory (AM1), which makes this a versatile and readily accessible tool.

### **6.1.1 Goals**

In this chapter a hypothesis-driven protocol for the construction of ternary supermolecules and co-crystals is presented where stoichiometry and primary intermolecular interactions can be readily rationalized. The approach is based upon four complementary steps:

1) Allow a series of ditopic molecules equipped with two different hydrogen-bond acceptors to react with a molecule containing two different hydrogen-bond donor moieties. Use structural data for the resulting binary 1:1 co-crystals to establish intermolecular binding preferences.

2) Once complementary hydrogen-bond interactions can be ranked according to frequency of occurrence, use covalent synthesis to deconstruct one of the ditopic compounds into mono-functional components, Figure 6.2.

3) Combine a ditopic ligand (with two hydrogen-bond acceptors) and two different hydrogen-bond donors in the deliberate synthesis of a specific ternary co-crystal (II), Figure 6.2. This approach requires a library of ditopic supramolecular reagents that contain either two different hydrogen-bond donors or two different hydrogen-bond acceptors that can be ranked according to relative hydrogen-bonding capability.

4) Use calculated molecular electrostatic potentials to predict/rationalize the specific binding events.

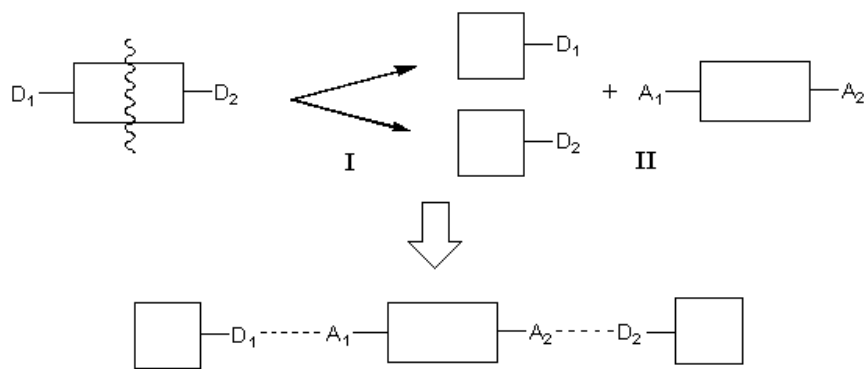


**Figure 6.2** Protocol for deconstructing and reconstructing ternary co-crystals.  $D_1$  and  $D_2$  = hydrogen-bond donors,  $A_1$  and  $A_2$  = hydrogen-bond acceptors.

In order to test our hypothesis we employed four asymmetric ditopic hydrogen-bond acceptors, (**11-14** and **30**), Figure 6.3 and two asymmetric ditopic hydrogen-bond donors, **31** and **4-hydroxybenzoic acid (4-OH BA)**, Figure 6.3. The maxima/minima on the AM1-based MEPs for all the supramolecular reagents are listed in Table 6.2. We now begin to construct co-crystals with the assumption that the hydrogen bonds in this system are primarily electrostatic in nature. Consequently, by applying the best donor/best acceptor, second-best donor/second-best acceptor rationale, in the context of the calculated charges in these molecules, we can postulate which molecular recognition events will most likely appear in the resulting crystal structures.

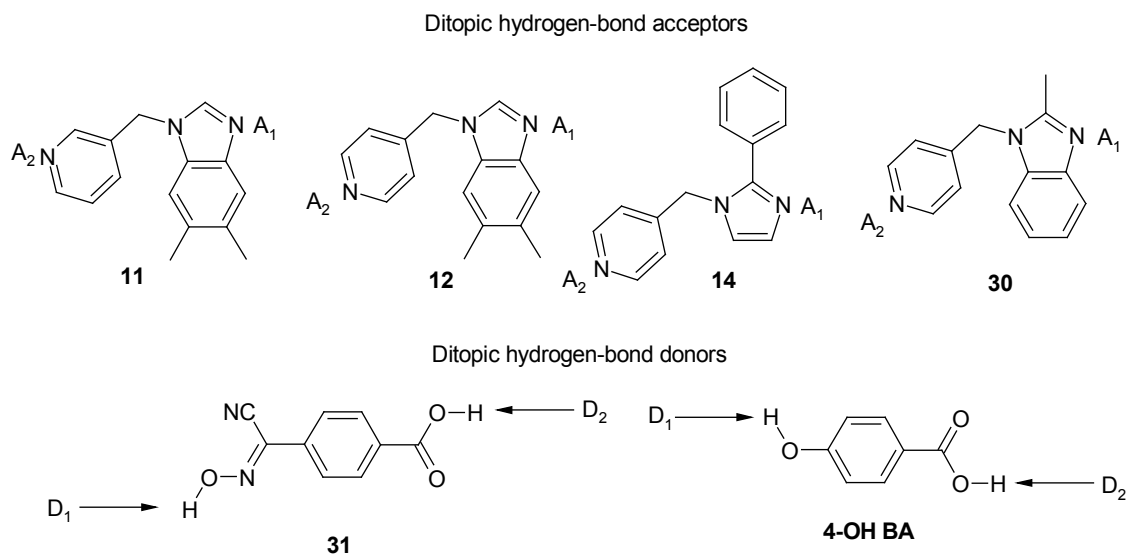


**Figure 6.3** Asymmetric ditopic donors and acceptors employed in this study.

## 6.2 Experimental

### 6.2.1 Synthesis of ditopic hydrogen-bond donor and acceptor molecules

The syntheses of supramolecular reagents **11**, **12** and **14** are reported in Chapter 3. 4-Hydroxybenzoic acid, 4-OH BA, was purchased from Aldrich and used without further purification.

#### 6.2.1.1 Synthesis of 4-(2-methylbenzimidazol-1-yl)methyl pyridine, **30**

2-Methylbenzimidazole (2.0 g, 15.13 mmol), was dissolved in 40 ml dry tetrahydrofuran with stirring under N<sub>2</sub>. NaOH (6.06 g, 150 mmol) was added and the mixture was left to stir for 2 h, upon which 4-picolyl chloride hydrochloride (2.46 g, mmol) was added in a suspension of dry THF. The mixture was left to stir under reflux for 2 days after which water (10 mL) was added to dissolve the NaOH and NaCl that had formed, and the two layers were separated. The water layer was washed with ethyl acetate and the fractions collected and combined with the THF layer. The organic layer was dried over magnesium sulfate and subsequently removed via rotary evaporation and the resulting brown solid was chromatographed on silica with a mixture of hexane/ethyl acetate as the eluent to produce a pale brown oil. Yield: 2.566 g (80%); <sup>1</sup>H NMR (CDCl<sub>3</sub>-d, 400 MHz) δ 2.54 (s, 3H), 5.31 (s, 2H), 6.93 (d, 2H, *J* = 6 Hz), 7.15-7.28 (m, 3H), 7.74 (d, 1H, *J* = 12 Hz), 8.54 (d, 2H, *J* = 8 Hz); <sup>13</sup>C NMR (200 MHz, CDCl<sub>3</sub>-d) δ 13.05, 45.19, 108.75, 118.46, 120.62, 121.25, 121.90, 122.14, 134.45, 141.70, 144.61, 149.57, 151.24.

#### 6.2.1.2 Synthesis of 1,4-carboxyphenylacetonitrile, **31**

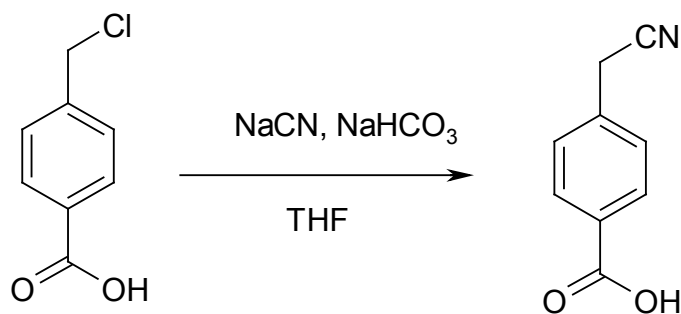


**Figure 6.4** Reaction scheme for the synthesis of 4-carboxyphenylacetonitrile, **31**



The synthesis of **31** was carried out according to a previously published procedure.<sup>7</sup> 4-chloro(methyl)benzoic acid (5.028g, 29.50 mmol) was dissolved in THF (40 mL). To this solution was added NaHCO<sub>3</sub> (saturated solution, 25 mL), whereby fizzing occurred. NaCN (8.49 g, 173 mmol) was added, followed by the addition of H<sub>2</sub>O (30 mL). The solution was left to stir for ~48 h after which it was cooled in an ice bath and acidified to pH=2. The THF was then removed under vacuum, where a brown precipitate emerged which was filtered off, and dissolved in 1M NaOH. Two spatulas of decolorizing charcoal were added to the solution and the mixture was filtered. The basic solution was then acidified with 1M HCl, upon which a tan-colored precipitate appeared, which was subsequently filtered off. Yield: 4.695g (98%); <sup>1</sup>H NMR (DMSO-d<sub>6</sub>, 200 MHz): δ 4.16 (s, 2H), 7.48 (d, 2H, J = 8 Hz), 7.96 (d, 2H, J = 8 Hz); IR: 3421 cm<sup>-1</sup> (O-H), 2248 cm<sup>-1</sup> (C≡N), 1680 cm<sup>-1</sup> (C=O); mp: 195-200 ° C.

#### 6.2.1.2 *Synthesis of 1,4-carboxyphenylcyanoxime, 32*

The conversion of 1,4-carboxyphenylacetonitrile into the corresponding cyanoxime was carried out using the method outline in Chapter 4. 2-Propanol (240 mL) was placed in a 500 mL Erlenmeyer flask. Nitrogen gas was bubbled through the solution for a few minutes after which sodium metal (0.049 g, 2.1 mmol) cut into small pieces and was added to the solution. After all the sodium had dissolved, **5** (0.344 g, 2.14 mmol) was dissolved in 2-propanol (~50 mL) with heat. This solution was then added to the iso-propoxide solution, upon which a small amount of precipitate was observed, and the solution turned yellow after a few minutes. 15 g of NaNO<sub>2</sub>, 100 mL distilled water, and 50 mL methanol were placed in a separate 500 mL three necked flask. The solution was stirred until all the NaNO<sub>2</sub> had dissolved. A greased septum was placed in one of the necks, a greased one-hole rubber stopper was placed in the central neck, and a dropper funnel (125 mL) was also greased and attached to the third neck with a Keck clip. A solution of H<sub>2</sub>O/H<sub>2</sub>SO<sub>4</sub> (2:1, 50 mL) was measured out and placed in an ice bath (4 °C). A glass U-tube was then placed through the hole in the rubber septum of the three-necked flask and into the Erlenmeyer flask. The acid/water solution was slowly added dropwise to the NaNO<sub>2</sub>/H<sub>2</sub>O/MeOH solution, and bubbles of evolving CH<sub>3</sub>ONO gas were immediately seen flowing into the Erlenmeyer flask containing the *i*-PrONa/acetonitrile solution. The acid/water mixture was continuously added to the NaNO<sub>2</sub>/H<sub>2</sub>O/MeOH

solution in small aliquots until all was added. The U-tube apparatus was dismantled, and the Erlenmeyer flask containing the yellow *i*-PrONa/acetonitrile/CH<sub>3</sub>ONO solution was stoppered and left to stir in an ice bath overnight. The next morning a small amount of solid had precipitated from the solution, which was filtered off. The remaining solvent was removed from the reaction mixture via rotary evaporation, resulting in a light yellow solid. This solid was filtered off and determined to be the sodium salt of the compound via <sup>1</sup>H NMR. All of the salt was collected in a beaker and dissolved in distilled water. A magnetic stir bar was added, and the beaker was placed in an ice bath on a stir plate. HCl (1M) was added in small aliquots until a white precipitate began to form. The addition of the acid was continued until the pH was around 5. The solid precipitated was filtered off and shown to be the free carboxyphenylcyanoxime. Yield: 0.316g (79%); <sup>1</sup>H NMR (DMSO-d<sub>6</sub>, 200 MHz): 7.84 (d, 2H, *J* = 8.8 Hz), 8.06 (d, 2H, *J* = 9 Hz), 14.1 (s, 1H); <sup>13</sup>C NMR (200 MHz, DMSO-d<sub>6</sub>) δ 109.22, 124.98, 129.43, 129.93, 131.78, 132.57, 165.78; IR: 3380 cm<sup>-1</sup> (O-H), 2228 cm<sup>-1</sup> (C≡N), 1710 cm<sup>-1</sup> (C=O); mp: 255-260 ° C (decomp.).

### 6.2.2 *Synthesis of co-crystals*

Several reactions were performed with various asymmetric ditopic hydrogen-bond acceptor and donor molecules, and several ternary co-crystallization reactions were attempted. Since selectivity of the molecules is being probed, only the reactions that produced crystals suitable for X-ray crystallography are discussed here.

#### 6.2.2.1 *Synthesis of 4-(5,6-dimethylbenzimidazol-1-yl)methylpyridine 4-carboxyphenylcyanoxime (1:1), 12:32*

**32** (0.010 g, 0.0526 mmol) was dissolved in methanol (2 mL) and to this solution was added a methanolic solution of **12** (0.006 g, 0.0236 mmol). Colorless prisms were obtained after three weeks; mp: 195-200 °C.

#### 6.2.2.2 *Synthesis of 4-(2-phenylimidazol-1-yl)methylpyridine 4-hydroxybenzoic acid (1:1), 14:4-OH BA*

**14** (0.015g, 0.063 mmol) was dissolved in 2 mL ethanol. 4-hydroxybenzoic acid (0.009 g, 0.063 mmol) was dissolved in ethanol with heat and subsequently added to the

ethanolic solution of **4-OH BA**. Colorless plates were obtained after approximately 12 days; mp: 165-168 °C.

### 6.2.2.3 Synthesis of pentamethylbenzoic acid 4-(2-methylbenzimidazol-1-yl)methylpyridinephenylcyanoxime (1:1:1) 30:PMBA:25

To a 2 mL solution of 4-(2-methylbenzimidazole-1-yl)methyl pyridine (0.017g, 0.076 mmol) in methanol was added pentamethylbenzoic acid (0.015 g, 0.076 mmol) in 3 mL methanol and phenylcyanoxime (0.011g, 0.076 mmol) in 3 mL methanol. Slow evaporation of the solvent yielded a white solid. This solid was subsequently redissolved in ethyl acetate to yield colorless plates after 2 weeks; mp: 122-126 °C.

## 6.3 Results

**Table 6.1** Hydrogen-bond geometries for **12:32**, **14:4-OH BA** and **30:PMBA:25**

Co-crystal	D-H...A	d(D-H)	d(H...A)	d(D...A)	<(DHA)
<b>12:32</b> <sup>i</sup>	O(41)-H(41)...N(31)	0.86(5)	1.79(5)	2.612(3)	161(5)
	O(48)-H(48)...N(13) <sup>a</sup>	0.98(4)	1.62(4)	2.603(3)	174(4)
<b>14:4-OH BA</b> <sup>ii</sup>	O(41)-H(41)...N(21)	0.87(3)	1.82(3)	2.693(2)	174(3)
	O(44)-H(44)...N(13) <sup>a</sup>	0.89(3)	1.78(3)	2.659(3)	166(3)
<b>30:PMBA:25</b>	O(37)-H(37)...N(13)	0.88(5)	1.76(5)	2.636(3)	173(4)
	O(51)-H(51)...N(21)	1.05(5)	1.58(5)	2.627(4)	171(4)

i) <sup>a</sup> x-1,y-1,z+1; ii) <sup>a</sup> x+1,y+1,z-1

### 6.3.1 Crystal structure of 4-(5,6-dimethylbenzimidazol-1-yl)methylpyridine 4-carboxyphenylcyanoxime (1:1), 12:32

The crystal structure of **12:32** shows one molecule of 4-(5,6-dimethylbenzimidazol-1-yl)methylpyridine and one molecule of 4-carboxyphenylcyanoxime. The carboxylic acid moiety binds to the pyridyl nitrogen atom and the cyanoxime moiety binds to the imidazole nitrogen atom, Figure 6.5. The result is an infinite one-dimensional chain.

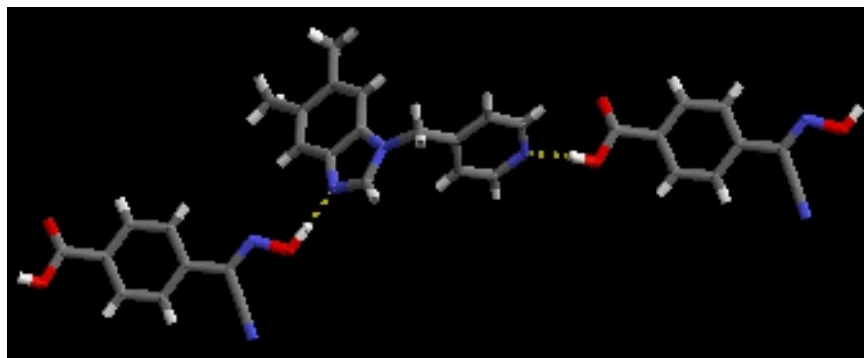


**Figure 6.5** Recognition events in the crystal structure of **12:32**.

### 6.3.2 *Crystal structure of 4-(2-phenylimidazol-1-yl)methylpyridine 4-hydroxybenzoic acid, 14:4-OH BA*

The crystal structure of **14:4-OH BA** shows one molecule of 4-(2-phenylimidazol-1-yl)methylpyridine and one molecule of 4-hydroxybenzoic acid. The hydroxyl group forms a hydrogen bond to the imidazole nitrogen atom and the carboxylic acid moiety forms a hydrogen bond to the pyridyl nitrogen atom, Figure 6.6. This results in the formation of a one-dimensional chain.

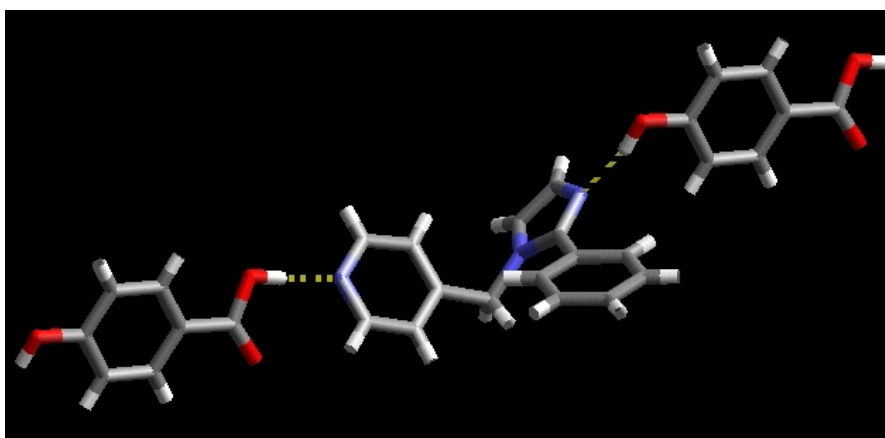


**Figure 6.6** Recognition events in the crystal structure of **14:4-OH BA**.

### 6.3.3 *Crystal structure of pentamethylbenzoic acid 4-(2-methylbenzimidazol-1-yl)methylpyridinephenylcyanoxime(1:1:1), 30:PMBA:25*

The crystal structure of **30:PMBA:25** shows one molecule of 4-(2-methylbenzimidazol-1-yl)methylpyridine, one molecule of pentamethylbenzoic acid, and

one molecule of phenylcyanoxime. The cyanoxime binds to the imidazole nitrogen atom and pentamethylbenzoic acid binds to the pyridine nitrogen atom, Figure 6.7.

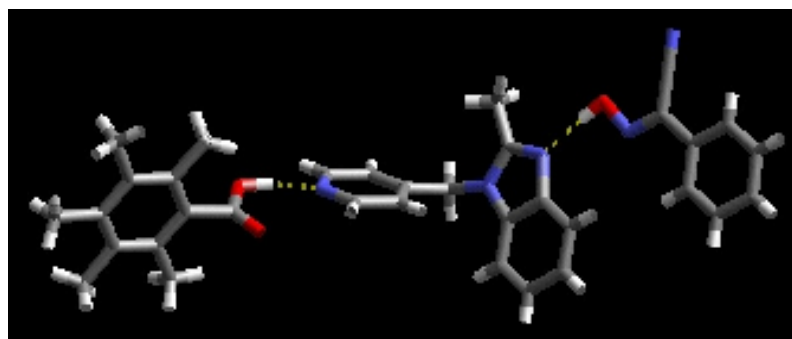


**Figure 6.7** Recognition events in the crystal structure of **30:PMBA:25**.

### 6.3.4 Molecular electrostatic potentials

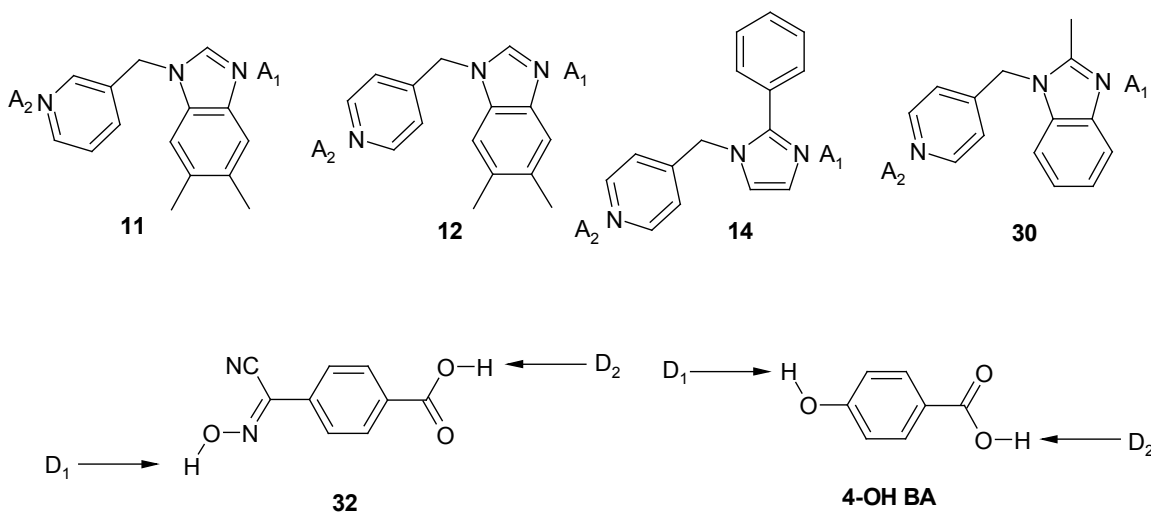


**Figure 6.8** Supramolecular reagents and their calculated molecular electrostatic potentials, Table 6.2.

**Table 6.2** Calculated molecular electrostatic potentials for molecules **30-33** and **35-39** <sup>8</sup>

Molecule	MEP for A <sub>1</sub> kJ mol <sup>-1</sup>	MEP for A <sub>2</sub> kJ mol <sup>-1</sup>
<b>30</b>	-301	-255
<b>31</b>	-299	-274
<b>32</b>	-311	-271
<b>33</b>	-299	-269
Molecule	MEP for D <sub>1</sub>	MEP for D <sub>2</sub>
<b>35</b>	+190	+152
<b>4-OH BA</b> *	+197	+136
Phenylcyanoxime, <b>25</b>	+171	-
<b>PMBA</b> *	+129	-

\* 4-OH BA = 4-hydroxybenzoic acid; PMBA = Pentamethylbenzoic acid.

## 6.4 Discussion

All of the binding events that took place in each of the crystal structures obtained were in agreement with the best-donor/best acceptor theory, and the calculated molecular electrostatic potentials can be used as a tool to accurately rank the specific binding sites in terms of charge. The binding preferences were first established in **31:35** and **32:36**, where, in both cases, the best donor, (the cyanoxime and the hydroxyl group, respectively) bound to the best acceptor (the imidazole nitrogen atom). It is conceivable, however, that the carboxylic acid is, in fact, determining the connectivity in both these cases by preferentially binding (and outcompeting the other donors) to the pyridine moiety. It was necessary therefore, to find out how a single oxime moiety would behave (in the absence of a competing donor) when faced with a ditopic molecule such as **11**, **12** **14** or **30**. These structures were reported in Chapter 3 (**11i**, **12f**, and **12g**).

All of these structures were of 1:1 stoichiometry and in each case the oxime moiety formed a hydrogen bond with the best acceptor of the two hydrogen-bond acceptor sites. We now have support, from six different crystal structures, that a binding preference and hierarchy of intermolecular interactions based upon simple MEPs can be employed as the basis for a versatile supramolecular synthetic strategy. In order to prepare a ternary co-crystal, a ditopic hydrogen-bond donor was deconstructed into separate fragments, that were subsequently allowed to react, in a 1:1:1 ratio, with the ditopic hydrogen-bond acceptor **30**. Phenylcyanoxime, **25**, ranks as a better hydrogen-bond donor than pentamethylbenzoic acid, **PMBA**, and the structural outcome is shown

in Figure 6.8. The connectivity in this supermolecule mirrors the intermolecular behavior observed in **12:32**, and can again be rationalized using an electrostatic argument based upon calculated molecular electrostatic potentials.

#### 6.4.1 Calculating the strength of intermolecular interactions

The calculated molecular electrostatic potentials of each hydrogen bond donor and acceptor molecule can be utilized to estimate the strength of the hydrogen bond that they participate in. The free energy,  $\Delta\Delta G$ , can be calculated and we can estimate which interaction is the most energetically favored, and therefore which one is most likely to form. This can be done for binary systems, when the incoming hydrogen-bond donor has a choice at which acceptor to bind to, Figure 6.9, or in ternary systems where the overall energy would govern the binding outcomes. This hypothesis goes hand-in-hand with the best-donor best acceptor approach, in terms of charges, since the best donor would contain the highest positive charge, and the best acceptor would contain the highest negative charge, and so the energy calculated between the two would have the highest (negative) value.

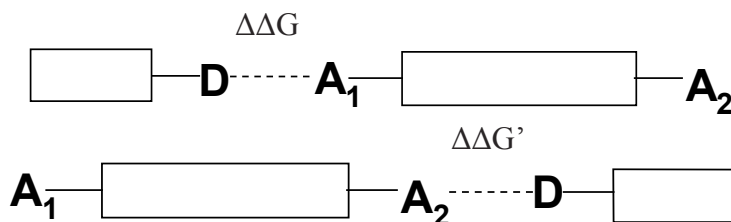


**Figure 6.9** Representation of the two possible binding outcomes between a ditopic hydrogen-bond acceptor molecule, and a monotopic donor. The interaction with the highest negative value of  $\Delta\Delta G$  would be the most favored.

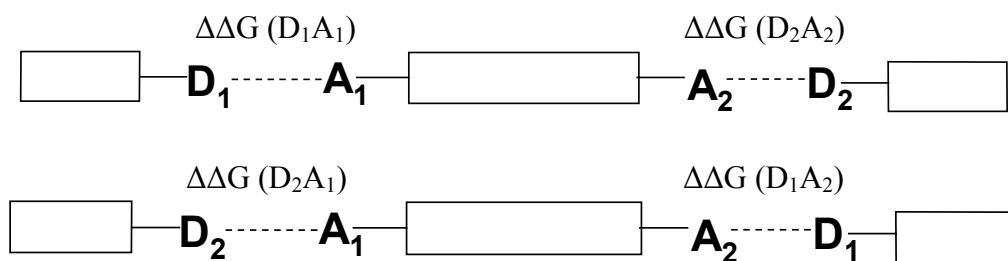


**Figure 6.10** Representation of the possible binding outcomes between two hydrogen bond donors of different hydrogen-bonding strength and a ditopic acceptor.

Figure 6.10 shows four possible outcomes of a co-crystallization between two different hydrogen-bond donors and a ditopic acceptor. The interaction energies  $\Delta\Delta G (D_1A_1)$  and  $\Delta\Delta G (D_2A_2)$  correspond to the energies of interactions between the best donor and best acceptor and the second best donor and second best acceptor. Whereas  $\Delta\Delta G (D_2A_1)$   $\Delta\Delta G (D_1A_2)$  correspond to the energies for the reverse interactions, Figure 6.10.

The calculated interaction energies for each of the crystal structures obtained here are displayed in Table 6.3.

**Table 6.3** Calculated interaction energies for co-crystals **12:32**, **14:4-OH BA**, **11i**, **12f**, **12g** and **30:PMBA:25**

Co-crystal	$\Delta\Delta G (D_1A_1)/$ $\text{kJ mol}^{-1}$	$\Delta\Delta G (D_2A_2)/$ $\text{kJ mol}^{-1}$	$\Sigma\Delta\Delta G/$ $\text{kJ mol}^{-1}$	$\Delta\Delta G (D_2A_1)/$ $\text{kJ mol}^{-1}$	$\Delta\Delta G (D_1A_2)/$ $\text{kJ mol}^{-1}$	$\Sigma\Delta\Delta G/$ $\text{kJ mol}^{-1}$
<b>12:32</b>	-21.46	-15.08	-36.54	-16.82	-19.24	-36.06
<b>14:4-OH BA</b>	-22.80	-13.52	-36.32	-15.60	-19.76	-35.36
<b>11i</b>	-20.88	-17.64	-	-	-	-
<b>12f</b>	-17.40	-15.90	-	-	-	-
<b>12g</b>	-20.30	-18.55	-	-	-	-
<b>30:PMBA:25</b>	-19.14	-13.00	-32.14	-14.50	-17.16	-31.66

In every case the most stable calculated interaction is reflected in the crystal structure. The differences of the sum of the total energies are marginal, and as a result cannot quantify the systems here in terms of energy, because the interaction energy calculations do not take into account factors such as the effect of solvent, or the distances between atoms (which would lead to an increase in energy). The charges of the



individual atoms, however, are a valuable tool in determining the best donor and best acceptor of a system, and hence in the predictability of intermolecular binding preferences. According to the bond energy calculations for  $\Delta\Delta G$  ( $D_1A_1$ ) and  $\Delta\Delta G$  ( $D_2A_1$ ), the best donor forms the strongest bond with the best acceptor than it does with the second best acceptor. This is true in every case.

## 6.5 Conclusions

The deceptively simple act of molecular recognition is achieved by balancing a range of relatively weak non-covalent, forces and to determine the reliability and limitations of the synthetic protocol presented here, a large number of reactions need to be examined in a systematic manner. The simplicity of the synthetic principles employed herein, should make it relatively easy to modify the nature of the different building blocks in order to maximize the supramolecular yield, and by translating molecular function into predictable intermolecular recognition, it may be possible to develop much more versatile supramolecular synthetic pathways for materials design and biological mimics.

---

## References

<sup>1</sup>(a) M. Vartanian, A. C. B. Lucassen, L. J. W. Shimon, M. E. van der Boom, *Cryst. Growth Des.*, 2008, **8**, 786; (b) W. W. Porter III, S. C. Elie, A. J. Matzger, *Cryst. Growth Des.*, 2008, **8**, 14; (c) T. Friscic, W. Jones, *Faraday Discuss.*, 2007, **136**, 167; (d) C. B. Aakeröy, N. Schultheiss, J. Desper, C. Moore, *New J. Chem.*, 2006, **30**, 1452; (e) M. Du, Z.-H. Zhang, X.-G. Wang, H.-F. Wu, Q. Wang, *Cryst. Growth Des.*, 2006, **6**, 1867; (f) M. Du, Z.-H. Zhang, X.-G. Wang, C.-P. Li, *J. Mol. Struct.*, 2006, **791**, 131; (g) P. Rizzo, C. Daniel, A. De Girolamo Del Mauro, G. Guerra, *Chem. Mater.*, 2007, **19**, 3864; (h) S. L. Childs, K. I. Hardcastle, *CrystEngComm*, 2007, **9**, 364; (i) S. L. Childs, K. Hardcastle, *Cryst. Growth Des.*, 2007, **7**, 1291; (j) M. Dabros, P. R. Emery, V. R. Thalladi, *Angew. Chemie, Int. Ed.*, 2007, **46**, 4132; (k) R.-H. Nair, *Mol. Pharm.*, 2007, **4**, 299; (l) J. A. Bis, P. Vishweshwar, D. Weyna, M. J. Zaworotko, *Mol. Pharm.*, 2007, **4**, 401; (m) J. N. Babu, S. L. Reddy, A. Nangia, *Mol. Pharm.*, 2007, **4**, 417; (n) S. Karki, T. Friscic, W. Jones, W. D. S. Motherwell, *Mol. Pharm.*, 2007, **4**, 347; (o) C. B. Aakeröy, M. E. Fasulo, J. Desper, *Mol. Pharm.*, 2007, **4**, 317; (p) M. R. Caira, *Mol. Pharm.*, 2007, **4**, 310; (q) A. V. Trask, *Mol. Pharm.*, 2007, **4**, 301.

<sup>2</sup> (a) B. R. Bhogala, S. Basavoju and A. Nangia, *CrystEngComm*, 2005, **7**, 551; (b) B. R. Bhogala, S. Basavoju, A. Nangia, *Cryst. Growth Des.*, 2005, **5**, 1683; (c) C. B. Aakeröy, A. M. Beatty, B. A. Helfrich, *Angew. Chem., Int. Ed.*, 2001, **40**, 3240; (d) T. Friscic, A. V. Trask, W. Jones, W. D. S. Motherwell, *Angew. Chem., Int. Ed.*, 2006, **45**, 7546; (e) T. Smolka, R. Boese, R. Sustmann, *Struct. Chem.*, 1999, **10**, 429; (f) C. B. Aakeröy, J. Desper, E. Elisabeth, B. A. Helfrich, B. Levin, J. F. Urbina, *Z. Kristallogr.*, 2005, **220**, 325.

<sup>3</sup> C. B. Aakeröy, J. Desper, J. F. Urbina, *Chem. Commun.*, 2005, 2820.

<sup>4</sup> B. G. Tehan, E. J. Lloyd, M. G. Wong, W. R. Pitt, J. G. Montana, D. T. Manallack, E. Gancia, *Quant. Struct. Act. Relat.*, 2002, **21**, 457.

<sup>5</sup> C. Laurence and H. Berthelot, *Perspect. Drug Discovery Des.*, 2000, **18**, 39.

<sup>6</sup> C. A. Hunter, *Angew. Chem., Int. Ed.*, 2004, **43**, 5310.

---

<sup>7</sup> A. M. Hayallah, J. Sandoval-Ramírez, U. Reith, U. Schobert, B. Preiss, B. Schumacher, J. W. Daly, C. E. Muller, *J. Med. Chem.* 2002, **45**, 1500.

<sup>8</sup> Molecular structures for 1–8 were constructed using Spartan '04 (Wavefunction, Inc. Irvine, CA). All seven molecules were optimized using AM1, with the maxima and minima in the electrostatic potential surface (0.002 e au<sup>-1</sup> isosurface) determined using a positive point charge in the vacuum as a probe.

# CHAPTER 7 - Application of Cyanoxime and Amide building blocks in the Supramolecular Assembly of Metal-Containing 1D-Architectures

## 7.1 Introduction

There is an increasing interest in the construction of metal-containing extended frameworks<sup>1</sup> because it is possible to impart specific properties through crystal engineering of metal-containing architectures, by organizing or assembling molecules through non-covalent interaction such as coordination bonds<sup>2</sup> and hydrogen bonds. One of the most challenging problems is the difficulty in controlling the orientation of the building blocks involved in order to achieve the desired connectivities and properties.

### 7.1.1 Supramolecular approach

A synthetic strategy for the construction of such metal-containing networks combines a suitable ligand moiety (for metal coordination), with an appropriate hydrogen-bond functionality (for the supramolecular chemistry). An example of such a ligand is isonicotinamide, which has been employed in coordination chemistry with a variety of metals, Figure 7.1.<sup>3</sup>

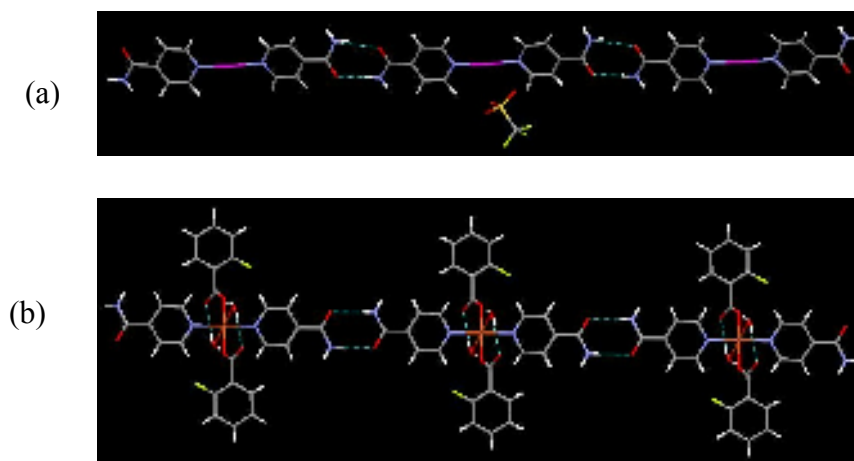


**Figure 7.1** Metal coordination and supramolecular chemistry in the crystal structures of (a) (isonicotinamide)silver(I)trifluoromethanesulfonate dihydrate<sup>4</sup> and (b) Diaqua-bis-(isonicotinamide-N)bis(2-fluorobenzoato)-O-copper(II).<sup>5</sup>

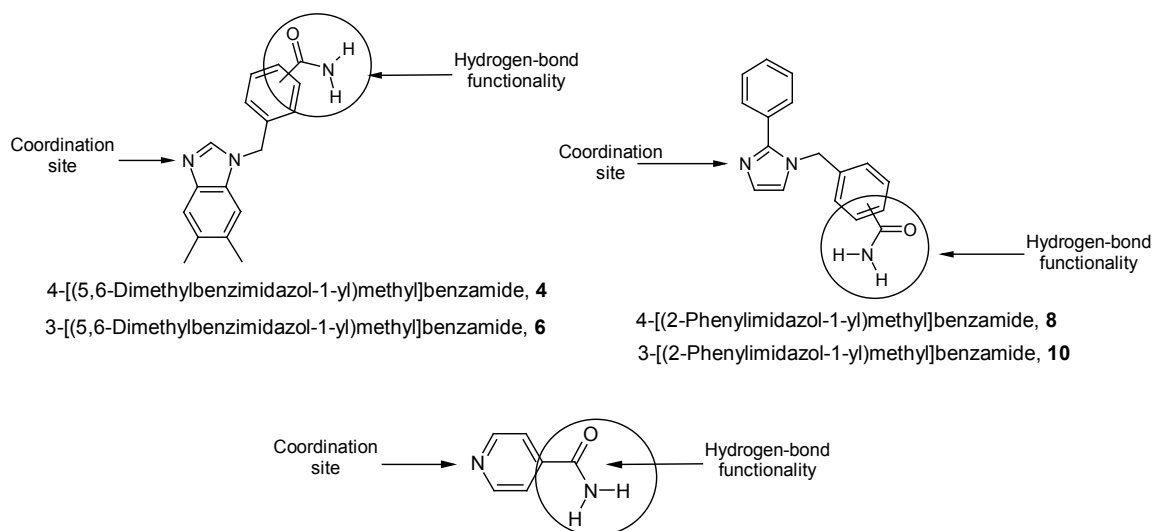


**Figure 7.2** (Benz-) and [(phenylimidazol-1-yl)methyl]benzamides vs isonicotinamide.

The pyridyl nitrogen atom provides coordination to the metal center with a 1-D chain propagated through carboxamide dimers. The amide moiety forms consistent and predictable supramolecular motifs, and so is a good choice for hydrogen bonding in metal-containing networks, Figure 7.1. This also reduces the chance of it competing for the metal ion itself. The carboxamide moiety frequently forms either dimeric or catemeric hydrogen-bonded patterns in the presence of potentially disruptive species (counterions, solvent molecules, *etc.*), and it is less likely to coordinate directly to the metal ion than are pyridyl- or imidazol-1-yl moieties. Carboxylic-acid containing ligands have also been employed in inorganic supramolecular synthesis,<sup>6</sup> however the carboxylic acid moiety is less reliable than the amide because of its propensity to bind directly to the metal cation.

We saw in Chapter 4 that cyanoximes have an excellent ability to form organic co-crystals, and cyanoximate anions have been employed in the construction of metal-organic networks,<sup>7</sup> and other metal complexes<sup>8</sup>. There are no organic co-crystals, nor metal-containing structures in the CSD that contain pyridyl cyanoximes, Figure 7.3.

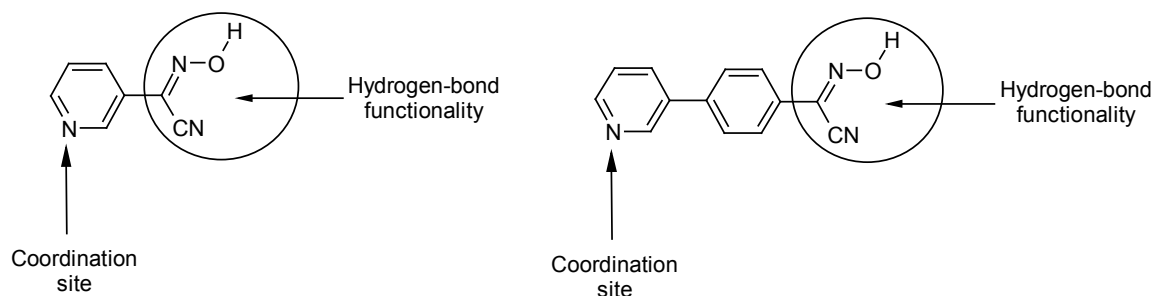


**Figure 7.3** 3-Pyridyl cyanoxime and [1-(pyridin-3-yl)-4-(cyanoxime)phenyl].

These ligands both contain a pyridyl moiety for metal coordination and a cyanoxime moiety for the supramolecular chemistry. Other oxime functionalities have been used to construct metal-containing networks,<sup>9</sup> including Ag(I) and Cu(II), Figure 7.4.

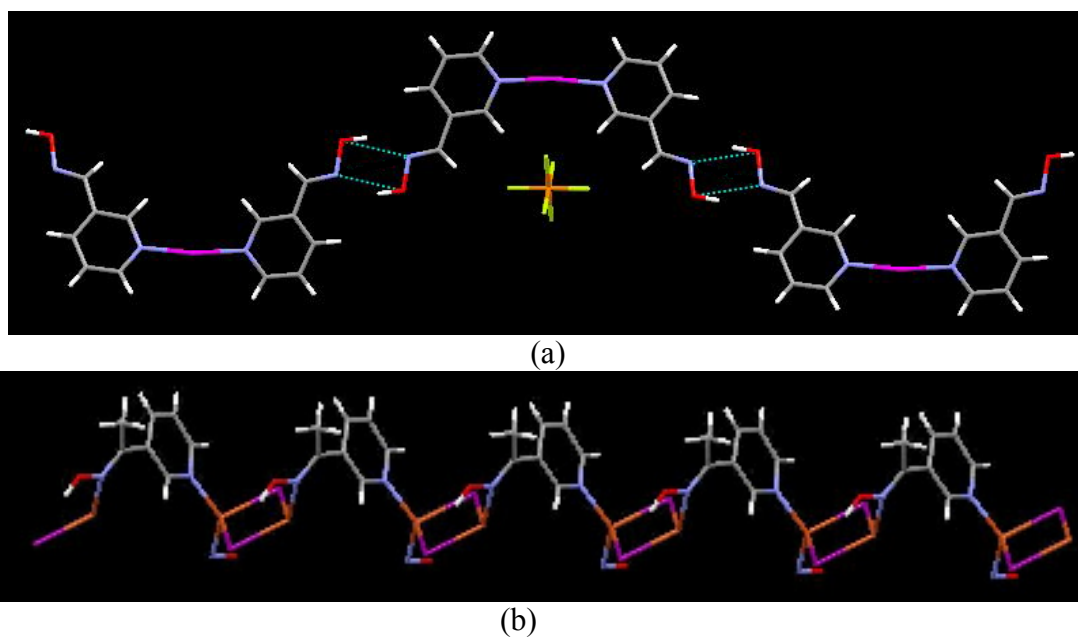


**Figure 7.4** (a) Metal coordination and supramolecular chemistry in the crystal structure of bis(3-aldoximepyridine)silver(I)hexafluorophosphate<sup>10</sup> and (b) coordination modes in the crystal structure of catena-((μ<sub>2</sub>-1-(3-pyridylethanoneoxime-N,N'))-(μ<sub>2</sub>-iodo)-copper(II)).<sup>11</sup>

### 7.1.2 Goals

The supramolecular reagents presented thus far have demonstrated a high degree of reliability and specificity in organic co-crystals. It will now be determined if the same

principles can be applied to the construction of extended metal frameworks with desired connectivities. This investigation will utilize ligands discussed in earlier chapters, as well as two new ones, Figure 7.3. Since there is no current data concerning pyridylcyanoximes as tools in supramolecular inorganic-organic synthesis, the approach is purely exploratory. This Chapter aims to do the following:

- 1) Utilize previously-synthesised [(benzimidazol-1-yl)methyl] and [(phenylimidazol-1-yl)methyl] ligands (Chapter 2) as building blocks in the construction of metal-organic networks (Ag(I), Cu(II), Ni(II)).
- 2) Establish their reliability and specificity at constructing such networks.
- 3) Establish the effect that counterions (in Ag(I) structures), solvent, and other potentially disruptive species have upon the supramolecular synthesis.
- 4) Synthesize two new supramolecular reagents, and employ them in inorganic supramolecular synthesis.
- 5) Establish the effect that extending the linker has on the resulting supramolecular architectures.

### 7.1.3 *Choice of metals*

The inorganic–organic supramolecular chemistry of [(benzimidazol-1-yl)methyl] and [(phenylimidazol-1-yl)methyl] benzamide ligands will be investigated by allowing them to react with a variety of Ag(I), Ni(II) and Cu(II) salts, to establish how effectively they can propagate a linear geometry of a complex ion into infinite 1-D chains with the aid of self-complementary hydrogen-bond interactions. Therefore, each metal complex is required to have exactly two available binding sites that can be occupied by N-heterocycle/amide ligands. Bidentate acetylacetonate (*acac*) and acetate “paddle-wheel” complexes are particularly useful in this context as they both produce neutral complexes (with  $M^{2+}$  metal ions) that present two open binding sites oriented in a trans-geometry, Figure 7.5.

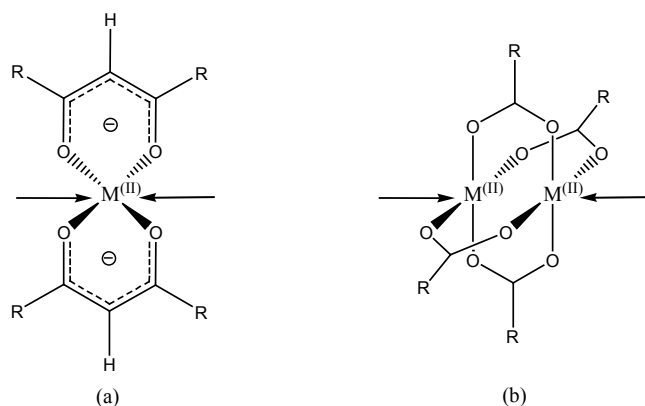


**Figure 7.5** Equatorial ‘blocked’ (a) *acac* complex and (b) “paddle-wheel” complex with axial sites (arrows) available for coordination.

The presence of various counterions in the Ag(I) complexes also allows for an examination of the structural complications that these units may present with respect to the desired supramolecular assembly process. In this way, it will be possible to make an assessment of the supramolecular yield, the capacity of this family of ligands to form specific and reproducible assemblies through intermolecular interactions.

## 7.2 Experimental

The synthesis of amides (**4-10**) were reported in Chapter 2. The syntheses of the other supramolecular reagents (**33** and **35**) discussed in this Chapter are as follows:



### 7.2.1 Synthesis of pyridylcyanoximes

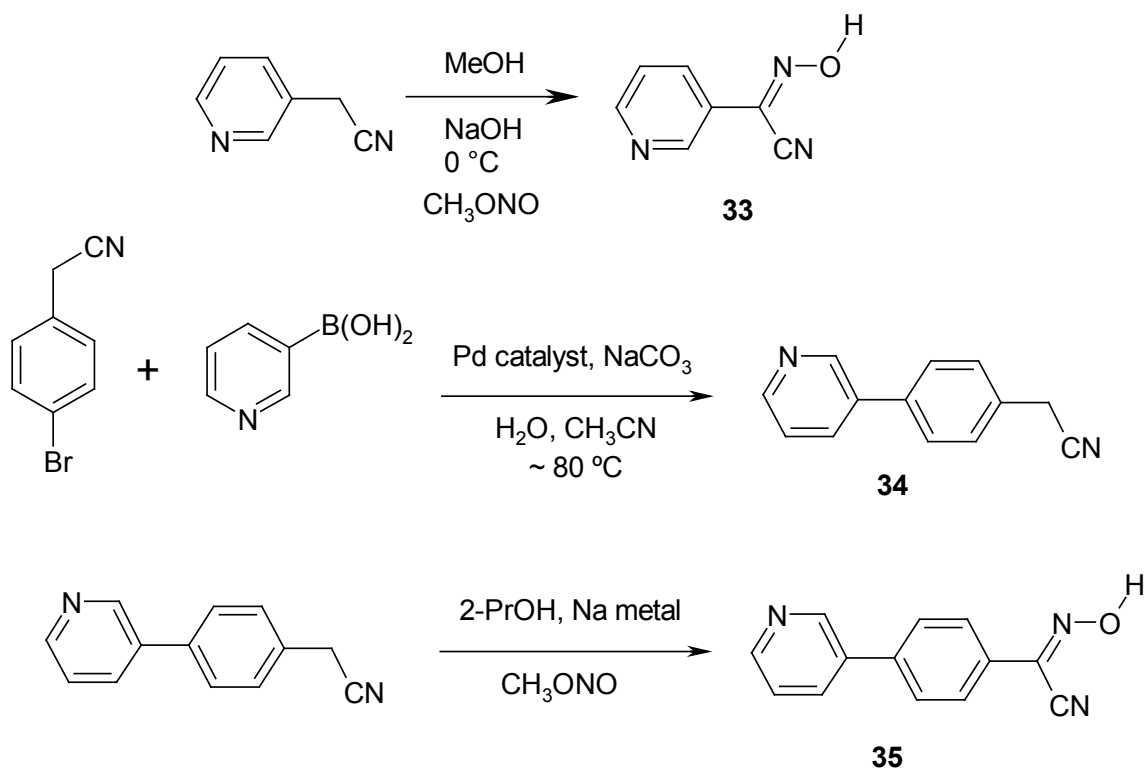


**Figure 7.6** Synthesis of pyridylcyanoximes.

#### 7.2.1.1 Synthesis of (3-pyridyl)-cyanoxime, 33

The synthesis of **33** was carried out according to a previously-published procedure.<sup>12</sup> Sodium hydroxide (0.34 g, 8.5 mmol) was dissolved in methanol (30 mL) over an approximate 2 h period. 3-pyridyl acetonitrile (1.0 g, 8.5 mmol) was added to the solution and it immediately turned from cloudy white to red. Methyl nitrite gas was generated by adding a 2:1 solution of water: sulphuric acid dropwise to a solution of sodium nitrite in methanol and water (10 g, 50 mL, and 100 mL, respectively). Upon bubbling the gas through the solution it immediately turned bright yellow. The solution was left to stir for around 4 h at 0° C. The solvent was reduced via rotary evaporation to produce a yellow solid. The solid was dissolved in water and a few drops of acetic acid were added, upon which a white solid precipitate appeared. Yield: 0.705 g, (56%); mp: 240-243 °C; <sup>1</sup>H NMR (200 MHz, DMSO-*d*<sub>6</sub>): δ 8.40-8.46 (m, 1H), 8.95-8.99 (m, 1H), 9.59 (s, 1H), 9.76 (s, 1H), 15.00 (s, 1H); <sup>13</sup>C NMR: (200 MHz, DMSO-*d*<sub>6</sub>) δ ; IR: ν 3436 cm<sup>-1</sup> (O-H), 2223 cm<sup>-1</sup> (C≡N), 2520 cm<sup>-1</sup> and 1818 cm<sup>-1</sup> (O-H···N).

### 7.2.1.2 Synthesis of 4-(3-pyridylphenylacetonitrile), 34

4-Bromophenylacetonitrile (4.334 g, 22 mmol) and 3-pyridyl boronic acid (2.84 g, 23.1 mmol) were dissolved in 20 ml H<sub>2</sub>O and 20 ml acetonitrile and the mixture was degassed with N<sub>2</sub> for 30 min. After which NaCO<sub>3</sub> (5.19 g, 49 mmol) and Pd (PPh<sub>3</sub>)<sub>3</sub> was added and the reaction was left to reflux and monitored by TLC. After 4 days H<sub>2</sub>O was added and the mixture was extracted with ethyl acetate which left behind a brown oil upon removal. The product was chromatographed on silica (10:1 hexane/ethyl acetate) to produce a light brown solid. Yield: 2.947 g (69%); mp: 43-46 °C. <sup>1</sup>H NMR (200 MHz, DMSO-*d*<sub>6</sub>): δ 4.11 (s, 2H), 7.44-7.51 (m, 3H), 7.76 (d, 2H, *J* = 8.4 Hz), 8.03-8.09 (m, 1H), 8.58 (dd, 1H, *J*<sub>1</sub> = 1.6 Hz, *J*<sub>2</sub> = 4.8 Hz), 8.91 (d, 1H, *J* = 2.2 Hz).

### 7.2.1.3 Synthesis of [1-(pyridin-3-yl)-4-(cyanoxime)phenyl], 35

Na metal (0.350 g, 15.2 mmol) was cut up into small pieces and left to dissolve in 540 ml 2-propanol over a period of 4 hours after which 4-(3-pyridylphenylacetonitrile) (2.947 g, 15.2 mmol) dissolved in 2-propanol was added. The resulting mixture was reddish-orange in colour. Methyl nitrite gas, generated *in situ*, by adding a 2:1 solution of water:sulphuric acid to a solution of sodium nitrite dissolved in methanol and water (10 g, 50 mL, 100 mL, respectively. was bubbled through the solution. The solution changed to an orange color and went cloudy. The reaction mixture was left to stir overnight, after which the precipitate that had formed was filtered off to leave a pale brown solid. The solid was dissolved in water (60 mL) and acidified with 1M HCl (20 mL). The solid formed was filtered off and recrystallized from hot toluene to give pale yellow plates. Yield: 1.834 g (54%); mp: 273-277 °C; <sup>1</sup>H NMR (400 MHz, DMSO-*d*<sub>6</sub>): δ 7.47-7.51 (m, 1H), 7.80 (d, 2H), 7.89 (d, 2H), 8.10-8.12 (m, 1H), 8.59 (m, 1H), 8.92 (s, 1H), 13.85 (s, 1H); <sup>13</sup>C NMR (200 MHz, DMSO-*d*<sub>6</sub>): δ 109.41, 123.37, 125.57, 127.06, 128.56, 130.13, 133.70, 138.55, 146.93, 148.35; IR: 3431 cm<sup>-1</sup> (O-H), 2223 cm<sup>-1</sup> (C≡N), 2509, 1808 cm<sup>-1</sup> (O-H···N).

## 7.2.2 Synthesis of metal complexes **4b-d**, **8a**, **10a**, **33a** and **33b**, **35a** and **35b**

### 7.2.2.1 Synthesis of bis[4-(5,6-dimethylbenzimidazol-1-yl)methylbenzamide]silver(I) tetrafluoroborate, **4b**

**4** (0.043 g, 0.155 mmol) was dissolved in 3 mL of acetonitrile with 1 mL of ethanol with heat in a 50 mL beaker. To it was added a solution of acetonitrile containing silver(I) tetrafluoroborate (0.01 g, 0.05 mmol), upon which the solution went cloudy. Ethanol (1 mL) was added and the solution was heated until it was clear. The resulting solution was covered in Al foil and stored in the dark. Colorless prisms suitable for X-ray crystallography were obtained after three days; mp >283 °C.

### 7.2.2.2 Synthesis of bis[4-(5,6-dimethylbenzimidazol-1-yl)methylbenzamide]silver(I) hexafluoroarsenate, **4c**

**4** (0.028 g, 0.102 mmol) was dissolved in acetonitrile (3mL) with ethanol (1mL) with heat in a 50mL beaker. To it was added a solution of acetonitrile containing silver(I) hexafluoroarsenate (0.01 g, 0.034 mmol). Amber prisms suitable for X-ray crystallography were obtained after five days; mp 265–270 °C (decomp.)

### 7.2.2.3 Synthesis of [4-(5,6-dimethylbenzimidazol-1-yl)methylbenzamide]bis-(hexafluoroacetylacetonato)copper(II), **4d**

**4** (0.02 g, 0.0628mmol) and bis-(hexafluoroacetylacetonato)copper(II) (0.01g, 0.0209mmol) were added to a vial and dissolved, with in heat in a methanol/acetonitrile mix and allowed to stand under ambient conditions. Green prisms, **4d**, suitable for X-ray diffraction were obtained after a few days. Mp 155-157°C.

### 7.2.2.4 Synthesis of tetrakis( $\mu$ -2-fluorobenzoato-*O,O'*)-bis(4-(2-phenylimidazol-1-yl)methylbenzamide)-dicopper(II), **8a**

**8** (0.015 g, 0.054 mmol) and Cu(II) 2-fluorobenzoate (0.01g, 0.018mmol) were added to a beaker and dissolved in acetonitrile. Green prisms, **8a**, suitable for X-ray diffraction were formed after a few days. Mp: 154-157 °C.

**7.2.2.5 Synthesis of tetrakis( $\mu$ -2-fluorobenzoato-O,O')-bis(3-(2-phenylimidazol-1-yl)methylbenzamide)-dicopper(II), 10a**

**10** (0.015 g, 0.054 mmol) and Cu(II) 2-fluorobenzoate (0.010 g, 0.018 mmol) were added to a beaker and dissolved in acetonitrile. Green prisms, **10a**, suitable for X-ray diffraction were formed after one hour. Mp: 144-146 °C.

**7.2.2.6 Synthesis of tetrakis( $\mu$ -2-fluorobenzoato-O,O')-bis(3-pyridyl-cyanoxime)-dicopper(II), 33a**

**33** (0.010 g, 0.068 mmol) and Cu(II) 2-fluorobenzoate (0.015 g, 0.022 mmol) were added to a beaker and dissolved in methanol. Green prisms, **33a**, suitable for X-ray diffraction were formed after approximately one week. Mp: 205-207 °C (decomp.).

**7.2.2.7 Synthesis of tetrakis( $\mu$ -acetato-O,O')-bis(3-pyridyl-cyanoxime)-dicopper(II), 33b**

**33** (0.010 g, 0.068 mmol) was dissolved in methanol and Cu acetate (0.005 g, 0.022 mmol) was added to it, upon which the solution went green and cloudy. A few drops of acetic acid were added and the solution went blue and clear. Blue blocks, **39b**, suitable for X-ray diffraction were obtained after three days. Mp: 205-207 °C.

**7.2.2.8 Synthesis of [1-(pyridin-3-yl)-4-(cyanoxime)phenyl]bis-(dibenzoylmethanato)nickel(II), 35a**

**35** (0.010 g, 0.048 mmol) was dissolved in methanol and toluene. To the solution was added *bis*-(dibenzoylmethanato)nickel(II). A powder was formed, which was redissolved in DMF to yield green plates, **35a**. Mp: 280-285 °C.

**7.2.2.9 Synthesis of tetrakis( $\mu$ -acetato-O,O')-bis([1-(pyridin-3-yl)-4-(cyanoxime)phenyl]-dicopper(II), 35b**

**35** (0.010 g, 0.048 mmol) was dissolved in methanol and toluene. To the solution was added copper acetate, and a precipitate was formed. Glacial acetic acid was added dropwise until the solution went clear. Blue blocks, **35b**, suitable for X-ray diffraction were obtained after a few days. Mp: 215-220 °C.

## 7.3 Results

**Table 7.1** Selected bond distances and angles for **4b-d**, **8a**, **10a**, **33a** and **33b**, **35a** and **35b**

Compound	M(II)-N (Å)	< N-M(II)-N (°)	< N-M(II)-M(II)-N (°)
<b>4b</b>	2.089(3)	180.0	-
<b>4c</b>	2.0707(19)	180.0	-
<b>4d</b>	1.995(2)	180.0	-
<b>8a</b>	2.162(3)	-	173.99(9)
<b>10a</b>	2.154(3)	-	172.67(7)
<b>33a</b>	2.15(3)	-	177(3)
	2.167(5)	-	178.3(6)
<b>33b</b>	2.1511(14)	-	176.23(4)
<b>35a</b>	2.086(2)	86.57(13)	-
<b>35b</b>	2.163 (3)	-	178.97(9)

**Table 7.2** Hydrogen-bond geometries for **4b-d**, **8a**, **10a**, **33a** and **33b**, **35a** and **35b**

Compound	D-H...A	D(D-H)	H... ·A/A°	D...A/A	D-H... A/°
<b>4b<sup>i</sup></b>	N(27)-(27A)...O(27) <sup>a</sup>	0.80(5)	2.13(5)	2.929(4)	178(5)
	N(27)-H(27B)...F(2) <sup>b</sup>	0.80(5)	2.20(5)	2.902(11)	148(5)
<b>4c<sup>ii</sup></b>	N(37)-H(37A)...O(37) <sup>a</sup>	0.88(4)	2.06(4)	2.944(3)	173(3)
	N(37)-H(37B)...F(1)	0.79(4)	2.28(4)	2.982(3)	148(3)
<b>4d<sup>iii</sup></b>	N(37)-H(37B)...N(1S)	0.74(4)	2.41(4)	3.121(3)	163(4)
	N(37)-H(37A)...O(37) <sup>a</sup>	0.87(4)	2.03(4)	2.896(3)	172(3)
<b>8a<sup>iv</sup></b>	N(37)-H(37B)...N(1S)	0.88	2.19	3.011(7)	154.3
	N(37)-H(37A)...O(37) <sup>a</sup>	0.88	2.02	2.879(5)	164.4
<b>10a<sup>v</sup></b>	N(31)-H(31A)...O(31) <sup>a</sup>	0.95(5)	1.91(5)	2.852(5)	169(4)
<b>33a<sup>vi</sup></b>	O(17A)-H(17A)...O(31) <sup>a</sup>	0.84	1.89	2.6973(18)	160.5
	O(17B)-H(17B)...O(31) <sup>a</sup>	0.84	1.99	2.562(8)	124.6
<b>33b<sup>vii</sup></b>	O(17A)-H(17A)...O(21) <sup>a</sup>	0.84	1.84	2.6716(17)	171.4
	O(17B)-H(17B)...O(21) <sup>a</sup>	0.84	1.92	2.756(13)	176.4
<b>35a<sup>viii</sup></b>	O(27A)-H(27A)...O(33) <sup>a</sup>	0.96(4)	1.67(4)	2.620(3)	172(3)
	O(27B)-H(27B)...O(33) <sup>a</sup>	0.95(4)	1.82(4)	2.765(14)	169(4)
<b>35b</b>					

i) <sup>a</sup> -x,-y,-z, <sup>b</sup> -x+1/2,y-1, -z+1/2; ii) <sup>a</sup> -x,-y+2,-z+1; iii) <sup>a</sup> -x+2,-y,-z; iv) <sup>a</sup> -x+ 2,-y+1,-z+1; v) <sup>a</sup> -x,-y,-z; vi) <sup>a</sup> -x+1,-y+1,-z+2; vii) <sup>a</sup> -x+1,-y+1,-z+1; viii) <sup>a</sup> -x,-y+1,-z; ix)

### 7.3.1 Crystal structure of bis[4-(5,6-dimethylbenzimidazol-1-yl)methylbenzamide] silver(I) tetrafluoroborate, **4b**

The crystal structure of **4b** contains Ag(I) ions coordinated to two ligands in a linear manner as well as a disordered [BF<sub>4</sub>]<sup>-</sup> anion. The ligands bind to the metal ion *via* the benzimidazol-1-yl nitrogen atoms, Figure 7.7. The linear geometry of the complex is propagated into infinite chains *via* a symmetric  $R_2^2(8)$  carboxamide...carboxamide hydrogen motif. *Anti* N–H protons of the carboxamide groups are engaged in hydrogen-bond interactions with [BF<sub>4</sub>]<sup>-</sup> anions. The through-space Ag...Ag separation within chains is 19.8 Å. Adjacent chains interact through  $\pi$ - $\pi$  stacking contacts (*ca.* 3.5 Å) involving 5,6-dimethylbenzimidazol-1-yl moieties, Fig. 7.8.

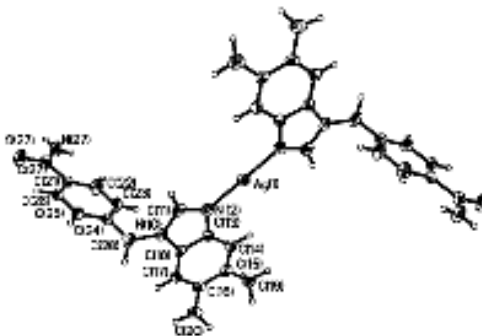


**Figure 7.7** Thermal ellipsoid plot (50% probability) and labeling scheme for **4b**.

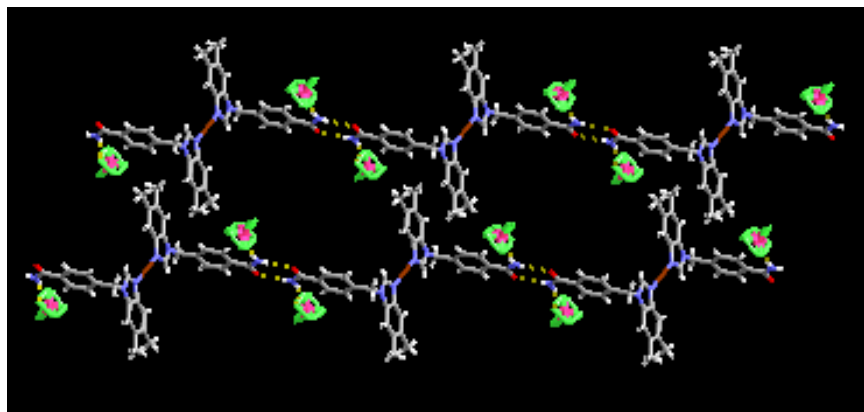


**Figure 7.8** View of **4b** showing  $\pi$ - $\pi$  interactions between adjacent 1-D chains; tetrafluoroborate anions are disordered.

### 7.3.2 Crystal structure of bis[4-(5,6-dimethylbenzimidazol-1-yl)methylbenzamide]silver(I) hexafluoroarsenate, 4c

In the crystal structure of **4c**, two 4-[(5,6-dimethylbenzimidazol-1-yl)methyl]benzamide ligands coordinate through their benzimidazol-1-yl nitrogen atoms to each Ag(I) ion in a linear fashion, Figure 7.9. Self-complementary  $R_2^2(8)$  carboxamide...carboxamide interactions extend the structural unit into an infinite 1-D assembly to yield an infinite chain, Figure. 7.10.

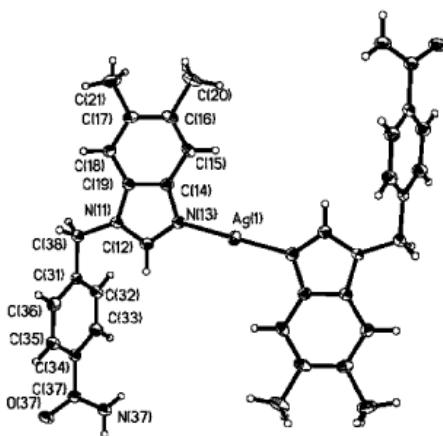


**Figure 7.9** Thermal ellipsoid plot (50% probability) and labeling scheme for **4c**.

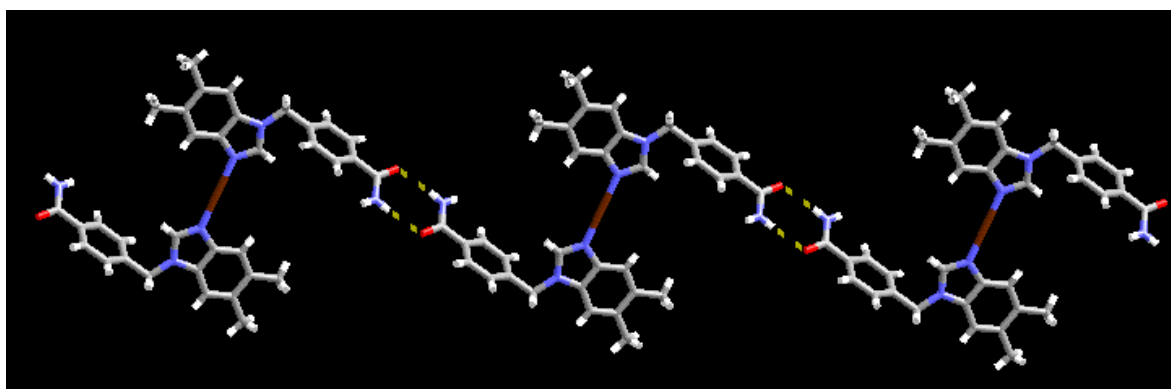


**Figure 7.10** Infinite 1-D cationic chain in **4b**;  $[\text{AsF}_6]^-$  anions have been removed for clarity.

### 7.3.3 Crystal structure of [4-(5,6-dimethylbenzimidazol-1-yl)methylbenzamide]bis(hexafluoroacetylacetonato)copper(II) acetonitrile, **4d**

The crystal structure of **4d** is constructed from two hexafluoroacetylacetonato (hfacac) ligands occupying the equatorial sites of the copper(II) ion and the axial sites coordinated by two 4-[(5,6-dimethylbenzimidazol-1-yl)methyl]benzamide ligands, (Cu-N, 1.995(5) Å) forming an octahedral metal complex. The octahedral complex is extended into a 1-D chain through amide-amide dimers via carboxamide...carboxamide interactions (N-H...O: 3.121 Å), Figure 7.11. The *anti*-amide proton forms a hydrogen bond to the included acetonitrile solvent molecule. Copper(II) ions within the chain are approximately 22 Å apart.

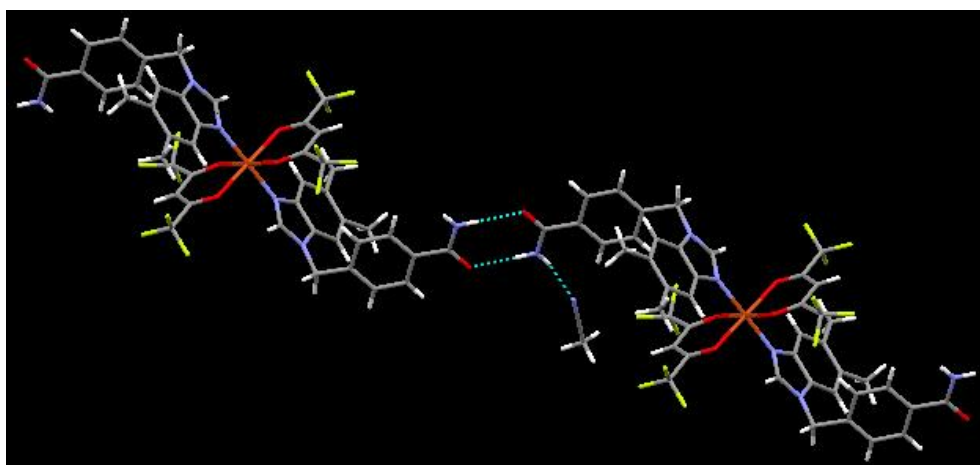


**Figure 7.11** One-dimensional chain in the crystal structure of **4d**.

### 7.3.4 Crystal structure of tetrakis( $\mu$ -2-fluorobenzoato-*O,O'*)-bis(4-(2-phenylimidazol-1-yl)methylbenzamide)-dicopper(II) acetonitrile, **8a**

The crystal structure of **8a** consists of two 4-[2-phenylimidazol-1-yl)methyl]benzamide ligands, coordinated via the imidazole nitrogen atoms to the axial positions of a copper(II) 2-fluorobenzoate “paddle wheel” unit, (Cu-N: 2.162(3) Å), Figure 7.12. The metal complex becomes part of an infinite 1-D chain as a result of self complementary homomeric amide-amide dimers involving the *syn*-hydrogen atom and the carbonyl oxygen of another amide, N-H...O, 2.879(5) Å. Additionally, the *anti*-hydrogen atom of the amide moiety interacts with an acetonitrile molecule via a N-



H $\cdots$ N hydrogen bond (3.011(7) Å) and the Cu-Cu distance within the “paddle wheel” is 2.6881(9) Å.

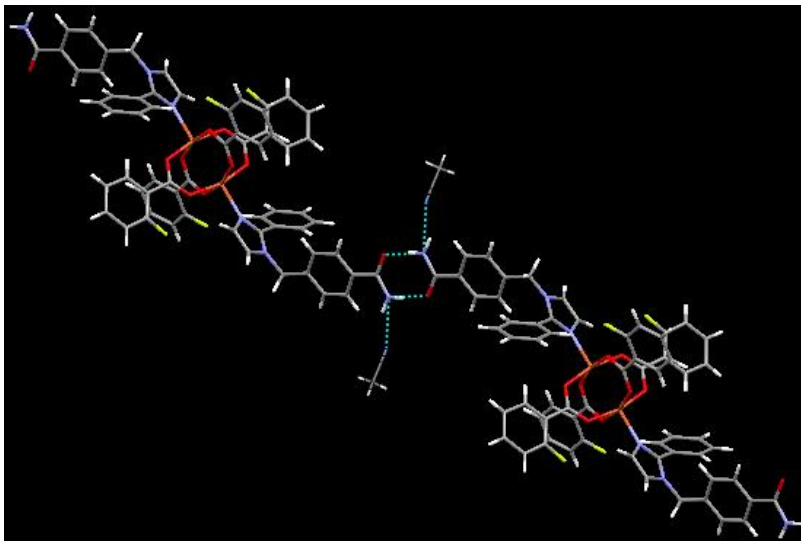


**Figure 7.12** One-dimensional chain in the crystal structure of **8a**.

### 7.3.5 Synthesis of *tetrakis(μ-2-fluorobenzoato-O,O′)-bis(3-(2-phenylimidazol-1-yl)methyl)methylbenzamide)-dicopper(II)*, **10a**

The crystal structure of **10a** contains two 3-[2-phenylimidazol-1-yl)methyl]-benzamide ligands, coordinated to the axial positions of the copper(II) 2-fluorobenzoate “paddle wheel” unit (Cu-N: 2.154(3) Å). 1-D chains are produced through self complementary homomeric amide-amide dimers via N-H $\cdots$ O hydrogen bonds (2.879 Å), between the *syn*-hydrogen atom and the carbonyl oxygen of another amide, Figure 7.13. The Cu-Cu distance within the “paddle wheel” unit is 2.6936(8) Å.

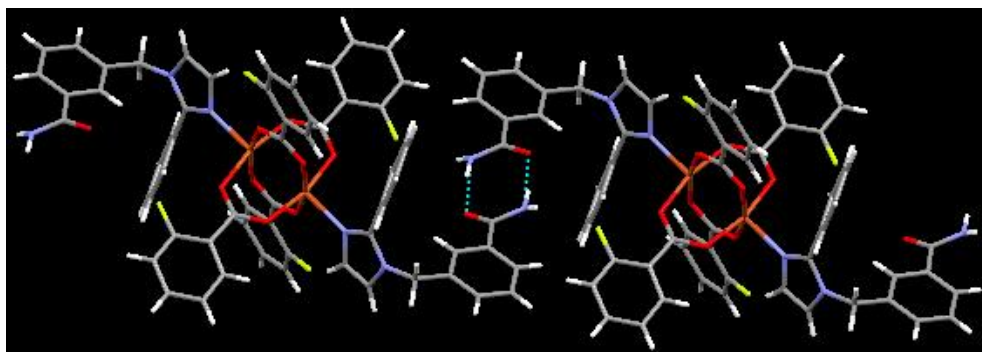


**Figure 7.13** 1-D ‘wavy’ chain in the crystal structure of **10a**

### 7.3.6 Synthesis of tetrakis( $\mu$ -2-fluorobenzoato- $O,O'$ )-bis-(3-pyridyl-cyanoxime)-dicopper(II), 33a

The crystal structure of **33a** contains two 3-pyridyl-cyanoxime ligands coordinated to the axial positions of the copper(II) 2-fluorobenzoate “paddle wheel” unit (Cu-N: 2.167 Å). 1-D chains are produced through O-H $\cdots$ O interactions between the oxime moieties and oxygen atoms of adjacent “paddle-wheel” units (2.697 Å), Figure 7.14. The Cu-Cu distance within the “paddle wheel” unit is 2.630 Å.

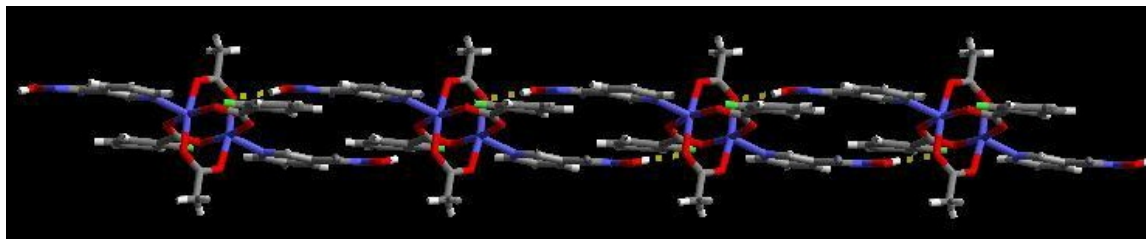


Figure 7.14 One-dimensional chain in the crystal structure of **33a**.

### 7.3.7 Crystal structure of tetrakis( $\mu$ -acetato- $O,O'$ )-bis-(3-pyridyl-cyanoxime)-dicopper(II), 33b

The crystal structure of **33b** contains two (3-pyridyl-cyanoxime) ligands coordinated to the axial positions of the copper(II) acetate “paddle wheel” unit (Cu-N: 2.151 Å). 1-D chains are produced through O-H $\cdots$ O interactions between the oxime moieties and oxygen atoms of adjacent “paddle-wheel” units (2.672 Å), Figure 7.15. The Cu-Cu distance within the “paddle wheel” unit is 2.617 Å.

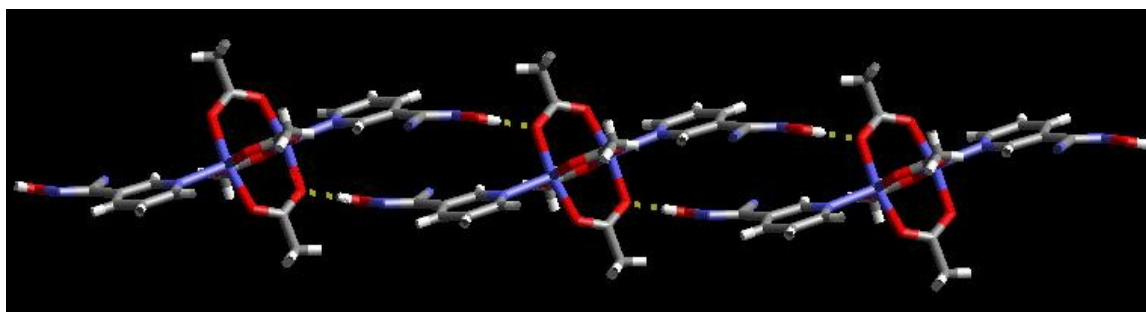
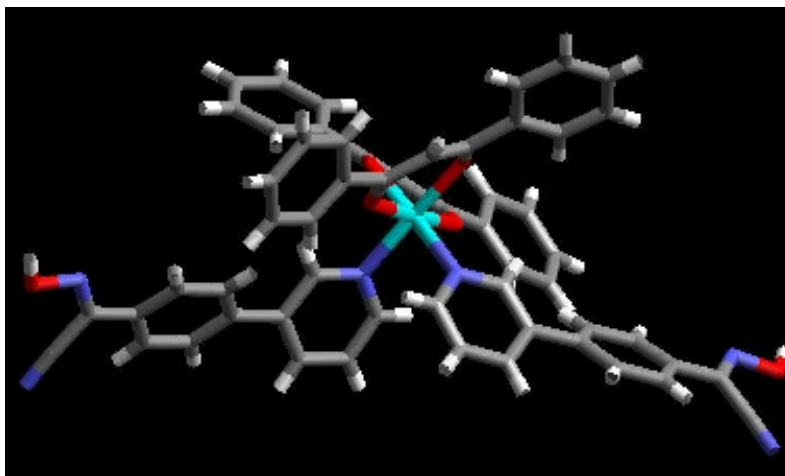


Figure 7.15 One dimensional chain in the crystal structure of **33b**.

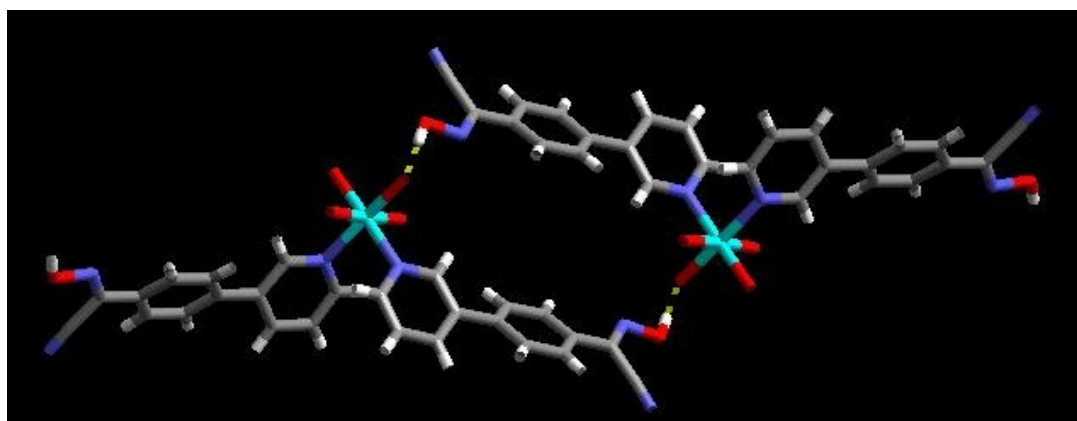
### 7.3.8 Crystal structure of [1-(pyridin-3-yl)-4-(cyanoxime)phenyl]bis-(dibenzoylmethanato)nickel(II), 35a

The crystal structure of **35a** contains two [1-(pyridin-3-yl)-4-(cyanoxime)phenyl] ligands, one coordinated to the axial position, and one to the equatorial position of the

Ni(II) center. (Ni-N: 2.086 Å). 1-D chains are produced through O-H...O interactions between the oxime moieties and oxygen atoms of adjacent dibenzoylmethanato units (2.621 Å), Figure 7.16. Nickel(II) ions within the chains are approximately 12.334 Å apart.



(a)



(b)

**Figure 7.16** (a) Ligand coordination around the metal center in the crystal structure of **6a** and (b) two Ni(II) centers with axial and equatorial coordination of [1-(pyridin-3-yl)-4-(cyanoxime)phenyl] ligands in the crystal structure of **35a**. Dibenzoylmethanate ligands have been removed for clarity.

### 7.3.9 Crystal structure of tetrakis( $\mu$ -acetato-O,O')-bis([1-(pyridin-3-yl)-4-(cyanoxime)phenyl]-dicopper(II), **35b**

The crystal structure of **35b** contains two [1-(pyridin-3-yl)-4-(cyanoxime)phenyl] ligands coordinated to the axial positions of the copper(II) acetate “paddle wheel” unit

(Cu-N: 2.163 Å). 1-D chains are produced through O-H...O interactions between the oxime moieties and oxygen atoms of adjacent “paddle-wheel” units (2.631 Å), Figure 7.17.  $\pi$ - $\pi$  stacking interactions occur between the phenyl rings of two adjacent ligands (3.811 Å). The Cu-Cu distance within the “paddle wheel” unit is 2.632 Å.

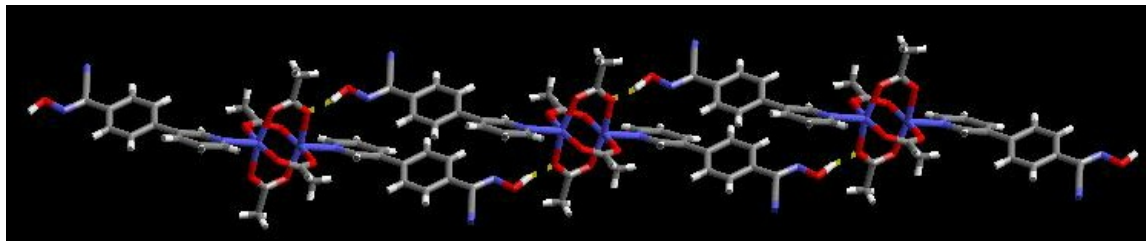
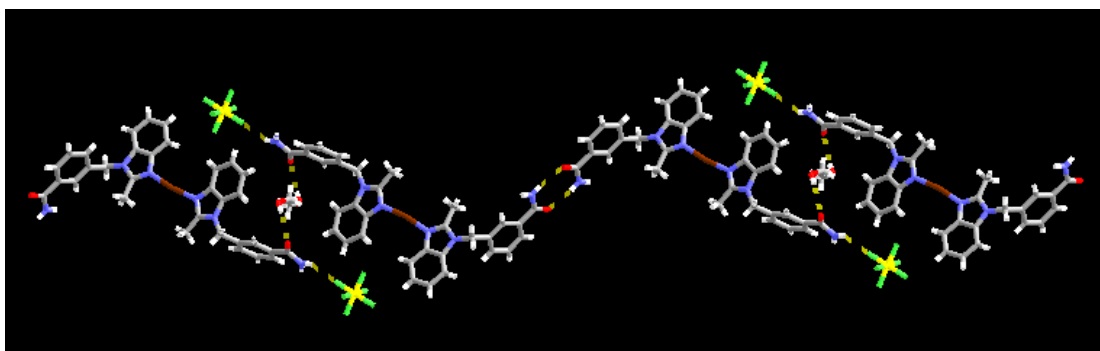


**Figure 7.17** One-dimensional chain in the crystal structure of **35b**.

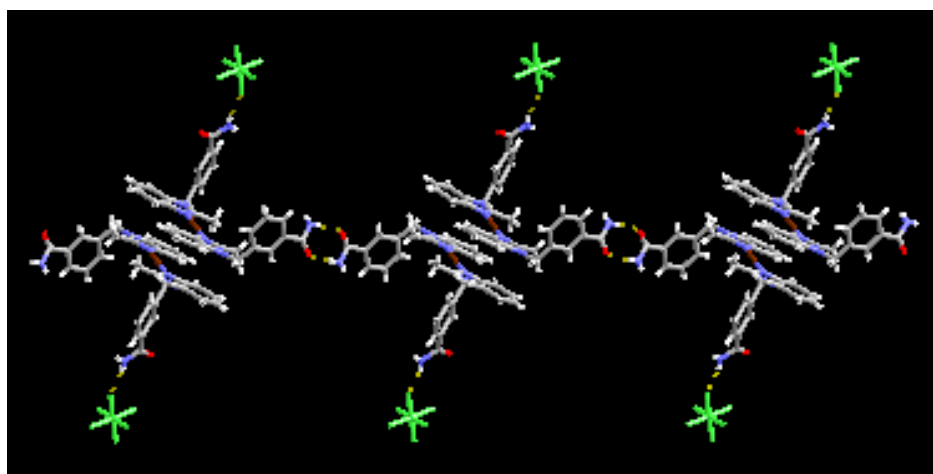
## 7.4 Discussion

Nine new metal complexes are presented here. Five of them contain N-heterocyclic amides, and four contain pyridyl-cyanoxime moieties. In the amide-containing structures, five out of five structures contained the desired coordination chemistry and geometry, with axial coordination through the imidazole-nitrogen atoms and infinite one-dimensional chains propagated through carboxamide-carboxamide interactions. This corresponds to a supramolecular yield of 100%, which is quite remarkable considering the competition offered by solvent molecules, counterions (in the Ag(I) systems), the ability of the amide moiety itself to coordinate to the metal center, or the amide to get “distracted” by the presence of various other hydrogen-bond acceptors. Six other Ag(I) complexes have been prepared using [(benzimidazol-1-yl)methyl]benzamide) ligands.<sup>13</sup> In each structure, two ligands are coordinated to the Ag(I) ion in a linear manner through the nitrogen atom of the benzimidazol-1-yl moiety. The amide moiety does not bind to the metal in any case, so it remains available to participate in the supramolecular process. Combining the results here with those presented in the literature, there are a total of eight linear silver (I) complexes. This means that there are sixteen amide moieties that need to be classified according to they type of hydrogen bond that they are involved in. Extended assemblies will arise from ligand-ligand based hydrogen bonds, (either  $R_2^2(8)$  or  $C(4)$  motifs) whereas hydrogen

bonding to solvent molecules, counterion, or solvent molecules will disrupt these extended assemblies, representing loss of control and directionality, and is considered a failed assembly event. In this family of compounds, adjacent amides produced nine  $R_2^2(8)$  motifs and five C(4) motifs. The intended supramolecular amide-amide interactions were disrupted in only two cases, once by a methanol molecule, Figure 7.18 (a), and once by an  $[\text{SbF}_6]^-$  anion, Figure 7.18(b).



(a)



(b)

**Figure 7.18** Examples of where the supramolecular events are disrupted in the crystal structures of (a) bis[3-(2-methylbenzimidazol-1-yl)methylbenzamide]silver(I) hexafluoroarsenate methanol and (b) bis[3-(2-methylbenzimidazol-1-yl)methylbenzamide]silver(I) hexafluoroantimonate.

These types of ligands are therefore capable of propagating the inherent linear geometry of the metal complex in six of the eight structures – a supramolecular yield of 75%. The fact that ligand-based amide–amide hydrogen bonds are capable of maneuvering complex ions of substantial size, also bodes well for the transferability and versatility of these ligands. What is interesting to note that the two [(benzimidazol-1-yl)methyl]benzamide) ligands with silver(I) reported herein contain methyl groups in the 5- and 6-positions on benzimidazole. It seems that this has an effect upon the orientation around the metal center. The other ligands contain methyl groups in the 2-positions and are all oriented in a *cis* manner around the silver metal center. However, those containing 5,6-dimethylbenzimidazole are of a *trans* configuration, Figure 7.19. The same is true for copper complexes **4d**, **8a** and **33a**. The simple tweaking of the ligand can impart differences into the overall structure of the metal complexes, which can lead to different properties.

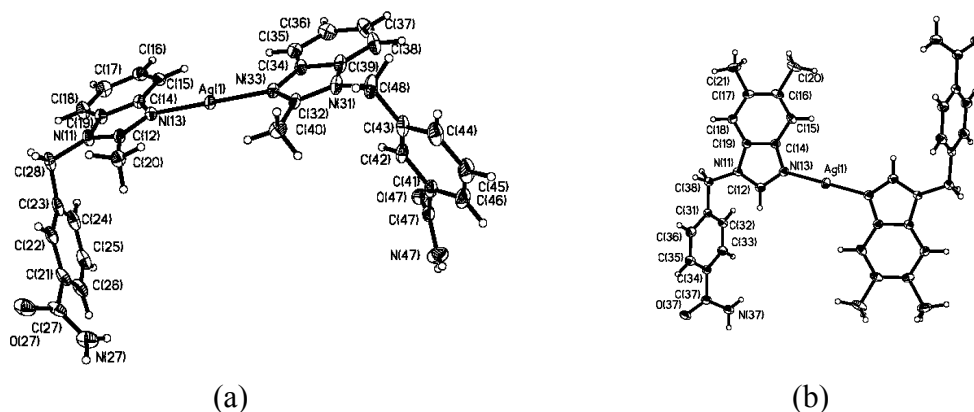


**Figure 7.19** Cis and trans configurations around Ag(I) in the crystal structures of (a) bis[3-(2-methylbenzimidazol-1-yl)methylbenzamide]silver(I) hexafluoroantimonate and (b) bis[4-(5,6-dimethylbenzimidazol-1-yl)methylbenzamide]silver(I)hexafluoroarsenate.

Such a handle on controlling the orientation around the metal center is not available in ligands such as isonicotinamide or nicotinamide and may be due to the flexibility of the methylene bridge, as well as to the imidazole moiety itself. The inter-chain Ag(I)-Ag(I) distances range from 18.6 to 23.6 Å, with no apparent trend as to the

type of ligand present (5,6-dimethylbenzimidazole or 2-methylbenzimidazole, or either the 3- or 4- isomer). These distances are significantly larger than those found in the corresponding structures with isonicotinamide<sup>14</sup> and nicotinamide,<sup>15</sup> with maximum Ag-Ag interchain distances of 17 and 15 Å, respectively. The same goes for the copper complexes, with interchain metal-metal distances ranging from 17.2 to 26.9 Å, compared to 16.5 and 19.6 Å in the corresponding nicotinamide complexes.<sup>16</sup> By employing these ligands we have successfully managed to increase the distances between the metal ions, and changing the ligand involved in the supramolecular synthesis can change the metrics of the systems.

In the structures containing cyanoximes, all four structures contained 1D chains propagated through O-H...O hydrogen bonds of the cyanoxime moiety to either the acetate, or “paddlewheel” unit. This would make sense since the acetate or “paddlewheel” oxygen atoms offer a better hydrogen-bond acceptor than the cyanoxime nitrile nitrogen atom. Nevertheless, a one-dimensional chain is formed. The only time the desired coordination geometry was not obtained was in the crystal structure of **35a**, where axial and equatorial coordination occurred. This corresponds to a supramolecular yield of 75%. The carboxamide-carboxamide interaction is clearly more robust than the cyanoxime catemeric self-complementary interaction. This is reflected in the calculated interaction energies of the amide-amide dimer compared to that of the catemeric cyanoxime interaction, Figure 7.20.

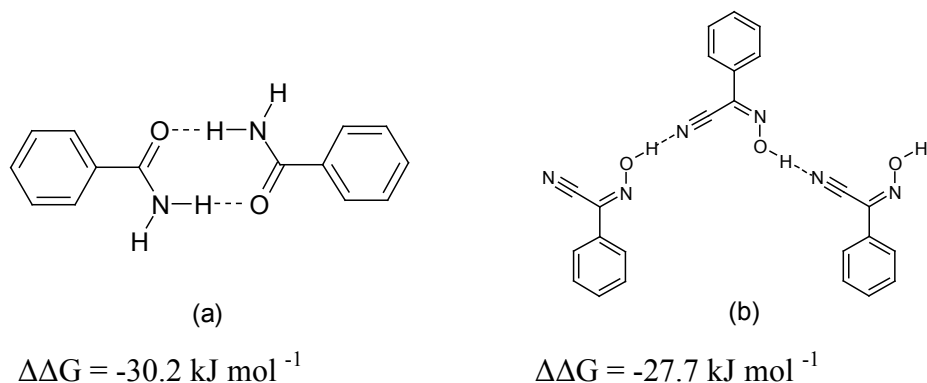


**Figure 7.20** Interaction energies of (a) amide-amide dimer and (b) cyanoxime catemer.

There is only a difference of  $2 \text{ kJ mol}^{-1}$  between the two interaction energies, and given the fact that the aldoxime dimer survives in the metal complexes containing it, despite the interaction being only  $18.2 \text{ kJ mol}^{-1}$ , then this finding may be explained in terms of kinetics rather than thermodynamics. The only difference between the amide-amide, the acetyloxime and aldoxime self-complementary dimers and the cyanoxime catemer is the number of points of interaction. The dimers contain a two-point interaction, and the catemer only one, Figure 7.21.

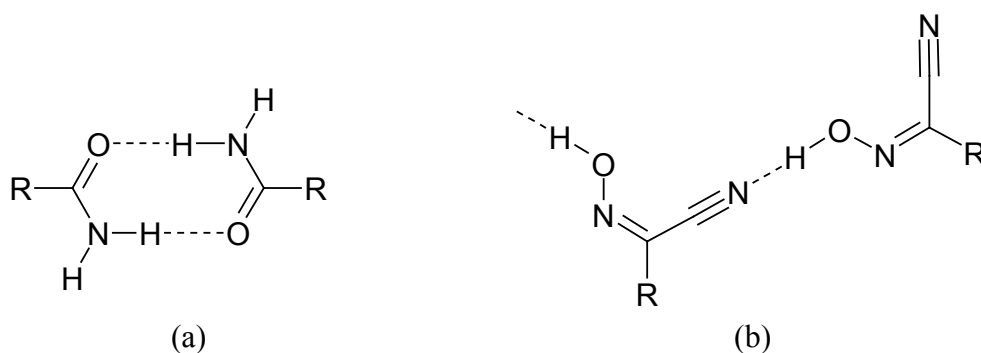


**Figure 7.21** Schematic representation of (a) two-point dimer interaction and (b) one-point catemeric interaction.

In the case of the two-point interaction, once one interaction has taken place it acts as a chelate to “lock” itself into place and hence facilitate the second interaction. This means that if one of the interactions is broken it can easily reconnect. With a one-point interaction, however, once the interaction is broken then it cannot be easily repaired. This helps to explain why the amide-amide and oxime dimers survive, while the cyanoxime catemer does not.

## 7.5 Conclusions

Self-complementary hydrogen-bond based amide-amide dimers are shown to be robust supramolecular synthons for the assembly and organization of *acac*- and paddle-wheel complex ions involving a variety of metals. Despite the potential that these interactions can be disrupted by counterions, solvent molecules, carboxylate and *acac* ligands, any supramolecular synthesis taking place with such ligands as those discussed here is likely to be successful. The pyridyl cyanoximes, despite it's the fact that the



potentially self-complementary O-H $\cdots$ N $\equiv$ C interactions did not materialize in these systems, showed a degree of consistency through hydrogen bonding to an oxygen atom of either carboxylate or *acac*.

---

---

## References

<sup>1</sup> (a) C. Yang, X. Wang, M. A. Omary, *J. Am. Chem. Soc.*, 2007, **129**, 15454; (b) J. Park, S. Hong, D. Moon, M. Park, K. Lee, S. Kang, Y. Zou, R. P. John, G. H. Kim, M. S. Lah, *Inorg. Chem.*, 2007, **46**, 10208; (c) D. L. Rogow, G. Zapeda, C. H. Swanson, X. Fan, C. F. Campana, A. G. Oliver, S. R. J. Oliver, *Chem. Mater.*, 2007, **19**, 4658; (d) T.-J. Won, J. K. Clegg, L. F. Lindoy, J. C. McMurtrie, *Cryst. Growth Des.*, 2007, **7**, 972; (e) A. K. Cheetham, C. N. R. Rao, R. K. Feller, *Chem. Commun.*, 2006, **46**, 4780; (f) T. Devic, C. Serre, N. Audebrand, J. Marrot, G. Ferey, *J. Am. Chem. Soc.*, 2005, **127**, 12788; (g) M. Eddaoudi, H. Li, O. M. Yaghi, *J. Am. Chem. Soc.*, 2000, **122**, 1391.

<sup>2</sup> (a) W. Sears, M. L. Hudolin, H. A. Jenkins, R. C. Mawhinney, C. D. Mackinnon, *J. Coord. Chem.*, 2008, **61**, 825; (b) T. Zhang, J. Kong, Y. Hu, X. Meng, H. Yin, D. Hu, C. Ji, *Inorg. Chem.*, ASAP; (c) M. Eddaoudi, J. Kim, N. Rosi, D. Vodak, J. Wachter, M. O'Keeffe, O. M. Yaghi, *Science*, 2002, **295**, 469; (d) J. Darriet, M. S. Haddad, E. N. Duesler, D. N. Hendrickson, *Inorg. Chem.*, 1979, **18**, 2679; (e) R. H. Groenman, L. R. MacGillivray, J. L. Atwood, *Chem. Commun.*, 1998, 2735; (f) K. Birahda, M. Aoyagi, M. Fujita, *J. Am. Chem. Soc.*, 2000, **122**, 2397.

<sup>3</sup> (a) C. B. Aakeröy, A. M. Beatty, *Cryst. Eng.*, 1998, **1**, 39; (b) B. R. Bhogala, P. K. Thallapally, A. Nangia, *Cryst. Growth Des.*, 2004, **4**, 215; (c) C. B. Aakeröy, A. M. Beatty, D. S. Leinen, K. R. Lorimer, *Chem. Commun.*, 2000, 935; (d) A. Angeloni, A. G. Orpen, *Chem. Commun.*, 2001, 343; (e) C. J. Kuehl, F. M. Tabellion, A. M. Arif, P. J. Stang, *Organometallics*, 2001, **20**, 1956; (f) Z. Qin, M. C. Jennings, R. J. Puddephatt, *Inorg. Chem.*, 2001, **40**, 6220; (g) J. K. Bera, T.-T. Vo, R. A. Walton, K. R. Dunbar, *Polyhedron*, 2003, **22**, 3009; (h) C. B. Aakeröy, A. M. Beatty, J. Desper, M. O'Shea, J. Valdes-Martinez, *Dalton Trans.*, 2003, 3956; (i) C. B. Aakeröy, A. M. Beatty, D. S. Leinen, *Angew. Chem., Int. Ed.*, 1999, **38**, 1815; (j) C. B. Aakeröy, J. Desper, J. Valdes-Martinez, *CrystEngComm*, 2004, **6**, 413.

<sup>4</sup> C. B. Aakeröy, A. M. Beatty, *Crystal Engineering*, 1998, **1**, 39.

<sup>5</sup> C. B. Aakeröy, A. M. Beatty, J. Desper, M. O'Shea, J. Valdes-Martinez, *Dalton Trans.*, 2003, 3956.

---

<sup>6</sup> (a) W.-Y. Sun, Y.-A. Zhang, T.-A. Okamura, T. Ye, N. Ueyama, *Chem. Lett.*, 2000, **10**, 1222; (b) J.-Z Zhang, W.-R. Cao, J.-X. Pan, Q.-W. Chen, *Inorg. Chem. Comm.*, 2007, **10**, 1360; (c) J. Fan, Y.-A. Zhang, T.-A. Okamura, Z.-H. Zou, N. Ueyama, W.-Y. Sun, *Inorg. Chem. Comm.*, 2001, **4**, 501; (d) S. M. Hawxwell, G. M. Espallargas, D. Bradshaw, M. J. Rosseinsky, T. J. Prior, A. J. Florence, J. van de Streek, L. Brammer, *Chem. Commun.*, 2007, 1532; (e) D. Braga, F. Grepioni, P. Sabatino, G. R. Desiraju, *Organometallics*, 1994, **13**, 3532.

<sup>7</sup> D. Robertson, J. F. Cannon, N. Gerasimchuk, *Inorg. Chem.*, 2005, **44**, 8326.

<sup>8</sup> (a) N. Gerasimchuk, T. Maher, P. Durham, K. V. Domasevitch, J. Wilking, A. Mokhir, *Inorg. Chem.*, 2007, **46**, 7268; (b) N. Gerasimchuk, N. K. Dalley, *J. Coord. Chem.*, 2004, **57**, 1431; (c) D. Robertson, C. Barnes, N. Gerasimchuk, *J. Coord. Chem.*, 2004, **57**, 1205-1216; (d) D. Eddings, C. Barnes, N. Gerasimchuk, P. Durham, K. Domasevich, *Inorg. Chem.*, 2004, **43**, 3894; (e) K. Domasevitch, N. Gerasimchuk, A. Mokhir, *Inorg. Chem.*, 2000, **39**, 1227; (f) A. Mokhir, K. Domasevich, N. K. Dalley, X. Kou, N. Gerasimchuk, O. A. Gerasimchuk, *Inorg. Chimica Acta*, 1999, **284**, 85.

<sup>9</sup> B. Zhang, S. Chu, X. Wang, G. Shen, R.-J. Wang, *Acta Cryst., Sect. E: Struct. Rep. Online*, 2003, **59**, m824; (b) C. B. Aakeröy, A. M. Beatty, D. S. Leinen, *Angew. Chem., Int. Ed.*, 1999, **38**, 1815; (c) C. J. Adams, P. C. Crawford, A. G. Orpen, T. J. Podesta, *Dalton Trans.*, 2006, 4078; (d) C. B. Aakeröy, A. M. Beatty, D. S. Leinen, *J. Am. Chem. Soc.*, 1998, **120**, 7383; (e) C. B. Aakeröy, A. M. Beatty, D. S. Leinen, K. R. Lorimer, *Chem. Commun.*, 2000, 935; (f) C. B. Aakeröy, A. M. Beatty, D. S. Leinen, *CrystEngComm*, 2002, **4**, 310.

<sup>10</sup> C. B. Aakeröy, A. M. Beatty, D. S. Leinen, *J. Am. Chem. Soc.*, 1998, **120**, 7383.

<sup>11</sup> I. Socorro, A. Neels, H. Stoeckli-Evans, *Acta Cryst., Sect. C: Cryst. Struct. Comm.*, 2004, **60**, m13.

<sup>12</sup> P. Sauerberg, P. H. Olesen, S. Nielsen, S. Treppendahl, M. J. Sheardown, T. Honoré, C. H. Mitch, J. S. Ward, A. J. Pike, F. P. Bymaster, B. D. Sawyer, and H. E. Shannon, *J. Med. Chem.*, 1992, **35**, 2274.

<sup>13</sup> C. B. Aakeröy, J. Desper, M. M. Smith, J. F. Urbina, *Dalton Trans.*, 2005, 2462.

- 
- <sup>14</sup> (a) B. R. Bhogala, P. K. Thallapally, A. Nangia, *Cryst. Growth Des.*, 2004, **4**, 215; (b) T. Dorn, K. M. Fromm, C. Janiak, *Aust. J. Chem.*, 2006, **59**, 22; (c) Z.-X. Lian, J. Cai, C.-H Chen, H.-B. Luo, *CrystEngComm*, 2007, **9**, 319; (d)
- <sup>14</sup> (a) C.-H Chen, J. Cai, X.-L. Feng, X.-M Chen, *Polyhedron*, 2002, **21**, 689; (b) C. B. Aakeröy, A. M. Beatty, *Chem. Commun.*, 1998, 1067; (c) C. B. Aakeröy, A. M. Beatty, *Cryst. Eng.*, 1998, **1**, 39.
- <sup>15</sup> (a) C.-H Chen, J. Cai, X.-L. Feng, X.-M Chen, *Polyhedron*, 2002, **21**, 689; (b) C. B. Aakeröy, A. M. Beatty, *Chem. Commun.*, 1998, 1067; (c) C. B. Aakeröy, A. M. Beatty, *Cryst. Eng.*, 1998, **1**, 39.
- <sup>16</sup> (a) B. Kozlevcar, I. Leban, I. Turel, P. Segedin, M. Petric, F. Pohleven, A. J. P. White, D. J. Williams, J. Sieler, *Polyhedron*, 1999, **18**, 755; (b) A. S. Antsyshkina, T. V. Koksharova, G. G. Sadikov, I. S. Gritsenko, V. S. Sergienko, O. A. Egorova, *Zh. Neorg. Khim. (Russ.) (Russ. J. Inorg. Chem.)*, 2006, **51**, 972; (c) B. Kozlevcar, N. Lah, I. Leban, I. Turel, P. Segedin, M. Petric, F. Pohleven, A. J. P. White, D. J. Williams, G. Giester, *Croat. Chem. Acta*, 1999, **72**, 427; (d) C. B. Aakeröy, A. M. Beatty, J. Desper, M. O'Shea, J. Valdes-Martinez, *Dalton Trans.*, 2003, 3956; (e) K. Smolander, M. Macko, M. Valko, M. Melnik, *Acta Chem. Scand.*, 1992, **46**, 29.

## Appendix A - $^1\text{H}$ and $^{13}\text{C}$ NMR Data

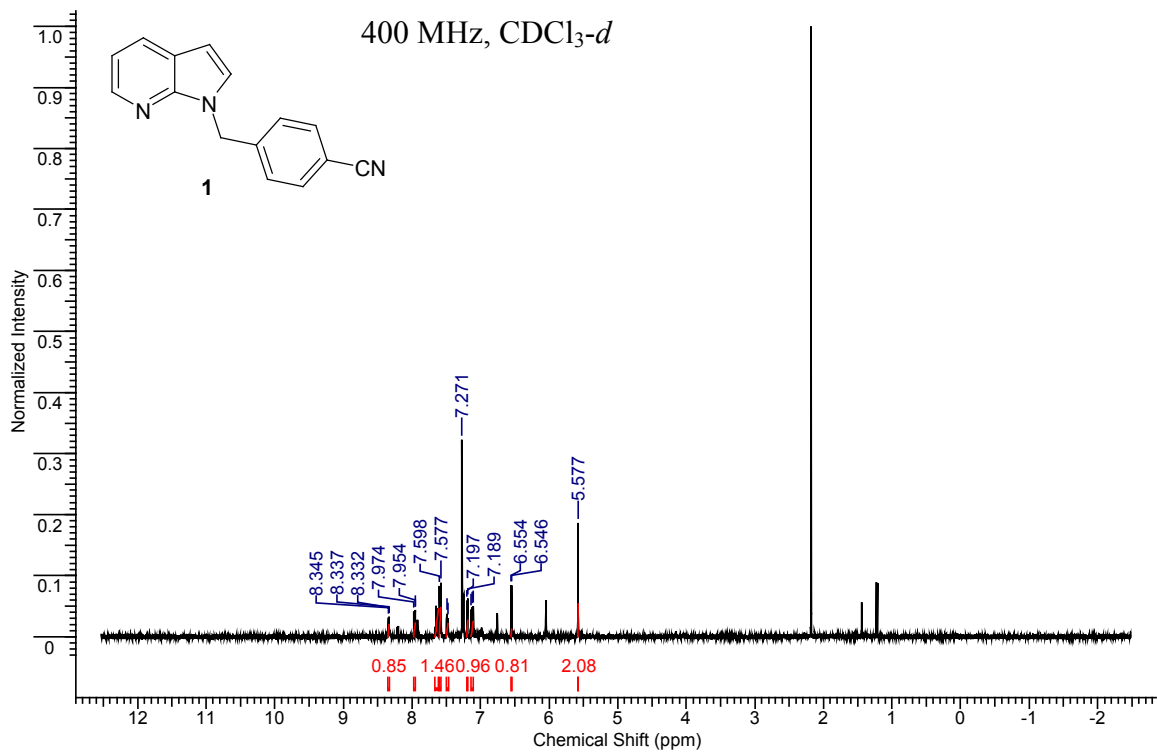
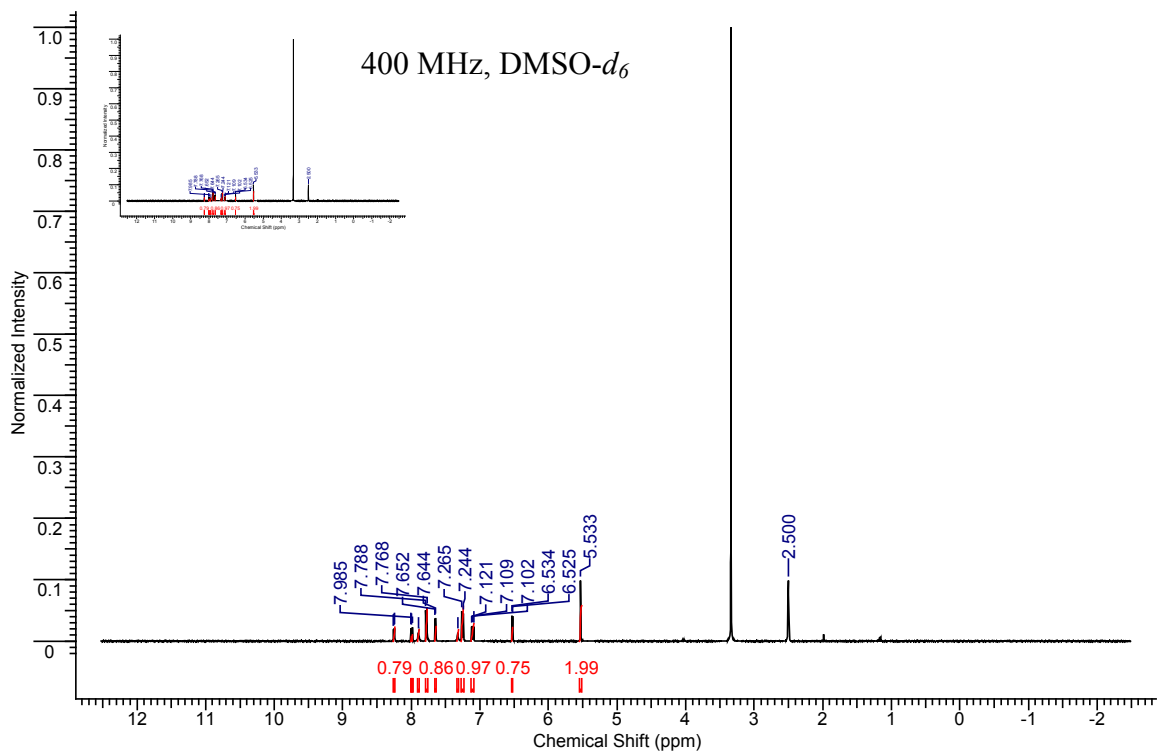
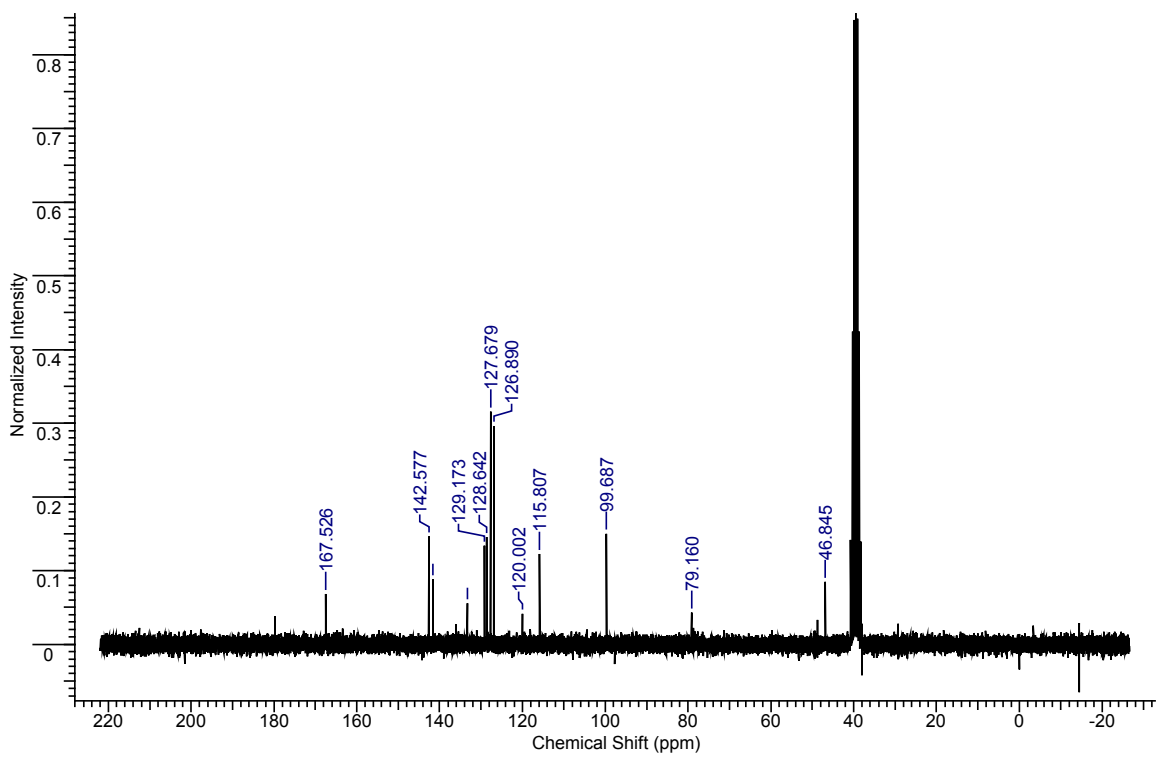


Figure A.1  $^1\text{H}$  NMR of **1**



(a)



(b)

Figure A.2 (a) <sup>1</sup>H and (b) <sup>13</sup>C NMR of 2

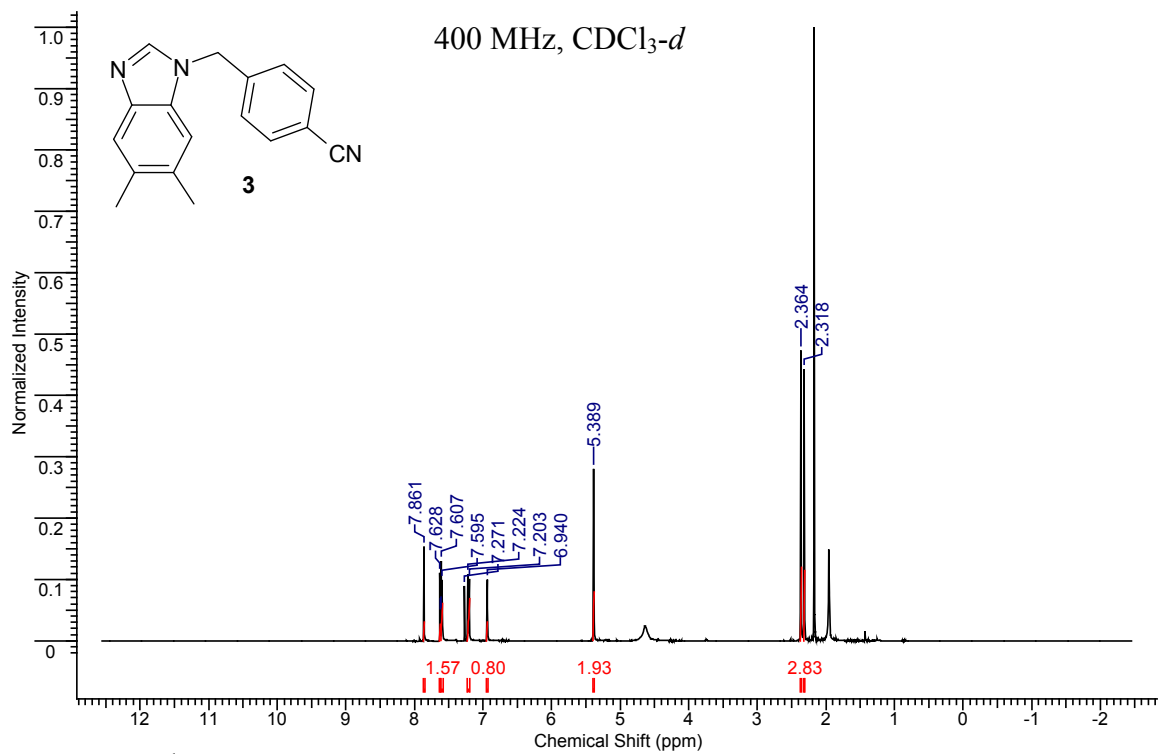


**Figure A.3** <sup>1</sup>H NMR of **3**

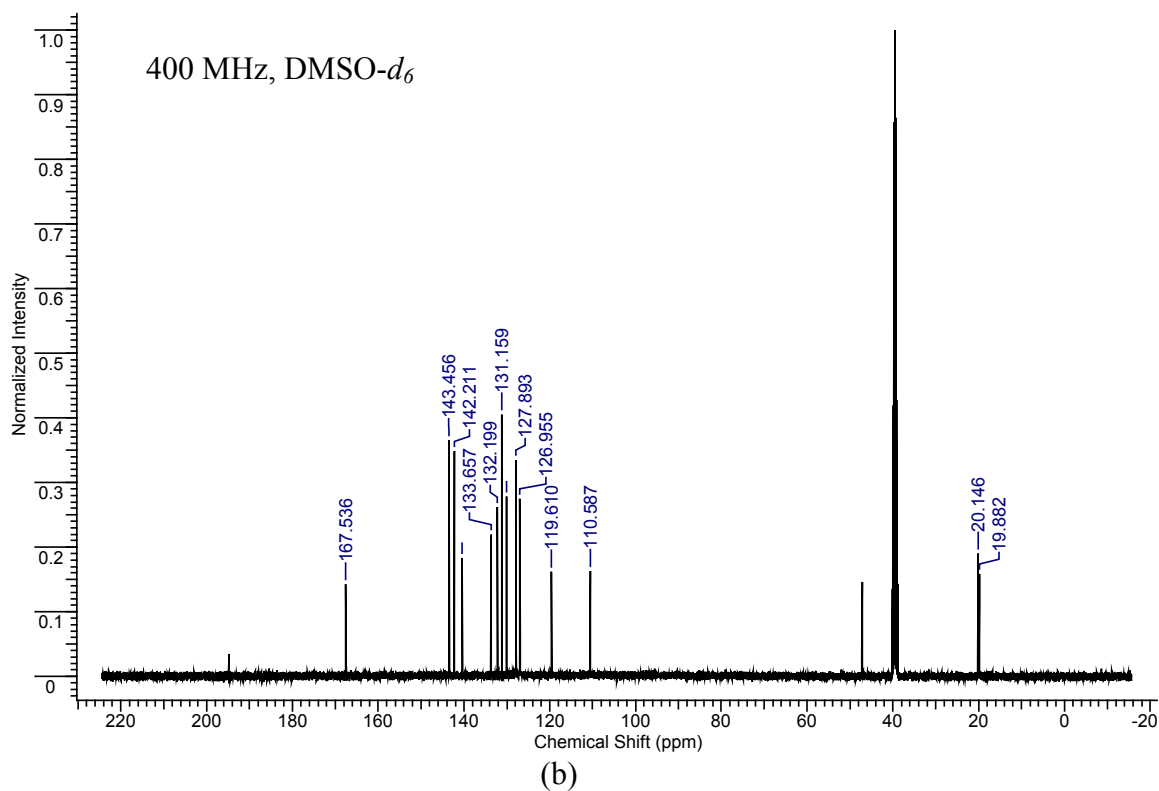
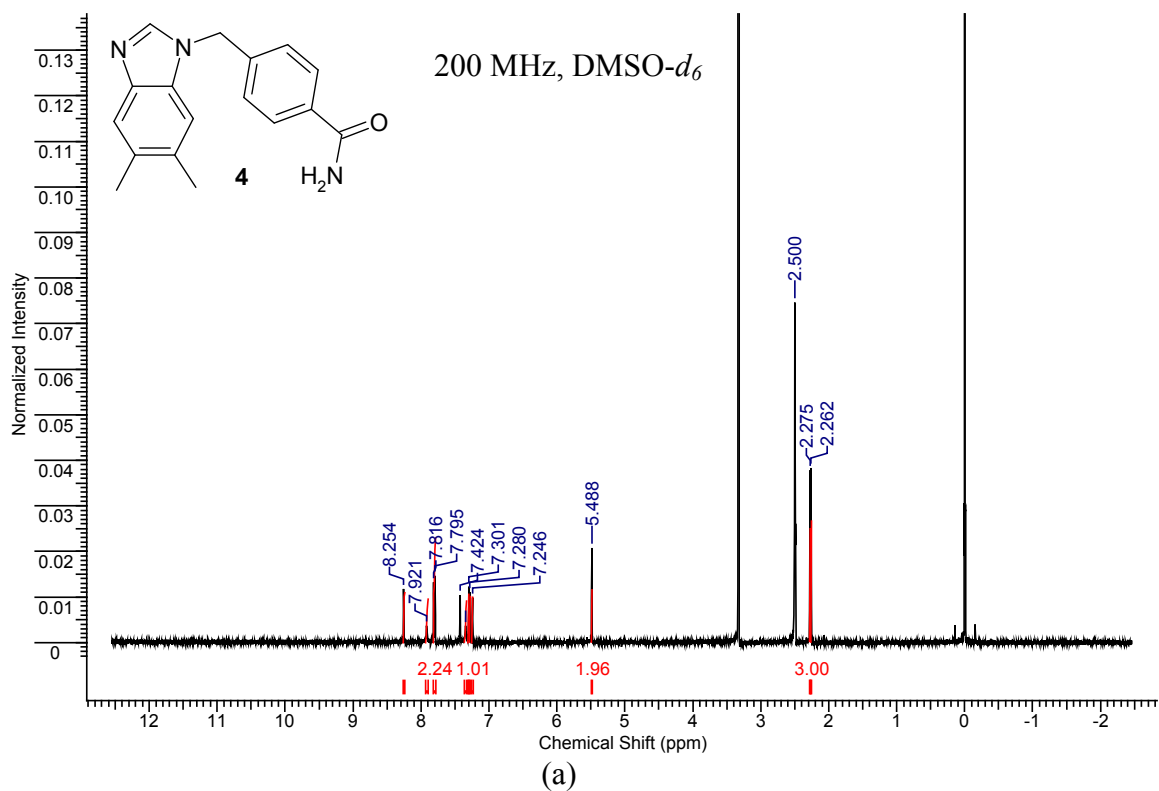


Figure A.4 (a)  $^1\text{H}$  and (b)  $^{13}\text{C}$  NMR of **4**



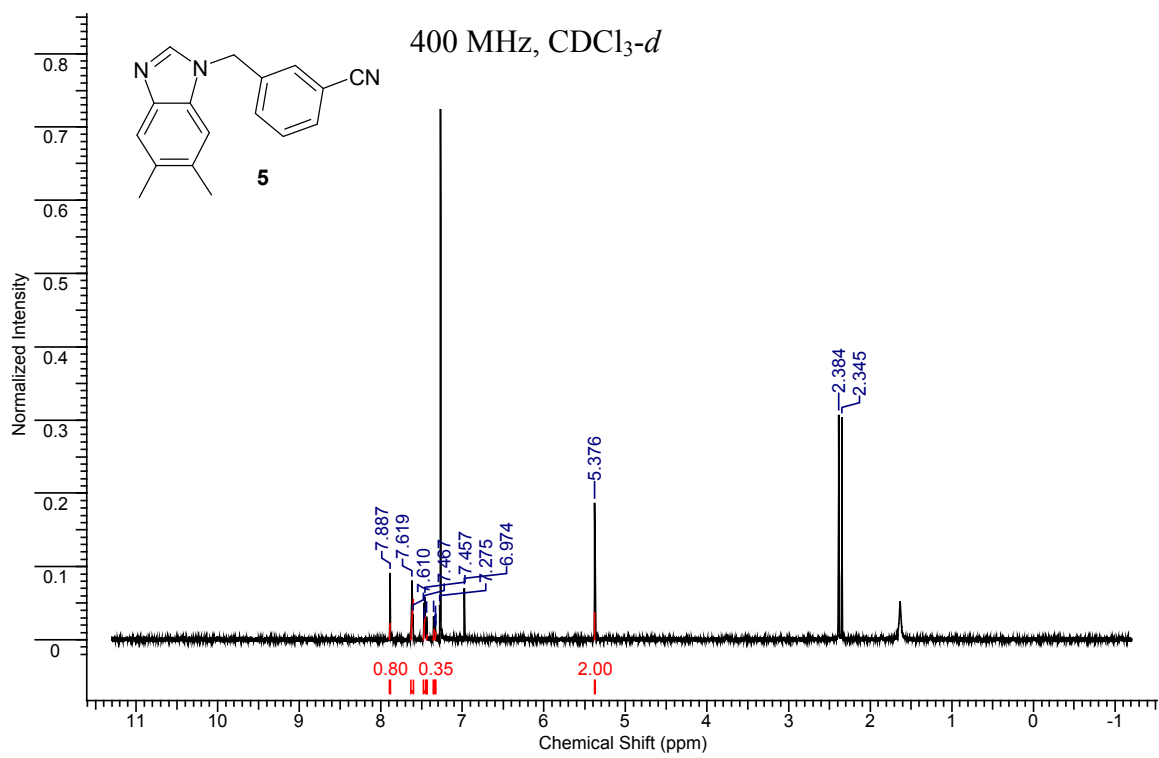
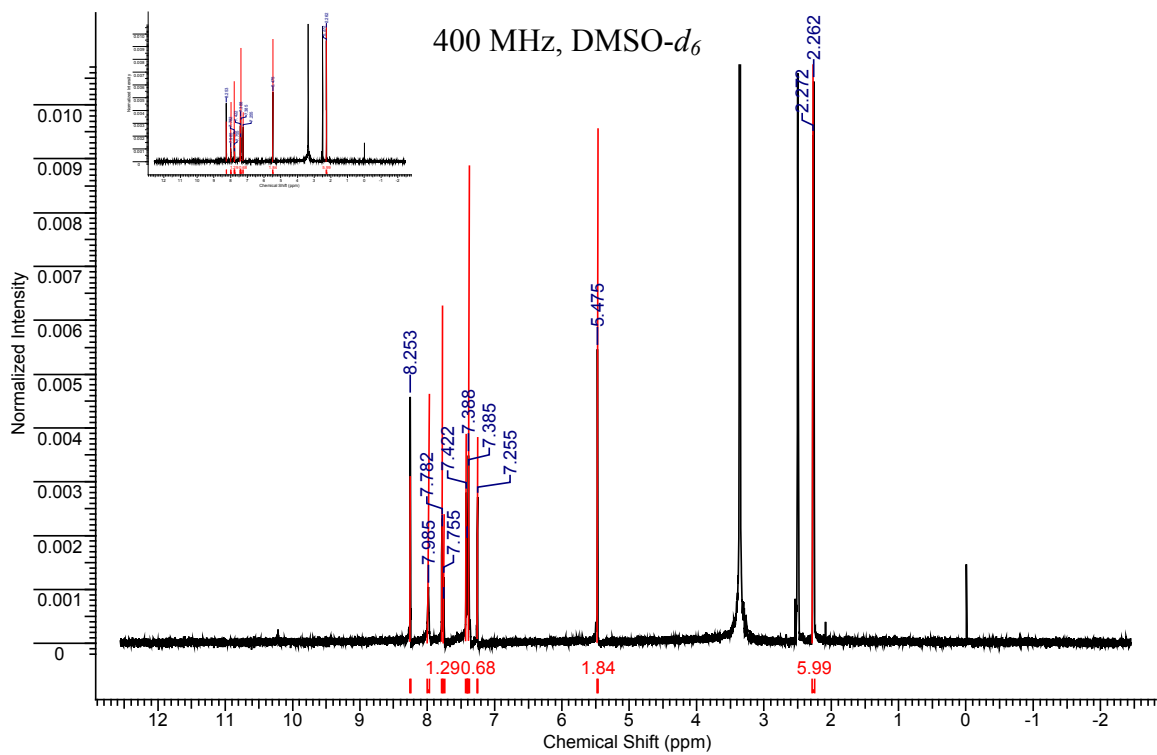
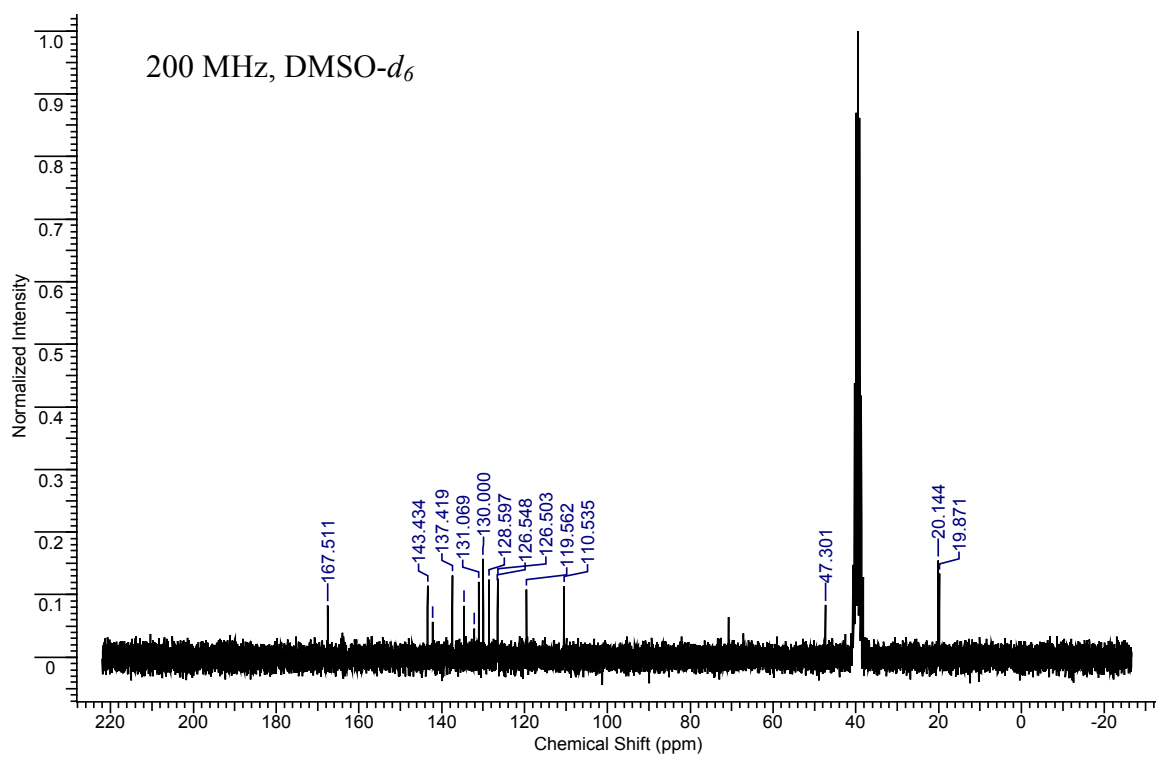


Figure A.5 <sup>1</sup>H NMR of **5**



(a)



(b)

Figure A.6 (a) <sup>1</sup>H and (b) <sup>13</sup>C NMR of **6**

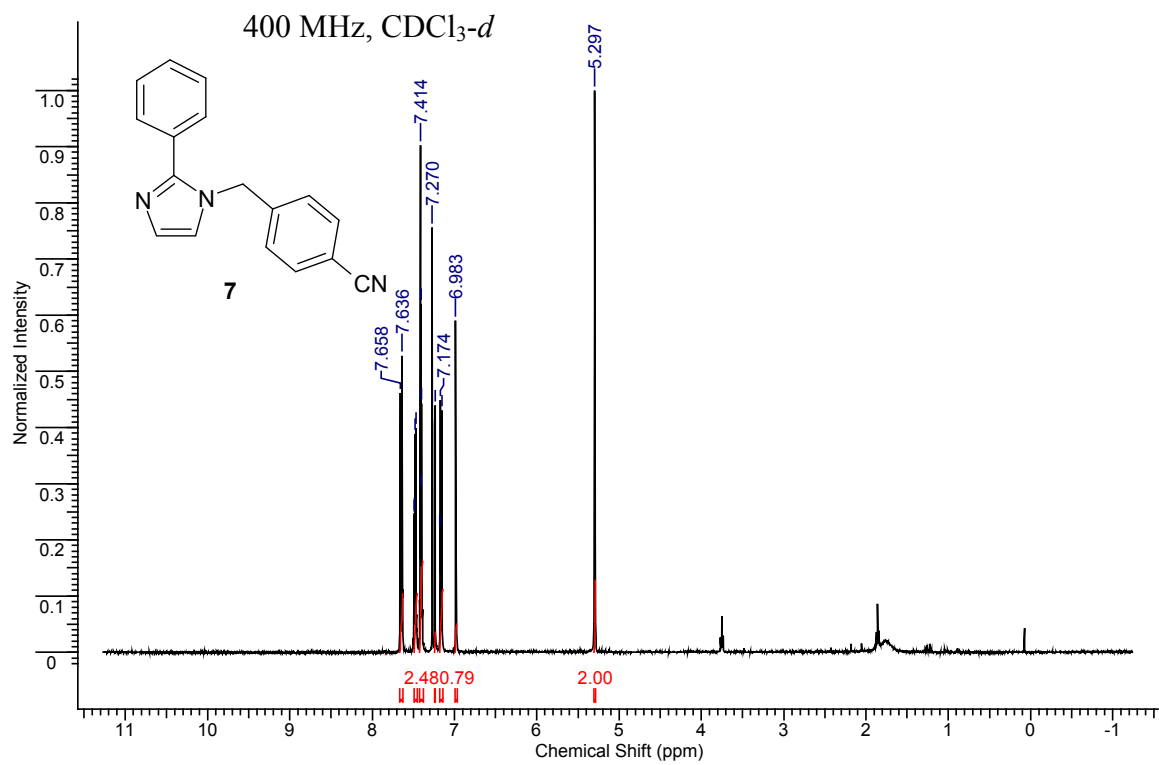
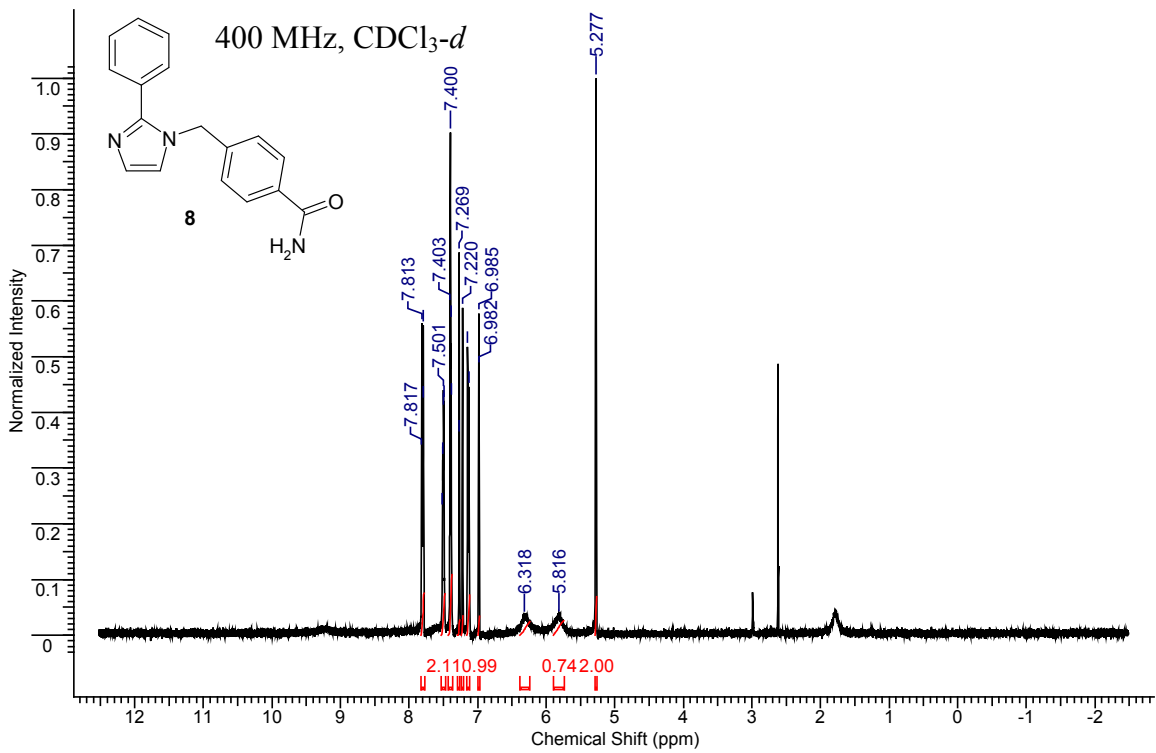
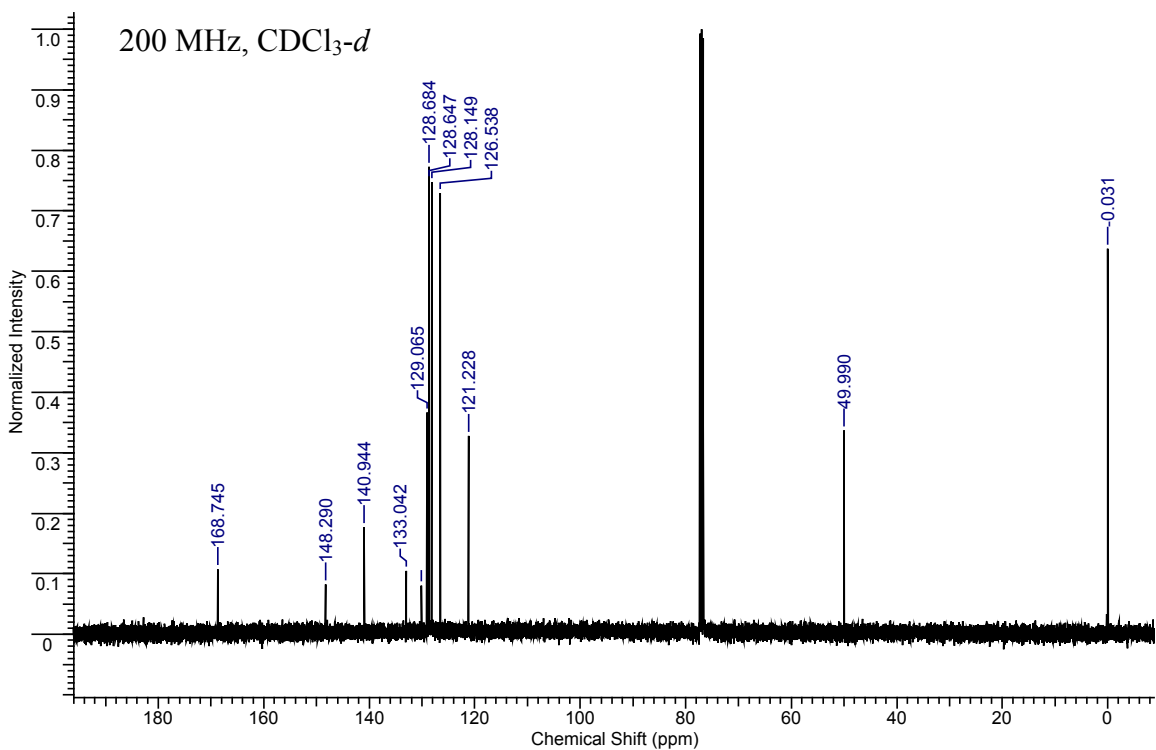


Figure A.7 <sup>1</sup>H NMR of 7



(a)



(b)

Figure A.8 (a) <sup>1</sup>H and (b) <sup>13</sup>C NMR of 8

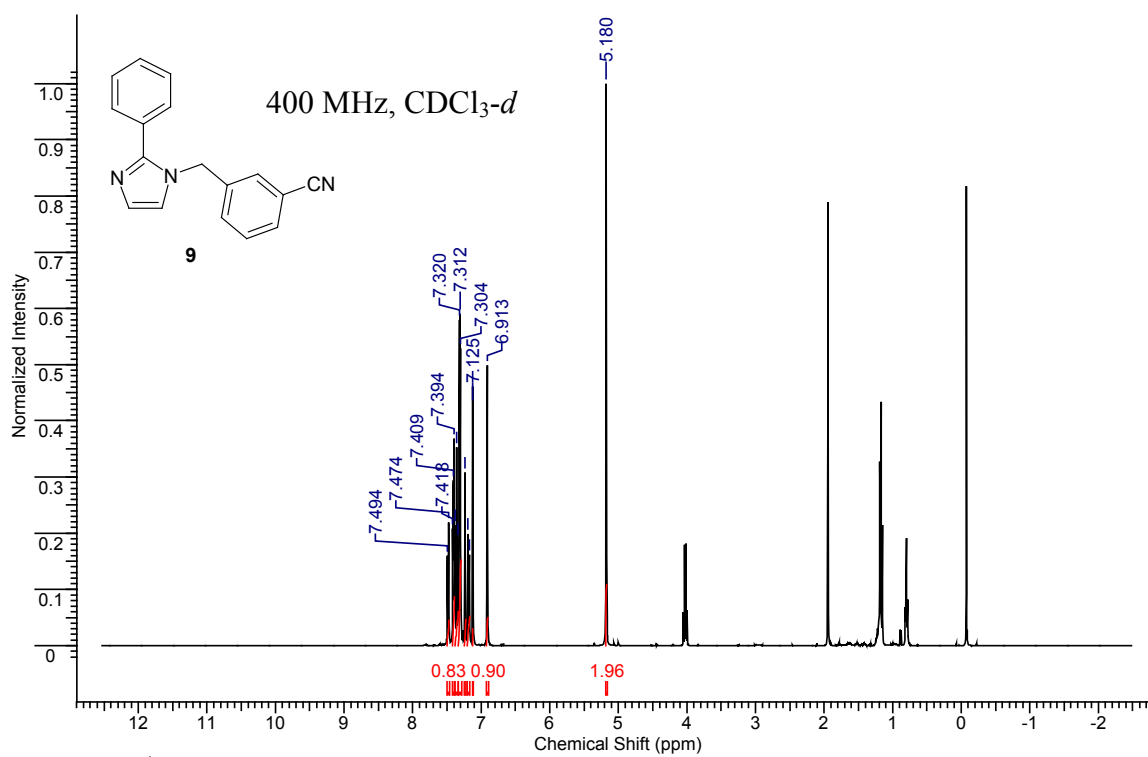
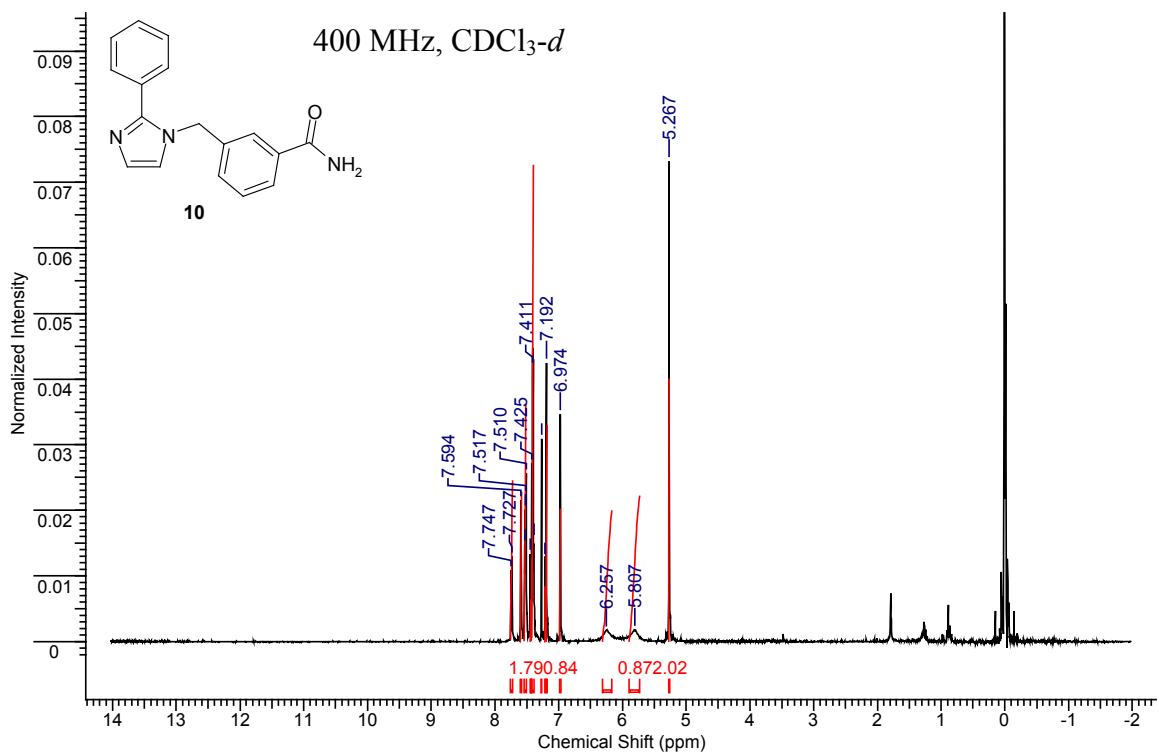
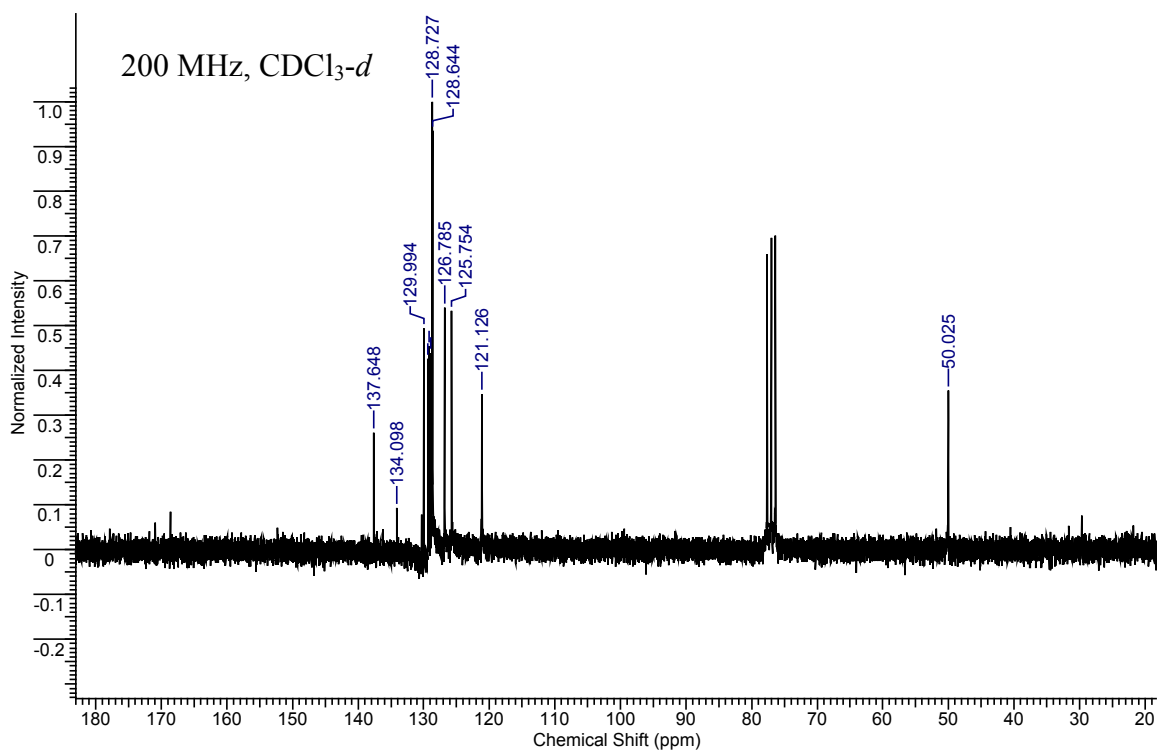


Figure A.9 <sup>1</sup>H NMR of 9



(a)



(b)

**Figure A.10** (a) <sup>1</sup>H and (b) <sup>13</sup>C NMR of **10**

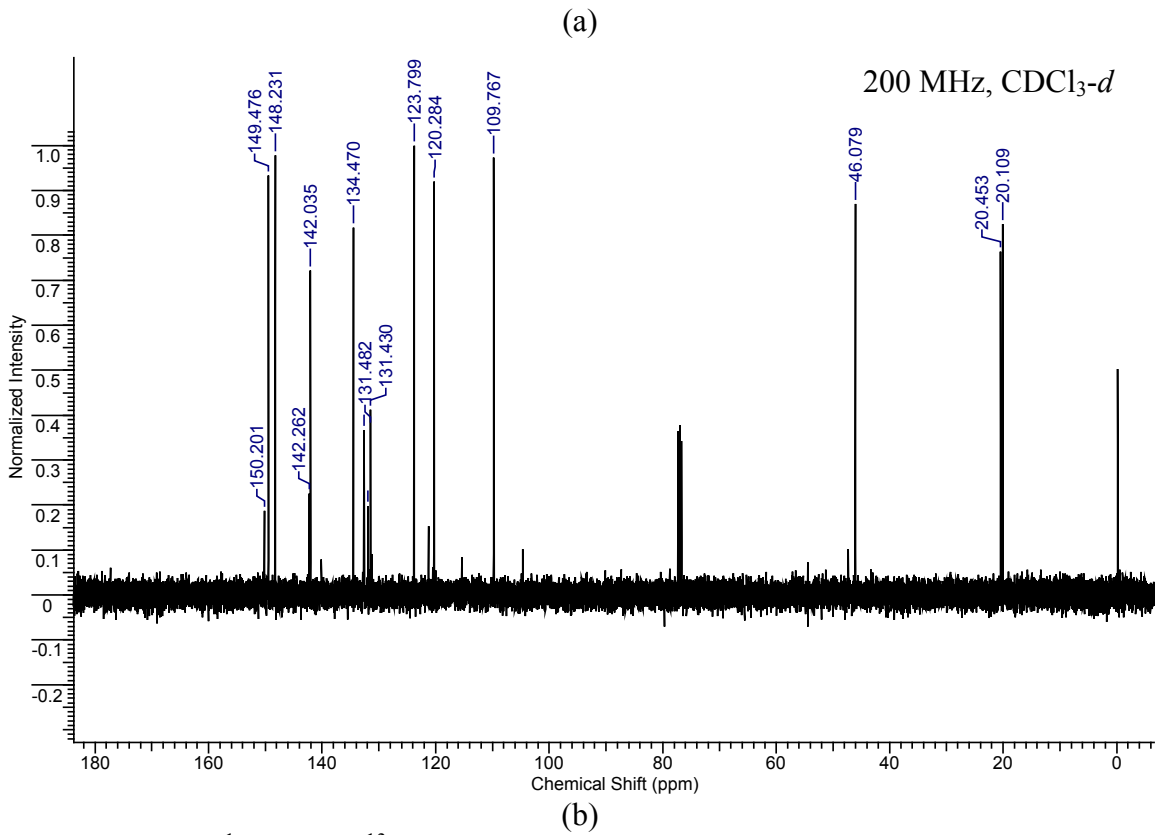
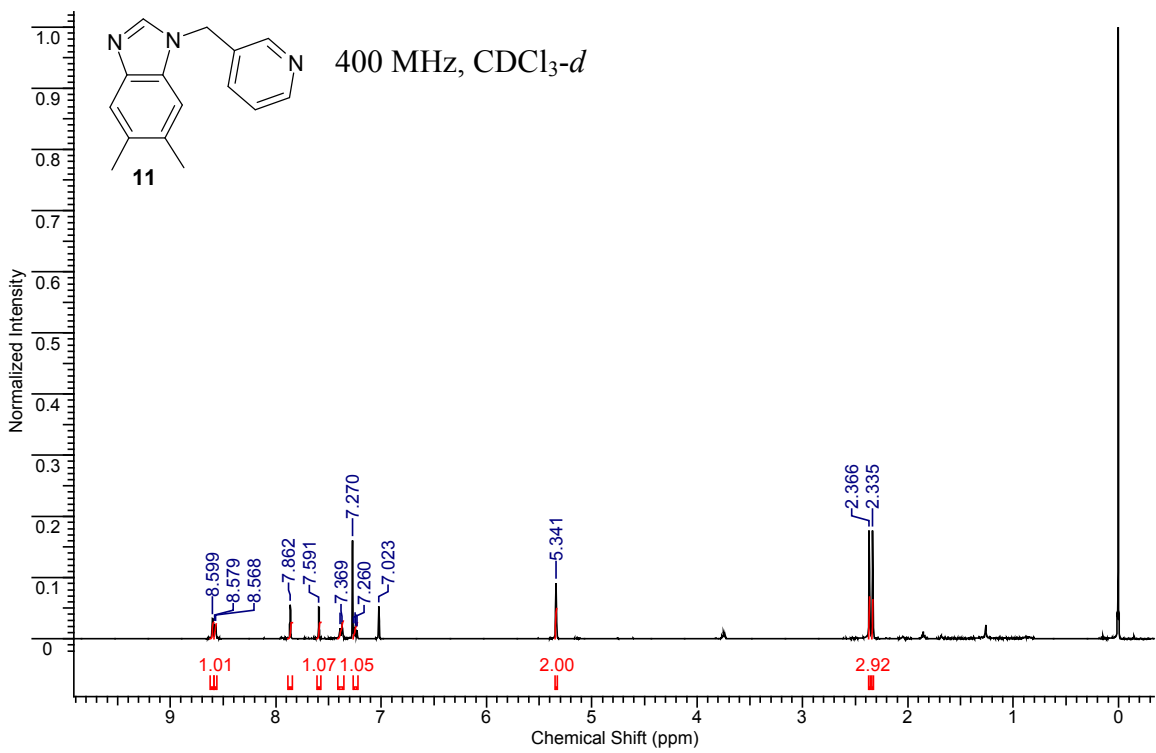
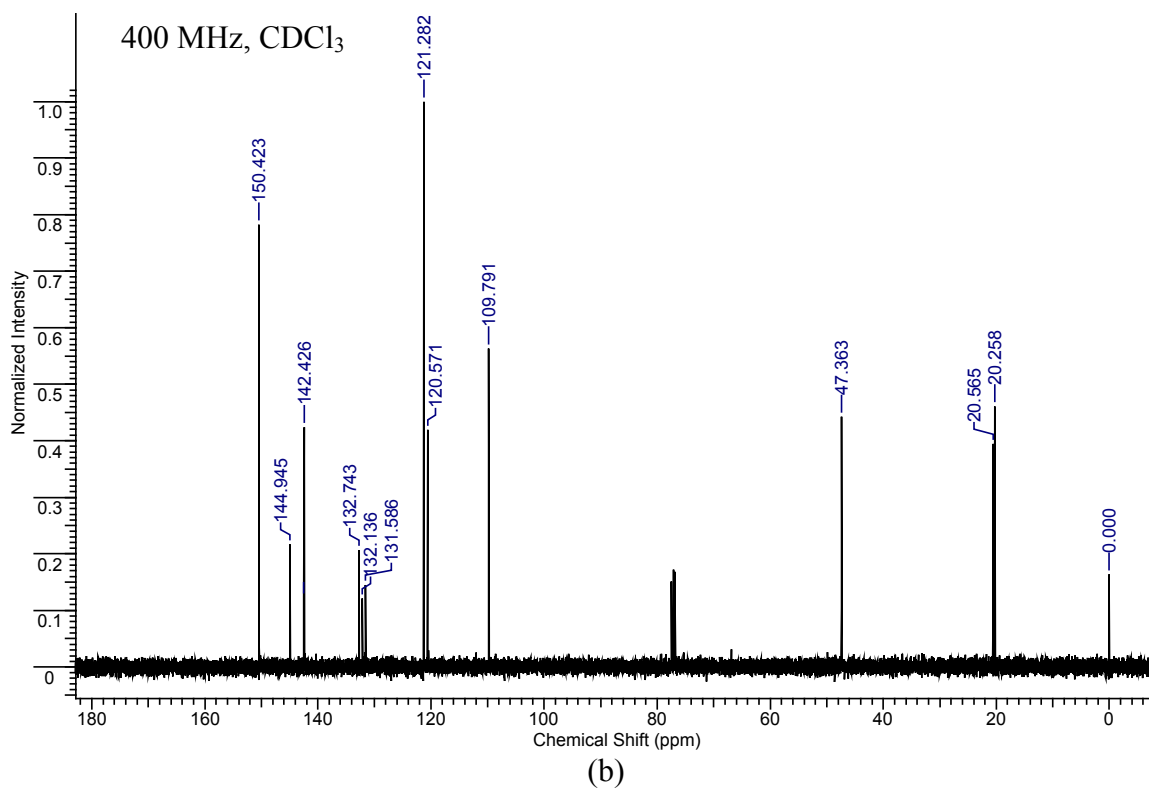
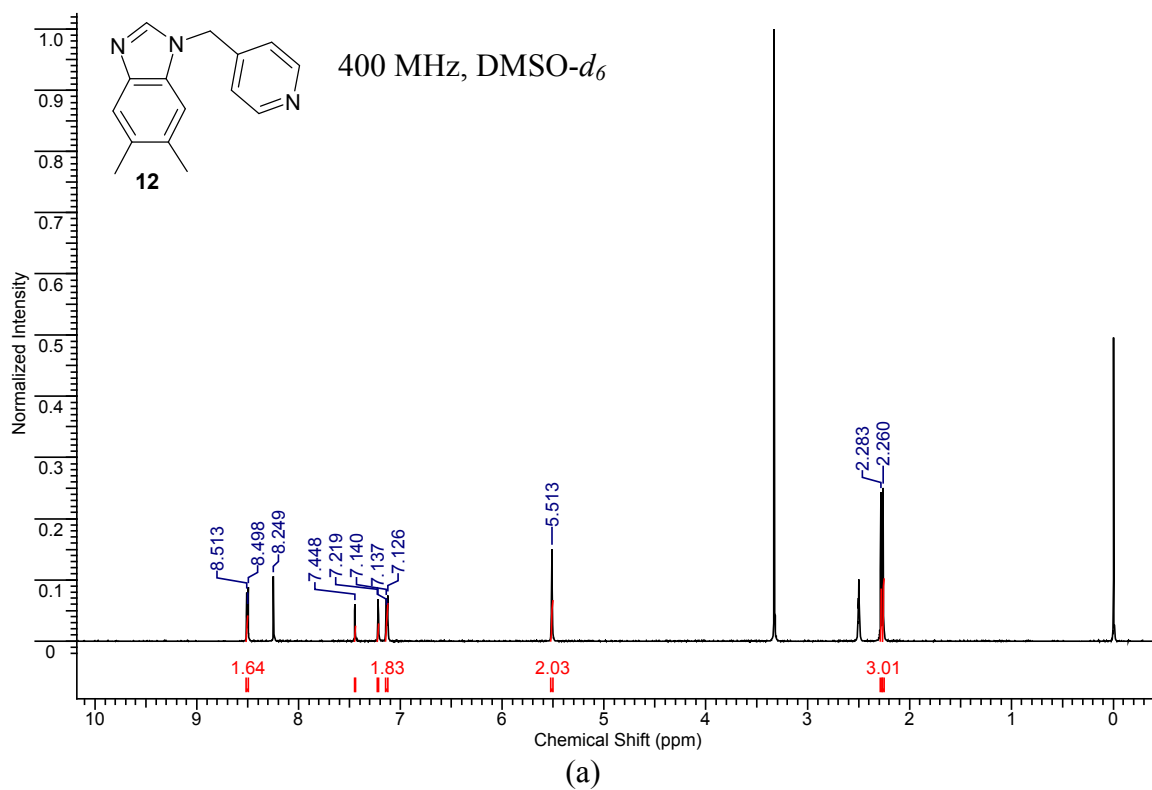
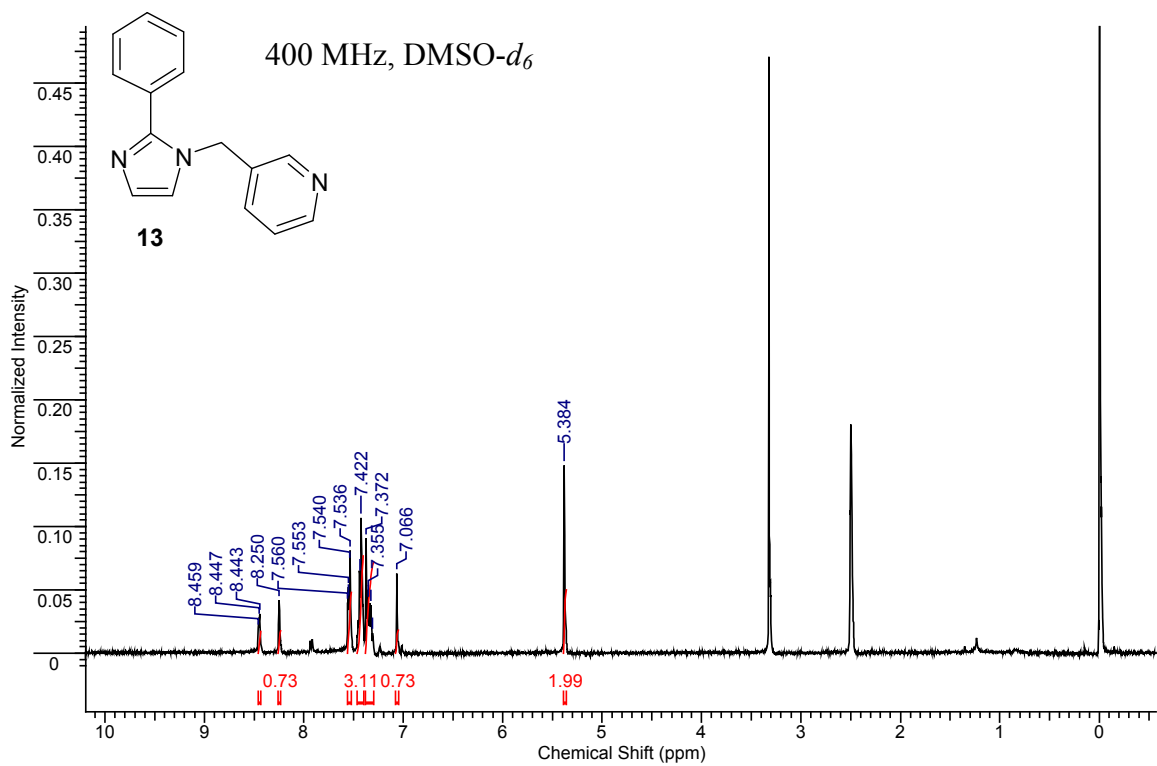


Figure A.11 (a) <sup>1</sup>H and (b) <sup>13</sup>C NMR of **11**

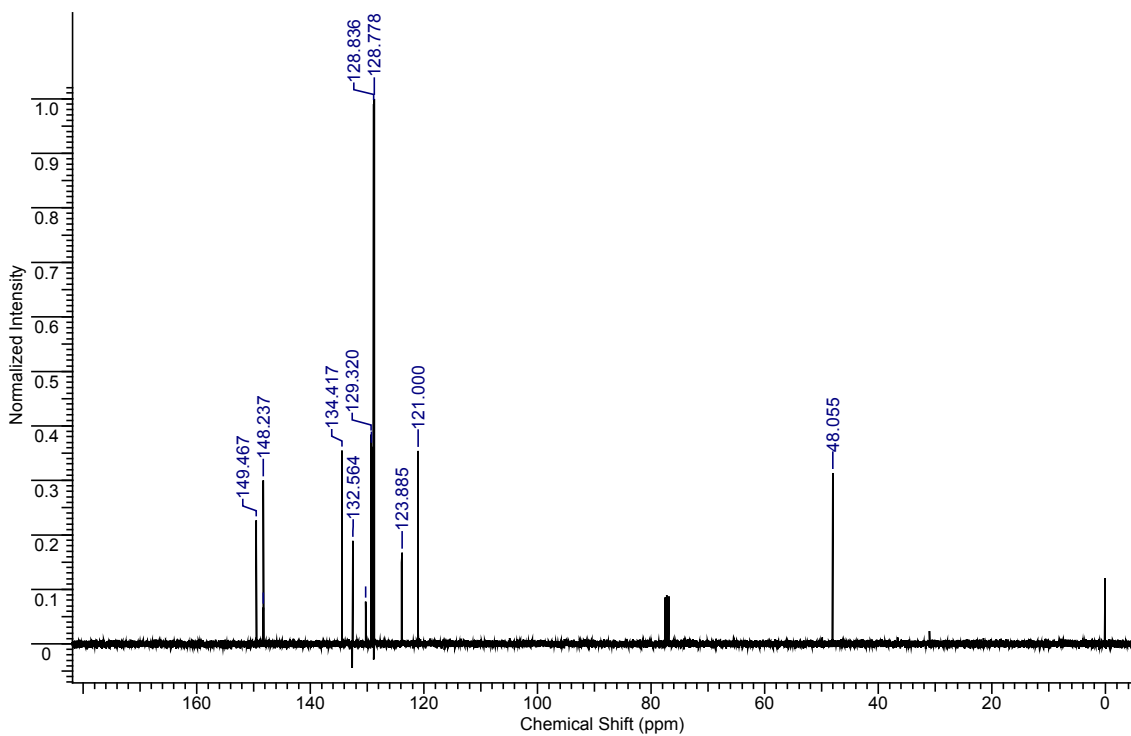


**Figure A.12** (a) <sup>1</sup>H and (b) <sup>13</sup>C NMR of **12**



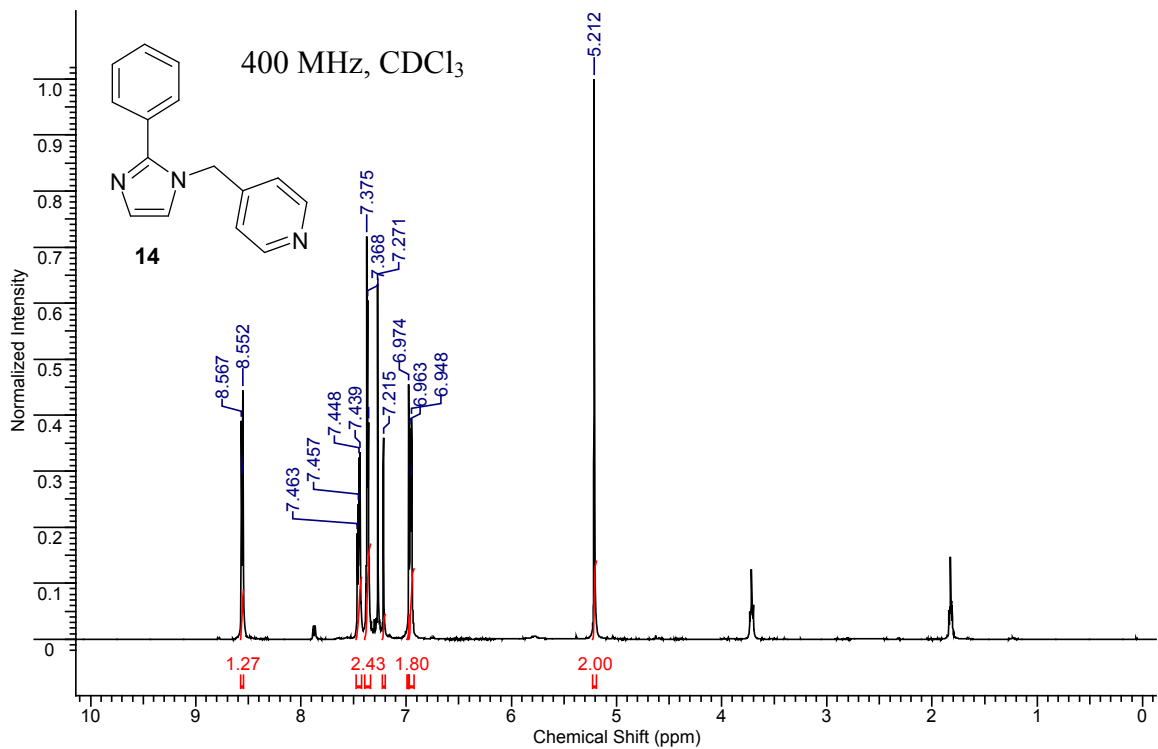


(a)

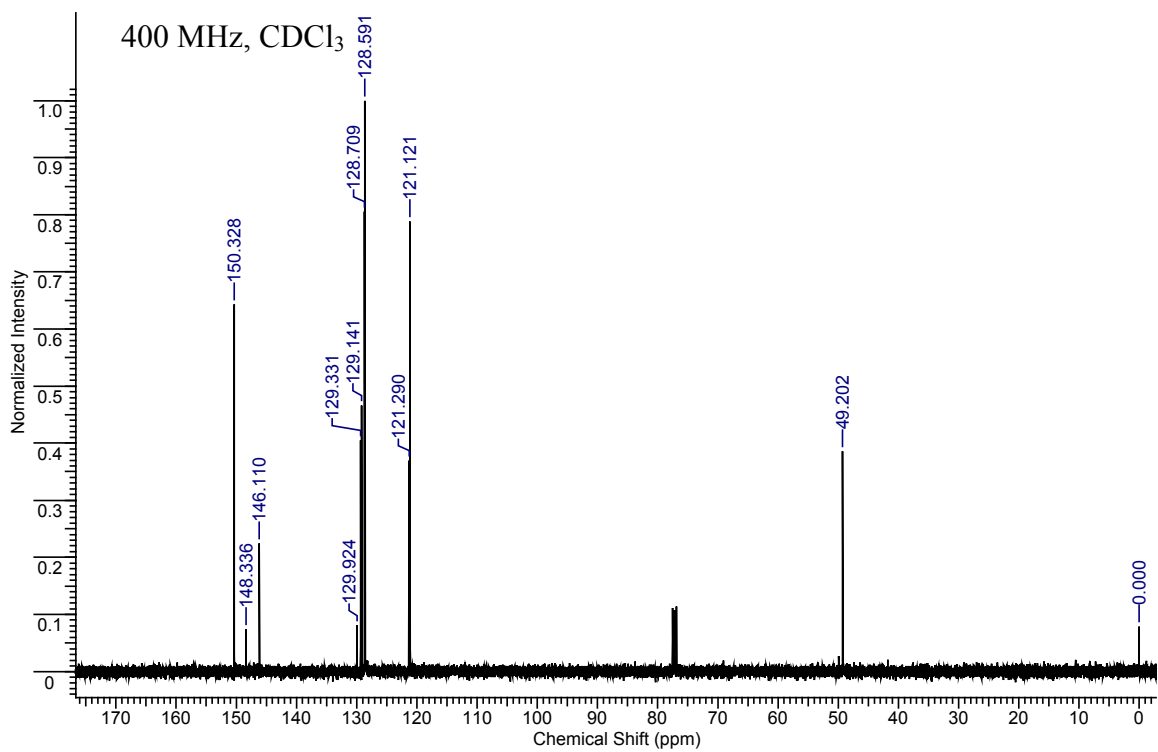


(b)

**Figure A.13** (a) <sup>1</sup>H and (b) <sup>13</sup>C NMR of **13**



(a)



(b)

Figure A.14 (a) <sup>1</sup>H and (b) <sup>13</sup>C NMR of **14**

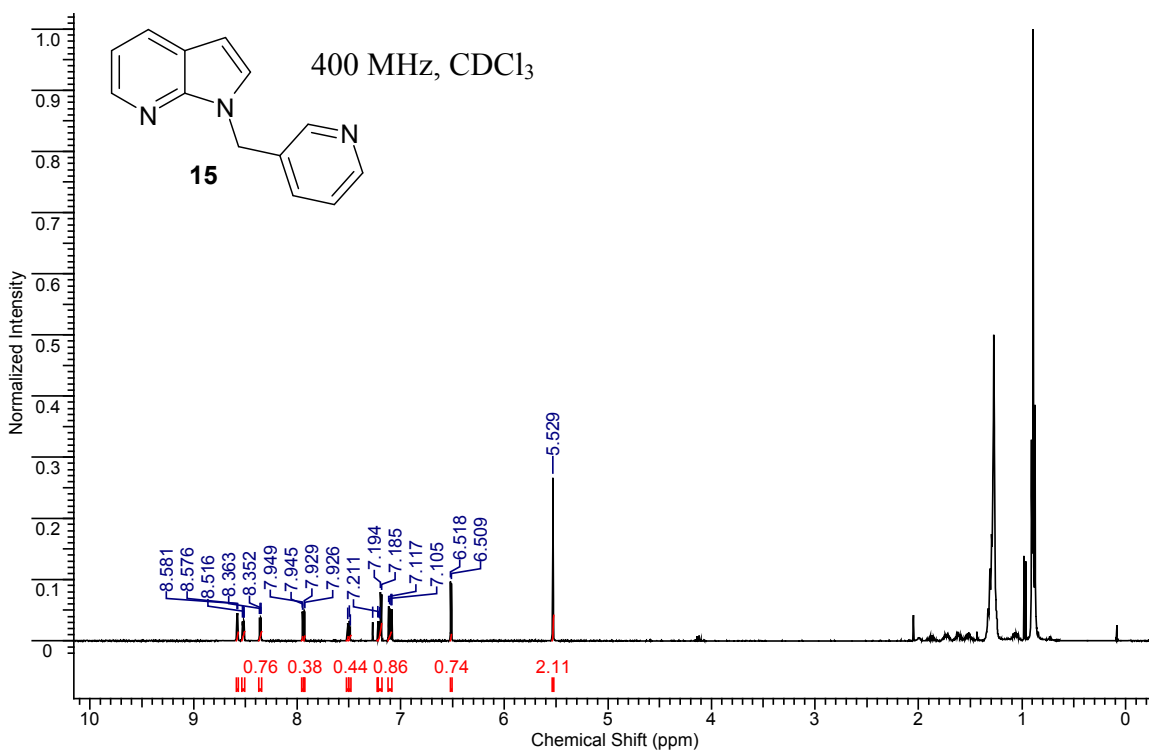


Figure A.15 <sup>1</sup>H NMR of **15**

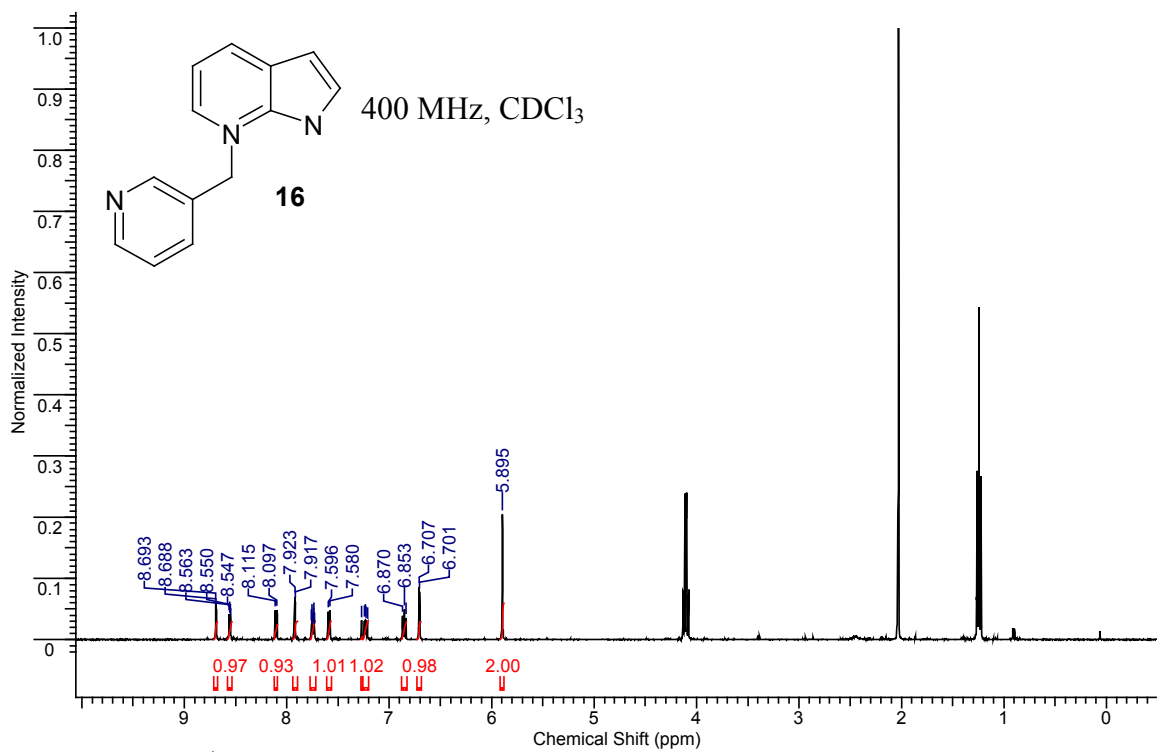
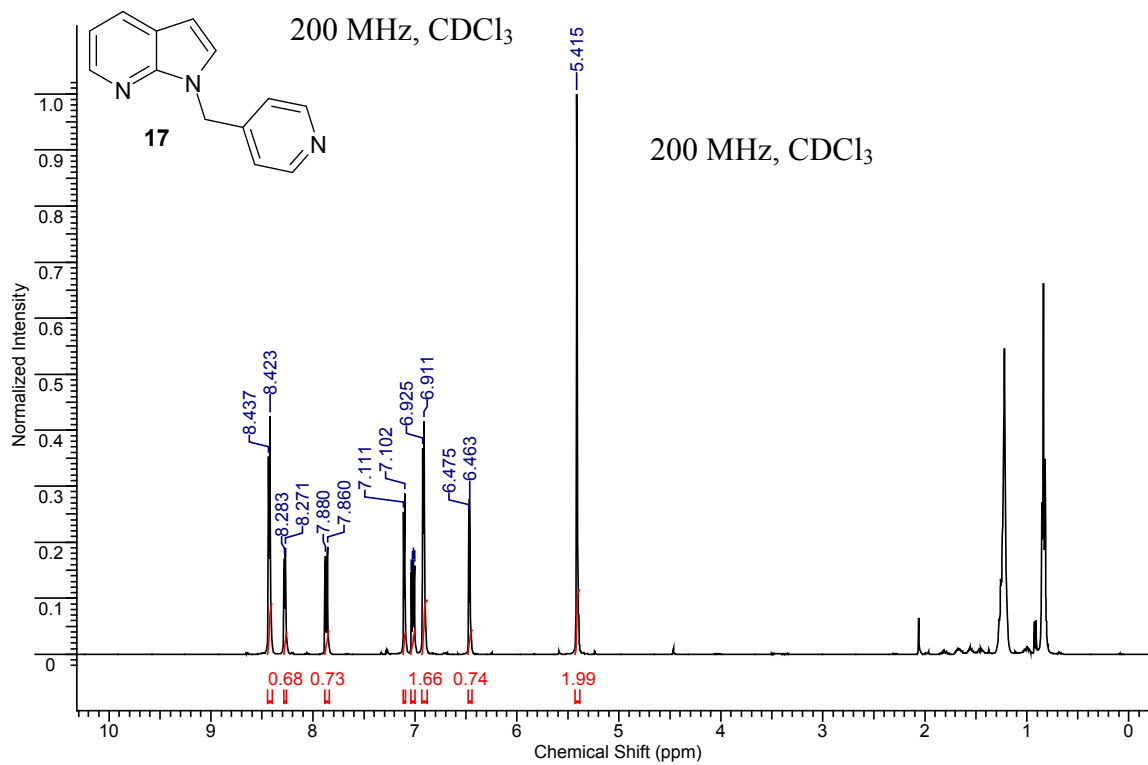
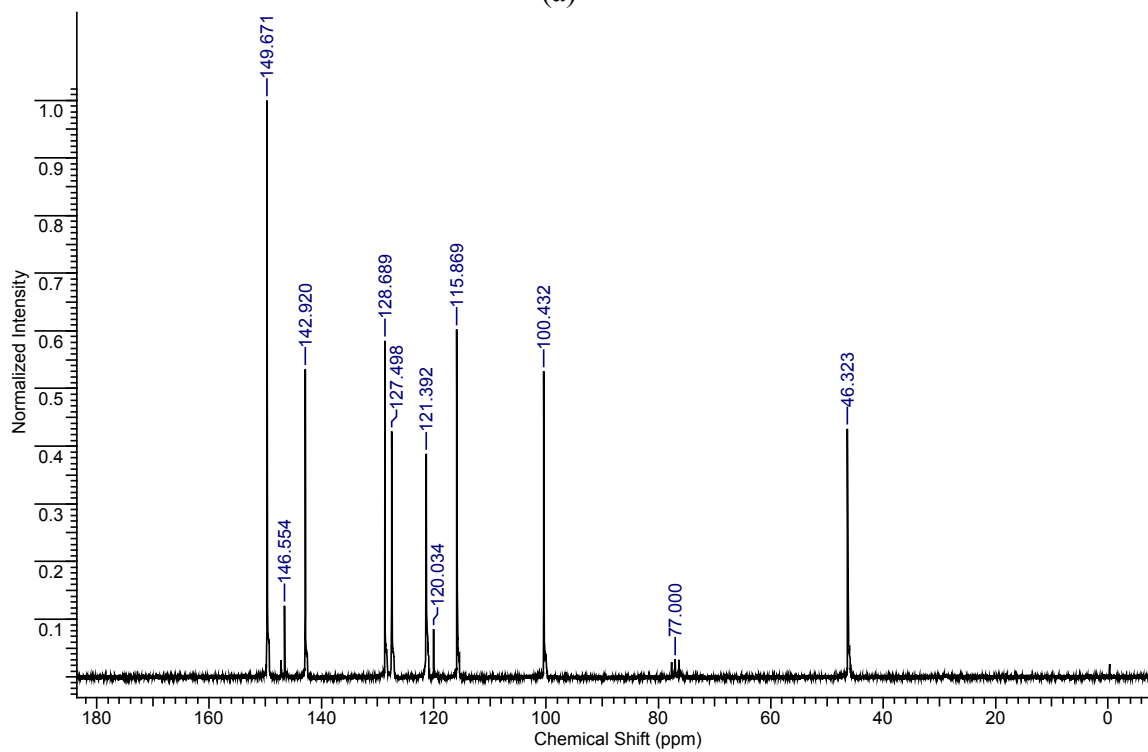


Figure A.16 <sup>1</sup>H NMR of **16**



(a)



(b)

Figure A.17 (a) <sup>1</sup>H and (b) <sup>13</sup>C NMR of 17

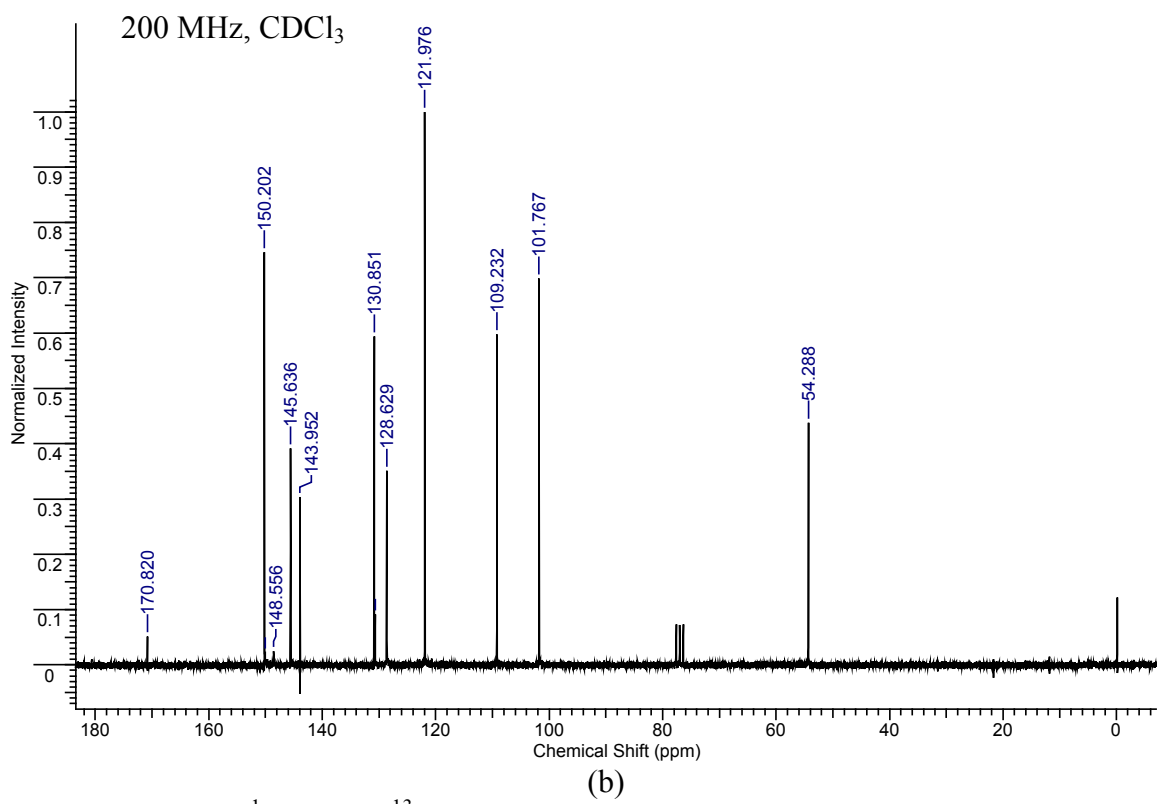
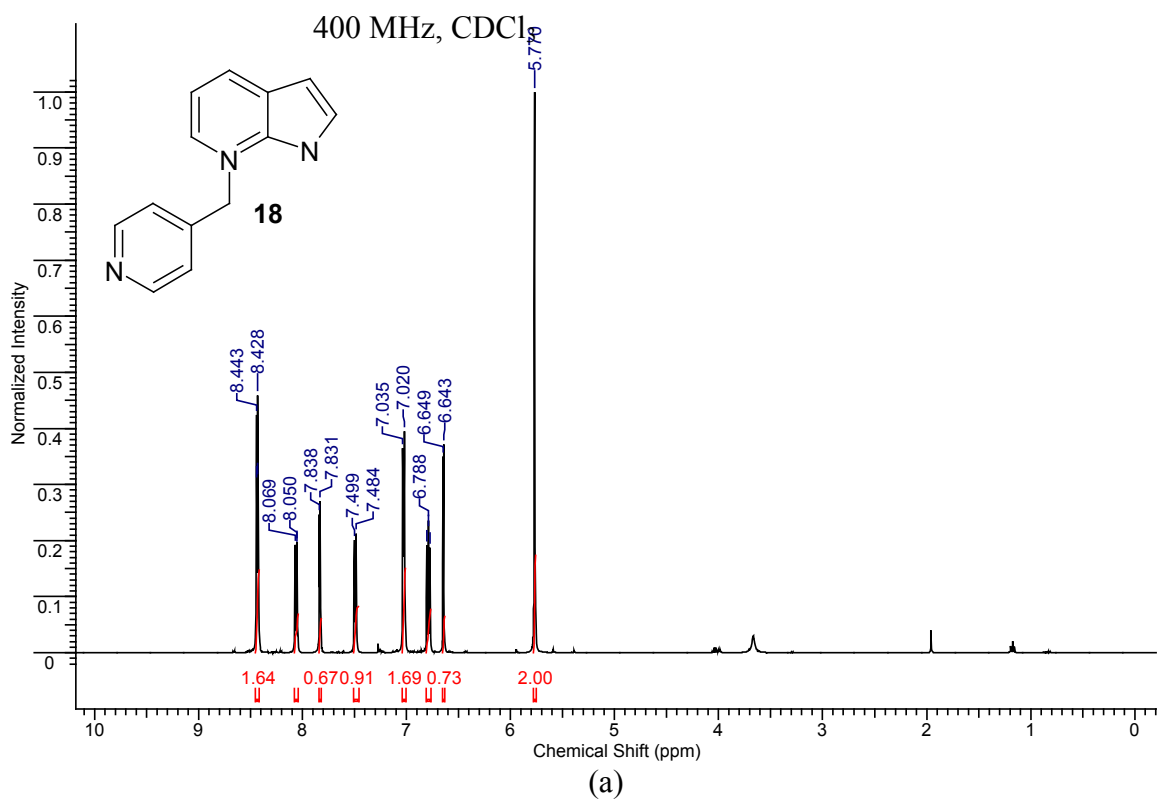


**Figure A.18** (a) <sup>1</sup>H and (b) <sup>13</sup>C NMR of **18**

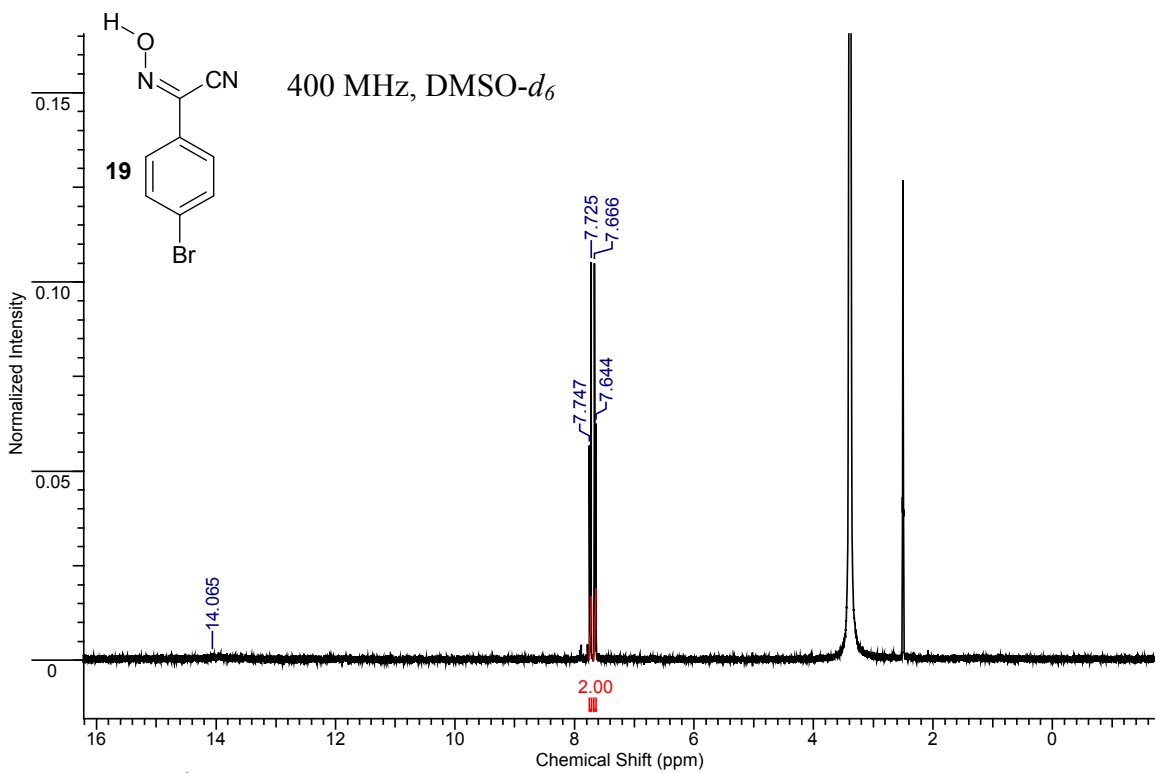


Figure A.19  $^1\text{H}$  NMR of 19

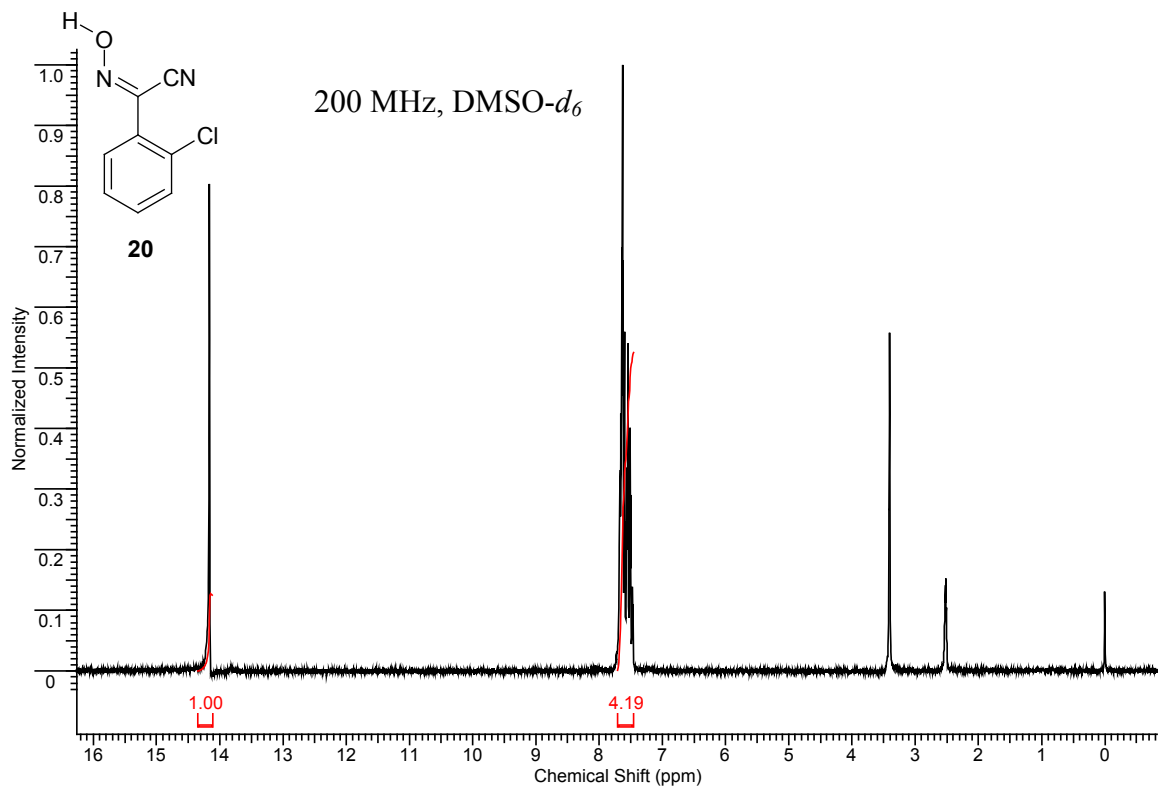


Figure A.20  $^1\text{H}$  NMR of 20

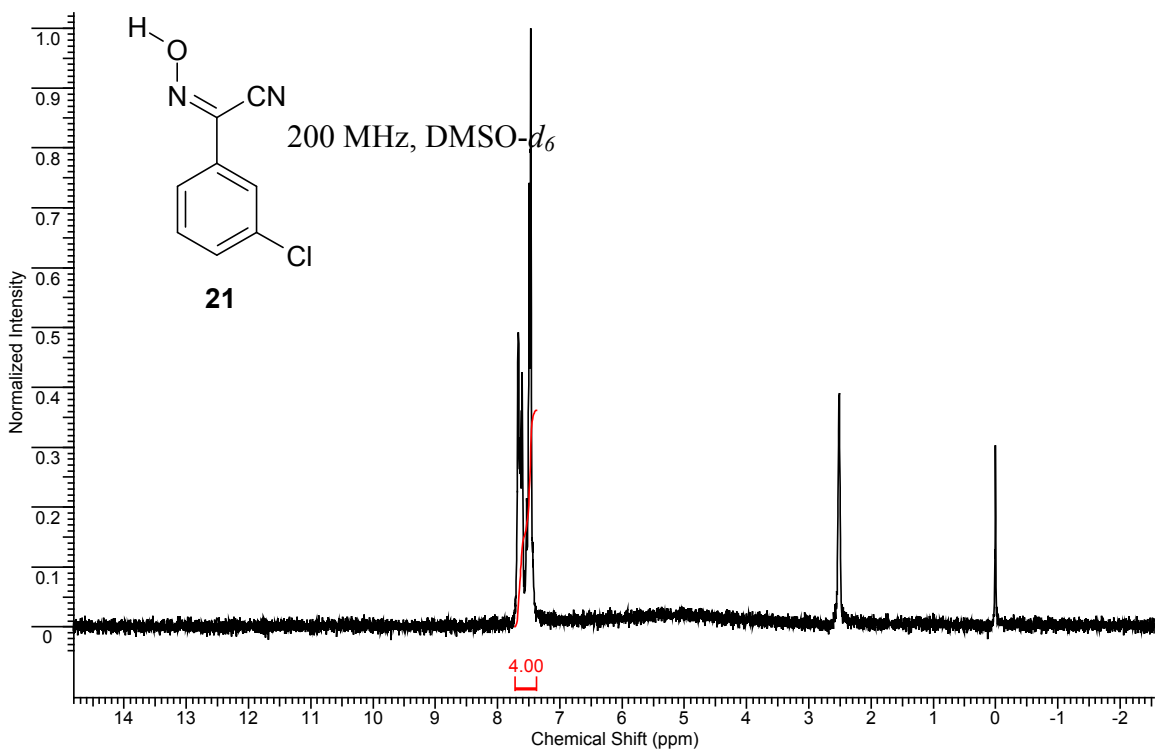


Figure A.21  $^1\text{H}$  NMR of **21**

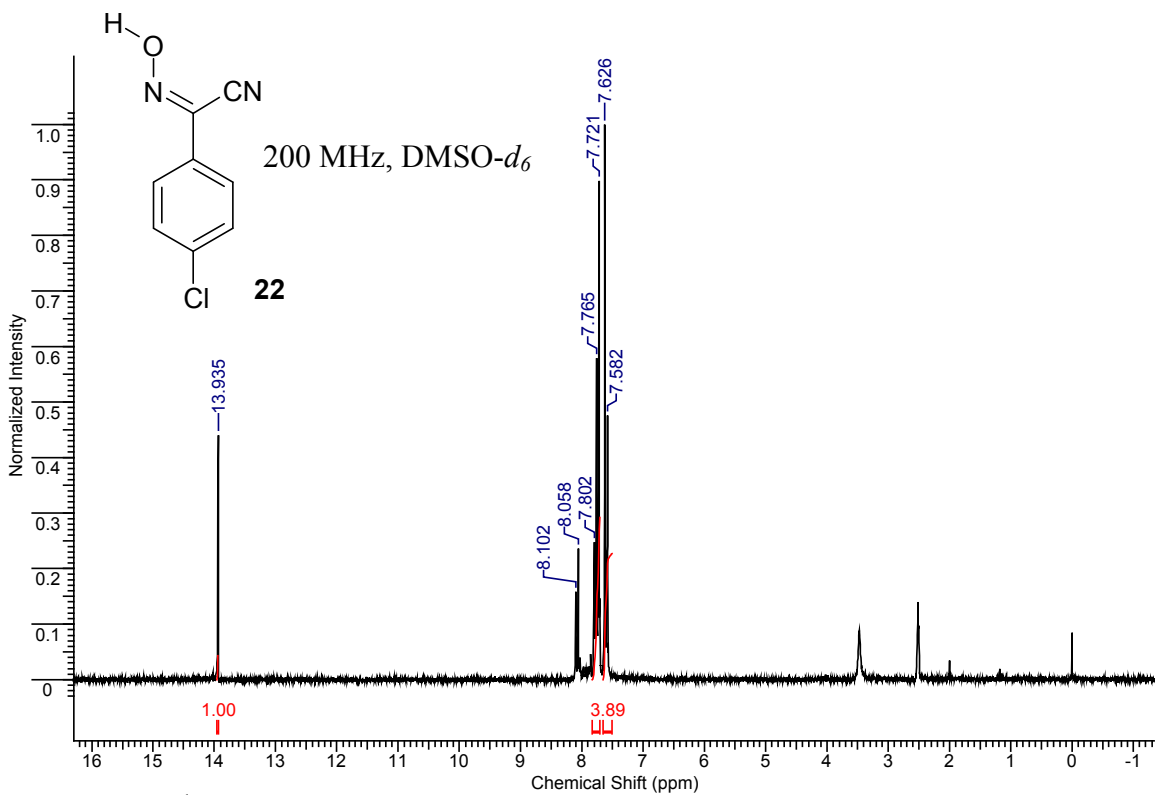
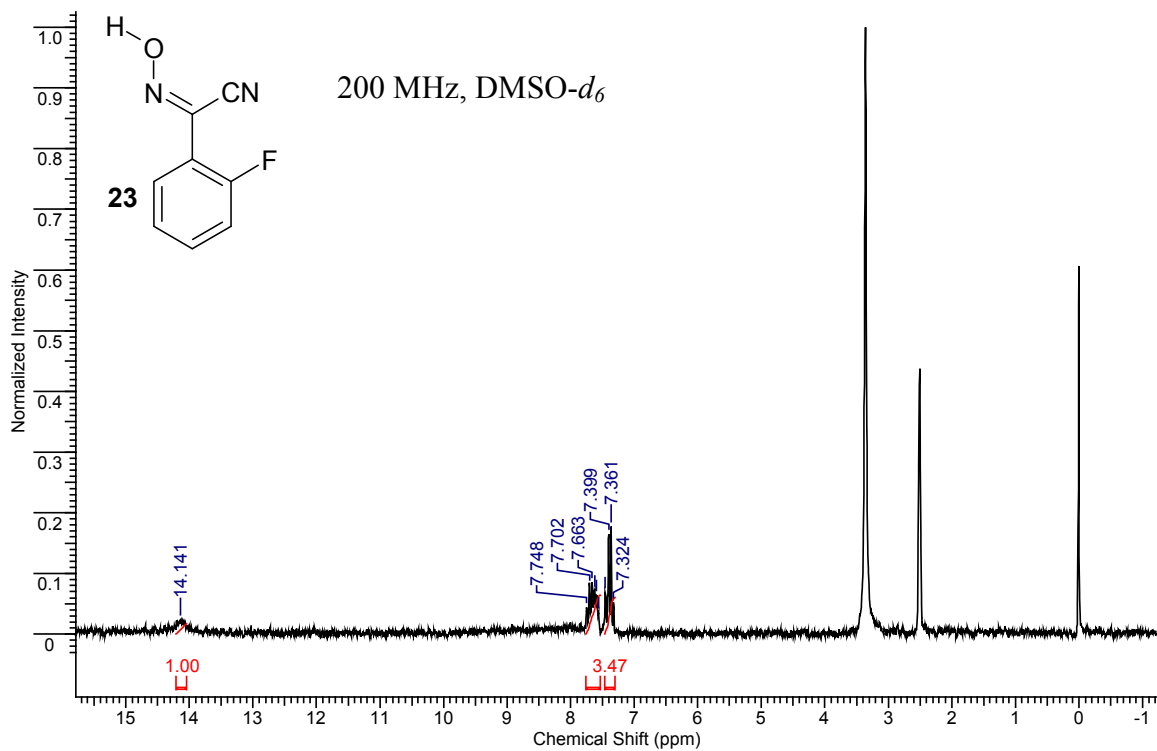
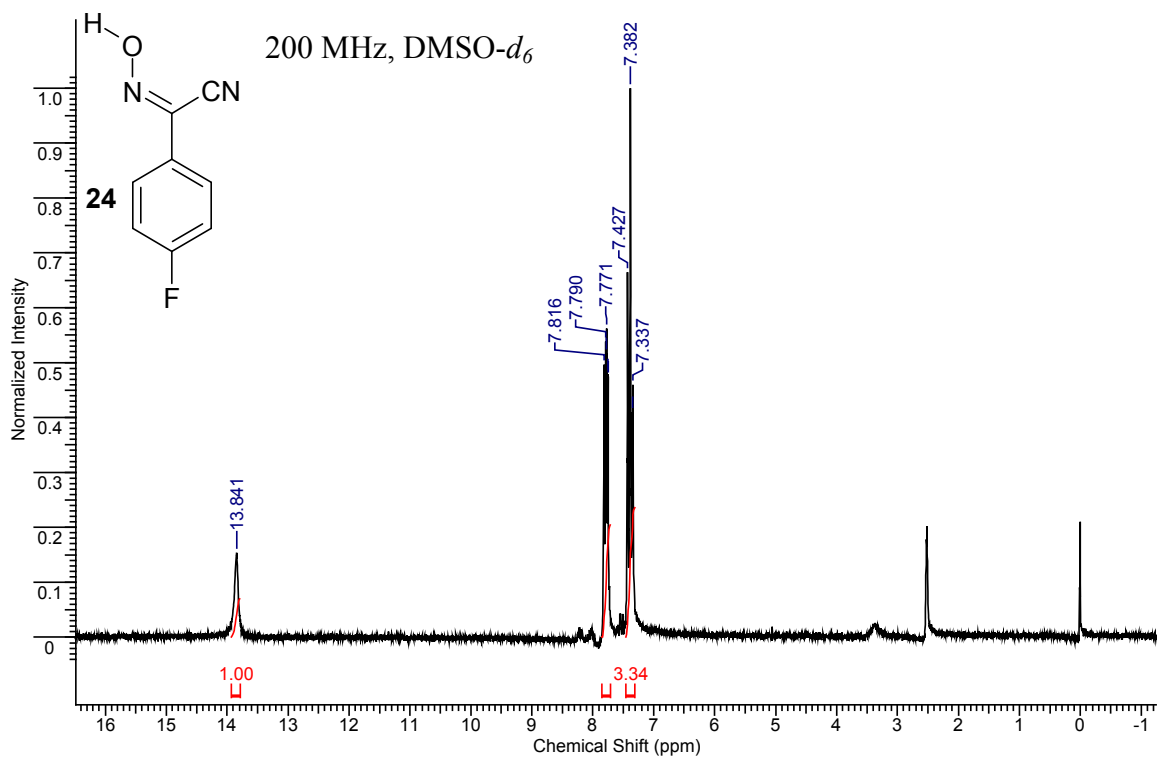


Figure A.22  $^1\text{H}$  NMR of **22**





**Figure A.23** <sup>1</sup>H NMR of **23**



**Figure A.24** <sup>1</sup>H NMR of **24**

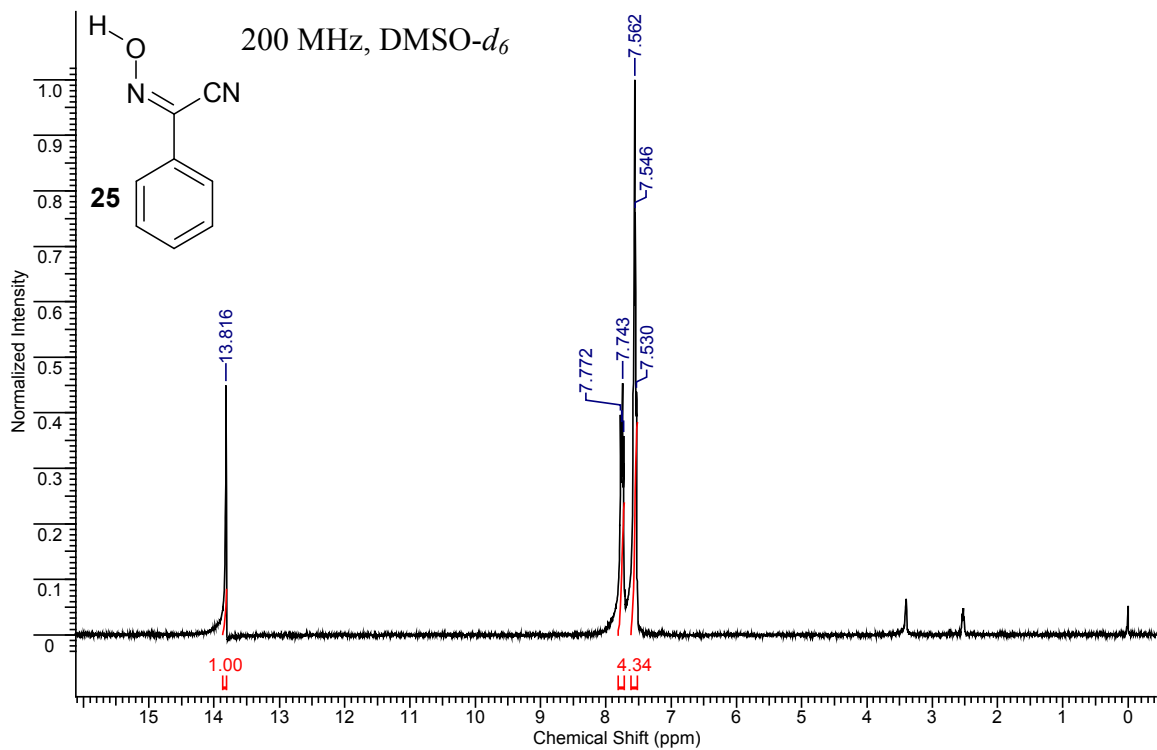


Figure A.25 <sup>1</sup>H NMR of **25**

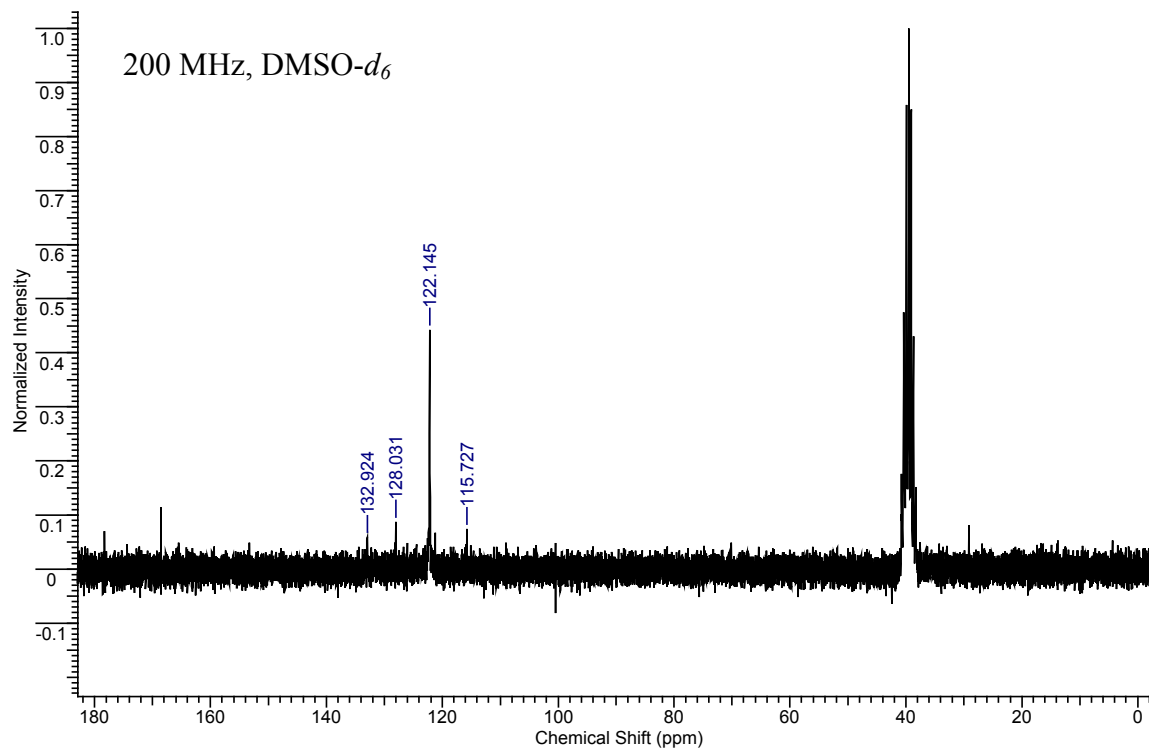
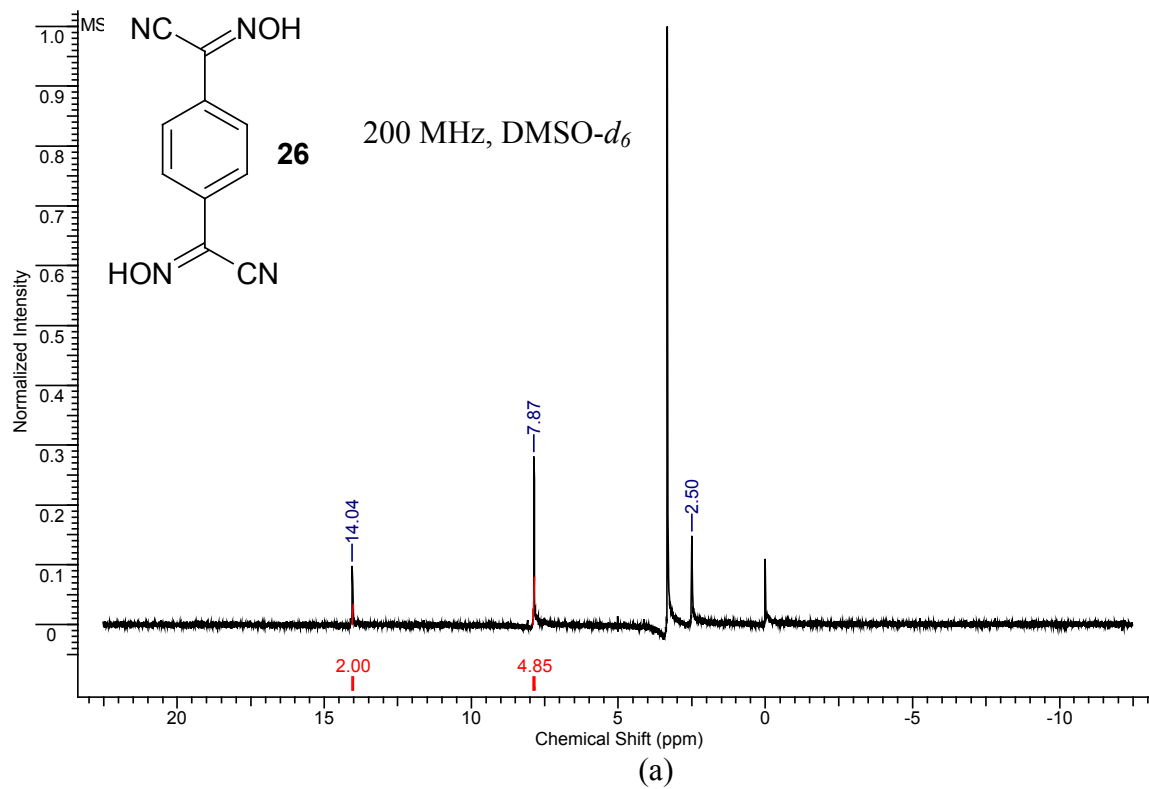
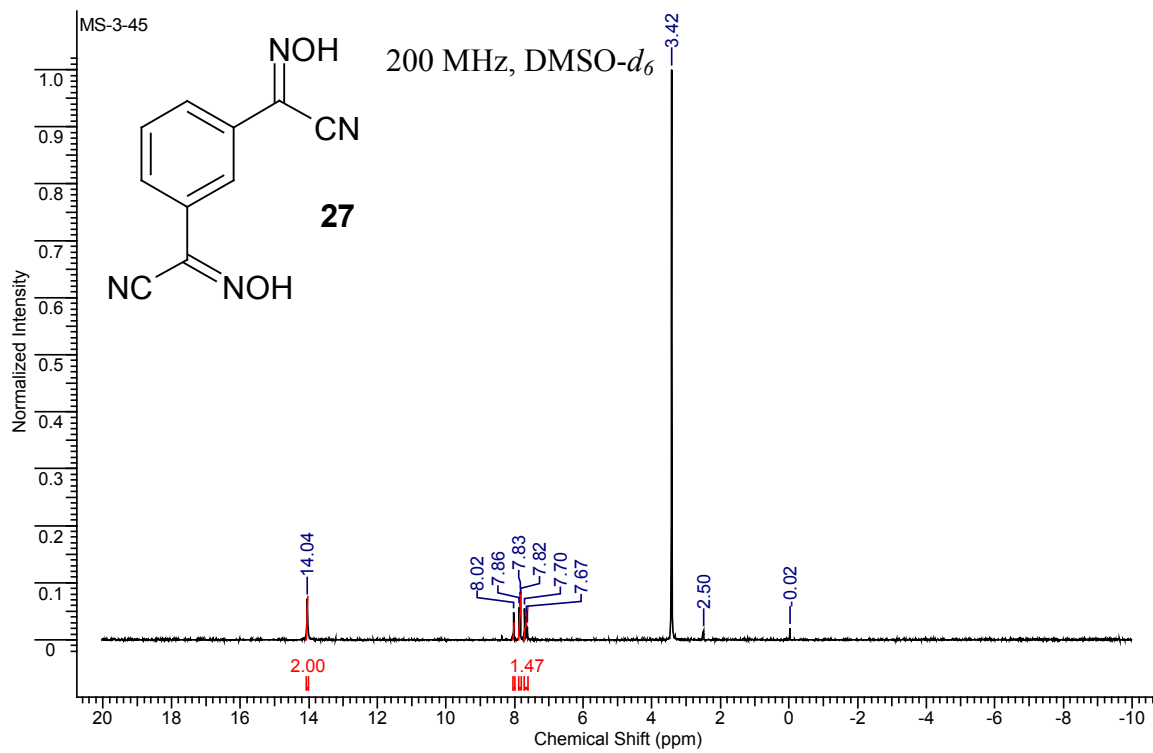
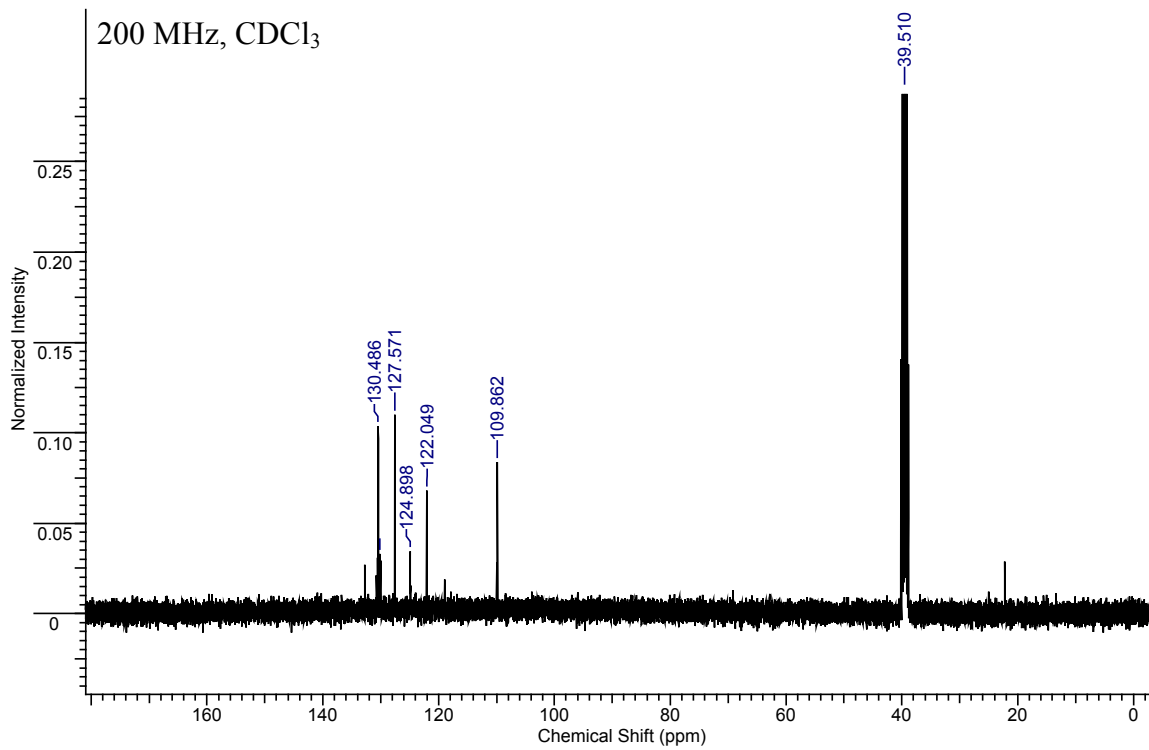


Figure A.26 (a) <sup>1</sup>H and (b) <sup>13</sup>C NMR of 26



(a)



(b)

Figure A.27 (a)  $^1\text{H}$  and (b)  $^{13}\text{C}$  NMR of 27

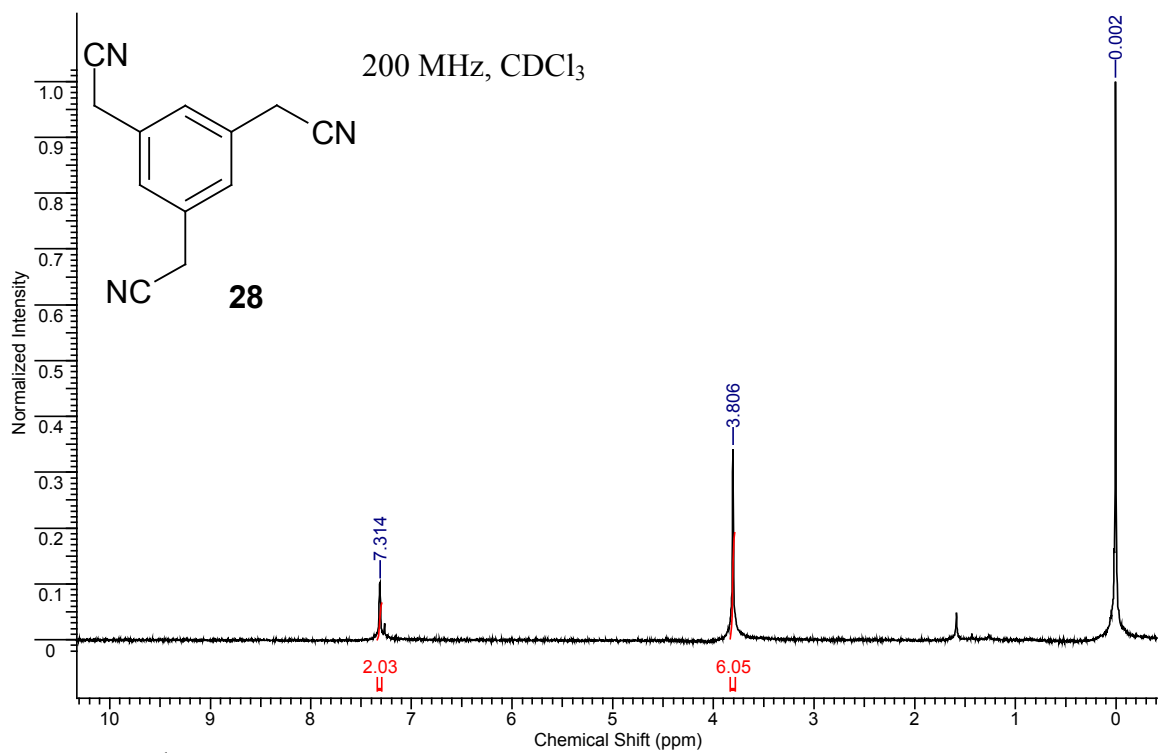
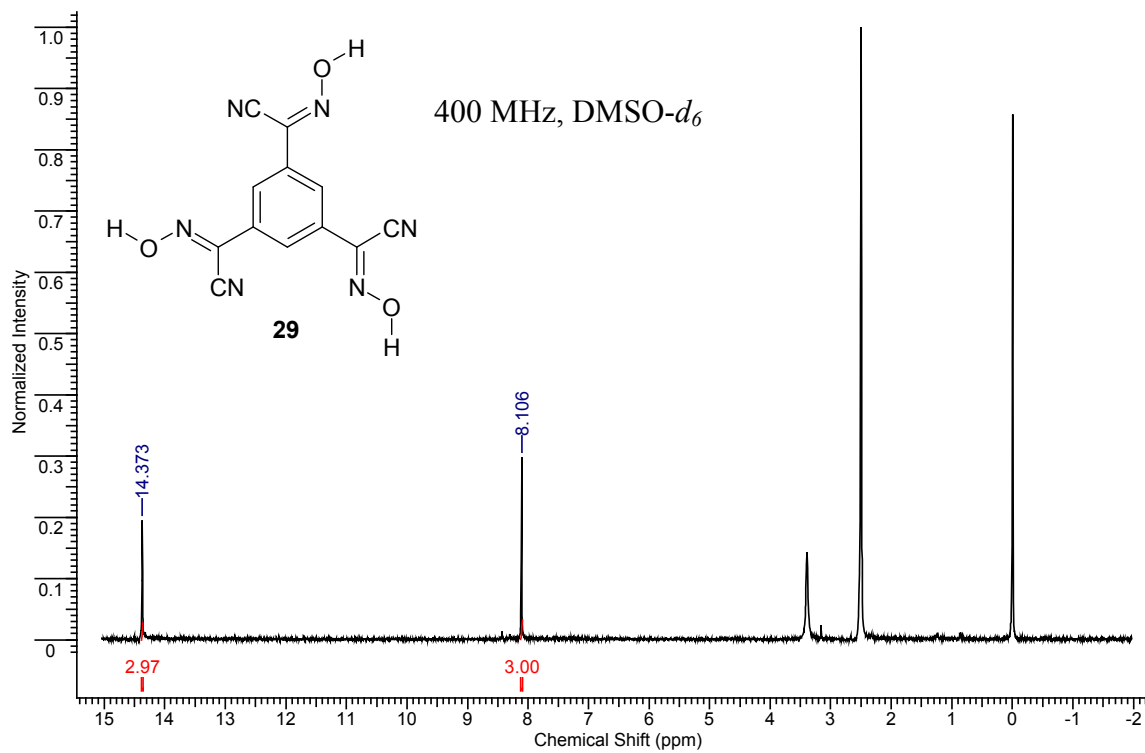
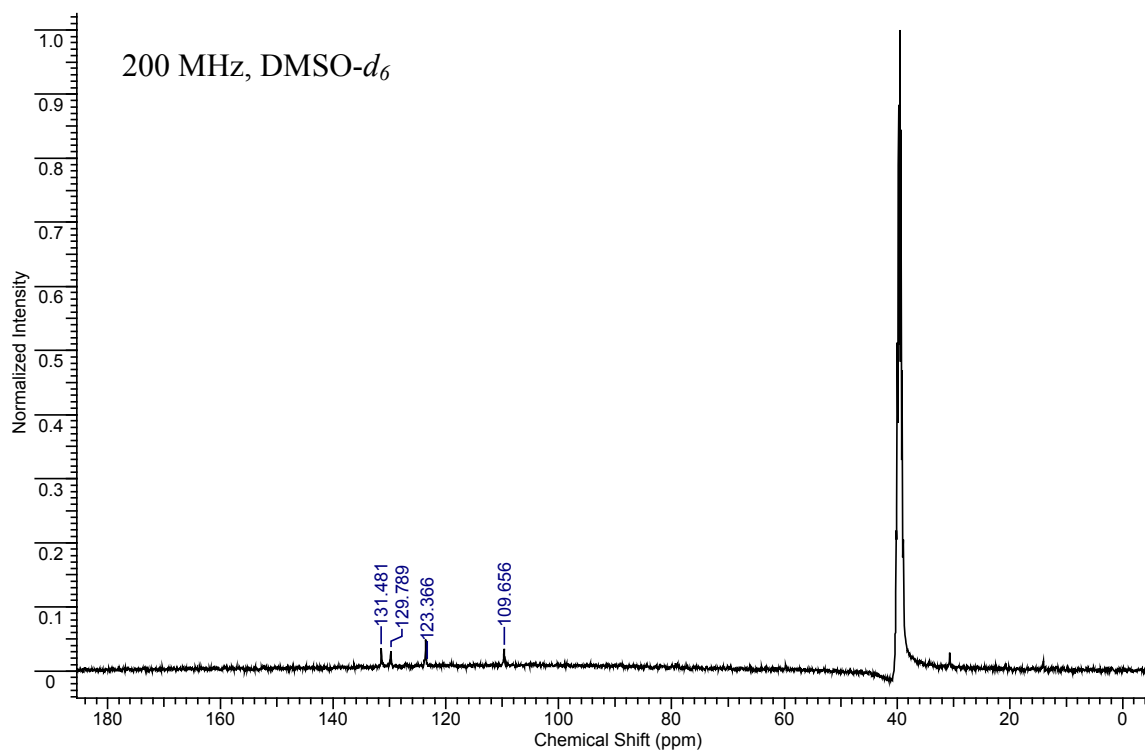


Figure A.28 <sup>1</sup>H NMR of **28**

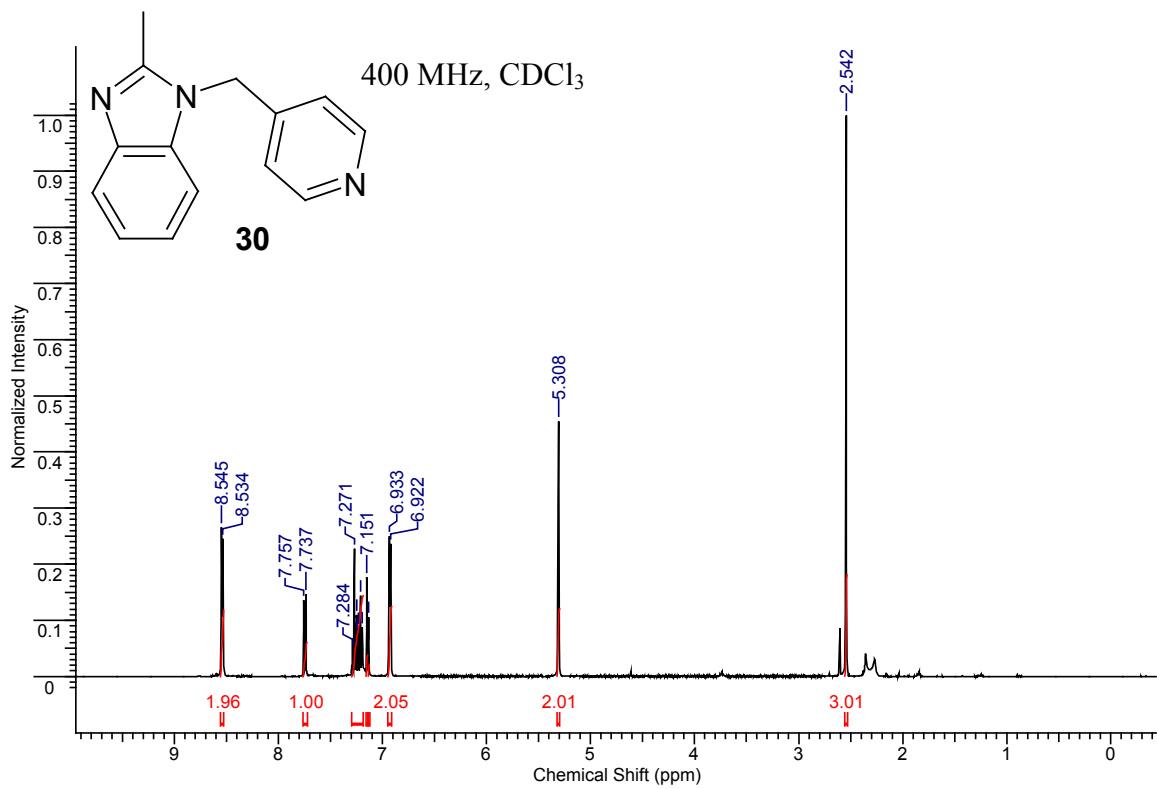


(a)

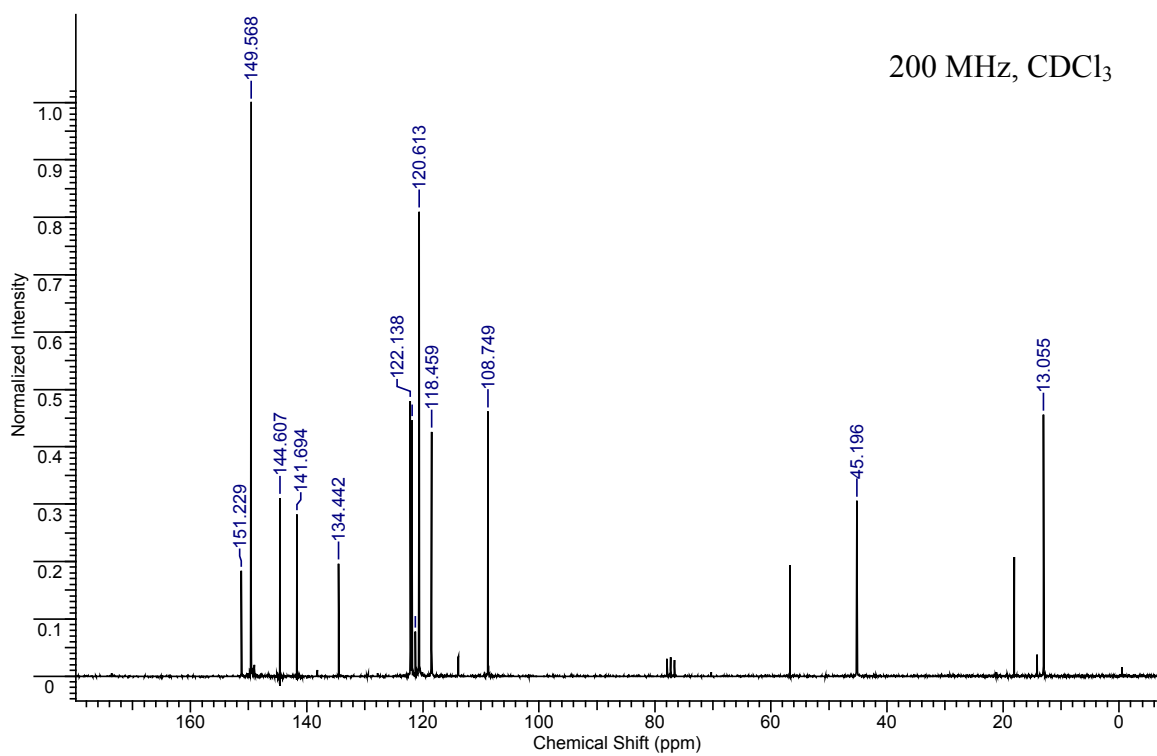


(b)

**Figure A.29** (a) <sup>1</sup>H and (b) <sup>13</sup>C NMR of **29**



(a)



(b)

**Figure A.30** (a) <sup>1</sup>H and (b) <sup>13</sup>C NMR of **30**

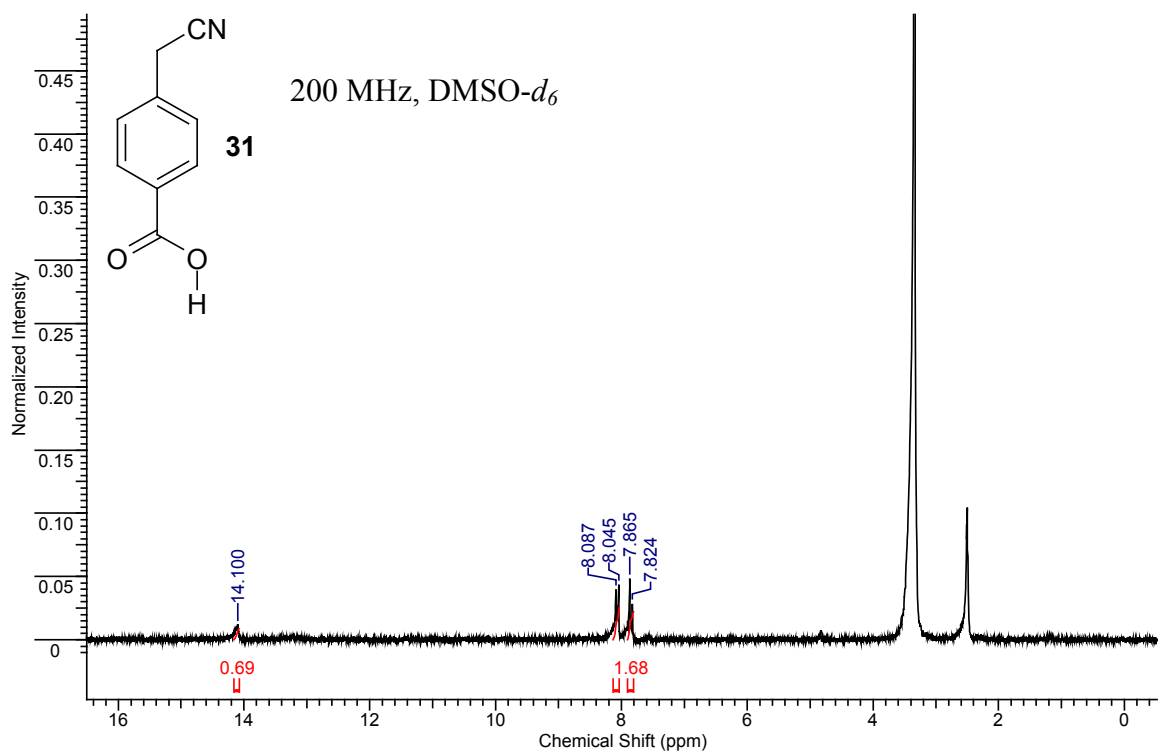
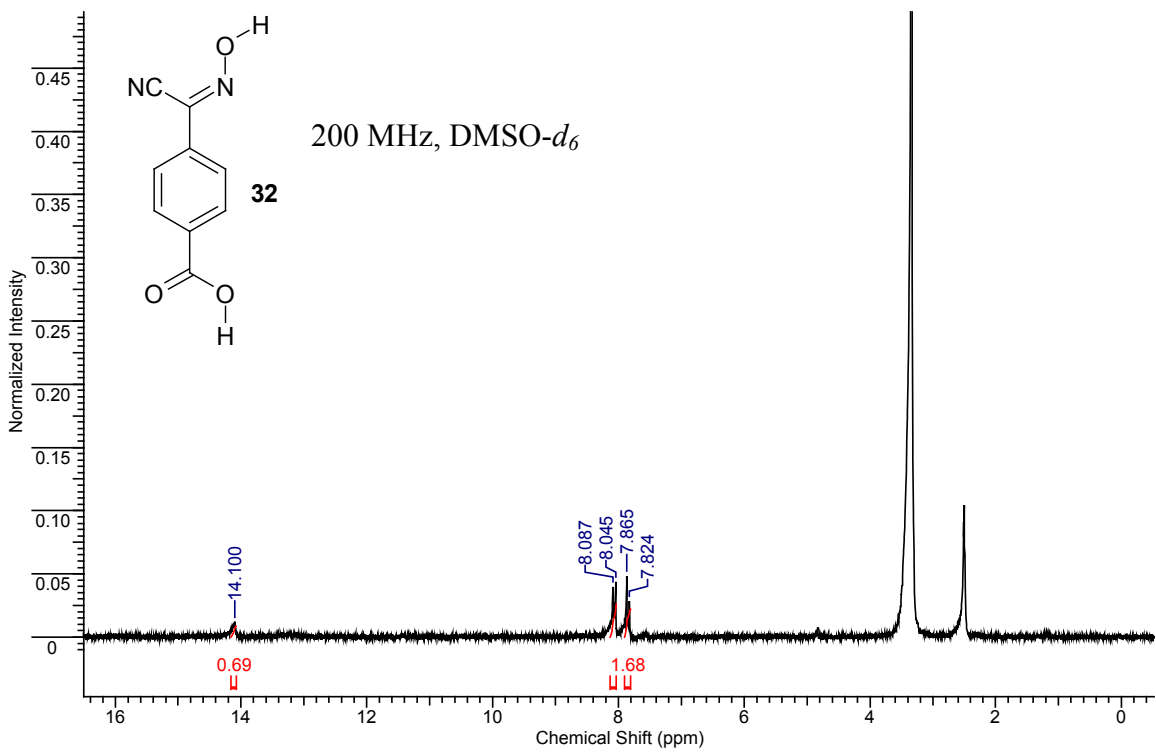
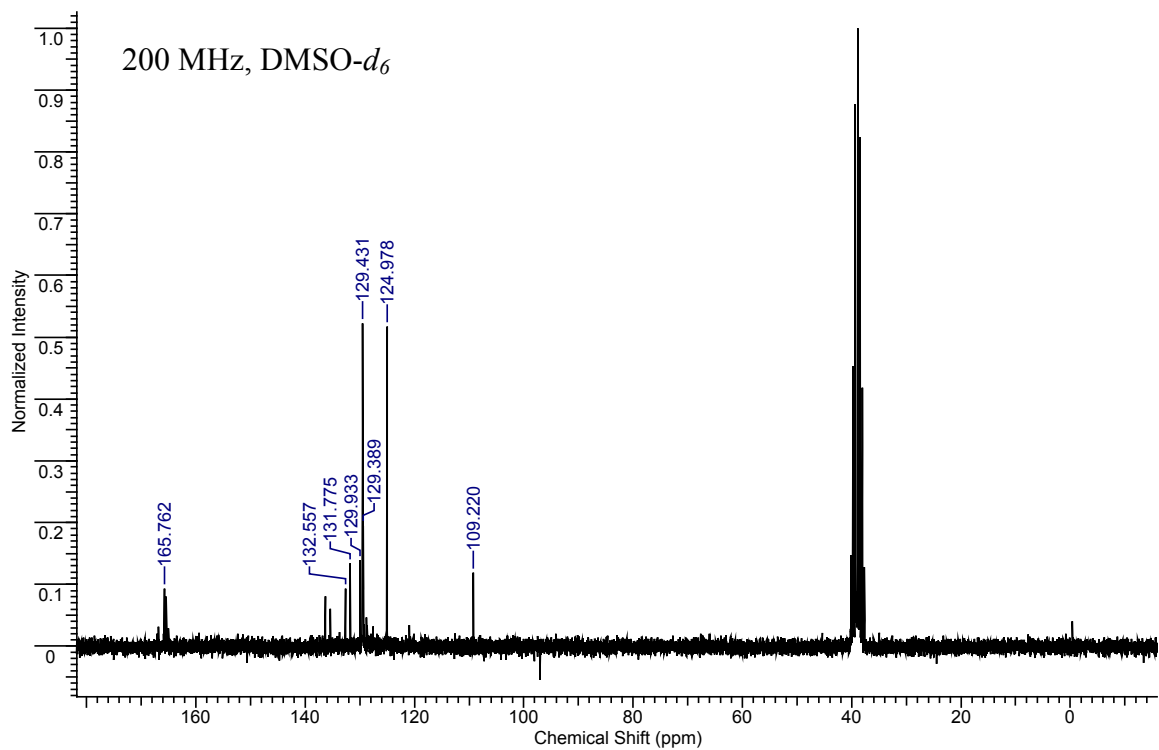


Figure A.31  $^1\text{H}$  NMR of 31





(a)



(b)

**Figure A.32** (a) <sup>1</sup>H and (b) <sup>13</sup>C NMR of **32**

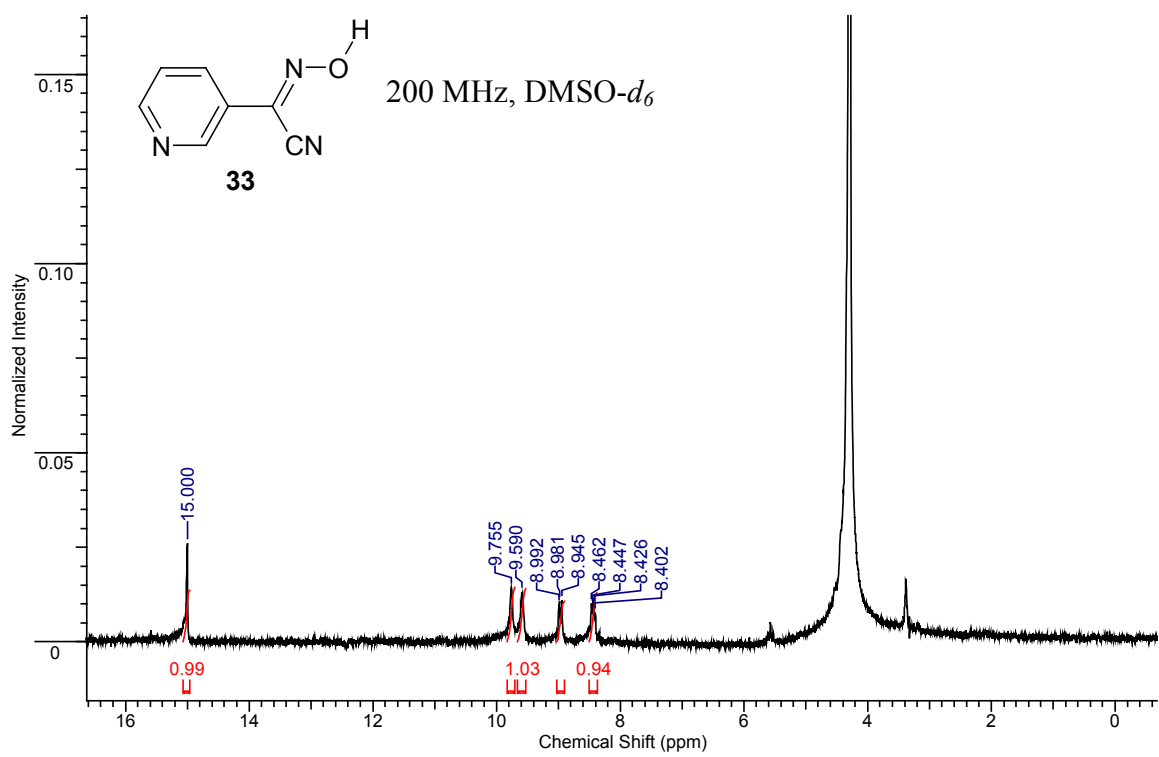


Figure A.33 <sup>1</sup>H NMR of **33**

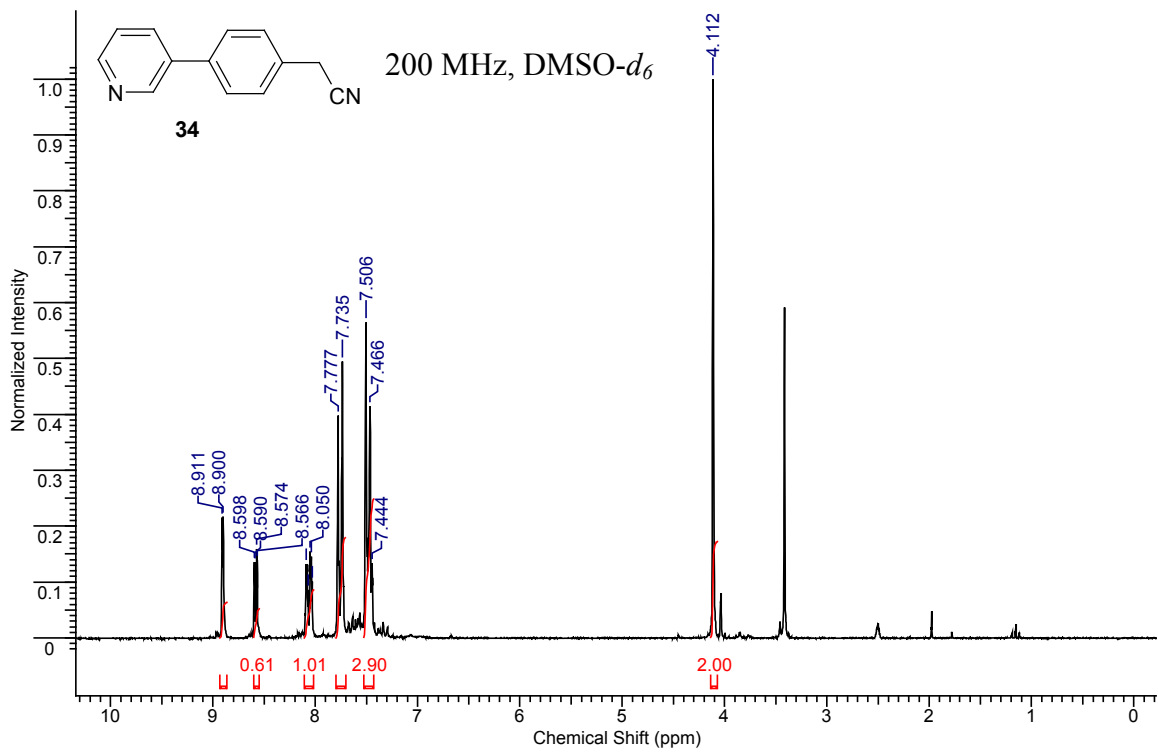


Figure A.34 (a) <sup>1</sup>H NMR of **34**

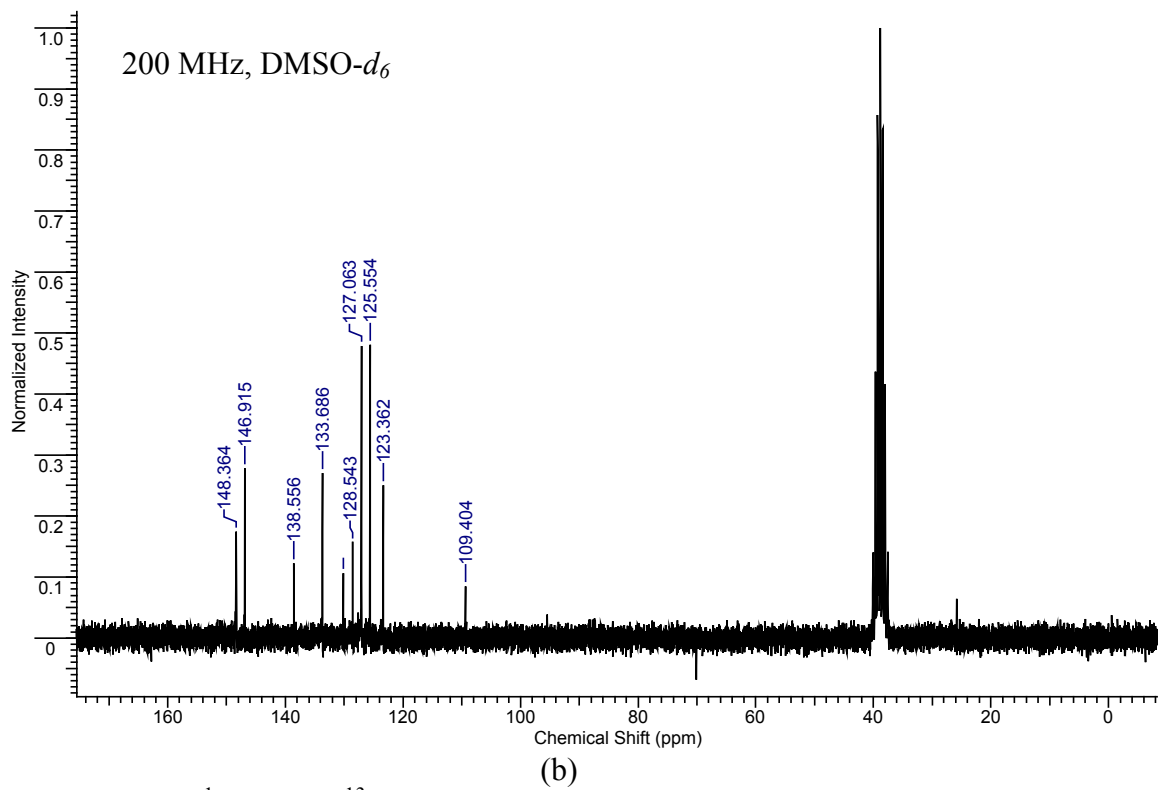
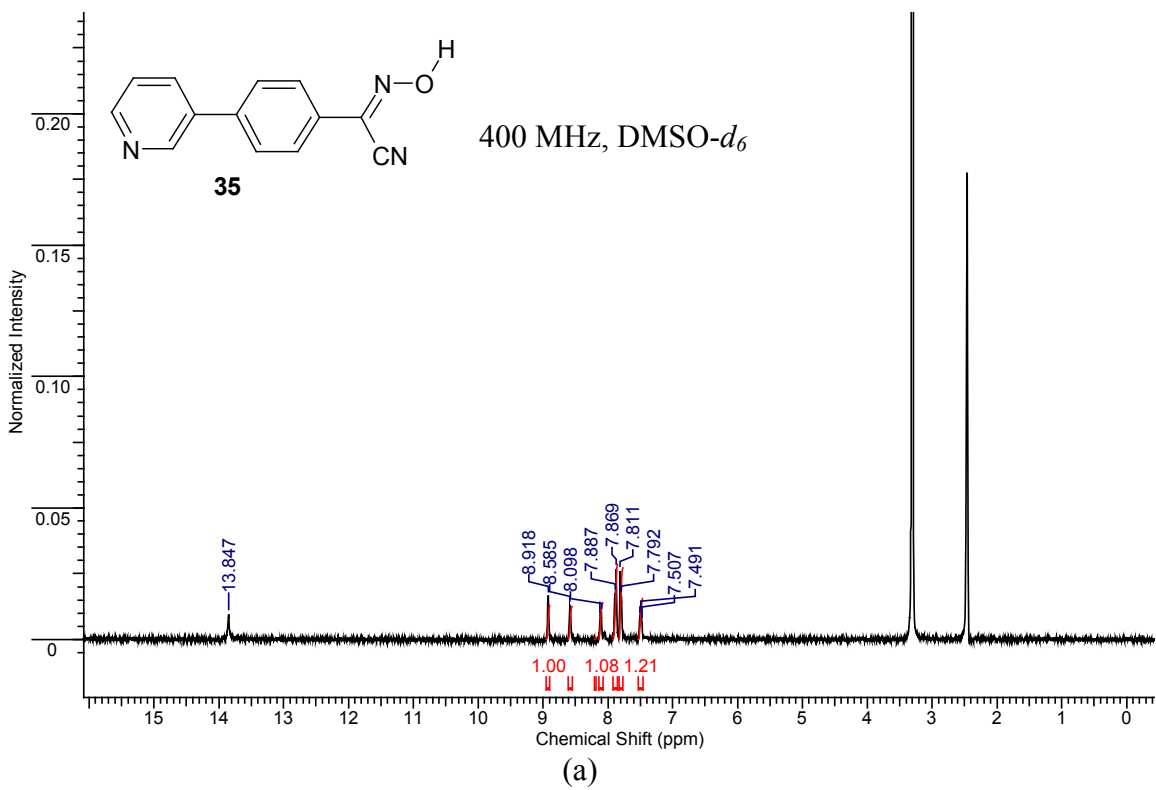


Figure A.35 (a) <sup>1</sup>H and (b) <sup>13</sup>C NMR of 35

## Appendix B - Crystal Data and Structure Refinements

**Table B.1** Crystal data and structure refinement for **2**

Empirical formula	C <sub>15</sub> H <sub>13</sub> N <sub>3</sub> O	
Formula weight	251.28	
Temperature	100(2) K	
Wavelength	0.71073 Å	
Crystal system	Monoclinic	
Space group	P2(1)/c	
Unit cell dimensions	a = 8.1547(6) Å	α = 90°.
	b = 21.7538(17) Å	β = 113.330(2)°.
	c = 7.2899(6) Å	γ = 90°.
Volume	1187.46(16) Å <sup>3</sup>	
Z	4	
Density (calculated)	1.406 g/cm <sup>3</sup>	
Absorption coefficient	0.092 mm <sup>-1</sup>	
F(000)	528	
Crystal size	0.18 x 0.19 x 0.33 mm <sup>3</sup>	
Theta range for data collection	1.87 to 30.15°.	
Index ranges	-10 ≤ h ≤ 11, -30 ≤ k ≤ 30, -10 ≤ l ≤ 10	
Reflections collected	13675	
Independent reflections	3492 [R(int) = 0.0257]	
Completeness to theta = 30.15°	99.4 %	
Absorption correction	Semi-empirical from equivalents	
Max. and min. transmission	1.00 and 0.83	
Refinement method	Full-matrix least-squares on F <sup>2</sup>	
Data / restraints / parameters	3492 / 23 / 208	
Goodness-of-fit on F <sup>2</sup>	1.157	
Final R indices [I > 2σ(I)]	R1 = 0.0554, wR2 = 0.1445	
R indices (all data)	R1 = 0.0612, wR2 = 0.1496	
Largest diff. peak and hole	0.549 and -0.180 e.Å <sup>-3</sup>	

**Table B.2** Crystal data and structure refinement for **2a**

Empirical formula	C <sub>29</sub> H <sub>23</sub> N <sub>5</sub> O <sub>9</sub>	
Formula weight	585.52	
Temperature	100(2) K	
Wavelength	0.71073 Å	
Crystal system	Monoclinic	
Space group	P2(1)/c	
Unit cell dimensions	a = 11.6977(5) Å	α = 90°.
	b = 20.0865(9) Å	β = 100.4580(10)°.
	c = 11.3232(5) Å	γ = 90°.
Volume	2616.4(2) Å <sup>3</sup>	
Z	4	
Density (calculated)	1.486 g/cm <sup>3</sup>	
Absorption coefficient	0.113 mm <sup>-1</sup>	
F(000)	1216	
Crystal size	0.27 x 0.31 x 0.34 mm <sup>3</sup>	
Theta range for data collection	1.77 to 30.03°.	
Index ranges	-13 ≤ h ≤ 16, -28 ≤ k ≤ 28, -15 ≤ l ≤ 15	
Reflections collected	27799	
Independent reflections	7640 [R(int) = 0.0285]	
Completeness to theta = 30.03°	99.9 %	
Absorption correction	None	
Refinement method	Full-matrix least-squares on F <sup>2</sup>	
Data / restraints / parameters	7640 / 0 / 400	
Goodness-of-fit on F <sup>2</sup>	1.053	
Final R indices [I > 2σ(I)]	R1 = 0.0495, wR2 = 0.1229	
R indices (all data)	R1 = 0.0576, wR2 = 0.1285	
Largest diff. peak and hole	0.532 and -0.437 e.Å <sup>-3</sup>	

**Table B.3** Crystal data and structure refinement for **2b**

Empirical formula	C <sub>22</sub> H <sub>17</sub> N <sub>5</sub> O <sub>7</sub>	
Formula weight	463.41	
Temperature	173(2) K	
Wavelength	0.71073 Å	
Crystal system	Monoclinic	
Space group	P2(1)/c	
Unit cell dimensions	a = 7.4415(7) Å	α = 90°.
	b = 7.5645(6) Å	β = 90.945(5)°.
	c = 36.589(3) Å	γ = 90°.
Volume	2059.4(3) Å <sup>3</sup>	
Z	4	
Density (calculated)	1.495 g/cm <sup>3</sup>	
Absorption coefficient	0.114 mm <sup>-1</sup>	
F(000)	960	
Crystal size	0.40 x 0.30 x 0.15 mm <sup>3</sup>	
Theta range for data collection	2.23 to 28.25°.	
Index ranges	-9 ≤ h ≤ 9, -10 ≤ k ≤ 9, -46 ≤ l ≤ 48	
Reflections collected	13605	
Independent reflections	4718 [R(int) = 0.0879]	
Completeness to theta = 28.25°	92.8 %	
Absorption correction	None	
Refinement method	Full-matrix least-squares on F <sup>2</sup>	
Data / restraints / parameters	4718 / 0 / 317	
Goodness-of-fit on F <sup>2</sup>	0.917	
Final R indices [I > 2σ(I)]	R1 = 0.0590, wR2 = 0.1409	
R indices (all data)	R1 = 0.1059, wR2 = 0.1586	
Extinction coefficient	0.020(2)	
Largest diff. peak and hole	0.398 and -0.291 e.Å <sup>-3</sup>	

**Table B.4** Crystal data and structure refinement for **4a**

Empirical formula	C <sub>24</sub> H <sub>21</sub> Cl <sub>2</sub> N <sub>3</sub> O <sub>3</sub>
Formula weight	470.34
Temperature	173(2) K
Wavelength	0.71073 Å
Crystal system	Monoclinic
Space group	P2(1)/n
Unit cell dimensions	a = 10.019(6) Å      α = 90°. b = 16.911(11) Å     β = 108.69(4)°. c = 14.182(9) Å      γ = 90°.
Volume	2276(2) Å <sup>3</sup>
Z	4
Density (calculated)	1.372 Mg/m <sup>3</sup>
Absorption coefficient	0.317 mm <sup>-1</sup>
F(000)	976
Crystal size	0.40 x 0.30 x 0.20 mm <sup>3</sup>
Theta range for data collection	1.94 to 27.41°.
Index ranges	-12 ≤ h ≤ 12, -18 ≤ k ≤ 18, -14 ≤ l ≤ 15
Reflections collected	8407
Independent reflections	4029 [R(int) = 0.0863]
Completeness to theta = 27.41°	77.7 %
Absorption correction	None
Refinement method	Full-matrix least-squares on F <sup>2</sup>
Data / restraints / parameters	4029 / 78 / 381
Goodness-of-fit on F <sup>2</sup>	1.097
Final R indices [I > 2σ(I)]	R1 = 0.0635, wR2 = 0.1732
R indices (all data)	R1 = 0.1040, wR2 = 0.2100
Largest diff. peak and hole	0.387 and -0.283 e.Å <sup>-3</sup>



**Table B.5** Crystal data and structure refinement for **6**

Empirical formula	C <sub>17</sub> H <sub>17</sub> N <sub>3</sub> O	
Formula weight	279.34	
Temperature	100(2) K	
Wavelength	0.71073 Å	
Crystal system	Triclinic	
Space group	P-1	
Unit cell dimensions	a = 10.2537(14) Å	α = 96.951(2)°.
	b = 12.1056(15) Å	β = 107.314(3)°.
	c = 12.3112(17) Å	γ = 98.436(3)°.
Volume	1421.0(3) Å <sup>3</sup>	
Z	4	
Density (calculated)	1.306 g/cm <sup>3</sup>	
Absorption coefficient	0.084 mm <sup>-1</sup>	
F(000)	592	
Crystal size	0.64 x 0.32 x 0.07 mm <sup>3</sup>	
Theta range for data collection	1.76 to 25.72°.	
Index ranges	-11 ≤ h ≤ 12, -14 ≤ k ≤ 14, -14 ≤ l ≤ 14	
Reflections collected	13294	
Independent reflections	3877 [R(int) = 0.1734]	
Completeness to theta = 25.72°	71.6 %	
Absorption correction	None	
Refinement method	Full-matrix least-squares on F <sup>2</sup>	
Data / restraints / parameters	3877 / 0 / 391	
Goodness-of-fit on F <sup>2</sup>	1.117	
Final R indices [I > 2σ(I)]	R1 = 0.0717, wR2 = 0.1681	
R indices (all data)	R1 = 0.0852, wR2 = 0.1763	
Largest diff. peak and hole	0.272 and -0.219 e.Å <sup>-3</sup>	

**Table B.6** Crystal data and structure refinement for **6a**

Empirical formula	C <sub>29</sub> H <sub>33</sub> N <sub>3</sub> O <sub>3</sub>	
Formula weight	471.58	
Temperature	100(2) K	
Wavelength	0.71073 Å	
Crystal system	Triclinic	
Space group	P-1	
Unit cell dimensions	a = 8.8538(8) Å	α = 110.7010(10)°.
	b = 11.5743(11) Å	β = 100.6800(10)°.
	c = 13.0813(12) Å	γ = 90.0370(10)°.
Volume	1229.1(2) Å <sup>3</sup>	
Z	2	
Density (calculated)	1.274 g/cm <sup>3</sup>	
Absorption coefficient	0.083 mm <sup>-1</sup>	
F(000)	504	
Crystal size	0.24 x 0.26 x 0.36 mm <sup>3</sup>	
Theta range for data collection	1.70 to 28.31°.	
Index ranges	-11 ≤ h ≤ 11, -14 ≤ k ≤ 15, -17 ≤ l ≤ 17	
Reflections collected	14697	
Independent reflections	5827 [R(int) = 0.0224]	
Completeness to theta = 28.31°	95.3 %	
Absorption correction	None	
Refinement method	Full-matrix least-squares on F <sup>2</sup>	
Data / restraints / parameters	5827 / 0 / 332	
Goodness-of-fit on F <sup>2</sup>	1.056	
Final R indices [I > 2σ(I)]	R1 = 0.0442, wR2 = 0.1142	
R indices (all data)	R1 = 0.0531, wR2 = 0.1198	
Largest diff. peak and hole	0.352 and -0.305 e.Å <sup>-3</sup>	

**Table B.7** Crystal data and structure refinement for **6b**

Empirical formula	C <sub>24</sub> H <sub>21</sub> N <sub>5</sub> O <sub>7</sub>	
Formula weight	491.46	
Temperature	173(2) K	
Wavelength	0.71073 Å	
Crystal system	Triclinic	
Space group	P-1	
Unit cell dimensions	a = 8.3134(6) Å	$\alpha = 77.357(3)^\circ$ .
	b = 9.9033(7) Å	$\beta = 85.484(4)^\circ$ .
	c = 13.8546(10) Å	$\gamma = 82.623(5)^\circ$ .
Volume	1102.27(14) Å <sup>3</sup>	
Z	2	
Density (calculated)	1.481 g/cm <sup>3</sup>	
Absorption coefficient	0.112 mm <sup>-1</sup>	
F(000)	512	
Crystal size	0.40 x 0.35 x 0.20 mm <sup>3</sup>	
Theta range for data collection	1.51 to 27.91°.	
Index ranges	-10 ≤ h ≤ 10, -12 ≤ k ≤ 12, -17 ≤ l ≤ 18	
Reflections collected	8221	
Independent reflections	4875 [R(int) = 0.1169]	
Completeness to theta = 27.91°	92.7 %	
Absorption correction	None	
Refinement method	Full-matrix least-squares on F <sup>2</sup>	
Data / restraints / parameters	4875 / 0 / 324	
Goodness-of-fit on F <sup>2</sup>	1.656	
Final R indices [I > 2σ(I)]	R1 = 0.0885, wR2 = 0.2351	
R indices (all data)	R1 = 0.1092, wR2 = 0.2575	
Extinction coefficient	0.051(11)	
Largest diff. peak and hole	0.498 and -0.610 e.Å <sup>-3</sup>	

**Table B.8** Crystal data and structure refinement for **11**

Empirical formula	C <sub>15</sub> H <sub>15</sub> N <sub>3</sub>	
Formula weight	237.30	
Temperature	100(2) K	
Wavelength	0.71073 Å	
Crystal system	Monoclinic	
Space group	P2(1)/n	
Unit cell dimensions	a = 13.764(2) Å	α = 90°.
	b = 6.2206(9) Å	β = 114.322(2)°.
	c = 15.440(2) Å	γ = 90°.
Volume	1204.7(3) Å <sup>3</sup>	
Z	4	
Density (calculated)	1.308 g/cm <sup>3</sup>	
Absorption coefficient	0.080 mm <sup>-1</sup>	
F(000)	504	
Crystal size	0.41 x 0.18 x 0.10 mm <sup>3</sup>	
Theta range for data collection	2.58 to 30.20°.	
Index ranges	-19 ≤ h ≤ 19, -8 ≤ k ≤ 8, -21 ≤ l ≤ 21	
Reflections collected	13122	
Independent reflections	3540 [R(int) = 0.1251]	
Completeness to theta = 30.20°	99.0 %	
Absorption correction	None	
Refinement method	Full-matrix least-squares on F <sup>2</sup>	
Data / restraints / parameters	3540 / 0 / 163	
Goodness-of-fit on F <sup>2</sup>	1.880	
Final R indices [I > 2σ(I)]	R1 = 0.0999, wR2 = 0.2486	
R indices (all data)	R1 = 0.1047, wR2 = 0.2510	
Largest diff. peak and hole	0.697 and -0.315 e.Å <sup>-3</sup>	

**Table B.9** Crystal data and structure refinement for **11a**

Empirical formula	C <sub>22</sub> H <sub>20</sub> Cl N <sub>3</sub> O <sub>2</sub>	
Formula weight	393.86	
Temperature	173(2) K	
Wavelength	0.71073 Å	
Crystal system	Triclinic	
Space group	P-1	
Unit cell dimensions	a = 6.7039(12) Å	α = 93.953(9)°.
	b = 10.2655(15) Å	β = 100.603(9)°.
	c = 14.468(2) Å	γ = 104.917(12)°.
Volume	938.6(3) Å <sup>3</sup>	
Z	2	
Density (calculated)	1.394 g/cm <sup>3</sup>	
Absorption coefficient	0.227 mm <sup>-1</sup>	
F(000)	412	
Crystal size	0.40 x 0.25 x 0.15 mm <sup>3</sup>	
Theta range for data collection	1.44 to 28.20°.	
Index ranges	-8 ≤ h ≤ 8, -12 ≤ k ≤ 13, -18 ≤ l ≤ 16	
Reflections collected	6738	
Independent reflections	4148 [R(int) = 0.0605]	
Completeness to theta = 28.20°	90.0 %	
Absorption correction	None	
Refinement method	Full-matrix least-squares on F <sup>2</sup>	
Data / restraints / parameters	4148 / 0 / 258	
Goodness-of-fit on F <sup>2</sup>	0.905	
Final R indices [I > 2σ(I)]	R1 = 0.0482, wR2 = 0.1157	
R indices (all data)	R1 = 0.0787, wR2 = 0.1281	
Largest diff. peak and hole	0.229 and -0.424 e.Å <sup>-3</sup>	

**Table B.10** Crystal data and structure refinement for **11b**

Empirical formula	C <sub>22</sub> H <sub>16</sub> F <sub>5</sub> N <sub>3</sub> O <sub>2</sub>	
Formula weight	449.38	
Temperature	120(2) K	
Wavelength	0.71073 Å	
Crystal system	Triclinic	
Space group	P-1	
Unit cell dimensions	a = 8.6933(6) Å	α = 70.154(3)°.
	b = 10.6404(7) Å	β = 81.042(3)°.
	c = 12.3254(9) Å	γ = 66.511(3)°.
Volume	983.25(12) Å <sup>3</sup>	
Z	2	
Density (calculated)	1.518 g/cm <sup>3</sup>	
Absorption coefficient	0.131 mm <sup>-1</sup>	
F(000)	460	
Crystal size	0.30 x 0.25 x 0.12 mm <sup>3</sup>	
Theta range for data collection	1.76 to 31.48°.	
Index ranges	-12 ≤ h ≤ 12, -15 ≤ k ≤ 15, -18 ≤ l ≤ 18	
Reflections collected	27019	
Independent reflections	6539 [R(int) = 0.0320]	
Completeness to theta = 31.48°	99.9 %	
Absorption correction	None	
Max. and min. transmission	0.9844 and 0.9617	
Refinement method	Full-matrix least-squares on F <sup>2</sup>	
Data / restraints / parameters	6539 / 0 / 294	
Goodness-of-fit on F <sup>2</sup>	1.059	
Final R indices [I > 2σ(I)]	R1 = 0.0468, wR2 = 0.1223	
R indices (all data)	R1 = 0.0644, wR2 = 0.1337	
Largest diff. peak and hole	0.387 and -0.418 e.Å <sup>-3</sup>	

**Table B.11** Crystal data and structure refinement for **11c**

Empirical formula	C <sub>19</sub> H <sub>21</sub> N <sub>3</sub> O <sub>5</sub>	
Formula weight	371.39	
Temperature	173(2) K	
Wavelength	0.71073 Å	
Crystal system	Triclinic	
Space group	P-1	
Unit cell dimensions	a = 4.2070(5) Å	α = 75.820(6)°.
	b = 10.5835(10) Å	β = 87.237(8)°.
	c = 20.653(2) Å	γ = 82.454(7)°.
Volume	883.70(17) Å <sup>3</sup>	
Z	2	
Density (calculated)	1.396 g/cm <sup>3</sup>	
Absorption coefficient	0.103 mm <sup>-1</sup>	
F(000)	392	
Crystal size	0.40 x 0.25 x 0.15 mm <sup>3</sup>	
Theta range for data collection	2.00 to 27.90°.	
Index ranges	-5 ≤ h ≤ 5, -13 ≤ k ≤ 13, -26 ≤ l ≤ 26	
Reflections collected	5937	
Independent reflections	3839 [R(int) = 0.1205]	
Completeness to theta = 27.90°	90.4 %	
Absorption correction	None	
Refinement method	Full-matrix least-squares on F <sup>2</sup>	
Data / restraints / parameters	3839 / 3 / 258	
Goodness-of-fit on F <sup>2</sup>	1.024	
Final R indices [I > 2σ(I)]	R1 = 0.0783, wR2 = 0.1918	
R indices (all data)	R1 = 0.1232, wR2 = 0.2139	
Extinction coefficient	0.099(13)	
Largest diff. peak and hole	0.506 and -0.398 e.Å <sup>-3</sup>	

**Table B.12** Crystal data and structure refinement for **11d**

Empirical formula	C <sub>39</sub> H <sub>47</sub> N <sub>3</sub> O <sub>4</sub>	
Formula weight	621.80	
Temperature	173(2) K	
Wavelength	0.71073 Å	
Crystal system	Triclinic	
Space group	P-1	
Unit cell dimensions	a = 9.0869(8) Å	α = 89.386(2)°.
	b = 11.0230(10) Å	β = 76.906(2)°.
	c = 18.4576(17) Å	γ = 71.067(2)°.
Volume	1699.4(3) Å <sup>3</sup>	
Z	2	
Density (calculated)	1.215 Mg/m <sup>3</sup>	
Absorption coefficient	0.078 mm <sup>-1</sup>	
F(000)	668	
Crystal size	0.26 x 0.41 x 0.50 mm <sup>3</sup>	
Theta range for data collection	1.96 to 30.10°.	
Index ranges	-12 ≤ h ≤ 12, -15 ≤ k ≤ 14, -25 ≤ l ≤ 25	
Reflections collected	17979	
Independent reflections	9707 [R(int) = 0.0291]	
Completeness to theta = 30.10°	96.9 %	
Absorption correction	None	
Refinement method	Full-matrix least-squares on F <sup>2</sup>	
Data / restraints / parameters	9707 / 0 / 433	
Goodness-of-fit on F <sup>2</sup>	1.336	
Final R indices [I > 2σ(I)]	R1 = 0.0577, wR2 = 0.1713	
R indices (all data)	R1 = 0.0632, wR2 = 0.1779	
Largest diff. peak and hole	0.552 and -0.333 e.Å <sup>-3</sup>	



**Table B.13** Crystal data and structure refinement for **11e**

Empirical formula	C <sub>24</sub> H <sub>22</sub> F <sub>4</sub> I N <sub>3</sub> O <sub>3</sub>	
Formula weight	603.35	
Temperature	120(2) K	
Wavelength	0.71073 Å	
Crystal system	Triclinic	
Space group	P-1	
Unit cell dimensions	a = 9.0965(6) Å	α = 83.050(2)°.
	b = 9.4786(6) Å	β = 82.618(2)°.
	c = 15.4097(10) Å	γ = 66.831(2)°.
Volume	1207.75(14) Å <sup>3</sup>	
Z	2	
Density (calculated)	1.659 g/cm <sup>3</sup>	
Absorption coefficient	1.388 mm <sup>-1</sup>	
F(000)	600	
Crystal size	0.25 x 0.20 x 0.15 mm <sup>3</sup>	
Theta range for data collection	2.34 to 30.96°.	
Index ranges	-13 ≤ h ≤ 13, -13 ≤ k ≤ 13, -21 ≤ l ≤ 21	
Reflections collected	31024	
Independent reflections	7305 [R(int) = 0.0247]	
Completeness to theta = 30.96°	95.1 %	
Absorption correction	None	
Max. and min. transmission	0.8188 and 0.7229	
Refinement method	Full-matrix least-squares on F <sup>2</sup>	
Data / restraints / parameters	7305 / 0 / 325	
Goodness-of-fit on F <sup>2</sup>	1.042	
Final R indices [I > 2σ(I)]	R1 = 0.0232, wR2 = 0.0581	
R indices (all data)	R1 = 0.0259, wR2 = 0.0598	
Largest diff. peak and hole	0.972 and -0.593 e.Å <sup>-3</sup>	

**Table B.14** Crystal data and structure refinement for **11f**

Empirical formula	C <sub>29</sub> H <sub>23</sub> N <sub>7</sub> O <sub>12</sub>	
Formula weight	661.54	
Temperature	100(2) K	
Wavelength	0.71073 Å	
Crystal system	Triclinic	
Space group	P-1	
Unit cell dimensions	a = 7.092(2) Å	α = 91.141(5)°.
	b = 7.395(2) Å	β = 93.438(5)°.
	c = 27.826(9) Å	γ = 97.548(5)°.
Volume	1443.4(8) Å <sup>3</sup>	
Z	2	
Density (calculated)	1.522 g/cm <sup>3</sup>	
Absorption coefficient	0.121 mm <sup>-1</sup>	
F(000)	684	
Crystal size	0.37 x 0.24 x 0.01 mm <sup>3</sup>	
Theta range for data collection	1.47 to 28.29°.	
Index ranges	-7 ≤ h ≤ 9, -9 ≤ k ≤ 9, -36 ≤ l ≤ 36	
Reflections collected	10087	
Independent reflections	6402 [R(int) = 0.0562]	
Completeness to theta = 28.29°	89.2 %	
Absorption correction	None	
Refinement method	Full-matrix least-squares on F <sup>2</sup>	
Data / restraints / parameters	6402 / 0 / 431	
Goodness-of-fit on F <sup>2</sup>	2.686	
Final R indices [I > 2σ(I)]	R1 = 0.2140, wR2 = 0.5062	
R indices (all data)	R1 = 0.2614, wR2 = 0.5155	
Largest diff. peak and hole	0.865 and -0.809 e.Å <sup>-3</sup>	

**Table B.15** Crystal data and structure refinement for **11g**

Empirical formula	C <sub>29</sub> H <sub>25</sub> N <sub>5</sub> O <sub>8</sub>	
Formula weight	571.54	
Temperature	173(2) K	
Wavelength	0.71073 Å	
Crystal system	Triclinic	
Space group	P-1	
Unit cell dimensions	a = 8.6831(7) Å	α = 95.958(4)°.
	b = 9.8757(8) Å	β = 96.830(5)°.
	c = 16.9312(13) Å	γ = 110.527(5)°.
Volume	1333.42(18) Å <sup>3</sup>	
Z	2	
Density (calculated)	1.424 g/cm <sup>3</sup>	
Absorption coefficient	0.106 mm <sup>-1</sup>	
F(000)	596	
Crystal size	0.40 x 0.40 x 0.10 mm <sup>3</sup>	
Theta range for data collection	1.23 to 27.87°.	
Index ranges	-11 ≤ h ≤ 10, -12 ≤ k ≤ 12, -22 ≤ l ≤ 22	
Reflections collected	10022	
Independent reflections	5954 [R(int) = 0.0965]	
Completeness to theta = 27.87°	94.1 %	
Absorption correction	None	
Refinement method	Full-matrix least-squares on F <sup>2</sup>	
Data / restraints / parameters	5954 / 0 / 387	
Goodness-of-fit on F <sup>2</sup>	1.004	
Final R indices [I > 2σ(I)]	R1 = 0.0661, wR2 = 0.1683	
R indices (all data)	R1 = 0.1042, wR2 = 0.1919	
Largest diff. peak and hole	0.318 and -0.351 e.Å <sup>-3</sup>	

**Table B.16** Crystal data and structure refinement for **11h**

Empirical formula	C <sub>51</sub> H <sub>45</sub> I <sub>3</sub> N <sub>6</sub> O <sub>6</sub>	
Formula weight	1218.63	
Temperature	100(2) K	
Wavelength	0.71073 Å	
Crystal system	Triclinic	
Space group	P-1	
Unit cell dimensions	a = 6.4635(6) Å	α = 89.891(4)°.
	b = 10.9609(11) Å	β = 86.426(4)°.
	c = 17.2934(17) Å	γ = 73.218(4)°.
Volume	1170.5(2) Å <sup>3</sup>	
Z	1	
Density (calculated)	1.729 g/cm <sup>3</sup>	
Absorption coefficient	2.060 mm <sup>-1</sup>	
F(000)	600	
Crystal size	0.25 x 0.15 x 0.08 mm <sup>3</sup>	
Theta range for data collection	1.94 to 30.50°.	
Index ranges	-9 ≤ h ≤ 9, -15 ≤ k ≤ 15, -24 ≤ l ≤ 24	
Reflections collected	91600	
Independent reflections	7150 [R(int) = 0.0329]	
Completeness to theta = 30.50°	100.0 %	
Absorption correction	Semi-empirical from equivalents	
Max. and min. transmission	0.8525 and 0.6269	
Refinement method	Full-matrix least-squares on F <sup>2</sup>	
Data / restraints / parameters	7150 / 23 / 340	
Goodness-of-fit on F <sup>2</sup>	1.128	
Final R indices [I > 2σ(I)]	R1 = 0.0229, wR2 = 0.0594	
R indices (all data)	R1 = 0.0241, wR2 = 0.0599	
Largest diff. peak and hole	1.145 and -0.856 e.Å <sup>-3</sup>	

**Table B.17** Crystal data and structure refinement for **11i**

Empirical formula	C <sub>23</sub> H <sub>20</sub> Br N <sub>5</sub> O
Formula weight	462.35
Temperature	133(2) K
Wavelength	0.71073 Å
Crystal system	Monoclinic
Space group	P2(1)/c
Unit cell dimensions	a = 15.9510(15) Å      α = 90°. b = 5.9914(6) Å      β = 103.494(4)°. c = 23.071(2) Å      γ = 90°.
Volume	2144.0(3) Å <sup>3</sup>
Z	4
Density (calculated)	1.432 g/cm <sup>3</sup>
Absorption coefficient	1.942 mm <sup>-1</sup>
F(000)	944
Crystal size	0.30 x 0.25 x 0.15 mm <sup>3</sup>
Theta range for data collection	1.82 to 33.14°.
Index ranges	-24 ≤ h ≤ 24, -9 ≤ k ≤ 9, -35 ≤ l ≤ 35
Reflections collected	81141
Independent reflections	8148 [R(int) = 0.0453]
Completeness to theta = 33.14°	99.8 %
Absorption correction	Semi-empirical from equivalents
Max. and min. transmission	0.7594 and 0.5935
Refinement method	Full-matrix least-squares on F <sup>2</sup>
Data / restraints / parameters	8148 / 0 / 276
Goodness-of-fit on F <sup>2</sup>	1.045
Final R indices [I > 2σ(I)]	R1 = 0.0363, wR2 = 0.0916
R indices (all data)	R1 = 0.0573, wR2 = 0.1001
Largest diff. peak and hole	0.789 and -0.522 e.Å <sup>-3</sup>

**Table B.18** Crystal data and structure refinement for **12a**

Empirical formula	C <sub>24</sub> H <sub>26</sub> N <sub>4</sub> O <sub>2</sub>	
Formula weight	402.49	
Temperature	173(2) K	
Wavelength	0.71073 Å	
Crystal system	Triclinic	
Space group	P-1	
Unit cell dimensions	a = 6.5178(11) Å	α = 101.474(8)°.
	b = 8.3747(15) Å	β = 91.394(12)°.
	c = 19.667(3) Å	γ = 104.728(13)°.
Volume	1014.3(3) Å <sup>3</sup>	
Z	2	
Density (calculated)	1.318 g/cm <sup>3</sup>	
Absorption coefficient	0.086 mm <sup>-1</sup>	
F(000)	428	
Crystal size	0.40 x 0.20 x 0.05 mm <sup>3</sup>	
Theta range for data collection	2.12 to 27.45°.	
Index ranges	-8 ≤ h ≤ 7, -10 ≤ k ≤ 10, -25 ≤ l ≤ 24	
Reflections collected	7514	
Independent reflections	4450 [R(int) = 0.1125]	
Completeness to theta = 27.45°	95.9 %	
Absorption correction	None	
Refinement method	Full-matrix least-squares on F <sup>2</sup>	
Data / restraints / parameters	4450 / 0 / 278	
Goodness-of-fit on F <sup>2</sup>	0.883	
Final R indices [I > 2σ(I)]	R1 = 0.0704, wR2 = 0.1702	
R indices (all data)	R1 = 0.1577, wR2 = 0.2130	
Largest diff. peak and hole	0.310 and -0.286 e.Å <sup>-3</sup>	

**Table B.19** Crystal data and structure refinement for **12b**

Empirical formula	C <sub>22</sub> H <sub>20</sub> I N <sub>3</sub> O <sub>2</sub>	
Formula weight	485.31	
Temperature	100(2) K	
Wavelength	0.71073 Å	
Crystal system	Triclinic	
Space group	P-1	
Unit cell dimensions	a = 6.5013(6) Å	α = 79.0860(10)°.
	b = 15.9500(14) Å	β = 87.0830(10)°.
	c = 19.1554(17) Å	γ = 86.8110(10)°.
Volume	1945.7(3) Å <sup>3</sup>	
Z	4	
Density (calculated)	1.657 Mg/m <sup>3</sup>	
Absorption coefficient	1.669 mm <sup>-1</sup>	
F(000)	968	
Crystal size	0.32 x 0.10 x 0.06 mm <sup>3</sup>	
Theta range for data collection	1.30 to 28.26°.	
Index ranges	-8 ≤ h ≤ 8, -21 ≤ k ≤ 21, -19 ≤ l ≤ 25	
Reflections collected	14151	
Independent reflections	8758 [R(int) = 0.0278]	
Completeness to theta = 28.26°	90.7 %	
Absorption correction	Semi-empirical from equivalents	
Max. and min. transmission	1.000 and 0.536	
Refinement method	Full-matrix least-squares on F <sup>2</sup>	
Data / restraints / parameters	8758 / 0 / 509	
Goodness-of-fit on F <sup>2</sup>	1.032	
Final R indices [I > 2σ(I)]	R1 = 0.0441, wR2 = 0.1044	
R indices (all data)	R1 = 0.0605, wR2 = 0.1120	
Largest diff. peak and hole	1.972 and -0.719 e.Å <sup>-3</sup>	

**Table B.20** Crystal data and structure refinement for **12c**

Empirical formula	C <sub>31</sub> H <sub>25</sub> N <sub>5</sub> O <sub>4</sub>	
Formula weight	531.56	
Temperature	100(2) K	
Wavelength	0.71073 Å	
Crystal system	Monoclinic	
Space group	P2(1)/n	
Unit cell dimensions	a = 7.9191(6) Å	$\alpha = 90^\circ$ .
	b = 12.5194(9) Å	$\beta = 94.5560(10)^\circ$ .
	c = 26.6039(18) Å	$\gamma = 90^\circ$ .
Volume	2629.2(3) Å <sup>3</sup>	
Z	4	
Density (calculated)	1.343 g/cm <sup>3</sup>	
Absorption coefficient	0.091 mm <sup>-1</sup>	
F(000)	1112	
Crystal size	0.24 x 0.24 x 0.15 mm <sup>3</sup>	
Theta range for data collection	1.80 to 28.28°.	
Index ranges	-10 ≤ h ≤ 10, -16 ≤ k ≤ 16, -35 ≤ l ≤ 35	
Reflections collected	22990	
Independent reflections	6329 [R(int) = 0.0269]	
Completeness to theta = 28.28°	96.9 %	
Absorption correction	None	
Refinement method	Full-matrix least-squares on F <sup>2</sup>	
Data / restraints / parameters	6329 / 0 / 369	
Goodness-of-fit on F <sup>2</sup>	1.038	
Final R indices [I > 2σ(I)]	R1 = 0.0416, wR2 = 0.1055	
R indices (all data)	R1 = 0.0523, wR2 = 0.1122	
Largest diff. peak and hole	0.359 and -0.241 e.Å <sup>-3</sup>	



**Table B.21** Crystal data and structure refinement for **12d**

Empirical formula	C <sub>19</sub> H <sub>23</sub> N <sub>3</sub> O <sub>5</sub>	
Formula weight	373.40	
Temperature	100(2) K	
Wavelength	0.71073 Å	
Crystal system	Monoclinic	
Space group	C2/c	
Unit cell dimensions	a = 21.0520(16) Å b = 20.4701(15) Å c = 9.7795(7) Å	α = 90°. β = 116.088(3)°. γ = 90°.
Volume	3785.0(5) Å <sup>3</sup>	
Z	8	
Density (calculated)	1.311 g/cm <sup>3</sup>	
Absorption coefficient	0.096 mm <sup>-1</sup>	
F(000)	1584	
Crystal size	0.30 x 0.25 x 0.15 mm <sup>3</sup>	
Theta range for data collection	2.93 to 32.58°.	
Index ranges	-31 ≤ h ≤ 31, -30 ≤ k ≤ 30, -14 ≤ l ≤ 14	
Reflections collected	63990	
Independent reflections	6818 [R(int) = 0.0364]	
Completeness to theta = 32.58°	98.8 %	
Absorption correction	None	
Max. and min. transmission	0.9857 and 0.9718	
Refinement method	Full-matrix least-squares on F <sup>2</sup>	
Data / restraints / parameters	6818 / 0 / 261	
Goodness-of-fit on F <sup>2</sup>	1.052	
Final R indices [I > 2σ(I)]	R1 = 0.0409, wR2 = 0.1136	
R indices (all data)	R1 = 0.0502, wR2 = 0.1212	
Largest diff. peak and hole	0.465 and -0.283 e.Å <sup>-3</sup>	

**Table B.22** Crystal data and structure refinement for **12e**

Empirical formula	C <sub>29</sub> H <sub>25</sub> F <sub>2</sub> N <sub>3</sub> O <sub>4</sub>	
Formula weight	517.52	
Temperature	120(2) K	
Wavelength	0.71073 Å	
Crystal system	Triclinic	
Space group	P-1	
Unit cell dimensions	a = 7.1921(4) Å	α = 86.977(2)°.
	b = 8.8171(5) Å	β = 80.472(3)°.
	c = 20.1473(12) Å	γ = 74.143(2)°.
Volume	1212.00(12) Å <sup>3</sup>	
Z	2	
Density (calculated)	1.418 g/cm <sup>3</sup>	
Absorption coefficient	0.106 mm <sup>-1</sup>	
F(000)	540	
Crystal size	0.30 x 0.10 x 0.05 mm <sup>3</sup>	
Theta range for data collection	2.05 to 30.51°.	
Index ranges	-10 ≤ h ≤ 10, -12 ≤ k ≤ 5, -28 ≤ l ≤ 28	
Reflections collected	22270	
Independent reflections	7201 [R(int) = 0.0678]	
Completeness to theta = 30.51°	97.3 %	
Absorption correction	None	
Max. and min. transmission	0.9947 and 0.9690	
Refinement method	Full-matrix least-squares on F <sup>2</sup>	
Data / restraints / parameters	7201 / 0 / 371	
Goodness-of-fit on F <sup>2</sup>	0.964	
Final R indices [I > 2σ(I)]	R1 = 0.0580, wR2 = 0.1247	
R indices (all data)	R1 = 0.1273, wR2 = 0.1526	
Largest diff. peak and hole	0.224 and -0.304 e.Å <sup>-3</sup>	

**Table B.23 Crystal data and structure refinement for 12f**

Empirical formula	C <sub>22</sub> H <sub>17</sub> F <sub>4</sub> I N <sub>4</sub> O	
Formula weight	556.30	
Temperature	120(2) K	
Wavelength	0.71073 Å	
Crystal system	Triclinic	
Space group	P-1	
Unit cell dimensions	a = 7.0386(4) Å	$\alpha = 93.272(4)^\circ$ .
	b = 10.4652(7) Å	$\beta = 101.688(3)^\circ$ .
	c = 15.6912(10) Å	$\gamma = 106.016(3)^\circ$ .
Volume	1080.06(12) Å <sup>3</sup>	
Z	2	
Density (calculated)	1.711 Mg/m <sup>3</sup>	
Absorption coefficient	1.539 mm <sup>-1</sup>	
F(000)	548	
Crystal size	0.30 x 0.25 x 0.10 mm <sup>3</sup>	
Theta range for data collection	2.04 to 33.14°.	
Index ranges	-10 ≤ h ≤ 10, -16 ≤ k ≤ 16, -24 ≤ l ≤ 24	
Reflections collected	32455	
Independent reflections	7883 [R(int) = 0.0283]	
Completeness to theta = 33.14°	95.8 %	
Absorption correction	None	
Max. and min. transmission	0.8613 and 0.6553	
Refinement method	Full-matrix least-squares on F <sup>2</sup>	
Data / restraints / parameters	7883 / 0 / 294	
Goodness-of-fit on F <sup>2</sup>	1.123	
Final R indices [I > 2σ(I)]	R1 = 0.0269, wR2 = 0.0630	
R indices (all data)	R1 = 0.0356, wR2 = 0.0662	
Largest diff. peak and hole	1.119 and -0.706 e.Å <sup>-3</sup>	

**Table B.24** Crystal data and structure refinement for **12g**

Empirical formula	C <sub>23</sub> H <sub>20</sub> F N <sub>5</sub> O	
Formula weight	401.44	
Temperature	120(2) K	
Wavelength	0.71073 Å	
Crystal system	Monoclinic	
Space group	P2(1)/n	
Unit cell dimensions	a = 16.1659(12) Å	$\alpha = 90^\circ$ .
	b = 6.4146(5) Å	$\beta = 105.945(5)^\circ$ .
	c = 21.0074(16) Å	$\gamma = 90^\circ$ .
Volume	2094.6(3) Å <sup>3</sup>	
Z	4	
Density (calculated)	1.273 g/cm <sup>3</sup>	
Absorption coefficient	0.088 mm <sup>-1</sup>	
F(000)	840	
Crystal size	0.30 x 0.15 x 0.05 mm <sup>3</sup>	
Theta range for data collection	1.42 to 30.50°.	
Index ranges	-21 ≤ h ≤ 23, -8 ≤ k ≤ 9, -29 ≤ l ≤ 29	
Reflections collected	20522	
Independent reflections	6367 [R(int) = 0.0654]	
Completeness to theta = 30.50°	99.7 %	
Absorption correction	None	
Max. and min. transmission	0.9956 and 0.9742	
Refinement method	Full-matrix least-squares on F <sup>2</sup>	
Data / restraints / parameters	6367 / 0 / 276	
Goodness-of-fit on F <sup>2</sup>	0.945	
Final R indices [I > 2σ(I)]	R1 = 0.0531, wR2 = 0.1011	
R indices (all data)	R1 = 0.1597, wR2 = 0.1323	
Largest diff. peak and hole	0.136 and -0.169 e.Å <sup>-3</sup>	

**Table B.25** Crystal data and structure refinement for **13**

Empirical formula	C <sub>15</sub> H <sub>13</sub> N <sub>3</sub>	
Formula weight	235.28	
Temperature	173(2) K	
Wavelength	0.71073 Å	
Crystal system	Monoclinic	
Space group	P2(1)	
Unit cell dimensions	a = 5.6978(5) Å	α = 90°.
	b = 8.4526(8) Å	β = 93.656(7)°.
	c = 12.5435(14) Å	γ = 90°.
Volume	602.88(10) Å <sup>3</sup>	
Z	2	
Density (calculated)	1.296 g/cm <sup>3</sup>	
Absorption coefficient	0.079 mm <sup>-1</sup>	
F(000)	248	
Crystal size	0.40 x 0.35 x 0.20 mm <sup>3</sup>	
Theta range for data collection	1.63 to 28.26°.	
Index ranges	-7 ≤ h ≤ 7, -10 ≤ k ≤ 11, -15 ≤ l ≤ 15	
Reflections collected	4216	
Independent reflections	1505 [R(int) = 0.0913]	
Completeness to theta = 28.26°	94.2 %	
Absorption correction	None	
Refinement method	Full-matrix least-squares on F <sup>2</sup>	
Data / restraints / parameters	1505 / 1 / 164	
Goodness-of-fit on F <sup>2</sup>	1.006	
Final R indices [I > 2σ(I)]	R1 = 0.0537, wR2 = 0.1267	
R indices (all data)	R1 = 0.0614, wR2 = 0.1333	
Absolute structure parameter	1(3)	
Extinction coefficient	0.064(16)	
Largest diff. peak and hole	0.267 and -0.246 e.Å <sup>-3</sup>	

**Table B.26** Crystal data and structure refinement for **13a**

Empirical formula	C <sub>29</sub> H <sub>23</sub> N <sub>5</sub> O <sub>8</sub>
Formula weight	569.52
Temperature	173(2) K
Wavelength	0.71073 Å
Crystal system	Monoclinic
Space group	Cc
Unit cell dimensions	a = 12.2918(9) Å      α = 90°. b = 34.041(3) Å      β = 123.601(4)°. c = 7.4350(5) Å      γ = 90°.
Volume	2591.1(3) Å <sup>3</sup>
Z	4
Density (calculated)	1.460 Mg/m <sup>3</sup>
Absorption coefficient	0.109 mm <sup>-1</sup>
F(000)	1184
Crystal size	0.40 x 0.35 x 0.15 mm <sup>3</sup>
Theta range for data collection	2.08 to 28.28°.
Index ranges	-16 ≤ h ≤ 16, -43 ≤ k ≤ 40, -9 ≤ l ≤ 9
Reflections collected	8925
Independent reflections	2989 [R(int) = 0.1389]
Completeness to theta = 28.28°	92.7 %
Absorption correction	None
Refinement method	Full-matrix least-squares on F <sup>2</sup>
Data / restraints / parameters	2989 / 2 / 380
Goodness-of-fit on F <sup>2</sup>	1.025
Final R indices [I > 2σ(I)]	R1 = 0.0622, wR2 = 0.1435
R indices (all data)	R1 = 0.0759, wR2 = 0.1565
Absolute structure parameter	0.2(16)
Extinction coefficient	0.0090(18)
Largest diff. peak and hole	0.498 and -0.388 e.Å <sup>-3</sup>

**Table B.27** Crystal data and structure refinement for **14a**

Empirical formula	C <sub>29</sub> H <sub>23</sub> N <sub>5</sub> O <sub>8</sub>	
Formula weight	569.52	
Temperature	100(2) K	
Wavelength	0.71073 Å	
Crystal system	Monoclinic	
Space group	P2(1)/c	
Unit cell dimensions	a = 9.6419(17) Å	α = 90°.
	b = 33.922(6) Å	β = 115.309(2)°.
	c = 8.8963(16) Å	γ = 90°.
Volume	2630.4(8) Å <sup>3</sup>	
Z	4	
Density (calculated)	1.438 g/cm <sup>3</sup>	
Absorption coefficient	0.107 mm <sup>-1</sup>	
F(000)	1184	
Crystal size	0.38 x 0.38 x 0.09 mm <sup>3</sup>	
Theta range for data collection	2.34 to 28.30°.	
Index ranges	-12 ≤ h ≤ 12, -44 ≤ k ≤ 45, -11 ≤ l ≤ 11	
Reflections collected	23110	
Independent reflections	6297 [R(int) = 0.0392]	
Completeness to theta = 28.30°	96.4 %	
Absorption correction	None	
Refinement method	Full-matrix least-squares on F <sup>2</sup>	
Data / restraints / parameters	6297 / 0 / 385	
Goodness-of-fit on F <sup>2</sup>	0.998	
Final R indices [I > 2σ(I)]	R1 = 0.0408, wR2 = 0.1016	
R indices (all data)	R1 = 0.0506, wR2 = 0.1077	
Largest diff. peak and hole	0.315 and -0.291 e.Å <sup>-3</sup>	

**Table B.28** Crystal data and structure refinement for **15a**

Empirical formula	C37 H43 N3 O4	
Formula weight	593.74	
Temperature	173(2) K	
Wavelength	0.71073 Å	
Crystal system	Triclinic	
Space group	P-1	
Unit cell dimensions	a = 8.7673(18) Å	$\alpha = 90.005(16)^\circ$ .
	b = 12.557(3) Å	$\beta = 77.019(16)^\circ$ .
	c = 15.151(4) Å	$\gamma = 78.247(11)^\circ$ .
Volume	1589.4(6) Å <sup>3</sup>	
Z	2	
Density (calculated)	1.241 g/cm <sup>3</sup>	
Absorption coefficient	0.081 mm <sup>-1</sup>	
F(000)	636	
Crystal size	0.30 x 0.30 x 0.20 mm <sup>3</sup>	
Theta range for data collection	1.38 to 27.19°.	
Index ranges	-11 ≤ h ≤ 11, -16 ≤ k ≤ 15, -19 ≤ l ≤ 18	
Reflections collected	11375	
Independent reflections	6824 [R(int) = 0.1625]	
Completeness to theta = 27.19°	96.3 %	
Absorption correction	None	
Refinement method	Full-matrix least-squares on F <sup>2</sup>	
Data / restraints / parameters	6824 / 0 / 413	
Goodness-of-fit on F <sup>2</sup>	0.904	
Final R indices [I > 2σ(I)]	R1 = 0.0942, wR2 = 0.2430	
R indices (all data)	R1 = 0.1788, wR2 = 0.3077	
Largest diff. peak and hole	0.419 and -0.400 e.Å <sup>-3</sup>	



**Table B.29** Crystal data and structure refinement for **21a**

Empirical formula	C <sub>38</sub> H <sub>28</sub> Cl <sub>2</sub> N <sub>8</sub> O <sub>2</sub>	
Formula weight	699.58	
Temperature	120(2) K	
Wavelength	0.71073 Å	
Crystal system	Monoclinic	
Space group	P2(1)/n	
Unit cell dimensions	a = 13.6335(10) Å	α = 90°.
	b = 4.4402(3) Å	β = 94.084(3)°.
	c = 27.297(2) Å	γ = 90°.
Volume	1648.2(2) Å <sup>3</sup>	
Z	2	
Density (calculated)	1.410 g/cm <sup>3</sup>	
Absorption coefficient	0.247 mm <sup>-1</sup>	
F(000)	724	
Crystal size	0.30 x 0.30 x 0.15 mm <sup>3</sup>	
Theta range for data collection	1.63 to 30.99°.	
Index ranges	-17 ≤ h ≤ 19, -6 ≤ k ≤ 6, -39 ≤ l ≤ 39	
Reflections collected	40395	
Independent reflections	5259 [R(int) = 0.0387]	
Completeness to theta = 30.99°	99.9 %	
Absorption correction	None	
Max. and min. transmission	0.9639 and 0.9297	
Refinement method	Full-matrix least-squares on F <sup>2</sup>	
Data / restraints / parameters	5259 / 0 / 229	
Goodness-of-fit on F <sup>2</sup>	1.078	
Final R indices [I > 2σ(I)]	R1 = 0.0418, wR2 = 0.1013	
R indices (all data)	R1 = 0.0634, wR2 = 0.1118	
Largest diff. peak and hole	0.337 and -0.347 e.Å <sup>-3</sup>	

**Table B.30** Crystal data and structure refinement for **23e**

Empirical formula	C <sub>28</sub> H <sub>20</sub> F <sub>2</sub> N <sub>6</sub> O <sub>2</sub>	
Formula weight	510.50	
Temperature	173(2) K	
Wavelength	0.71073 Å	
Crystal system	Triclinic	
Space group	P-1	
Unit cell dimensions	a = 3.8189(6) Å	α = 98.884(10)°.
	b = 11.2941(18) Å	β = 93.147(11)°.
	c = 14.107(2) Å	γ = 94.624(10)°.
Volume	597.79(16) Å <sup>3</sup>	
Z	1	
Density (calculated)	1.418 g/cm <sup>3</sup>	
Absorption coefficient	0.104 mm <sup>-1</sup>	
F(000)	264	
Crystal size	0.40 x 0.20 x -0.08 mm <sup>3</sup>	
Theta range for data collection	1.46 to 27.47°.	
Index ranges	-4 ≤ h ≤ 4, -14 ≤ k ≤ 14, -17 ≤ l ≤ 17	
Reflections collected	4295	
Independent reflections	2606 [R(int) = 0.1106]	
Completeness to theta = 27.47°	96.0 %	
Absorption correction	None	
Refinement method	Full-matrix least-squares on F <sup>2</sup>	
Data / restraints / parameters	2606 / 0 / 180	
Goodness-of-fit on F <sup>2</sup>	1.017	
Final R indices [I > 2σ(I)]	R1 = 0.0597, wR2 = 0.1588	
R indices (all data)	R1 = 0.0869, wR2 = 0.1754	
Largest diff. peak and hole	0.295 and -0.304 e.Å <sup>-3</sup>	

**Table B.31** Crystal data and structure refinement for **26**

Empirical formula	C10 H6 N4 O2
Formula weight	214.19
Temperature	120(2) K
Wavelength	0.71073 Å
Crystal system	Orthorhombic
Space group	Pbca
Unit cell dimensions	a = 5.1610(6) Å $\alpha = 90^\circ$ . b = 11.1506(12) Å $\beta = 90^\circ$ . c = 16.0413(18) Å $\gamma = 90^\circ$ .
Volume	923.15(18) Å <sup>3</sup>
Z	4
Density (calculated)	1.541 Mg/m <sup>3</sup>
Absorption coefficient	0.114 mm <sup>-1</sup>
F(000)	440
Crystal size	0.30 x 0.20 x 0.10 mm <sup>3</sup>
Theta range for data collection	2.54 to 30.96°.
Index ranges	-7<=h<=7, -15<=k<=15, -16<=l<=23
Reflections collected	13112
Independent reflections	1443 [R(int) = 0.0418]
Completeness to theta = 30.96°	98.6 %
Absorption correction	None
Max. and min. transmission	0.9887 and 0.9667
Refinement method	Full-matrix least-squares on F <sup>2</sup>
Data / restraints / parameters	1443 / 0 / 76
Goodness-of-fit on F <sup>2</sup>	1.365
Final R indices [I>2sigma(I)]	R1 = 0.0437, wR2 = 0.1351
R indices (all data)	R1 = 0.0529, wR2 = 0.1418
Largest diff. peak and hole	0.348 and -0.266 e.Å <sup>-3</sup>

**Table B.32** Crystal data and structure refinement for **26a**

Empirical formula	C <sub>22</sub> H <sub>18</sub> N <sub>6</sub> O <sub>2</sub>	
Formula weight	398.42	
Temperature	120(2) K	
Wavelength	0.71073 Å	
Crystal system	Monoclinic	
Space group	P2(1)/c	
Unit cell dimensions	a = 9.5945(3) Å	α = 90°.
	b = 7.6585(3) Å	β = 96.5170(10)°.
	c = 13.5188(4) Å	γ = 90°.
Volume	986.94(6) Å <sup>3</sup>	
Z	2	
Density (calculated)	1.341 Mg/m <sup>3</sup>	
Absorption coefficient	0.091 mm <sup>-1</sup>	
F(000)	416	
Crystal size	0.30 x 0.25 x 0.15 mm <sup>3</sup>	
Theta range for data collection	2.14 to 30.98°.	
Index ranges	-7 ≤ h ≤ 13, -11 ≤ k ≤ 11, -19 ≤ l ≤ 19	
Reflections collected	17171	
Independent reflections	3085 [R(int) = 0.0329]	
Completeness to theta = 30.98°	98.4 %	
Absorption correction	None	
Max. and min. transmission	0.9865 and 0.9733	
Refinement method	Full-matrix least-squares on F <sup>2</sup>	
Data / restraints / parameters	3085 / 6 / 155	
Goodness-of-fit on F <sup>2</sup>	1.060	
Final R indices [I > 2σ(I)]	R1 = 0.0431, wR2 = 0.1120	
R indices (all data)	R1 = 0.0551, wR2 = 0.1192	
Largest diff. peak and hole	0.314 and -0.237 e.Å <sup>-3</sup>	

**Table B.33** Crystal data and structure refinement for **26b**

Empirical formula	C <sub>25</sub> H <sub>21</sub> N <sub>7</sub> O <sub>2</sub>
Formula weight	451.49
Temperature	120(2) K
Wavelength	0.71073 Å
Crystal system	Triclinic
Space group	P-1
Unit cell dimensions	a = 8.1531(4) Å $\alpha$ = 110.186(2)° b = 12.1495(6) Å $\beta$ = 104.862(2)° c = 12.4728(6) Å $\gamma$ = 97.578(2)°
Volume	1087.25(9) Å <sup>3</sup>
Z	2
Density (calculated)	1.379 g/cm <sup>3</sup>
Absorption coefficient	0.092 mm <sup>-1</sup>
F(000)	472
Crystal size	0.25 x 0.25 x 0.20 mm <sup>3</sup>
Theta range for data collection	1.84 to 30.50°.
Index ranges	-11 ≤ h ≤ 10, -12 ≤ k ≤ 17, -17 ≤ l ≤ 17
Reflections collected	19693
Independent reflections	6439 [R(int) = 0.0341]
Completeness to theta = 30.50°	97.0 %
Absorption correction	None
Max. and min. transmission	0.9817 and 0.9772
Refinement method	Full-matrix least-squares on F <sup>2</sup>
Data / restraints / parameters	6439 / 0 / 315
Goodness-of-fit on F <sup>2</sup>	1.051
Final R indices [I > 2σ(I)]	R1 = 0.0479, wR2 = 0.1210
R indices (all data)	R1 = 0.0665, wR2 = 0.1311
Largest diff. peak and hole	0.364 and -0.316 e.Å <sup>-3</sup>

**Table B.34** Crystal data and structure refinement for **26c**

Empirical formula	C <sub>23</sub> H <sub>17</sub> N <sub>7</sub> O <sub>2</sub>	
Formula weight	423.44	
Temperature	120(2) K	
Wavelength	0.71073 Å	
Crystal system	Monoclinic	
Space group	P2(1)/n	
Unit cell dimensions	a = 13.209(2) Å	α = 90°.
	b = 4.2872(7) Å	β = 91.588(8)°.
	c = 36.572(6) Å	γ = 90°.
Volume	2070.3(6) Å <sup>3</sup>	
Z	4	
Density (calculated)	1.359 g/cm <sup>3</sup>	
Absorption coefficient	0.092 mm <sup>-1</sup>	
F(000)	880	
Crystal size	0.20 x 0.10 x 0.04 mm <sup>3</sup>	
Theta range for data collection	1.11 to 29.57°.	
Index ranges	-18 ≤ h ≤ 15, -5 ≤ k ≤ 5, -50 ≤ l ≤ 50	
Reflections collected	26062	
Independent reflections	5751 [R(int) = 0.1017]	
Completeness to theta = 29.57°	99.6 %	
Absorption correction	None	
Max. and min. transmission	0.9963 and 0.9818	
Refinement method	Full-matrix least-squares on F <sup>2</sup>	
Data / restraints / parameters	5751 / 0 / 295	
Goodness-of-fit on F <sup>2</sup>	1.015	
Final R indices [I > 2σ(I)]	R1 = 0.0692, wR2 = 0.1415	
R indices (all data)	R1 = 0.1601, wR2 = 0.1752	
Largest diff. peak and hole	0.249 and -0.314 e.Å <sup>-3</sup>	

**Table B.35** Crystal data and structure refinement for **26d**

Empirical formula	C <sub>25</sub> H <sub>19</sub> N <sub>7</sub> O <sub>2</sub>	
Formula weight	449.47	
Temperature	120(2) K	
Wavelength	0.71073 Å	
Crystal system	Triclinic	
Space group	P-1	
Unit cell dimensions	a = 7.8608(3) Å b = 9.2579(4) Å c = 15.0534(5) Å	α = 82.518(2)°. β = 78.3330(10)°. γ = 86.741(2)°.
Volume	1063.21(7) Å <sup>3</sup>	
Z	2	
Density (calculated)	1.404 g/cm <sup>3</sup>	
Absorption coefficient	0.094 mm <sup>-1</sup>	
F(000)	468	
Crystal size	0.22 x 0.18 x 0.10 mm <sup>3</sup>	
Theta range for data collection	1.39 to 30.50°.	
Index ranges	-11 ≤ h ≤ 11, -12 ≤ k ≤ 13, -12 ≤ l ≤ 21	
Reflections collected	19480	
Independent reflections	6331 [R(int) = 0.0378]	
Completeness to theta = 30.50°	97.3 %	
Absorption correction	None	
Max. and min. transmission	0.9906 and 0.9795	
Refinement method	Full-matrix least-squares on F <sup>2</sup>	
Data / restraints / parameters	6331 / 8 / 322	
Goodness-of-fit on F <sup>2</sup>	1.108	
Final R indices [I > 2σ(I)]	R1 = 0.0527, wR2 = 0.1342	
R indices (all data)	R1 = 0.0766, wR2 = 0.1484	
Largest diff. peak and hole	0.330 and -0.329 e.Å <sup>-3</sup>	

**Table B.36** Crystal data and structure refinement for **26e**

Empirical formula	C18 H18 N6 O2	
Formula weight	350.38	
Temperature	120(2) K	
Wavelength	0.71073 Å	
Crystal system	Monoclinic	
Space group	P2(1)/n	
Unit cell dimensions	a = 7.6037(3) Å	$\alpha = 90^\circ$ .
	b = 9.4596(4) Å	$\beta = 104.125(2)^\circ$ .
	c = 12.6039(5) Å	$\gamma = 90^\circ$ .
Volume	879.16(6) Å <sup>3</sup>	
Z	2	
Density (calculated)	1.324 g/cm <sup>3</sup>	
Absorption coefficient	0.091 mm <sup>-1</sup>	
F(000)	368	
Crystal size	0.30 x 0.25 x 0.20 mm <sup>3</sup>	
Theta range for data collection	2.72 to 30.50°.	
Index ranges	-10 ≤ h ≤ 10, -13 ≤ k ≤ 13, -17 ≤ l ≤ 15	
Reflections collected	14686	
Independent reflections	2686 [R(int) = 0.0275]	
Completeness to theta = 30.50°	100.0 %	
Absorption correction	None	
Max. and min. transmission	0.9820 and 0.9732	
Refinement method	Full-matrix least-squares on F <sup>2</sup>	
Data / restraints / parameters	2686 / 0 / 123	
Goodness-of-fit on F <sup>2</sup>	1.057	
Final R indices [I > 2σ(I)]	R1 = 0.0390, wR2 = 0.1100	
R indices (all data)	R1 = 0.0449, wR2 = 0.1155	
Largest diff. peak and hole	0.447 and -0.311 e.Å <sup>-3</sup>	



**Table B.37** Crystal data and structure refinement for **29a**

Empirical formula	C <sub>24</sub> H <sub>18</sub> Br <sub>2</sub> N <sub>8</sub> O <sub>3</sub>	
Formula weight	626.28	
Temperature	120(2) K	
Wavelength	0.71073 Å	
Crystal system	Monoclinic	
Space group	P2(1)/c	
Unit cell dimensions	a = 11.2343(7) Å	α = 90°.
	b = 16.2173(9) Å	β = 90.063(3)°.
	c = 14.2298(8) Å	γ = 90°.
Volume	2592.5(3) Å <sup>3</sup>	
Z	4	
Density (calculated)	1.605 g/cm <sup>3</sup>	
Absorption coefficient	3.169 mm <sup>-1</sup>	
F(000)	1248	
Crystal size	0.25 x 0.20 x 0.15 mm <sup>3</sup>	
Theta range for data collection	2.21 to 31.50°.	
Index ranges	-16 ≤ h ≤ 16, -22 ≤ k ≤ 23, -20 ≤ l ≤ 20	
Reflections collected	52753	
Independent reflections	8599 [R(int) = 0.0529]	
Completeness to theta = 31.50°	99.8 %	
Absorption correction	None	
Max. and min. transmission	0.6478 and 0.5046	
Refinement method	Full-matrix least-squares on F <sup>2</sup>	
Data / restraints / parameters	8599 / 0 / 345	
Goodness-of-fit on F <sup>2</sup>	1.041	
Final R indices [I > 2σ(I)]	R1 = 0.0407, wR2 = 0.1009	
R indices (all data)	R1 = 0.0740, wR2 = 0.1131	
Largest diff. peak and hole	0.937 and -0.874 e.Å <sup>-3</sup>	

**Table B.38** Crystal data and structure refinement for **29b**

Empirical formula	C <sub>65</sub> H <sub>58.50</sub> N <sub>19</sub> O <sub>7.50</sub>	
Formula weight	1225.81	
Temperature	120(2) K	
Wavelength	0.71073 Å	
Crystal system	Triclinic	
Space group	P-1	
Unit cell dimensions	a = 11.310(2) Å	α = 88.010(10)°.
	b = 17.162(3) Å	β = 82.742(10)°.
	c = 17.335(3) Å	γ = 70.891(10)°.
Volume	3153.8(11) Å <sup>3</sup>	
Z	2	
Density (calculated)	1.291 g/cm <sup>3</sup>	
Absorption coefficient	0.089 mm <sup>-1</sup>	
F(000)	1283	
Crystal size	0.30 x 0.20 x 0.06 mm <sup>3</sup>	
Theta range for data collection	1.92 to 29.35°.	
Index ranges	-15 ≤ h ≤ 15, -23 ≤ k ≤ 23, -23 ≤ l ≤ 23	
Reflections collected	69025	
Independent reflections	69025 [R(int) = 0.0000]	
Completeness to theta = 25.00°	99.2 %	
Absorption correction	None	
Max. and min. transmission	0.9947 and 0.9739	
Refinement method	Full-matrix least-squares on F <sup>2</sup>	
Data / restraints / parameters	69025 / 435 / 899	
Goodness-of-fit on F <sup>2</sup>	1.435	
Final R indices [I > 2σ(I)]	R1 = 0.0816, wR2 = 0.2282	
R indices (all data)	R1 = 0.1138, wR2 = 0.2468	
Largest diff. peak and hole	0.938 and -0.559 e.Å <sup>-3</sup>	

**Table B.39** Crystal data and structure refinement for **12:32**

Empirical formula	C <sub>24</sub> H <sub>21</sub> N <sub>5</sub> O <sub>3</sub>
Formula weight	427.46
Temperature	173(2) K
Wavelength	0.71073 Å
Crystal system	Monoclinic
Space group	Pc
Unit cell dimensions	a = 11.0553(13) Å      α = 90°. b = 7.3121(9) Å      β = 94.693(7)°. c = 13.2662(17) Å      γ = 90°.
Volume	1068.8(2) Å <sup>3</sup>
Z	2
Density (calculated)	1.328 g/cm <sup>3</sup>
Absorption coefficient	0.091 mm <sup>-1</sup>
F(000)	448
Crystal size	0.35 x 0.30 x 0.25 mm <sup>3</sup>
Theta range for data collection	1.85 to 28.25°.
Index ranges	-14 ≤ h ≤ 14, -8 ≤ k ≤ 9, -16 ≤ l ≤ 17
Reflections collected	12367
Independent reflections	2511 [R(int) = 0.1420]
Completeness to theta = 28.25°	94.8 %
Absorption correction	None
Refinement method	Full-matrix least-squares on F <sup>2</sup>
Data / restraints / parameters	2511 / 2 / 297
Goodness-of-fit on F <sup>2</sup>	1.030
Final R indices [I > 2σ(I)]	R1 = 0.0527, wR2 = 0.1298
R indices (all data)	R1 = 0.0563, wR2 = 0.1346
Absolute structure parameter	0.7(13)
Largest diff. peak and hole	0.287 and -0.241 e.Å <sup>-3</sup>

**Table B.40** Crystal data and structure refinement for **14:4-OH BA**

Empirical formula	C <sub>22</sub> H <sub>19</sub> N <sub>3</sub> O <sub>3</sub>	
Formula weight	373.40	
Temperature	173(2) K	
Wavelength	0.71073 Å	
Crystal system	Triclinic	
Space group	P-1	
Unit cell dimensions	a = 8.0137(8) Å	α = 82.364(6)°.
	b = 9.8024(9) Å	β = 86.045(7)°.
	c = 12.0784(13) Å	γ = 75.888(6)°.
Volume	911.35(16) Å <sup>3</sup>	
Z	2	
Density (calculated)	1.361 g/cm <sup>3</sup>	
Absorption coefficient	0.092 mm <sup>-1</sup>	
F(000)	392	
Crystal size	0.40 x 0.40 x 0.15 mm <sup>3</sup>	
Theta range for data collection	1.70 to 27.48°.	
Index ranges	-10 ≤ h ≤ 10, -12 ≤ k ≤ 11, -14 ≤ l ≤ 15	
Reflections collected	6742	
Independent reflections	3987 [R(int) = 0.0859]	
Completeness to theta = 27.48°	95.1 %	
Absorption correction	None	
Refinement method	Full-matrix least-squares on F <sup>2</sup>	
Data / restraints / parameters	3987 / 0 / 260	
Goodness-of-fit on F <sup>2</sup>	1.136	
Final R indices [I > 2σ(I)]	R1 = 0.0689, wR2 = 0.1795	
R indices (all data)	R1 = 0.0975, wR2 = 0.1993	
Extinction coefficient	0.051(9)	
Largest diff. peak and hole	0.447 and -0.358 e.Å <sup>-3</sup>	

**Table B.41** Crystal data and structure refinement for **30:PMBA:25**

Empirical formula	C <sub>34</sub> H <sub>35</sub> N <sub>5</sub> O <sub>3</sub>	
Formula weight	561.67	
Temperature	173(2) K	
Wavelength	0.71073 Å	
Crystal system	Monoclinic	
Space group	P2(1)	
Unit cell dimensions	a = 5.8013(4) Å	α = 90°.
	b = 31.248(2) Å	β = 106.337(5)°.
	c = 8.4490(6) Å	γ = 90°.
Volume	1469.80(18) Å <sup>3</sup>	
Z	2	
Density (calculated)	1.269 g/cm <sup>3</sup>	
Absorption coefficient	0.083 mm <sup>-1</sup>	
F(000)	596	
Crystal size	0.40 x 0.20 x 0.08 mm <sup>3</sup>	
Theta range for data collection	1.30 to 28.33°.	
Index ranges	-7 ≤ h ≤ 7, -41 ≤ k ≤ 40, -11 ≤ l ≤ 11	
Reflections collected	18492	
Independent reflections	3539 [R(int) = 0.1495]	
Completeness to theta = 28.33°	94.8 %	
Absorption correction	None	
Max. and min. transmission	0.9934 and 0.9676	
Refinement method	Full-matrix least-squares on F <sup>2</sup>	
Data / restraints / parameters	3539 / 1 / 391	
Goodness-of-fit on F <sup>2</sup>	1.027	
Final R indices [I > 2σ(I)]	R1 = 0.0523, wR2 = 0.1324	
R indices (all data)	R1 = 0.0688, wR2 = 0.1440	
Absolute structure parameter	-1.1(16)	
Largest diff. peak and hole	0.294 and -0.269 e.Å <sup>-3</sup>	

**Table B.42** Crystal data and structure refinement for **4b**

Empirical formula	C <sub>34</sub> H <sub>34</sub> Ag B F <sub>4</sub> N <sub>6</sub> O <sub>2</sub>	
Formula weight	753.35	
Temperature	173(2) K	
Wavelength	0.71073 Å	
Crystal system	Monoclinic	
Space group	P2/n	
Unit cell dimensions	a = 9.9140(7) Å	α = 90°.
	b = 8.4229(6) Å	β = 102.108(3)°.
	c = 19.7055(13) Å	γ = 90°.
Volume	1608.89(19) Å <sup>3</sup>	
Z	2	
Density (calculated)	1.555 g/cm <sup>3</sup>	
Absorption coefficient	0.692 mm <sup>-1</sup>	
F(000)	768	
Crystal size	0.20 x 0.20 x 0.20 mm <sup>3</sup>	
Theta range for data collection	2.11 to 28.27°.	
Index ranges	-13 ≤ h ≤ 13, -10 ≤ k ≤ 11, -23 ≤ l ≤ 25	
Reflections collected	11041	
Independent reflections	3711 [R(int) = 0.1071]	
Completeness to theta = 28.27°	93.0 %	
Absorption correction	None	
Refinement method	Full-matrix least-squares on F <sup>2</sup>	
Data / restraints / parameters	3711 / 20 / 240	
Goodness-of-fit on F <sup>2</sup>	1.042	
Final R indices [I > 2σ(I)]	R1 = 0.0558, wR2 = 0.1341	
R indices (all data)	R1 = 0.0763, wR2 = 0.1461	
Largest diff. peak and hole	0.590 and -1.773 e.Å <sup>-3</sup>	

**Table B.43** Crystal data and structure refinement for **4c**

Empirical formula	C <sub>34</sub> H <sub>34</sub> Ag As F <sub>6</sub> N <sub>6</sub> O <sub>2</sub>	
Formula weight	855.46	
Temperature	183(2) K	
Wavelength	0.71073 Å	
Crystal system	Triclinic	
Space group	P-1	
Unit cell dimensions	a = 9.1269(6) Å	α = 97.921(4)°.
	b = 9.2459(5) Å	β = 89.950(4)°.
	c = 10.0615(7) Å	γ = 98.904(4)°.
Volume	830.64(9) Å <sup>3</sup>	
Z	1	
Density (calculated)	1.710 Mg/m <sup>3</sup>	
Absorption coefficient	1.671 mm <sup>-1</sup>	
F(000)	430	
Crystal size	0.40 x 0.35 x 0.25 mm <sup>3</sup>	
Theta range for data collection	2.04 to 27.47°.	
Index ranges	-11 ≤ h ≤ 11, -10 ≤ k ≤ 11, -12 ≤ l ≤ 13	
Reflections collected	6058	
Independent reflections	3620 [R(int) = 0.0286]	
Completeness to theta = 27.47°	95.2 %	
Absorption correction	Semi-empirical from equivalents	
Max. and min. transmission	1.000 and 0.819	
Refinement method	Full-matrix least-squares on F <sup>2</sup>	
Data / restraints / parameters	3620 / 0 / 235	
Goodness-of-fit on F <sup>2</sup>	1.141	
Final R indices [I > 2σ(I)]	R1 = 0.0385, wR2 = 0.1049	
R indices (all data)	R1 = 0.0418, wR2 = 0.1083	
Largest diff. peak and hole	0.639 and -1.282 e.Å <sup>-3</sup>	

**Table B.44** Crystal data and structure refinement for **4d**

Empirical formula	C <sub>48</sub> H <sub>42</sub> Cu F <sub>12</sub> N <sub>8</sub> O <sub>6</sub>	
Formula weight	1118.44	
Temperature	100(2) K	
Wavelength	0.71073 Å	
Crystal system	Triclinic	
Space group	P-1	
Unit cell dimensions	a = 10.349(3) Å	α = 98.217(6)°.
	b = 10.688(3) Å	β = 110.457(5)°.
	c = 12.680(3) Å	γ = 104.465(5)°.
Volume	1230.8(6) Å <sup>3</sup>	
Z	1	
Density (calculated)	1.509 g/cm <sup>3</sup>	
Absorption coefficient	0.547 mm <sup>-1</sup>	
F(000)	571	
Crystal size	0.21 x 0.47 x 0.52 mm <sup>3</sup>	
Theta range for data collection	2.22 to 29.95°.	
Index ranges	-14 ≤ h ≤ 14, -14 ≤ k ≤ 14, -17 ≤ l ≤ 17	
Reflections collected	13002	
Independent reflections	6946 [R(int) = 0.0288]	
Completeness to theta = 29.95°	97.2 %	
Absorption correction	None	
Refinement method	Full-matrix least-squares on F <sup>2</sup>	
Data / restraints / parameters	6946 / 24 / 357	
Goodness-of-fit on F <sup>2</sup>	1.047	
Final R indices [I > 2σ(I)]	R1 = 0.0653, wR2 = 0.1574	
R indices (all data)	R1 = 0.0772, wR2 = 0.1650	
Largest diff. peak and hole	1.191 and -0.949 e.Å <sup>-3</sup>	



**Table B.45** Crystal data and structure refinement for **8a**

Empirical formula	C72 H61 Cu2 F4 N11 O10
Formula weight	1443.40
Temperature	173(2) K
Wavelength	0.71073 Å
Crystal system	Triclinic
Space group	P-1
Unit cell dimensions	a = 10.9536(9) Å $\alpha = 77.570(6)^\circ$ . b = 11.2155(8) Å $\beta = 78.159(4)^\circ$ . c = 14.9765(12) Å $\gamma = 74.526(5)^\circ$ .
Volume	1710.1(2) Å <sup>3</sup>
Z	1
Density (calculated)	1.402 g/cm <sup>3</sup>
Absorption coefficient	0.700 mm <sup>-1</sup>
F(000)	744
Crystal size	0.30 x 0.25 x 0.15 mm <sup>3</sup>
Theta range for data collection	1.41 to 27.49°.
Index ranges	-12 ≤ h ≤ 13, -14 ≤ k ≤ 14, -19 ≤ l ≤ 18
Reflections collected	12745
Independent reflections	7533 [R(int) = 0.1070]
Completeness to theta = 27.49°	95.8 %
Absorption correction	Semi-empirical from equivalents
Max. and min. transmission	1.000 and 0.687
Refinement method	Full-matrix least-squares on F <sup>2</sup>
Data / restraints / parameters	7533 / 9 / 448
Goodness-of-fit on F <sup>2</sup>	1.356
Final R indices [I > 2σ(I)]	R1 = 0.0782, wR2 = 0.2108
R indices (all data)	R1 = 0.0964, wR2 = 0.2236
Largest diff. peak and hole	0.787 and -0.940 e.Å <sup>-3</sup>

**Table B.46** Crystal data and structure refinement for **10a**

Empirical formula	C70 H58 Cu2 F4 N10 O10
Formula weight	1402.34
Temperature	173(2) K
Wavelength	0.71073 Å
Crystal system	Triclinic
Space group	P-1
Unit cell dimensions	a = 10.9819(16) Å $\alpha = 99.042(8)^\circ$ . b = 11.2072(15) Å $\beta = 91.419(6)^\circ$ . c = 14.926(2) Å $\gamma = 116.183(7)^\circ$ .
Volume	1618.8(4) Å <sup>3</sup>
Z	1
Density (calculated)	1.438 g/cm <sup>3</sup>
Absorption coefficient	0.737 mm <sup>-1</sup>
F(000)	722
Crystal size	0.40 x 0.20 x 0.08 mm <sup>3</sup>
Theta range for data collection	2.06 to 27.56°.
Index ranges	-13 ≤ h ≤ 14, -13 ≤ k ≤ 14, -18 ≤ l ≤ 19
Reflections collected	12440
Independent reflections	7276 [R(int) = 0.0912]
Completeness to theta = 27.56°	97.0 %
Absorption correction	Semi-empirical from equivalents
Max. and min. transmission	1.000 and 0.733
Refinement method	Full-matrix least-squares on F <sup>2</sup>
Data / restraints / parameters	7276 / 0 / 442
Goodness-of-fit on F <sup>2</sup>	1.089
Final R indices [I > 2σ(I)]	R1 = 0.0647, wR2 = 0.1759
R indices (all data)	R1 = 0.0834, wR2 = 0.1927
Largest diff. peak and hole	0.773 and -0.569 e.Å <sup>-3</sup>

**Table B.47** Crystal data and structure refinement for **33a**

Empirical formula	C <sub>32</sub> H <sub>24</sub> Cu <sub>2</sub> F <sub>2</sub> N <sub>6</sub> O <sub>10</sub>	
Formula weight	817.65	
Temperature	120(2) K	
Wavelength	0.71073 Å	
Crystal system	Triclinic	
Space group	P-1	
Unit cell dimensions	a = 7.8479(3) Å	α = 80.757(2)°.
	b = 8.5641(3) Å	β = 73.882(2)°.
	c = 12.5957(5) Å	γ = 79.976(2)°.
Volume	795.21(5) Å <sup>3</sup>	
Z	1	
Density (calculated)	1.707 g/cm <sup>3</sup>	
Absorption coefficient	1.420 mm <sup>-1</sup>	
F(000)	414	
Crystal size	0.20 x 0.15 x 0.10 mm <sup>3</sup>	
Theta range for data collection	2.73 to 32.58°.	
Index ranges	-11 ≤ h ≤ 11, -12 ≤ k ≤ 12, -19 ≤ l ≤ 19	
Reflections collected	19783	
Independent reflections	5601 [R(int) = 0.0273]	
Completeness to theta = 32.58°	97.1 %	
Absorption correction	None	
Max. and min. transmission	0.8711 and 0.7644	
Refinement method	Full-matrix least-squares on F <sup>2</sup>	
Data / restraints / parameters	5601 / 36 / 298	
Goodness-of-fit on F <sup>2</sup>	1.065	
Final R indices [I > 2σ(I)]	R1 = 0.0317, wR2 = 0.0778	
R indices (all data)	R1 = 0.0405, wR2 = 0.0824	
Largest diff. peak and hole	0.788 and -0.572 e.Å <sup>-3</sup>	

**Table B.48** Crystal data and structure refinement for **33b**

Empirical formula	C <sub>22</sub> H <sub>22</sub> Cu <sub>2</sub> N <sub>6</sub> O <sub>10</sub>	
Formula weight	657.54	
Temperature	120(2) K	
Wavelength	0.71073 Å	
Crystal system	Monoclinic	
Space group	P2(1)/c	
Unit cell dimensions	a = 12.6958(6) Å	α = 90°.
	b = 14.7329(7) Å	β = 99.951(2)°.
	c = 7.1734(4) Å	γ = 90°.
Volume	1321.57(12) Å <sup>3</sup>	
Z	2	
Density (calculated)	1.652 g/cm <sup>3</sup>	
Absorption coefficient	1.675 mm <sup>-1</sup>	
F(000)	668	
Crystal size	0.20 x 0.10 x 0.05 mm <sup>3</sup>	
Theta range for data collection	2.14 to 27.11°.	
Index ranges	-16 ≤ h ≤ 16, -18 ≤ k ≤ 18, -9 ≤ l ≤ 9	
Reflections collected	25834	
Independent reflections	2910 [R(int) = 0.0288]	
Completeness to theta = 27.12°	99.8 %	
Absorption correction	None	
Refinement method	Full-matrix least-squares on F <sup>2</sup>	
Data / restraints / parameters	2910 / 14 / 206	
Goodness-of-fit on F <sup>2</sup>	1.073	
Final R indices [I > 2σ(I)]	R1 = 0.0232, wR2 = 0.0601	
R indices (all data)	R1 = 0.0287, wR2 = 0.0628	
Largest diff. peak and hole	0.321 and -0.301 e.Å <sup>-3</sup>	

**Table B.49** Crystal data and structure refinement for **35a**

Empirical formula	C <sub>56</sub> H <sub>40</sub> N <sub>6</sub> Ni O <sub>6</sub>	
Formula weight	951.65	
Temperature	173(2) K	
Wavelength	0.71073 Å	
Crystal system	Orthorhombic	
Space group	Pbcn	
Unit cell dimensions	a = 19.447(4) Å	α = 90°.
	b = 9.6392(18) Å	β = 90°.
	c = 24.661(4) Å	γ = 90°.
Volume	4622.8(14) Å <sup>3</sup>	
Z	4	
Density (calculated)	1.367 Mg/m <sup>3</sup>	
Absorption coefficient	0.480 mm <sup>-1</sup>	
F(000)	1976	
Crystal size	0.36 x 0.20 x 0.12 mm <sup>3</sup>	
Theta range for data collection	1.65 to 28.51°.	
Index ranges	-25 ≤ h ≤ 24, -12 ≤ k ≤ 12, -32 ≤ l ≤ 32	
Reflections collected	26027	
Independent reflections	5418 [R(int) = 0.1479]	
Completeness to theta = 28.51°	92.4 %	
Absorption correction	Semi-empirical from equivalents	
Max. and min. transmission	1.000 and 0.620	
Refinement method	Full-matrix least-squares on F <sup>2</sup>	
Data / restraints / parameters	5418 / 39 / 364	
Goodness-of-fit on F <sup>2</sup>	0.960	
Final R indices [I > 2σ(I)]	R1 = 0.0558, wR2 = 0.1379	
R indices (all data)	R1 = 0.1201, wR2 = 0.1652	
Largest diff. peak and hole	0.475 and -0.578 e.Å <sup>-3</sup>	

**Table B.50** Crystal data and structure refinement for **35b**

Empirical formula	C <sub>34</sub> H <sub>30</sub> Cu <sub>2</sub> N <sub>6</sub> O <sub>10</sub>	
Formula weight	809.72	
Temperature	173(2) K	
Wavelength	0.71073 Å	
Crystal system	Triclinic	
Space group	P-1	
Unit cell dimensions	a = 7.5176(11) Å	α = 80.610(10)°.
	b = 7.9779(11) Å	β = 83.614(8)°.
	c = 15.951(2) Å	γ = 65.515(10)°.
Volume	858.0(2) Å <sup>3</sup>	
Z	1	
Density (calculated)	1.567 Mg/m <sup>3</sup>	
Absorption coefficient	1.307 mm <sup>-1</sup>	
F(000)	414	
Crystal size	0.30 x 0.20 x 0.10 mm <sup>3</sup>	
Theta range for data collection	2.59 to 27.52°.	
Index ranges	-9 ≤ h ≤ 9, -10 ≤ k ≤ 10, -20 ≤ l ≤ 19	
Reflections collected	6988	
Independent reflections	3808 [R(int) = 0.0476]	
Completeness to theta = 27.52°	96.6 %	
Absorption correction	Semi-empirical from equivalents	
Max. and min. transmission	1.000 and 0.513	
Refinement method	Full-matrix least-squares on F <sup>2</sup>	
Data / restraints / parameters	3808 / 0 / 244	
Goodness-of-fit on F <sup>2</sup>	1.031	
Final R indices [I > 2σ(I)]	R1 = 0.0584, wR2 = 0.1544	
R indices (all data)	R1 = 0.0758, wR2 = 0.1670	
Largest diff. peak and hole	0.785 and -1.089 e.Å <sup>-3</sup>	

## Appendix C - Infra Red Spectra

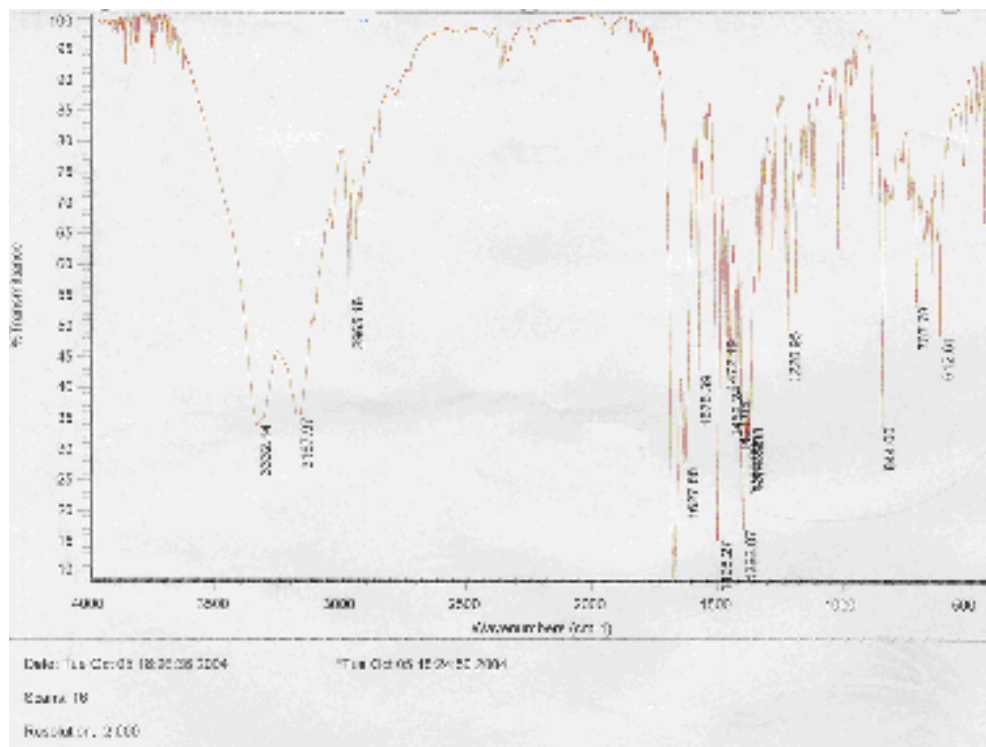


Figure C.1 IR spectrum of 6.

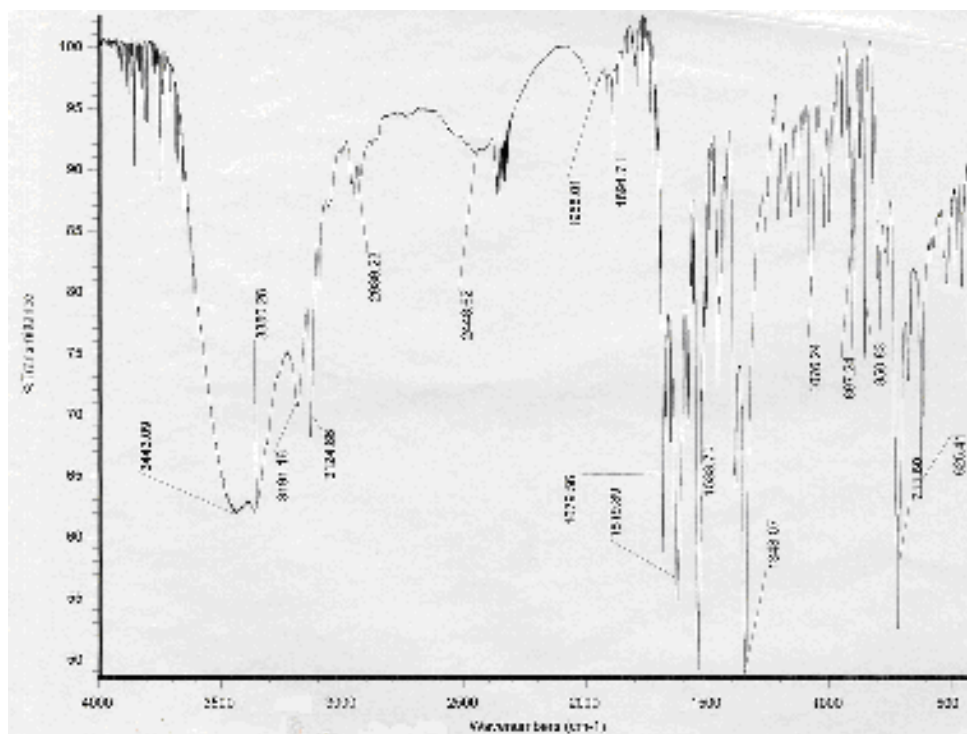


Figure C.2 IR spectrum of co-crystal of 6 and 3,5-dinitrobenzoic acid.